Microphysique du manteau neigeux : évolution de la surface spécifique de la neige dans les Alpes et l'Antarctique ; impact sur la chimie atmosphèrique

Axel Cabanes

CENTRE NATIONAL DE LA RECHERCHE SCIENTIFIQUE

LABORATOIRE DE GLACIOLOGIE ET GEOPHYSIQUE DE L'ENVIRONNEMENT

Associé à l'UNIVERSITE JOSEPH FOURIER - GRENOBLE I

Microphysique du manteau neigeux. Evolution de la surface spécifique de la neige dans les Alpes et l'Arctique. Impact sur la chimie atmosphérique.

Axel CABANES

Thèse de doctorat de l'Université Joseph Fourier - Grenoble I
(Arrêtés ministériels du 5 Juillet 1984 et 30 mars 1992)

Spécialité : Sciences de la Terre et de l'Univers

Date de la soutenance : 25 Janvier 2002

Composition du jury :

M.	Patrick Baussand	Président du Jury
M.	Michel Rossi	Rapporteur
M.	Jean Bruno Brzoska	Rapporteur
M.	Michel Pirre	Examinateur
M.	Wolfram Wobrock	Examinateur
M.	Florent Dominé	Directeur de Thèse

Laboratoire de Glaciologie et Géophysique de l'Environnement - CNRS
Tél (33) 04.76.82.42.00 - Fax (33) 04.76.82.42.01
54, Rue Molière - BP 96 - 38402 Saint Martin d'Hères Cedex France

Avant-Propos

Je tiens tout d'abord à remercier les membres du jury qui ont accepté de juger ce travail, et en particulier Mr Patrick Baussand, d'avoir accepté de présider mon jury de thèse. Je remercie Mr Michel Rossi et Mr Jean Bruno Brzoska pour l'intérêt qu'ils ont porté à ce travail en acceptant d'être rapporteur, ainsi que Mr Michel Pirre et Mr Wolfram Wobrock qui ont également participé au jury de cette these.

Je remercie vivement Mr Florent Dominé, mon directeur de thèse pour ses conseils, l'importance de la rigueur scientifique qui s'est efforcé de me transmettre au cours de ces 4 années. Je le remercie également pour les discussions scientifiques ou extra-scientifiques que nous avons eues ainsi que pour la bonne ambiance à laquelle il a contribué notamment lors de cette longue nuit polaire de 25 jours passée au nord du Canada.

Je tiens à remercier Leonard Barrie sans qui nous n'aurions pas participé à cette très enrichissante campagne de terrain, ainsi que Paul Shepson, Jan Bottenheim et leur équipes pour la coordination scientifique et logistique.

Mes remerciements s'adressent également à Werner Kuhs et son équipe ainsi qu'aux membres du CEN pour leur collaboration.

Un grand merci à Loic Legagneux pour sa contribution dans l'obtention des nombreux résultats de ce travail, ainsi qu'à Sébastien Perrier et Stéphane Houdier pour leur aide et leur bonne humeur.

J'exprime tout ma reconnaissance aux personnels du laboratoire qui ont pu contribué par leur aide, et leur conseils, à la réalisation de ce travail. Toute ma sympathie va également aux permanents, thésards, mes 'collocs' de bureau (Vince, Christophe) qui ont assuré une bonne ambiance durant ces 4 années.

Merci à tous mes amis de Montpellier, Béziers, Grenoble, qui se reconnaîtront et que j'ai toujours le plaisir de retrouver les week-ends, pour de bons moments de détente, de ski, de descente de rivière (j'ai maintenant un super casque !!)... et qui m'ont permis de garder toute ma motivation.

Merci à Sophie pour son soutien permanent notamment durant ces derniers mois de rédaction pas toujours très faciles. Enfin, un grand merci à mes proches pour leurs encouragements et à mes parents qui m'ont fait confiance durant ces longues années d'étude. Une dernière pensée pour mon papa qui n'aura malheureusement pas pu voir l'aboutissement de ce long et passionnant travail.

Résumé

La neige recouvre jusqu'à 50 % des surfaces émergées de l'hémisphère Nord en hiver. Une telle importance de la glace à la surface de la terre suggère un fort potentiel d'interaction avec l'atmosphère. De telles interactions ont été mises en évidence ces dernières années, et impliquent des processus complexes, comme la catalyse de réactions hétérogènes ou l'échange de gaz traces réactifs adsorbés à la surface des cristaux de neige, la diffusion en phase solide, les cycles de sublimation/condensation de glace qui entraînent des solutés. Leur compréhension et leur quantification requièrent la connaissance de divers paramètres physiques dont la surface spécifique (SS) de la neige, définie comme la surface accessible aux gaz par unité de masse. L'importance de ce paramètre et le peu de données existant dans la littérature a incité à effectuer ce travail sur l'étude de la SS de la neige et son évolution dans le manteau neigeux.

La SS a été déterminée par adsorption de méthane à la température de l'azote liquide (77 K). Afin de comprendre les processus responsables de l'évolution de la SS, des macrophotographies et des images obtenues par microscopie électronique à balayage ont été utilisées.

L'ensemble de nos résultats (176 mesures de SS) obtenus dans les Alpes et l'Arctique a montré que la SS de la neige est très variable : elle est comprise entre 1540 et 400 cm^2/g pour les neiges fraîches et peut descendre jusqu'à 100 cm^2/g pour des vieilles neiges. L'étude de l'évolution de la SS indique une décroissance avec le temps qui est due aux transformations morphologiques liées au métamorphisme de la neige. Celles-ci sont essentiellement caractérisées par un arrondissement et un grossissement des cristaux, et par la sublimation des petites structures.

La vitesse de décroissance de la SS a également été étudiée à différentes températures. Nos résultats ont montré que la température et le vent sont les deux principaux facteurs qui déterminent la cinétique de décroissance de la SS.

A Alert, (Arctique canadien), l'étude détaillée de la microphysique du manteau neigeux a permis de mesurer directement la capacité d'adsorption de gaz traces réactifs par le manteau neigeux. Sa surface totale a été mesurée entre 1160 et 3710 m^2/m^2. Nous avons ainsi démontré que le manteau neigeux pouvait séquestrer une grande partie des espèces présentes dans le système (neige + couche limite). Les mesures de SS ont également été utilisées pour déterminer les processus d'incorporation du formaldéhyde dans la neige.

Abstract

Snow covers up to 50% of land masses in the northern hemisphere in winter and its potential for interaction with the atmosphere has been demonstrated by studies in Polar Regions. This can proceed by complex processes that include heterogeneous reactions on the snow surface, adsorption/ desorption of gases, sublimation of snow and its solutes and co-condensation of water vapor and other gases. Understanding and quantifying theses processes requires the knowledge of physical parameters among which the specific surface area (SSA) of snow. It represents the surface area accessible to gases per mass unit.

In spite of the importance of this parameter, few data have been obtained earlier, which led us to perform this study on the SSA of snow and its evolution in the snowpack.

SSA was measured by methane adsorption at liquid nitrogen temperature (77K). In order to understand processes involved in SSA evolution, photomacrographs and pictures obtained by scanning electronic microscopy were used.

SSA values obtained were in the range 1540 to 400 cm^2/g for fresh snow. Values decrease down to 100 cm^2/g for aged snow. This decrease results from morphological changes associated to snow metamorphism. Temperature and wind are the main factors which drive the kinetics of SSA decrease.

At Alert (Canadian Arctic), a detailed study of the microphysics of the snowpack allowed the measurement of the uptake capacity of adsorbable trace gases by the snowpack. The total surface area of the snowpack ranged from 1160 to 3710 m^2/m^2. Therefore, we demonstrated that snowpack may sequester most of the species in the (snow + boundary layer) system. SSA values were also used to determinate incorporation processes of formaldehyde in snow.

SOMMAIRE

Chapitre I

Chapitre II

Chapitre III

INTRODUCTION

LA GLACE DANS LES NUAGES ET SUR TERRE

La glace constitue 45 % de la masse d'eau des nuages et se retrouve sur terre sous forme de glaciers, neige et calottes polaires où elle constitue plus de 98% des réserves d'eau douce de la planète (Van de Veen, 1991 ; Paterson, 1994). Sous forme de neige, elle recouvre de façon saisonnière une fraction importante des continents : jusqu'à 50% des terres émergées de l'hémisphère Nord pendant l'hiver (Robinson et al., 1993) comme le montre la figure **I.1**.

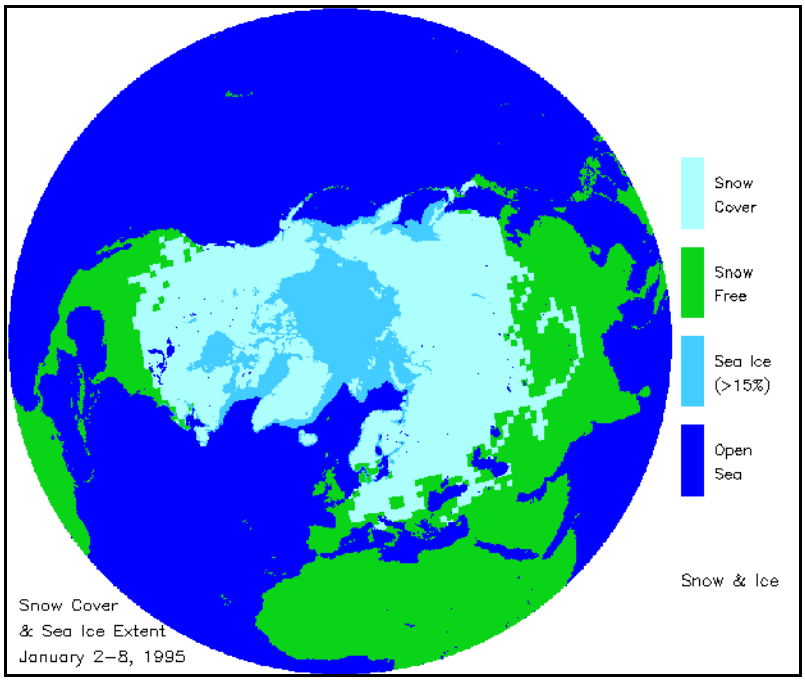

Figure I.1 : Surface du globe recouverte de neige ou de glace de mer dans l'hémisphère nord au mois de Janvier 1995.

Une telle importance de la glace dans l'atmosphère et à la surface de la terre suggère que ce solide puisse avoir une forte influence sur la chimie atmosphérique en catalysant des réactions hétérogènes comme cela a été observé dans la stratosphère polaire. Dans ce cas, des composés chlorés résultant de la dégradation des chlorofluorocarbures (CFC) d'origine anthropique, sont transformés à la surface des cristaux de glace et d'autres aérosols, en espèces photolysables qui détruisent l'ozone (Solomon, 1988 ; Leu, 1988 ; Hanson et Ravishankara, 1992 ; Chu et al., 1993).

Outre des processus de catalyse, l'impact de la glace peut aussi se manifester par la séquestration de gaz traces réactifs à sa surface ou dans son réseau cristallin. Il a par exemple été prédit que dans les cirrus, situés dans la haute troposphère, HNO_3 pouvait s'adsorber fortement à la surface de la glace jusqu'à être presque totalement éliminé de la phase gazeuse (Abbatt, 1997). Thibert et Dominé

(1997), après avoir mesuré le coefficient de diffusion de HCl dans la glace I_h, ont estimé le partage de ce gaz entre la phase gaz et le volume de la glace dans les cirrus et les traînées de condensation d'avion. Ils ont montré que les particules de glace de ces nuages pouvaient contenir dans leur volume 65 à 99 % du HCl contenu dans ces nuages.

Hormis les acides minéraux et organiques, des composés organiques apolaires ou faiblement polaires peuvent aussi s'adsorber de manière importante à la surface de la glace comme cela a été montré pour les hydrocarbures ou leurs dérivés chlorés (Hoff et al., 1995) ainsi que pour l'acétone (Rey-Hanot, 1999).

Ces quelques exemples illustrent l'effet important de la glace des nuages, qui soustrait des espèces chimiques à la phase gaz et modifie donc la composition de l'atmosphère.

IMPORTANCE DU MANTEAU NEIGEUX POUR LA CHIMIE ATMOSPHERIQUE

Le manteau neigeux contient une quantité de glace beaucoup plus importante que les nuages. Il suffit pour s'en rendre compte, d'estimer la quantité totale de glace contenue dans une colonne d'air de 1 m^2 traversée par un nuage de 1000 mètres d'épaisseur. Avec une valeur typique de 0.1g/m^3 (Snider et Murphy, 1995 ; Voisin et al., 2000), on obtient une quantité totale de glace de 100 g/m^2. Par comparaison, une couche de neige fraîche légère (masse volumique 0.05 g/cm^3) de seulement 10 cm d'épaisseur contient 5000 g de neige soit 50 fois plus. Cette masse atteint 300 000 g pour une couche de neige âgée (0.3 g/cm^3) de 1 mètre d'épaisseur, soit 3000 fois plus que dans le nuage décrit précédemment. Il est donc fort probable que le manteau neigeux, qui atteint généralement plusieurs dizaines de cm d'épaisseur, voire plusieurs mètres, interagisse fortement avec l'atmosphère et joue un rôle important sur sa chimie.

De nombreuses études menées depuis plus de 10 ans en régions polaires suggèrent effectivement l'existence de telles interactions. Parmi celles étudiées, la destruction de l'ozone observée dans la couche limite marine de l'Arctique est sans doute la mieux documentée (Bottenheim et al., 1986, 1990 ; Barrie et al., 1988, 1994 ; Mickle et al., 1989 ; Anlauf et al., 1994 ; Solberg et al., 1994). En effet, au printemps, à la période du levée de soleil polaire, il n'est pas rare que le rapport de mélange de l'ozone chute de son niveau normal (40 à 60 ppbv) jusqu'à une valeur inférieure à la limite de détection (~ 0.5 ppbv), au niveau du sol et jusqu'à une hauteur de 1000 mètres (Fig. **I.2**).

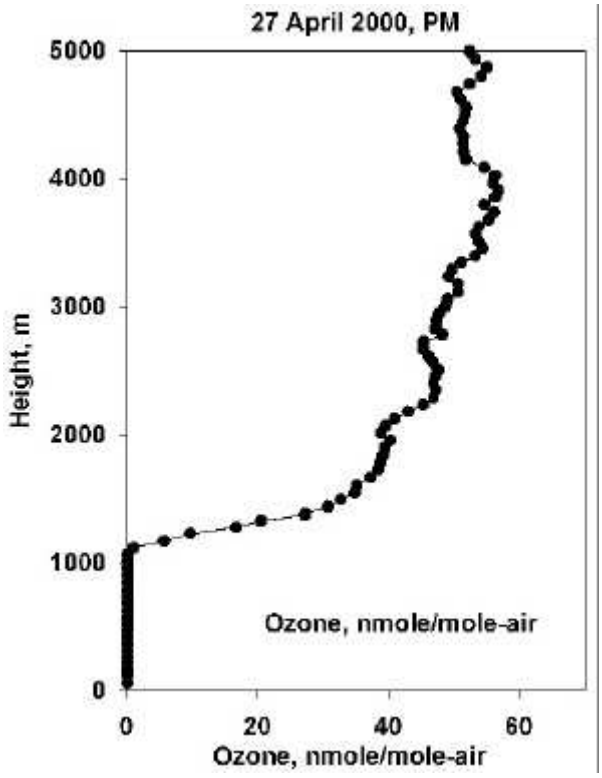

Figure I.2 : Profil vertical d'ozone lors d'un épisode de destruction, montrant la disparition totale de ce gaz sur 1100 m d'épaisseur. L'ozone ne retrouve sa concentration normale que vers 1500m.

L'explication de ce phénomène fait appel à des réactions en chaîne impliquant Br et BrO (Barrie et al. 1988 ; Jobson et al., 1994 ; Hausmann et Platt, 1994) selon les réactions :

$$Br + O_3 \rightarrow BrO + O_2 \qquad (I.1)$$

$$BrO + BrO \rightarrow 2\,Br + O_2 \qquad (I.2)$$

En atmosphère marine, la neige contient plusieurs ppbw de bromure Br^- qui peut donner lieu à des réactions hétérogènes (Tang et Mc Connell, 1996 ; Impey et al., 1997 et 1999). La production d'atomes de brome Br à partir de bromure Br^- peut donc être initiée sur des surfaces de glace, et peut-être d'autres aérosols, par l'ozone, selon la réaction (Oum et al., 1998) :

$$O_3 + Br^- (+ H^+) \rightarrow HOBr + O_2 \qquad (I.3)$$

HOBr peut ensuite réagir avec le bromure contenu sur les cristaux de neige, et libérer du brome moléculaire en phase gazeuse (Fan et Jacob, 1992; Abbatt 1994), dont la photolyse produit les atomes de brome actifs dans la destruction de l'ozone.

$$HOBr_{(surface)} + Br^- (+ H^+) \rightarrow Br_{2(gaz)} + H_2O \qquad (I.4)$$

$$Br_2 + h\nu \rightarrow 2Br \qquad (I.5)$$

Il est à noter que la production de fortes concentrations de Br_2 peut être rapide, car la production d'une seule molécule de HOBr par la réaction (I.3) mène à la formation de 2 atomes de brome. De plus, les réactions de terminaison de la chaîne constituée par les réactions (I.1) et (I.2) régénèrent HBr et HOBr selon :

$$Br + RCHO \rightarrow HBr + RC(O) \qquad (I.6)$$

$$BrO + HO_2 \rightarrow HOBr + O_2 \qquad (I.7)$$

qui sont les précurseurs de Br, et une cascade de réactions multipliant exponentiellement la concentration de brome peut alors avoir lieu, détruisant l'ozone sur de grandes épaisseurs en quelques jours.

Le cas de l'ozone n'est cependant qu'un exemple où les surfaces de glace ont un impact important sur la chimie de l'atmosphère. Plus récemment, des campagnes de terrain ont révélé d'autres espèces chimiques dont les concentrations étaient modifiées par la présence de la neige. Ainsi, une production de NO_x ($NO + NO_2$) par le manteau neigeux a été observée au Groenland et en Antarctique (Dibb et al., 1998, Honrath et al., 1999 ; Weller et al., 1999 ; Jones et al., 2001) ainsi qu'aux moyennes latitudes (Honrath et al., 2000a). L'émission de composés carbonylés tels que le formaldéhyde et l'acétaldéhyde a également été observée dans l'Arctique (Hutterli et al., 1999 ; Sumner and Shepson, 1999). Le relargage par le manteau neigeux de ces deux espèces chimiques ainsi que l'acétone a aussi été observé aux moyennes latitudes (Couch et al., 2000).

Les modèles de chimie atmosphérique au-dessus des surfaces enneigées n'arrivent pas à rendre compte de ces observations. A titre d'exemples, les modèles de Sander et al. (1997) et Michalowski et al. (2000) ne parviennent pas à reproduire correctement la destruction de l'ozone troposphérique et conduisent à des concentrations en aldéhydes beaucoup plus basses que celles mesurées (De Serves, 1994 ; Sumner et Shepson, 1999) lors de campagnes de terrain. L'étude des processus ayant lieu dans le manteau neigeux est donc nécessaire et doit être prise en compte dans les modèles de chimie atmosphérique.

La chimie atmosphérique actuelle n'est pas le seul domaine où les interactions air-neige ont un intérêt. Dans les régions polaires où la neige s'accumule depuis des milliers d'années et se transforme en calottes polaires ou glaciers, l'analyse de carottes de glace permet de fournir des informations sur la composition passée de l'atmosphère. Cependant, la relation reliant la concentration d'un gaz trace dans la glace à sa concentration dans l'air, appelée fonction de transfert '' air-neige'' (Jaffrezo et al., 1994 ; Dominé et al., 1995) est très complexe. Ainsi, la reconstitution détaillée de la composition des atmosphères passées requiert une connaissance des processus qui donnent à la neige sa composition. De plus, dans le cadre du réchauffement global, comprendre l'effet de la neige est aussi nécessaire pour évaluer l'impact atmosphérique de la diminution de la couverture neigeuse.

Tous ces exemples nous montrent clairement l'importance des échanges et interactions entre le manteau neigeux et l'atmosphère ainsi que les difficultés rencontrées par les modèles de chimie atmosphérique. On voit donc la nécessité d'être capable de quantifier les processus ayant lieu dans le manteau neigeux pour comprendre et modéliser la chimie de la troposphère au-dessus des régions enneigées, mais aussi pour mieux interpréter la quantité d'informations extraites des carottes de glace.

DES PROCESSUS PHYSICO-CHIMIQUES DANS LE MANTEAU NEIGEUX

Le manteau neigeux comprend un solide divisé, la neige et de l'air interstitiel. Il est donc très probable que l'impact chimique du manteau neigeux soit la résultante de processus physiques et chimiques. Etant dans un état thermodynamiquement instable, le manteau neigeux est en perpétuelle évolution. Ceci se manifeste par de nombreux processus physiques très actifs regroupés sous le terme de 'métamorphisme du manteau neigeux' (Seligman, 1936 ; de Quervain, 1958, 1963). Le métamorphisme fait intervenir des cycles de sublimation-condensation de la neige qui génèrent d'importants flux de vapeur d'eau. Ceux-ci peuvent résulter de gradients de rayon de courbure à l'échelle des cristaux qui génèrent des gradients de vapeur d'eau en vertu de la loi de Kelvin, et de la présence d'un gradient thermique à l'intérieur du manteau neigeux. Il est clair que ces flux peuvent entraîner les solutés contenus dans la neige et le métamorphisme peut donc modifier la composition chimique de la neige et de l'air interstitiel.

D'autres processus que les flux de vapeur d'eau peuvent entraîner des modifications chimiques dans le manteau neigeux. Il peut s'agir (i) de l'adsorption/désorption de gaz traces à la surface des cristaux de neige, (ii) de la diffusion d'espèces chimiques dans le volume de la glace, ou (iii) de réactions hétérogènes ayant lieu à la surface de la glace. La compréhension et la quantification de ces processus complexes requièrent la connaissance de divers paramètres physiques dont la **surface spécifique de la neige**, définie comme la surface totale développée par un cristal par unité de masse, et exprimée en m^2/g. On peut également la définir comme la surface totale de neige accessible aux gaz, par unité de masse. Les exemples suivants illustrent l'implication de la surface spécifique pour les trois processus décrits précédemment.

Dans la neige, certains hydrocarbures chlorés comme le paradichlorobenzène et le p,p'-DDT sont localisés majoritairement à la surface de la glace (Wania, 1997) de telle sorte que leur concentration est directement proportionnelle à la surface spécifique de la neige, et à leur pression partielle dans l'air interstitiel. A la suite d'un réchauffement, une fraction de ces espèces chimiques peut être relarguée dans l'atmosphère, modifiant ainsi sa composition et celle de la neige. La quantification de tels échanges fait intervenir des termes de surface et nécessite donc la connaissance de la surface spécifique de la neige.

Supposons maintenant qu'un gaz comme HCl ou HNO_3 dissout dans la glace soit en déséquilibre thermodynamique avec sa concentration atmosphérique (Dominé et Thibert, 1996). Le rééquilibrage se fera par diffusion en phase solide dont une étape est le franchissement de l'interface gaz-glace. Le flux de gaz à travers cette interface sera proportionnel à la surface d'échange, et le calcul de la vitesse de rééquilibrage nécessite également de connaître la surface spécifique.

Dans le cas d'une réaction hétérogène ayant lieu à la surface des cristaux de neige, de type

$$A_{(surface)} + B \rightarrow AB_{(gaz)} \qquad (I.8)$$

la vitesse de formation de l'espèce chimique AB va être proportionnelle à la concentration totale (molec/cm^3) de l'espèce chimique A localisée à la surface de la glace. Celle-ci est égale à sa concentration de surface (molec/cm^2) multipliée par la surface totale de glace (cm^2/cm^3). Sa

quantification fait donc encore une fois intervenir la surface spécifique de la neige, qui est donc un paramètre crucial dans la quantification des interactions air-neige.

De plus, à cause des processus physiques du métamorphisme qui modifient la structure des cristaux, la surface spécifique évolue. Sa valeur et son évolution sont étroitement liées aux autres paramètres physiques de la neige que sont la taille des grains, leur forme et la densité de la neige, ce qui en fait de plus paramètre important de la microphysique du manteau neigeux.

Malgré son importance pour la chimie de l'atmosphère des zones enneigées et pour la physique du manteau neigeux, l'étude de cette SS a suscité peu d'intérêt puisque seules des mesures isolées, dont la validité est d'ailleurs discutable, ont été effectuées avant 1998. Ce manque de données nous a donc incités à effectuer ce travail consacré à l'étude de la SS de la neige et à son évolution dans le manteau neigeux.

DEMARCHE ADOPTEE

La SS de la neige est donc un thème nouveau puisque comme nous l'avons dit précédemment peu de données existent dans la littérature. Ce sujet a été initié au laboratoire par (i) des premières mesures effectuées en 1995 (Rey, 1995) et 1996 (Chaix et al., 1996) sur des échantillons prélevés près de Grenoble au col de Porte et à Chamrousse, et à proximité du laboratoire, (ii) puis par une étude portant sur l'évolution de la SS d'une couche de neige en Janvier 1998 (Hanot et Dominé, 1999). Ces premiers résultats ont mis en évidence la capacité de la neige à pouvoir stocker une grande quantité de gaz et ont montré l'importance de faire une étude plus approfondie sur ce paramètre clé de la microphysique de la neige.

L'objectif de cette étude est donc de fournir des données de la SS qui servent dans la quantification du rôle de la neige sur la chimie atmosphérique. Pour cela, trois points essentiels sont visés. Il s'agit : (i) de corréler la SS avec ses caractéristiques physiques macroscopiques, (ii) d'étudier l'évolution de la SS de la neige fraîche, (iii) de comprendre la relation entre le métamorphisme de la neige et l'évolution de la SS ceci à l'aide d'images de cristaux obtenues par macrophotographies ou microscopie électronique à balayage (MEB). La prédiction, par la modélisation, de l'évolution de la surface spécifique peut être considérée comme l'objectif ultime de cette thématique. Ce travail s'inscrit comme une première étape vers cet objectif, et comprend un important travail d'observation et un début de compréhension des phénomènes déterminant la surface spécifique et son évolution.

La première partie de cette étude a consisté à mettre au point une méthode de mesure fiable et sensible de la surface spécifique de la neige. Le problème est délicat, car la SS de la neige est faible comparée à celle de la glace synthétisée à basse température en laboratoire, et ne dépasse pas 0.15 m^2/g. C'est la méthode d'adsorption de méthane à la température de l'azote liquide (77K) qui a été utilisée. La neige ayant en général une faible SS comparée à d'autres matériaux, le choix d'une unité en cm^2/g a été préféré au m^2/g.

Ensuite des études de la SS de la neige et son évolution ont pu être effectuées dans les Alpes et l'Arctique. Dans les Alpes, la plupart des études ont été effectuées au col de Porte (12 km de Grenoble) où nous avons pu bénéficier des enregistrements météorologiques fournis par le Centre d'Etude de la Neige (CEN, Météo France), ces données étant utiles dans l'interprétation de l'évolution de la SS. Dans l'Arctique, nous avons participé en Février et Avril 2000 à la campagne de terrain ALERT 2000 à Alert (82°30'N, 62°20'W, Nunavut, Canada) dont le but était d'étudier l'impact du manteau neigeux sur la chimie de la basse troposphère et la destruction de l'ozone au niveau du sol. De nombreuses mesures de la SS ont pu être effectuées avec succès lors de cette campagne. Lors d'une seconde campagne, NICE, menée dans l'archipel du Svalbard près de Ny-Alesund (79°N, 12°E) en Avril 2001, de nouvelles données ont pu être obtenues. Afin de comprendre l'évolution de la SS de la neige, nous avons étudié les changements morphologiques des cristaux de neige par macrophotographies et par microscopie électronique à balayage (MEB). L'ensemble de toutes nos données nous a permis de présenter une compilation des valeurs de SS qui ont pu être regroupées en 14 catégories en fonction du type de neige et de son âge. De plus, à partir des différentes couches de neige étudiées, nous avons proposé de faire une paramétrisation préliminaire de la vitesse de l'évolution de la SS de la neige fraîche avec le temps.

PLAN DU MANUSCRIT

Le travail effectué durant cette étude s'est inscrit dans un travail d'équipe qui consistait à étudier de manière couplée la physique et la chimie de la neige. Il a permis notamment la mise au point d'une méthode fiable et précise de mesure de la SS, qui a motivé notre participation aux campagnes de terrain dans l'Arctique. Durant les campagnes ALERT 2000 et NICE, le partage du travail consistait à échantillonner la neige, mesurer sa SS, photographier les cristaux échantillonnés, et étudier la chimie de la neige. La réussite de ce travail d'équipe a déjà débouché sur des applications atmosphériques au sein de notre équipe lors de la campagne ALERT 2000 (Perrier et al., sous presse ; Houdier et al., sous presse).

L'aspect novateur de la mesure de la SS de neige a conduit à la rédaction de plusieurs articles publiés, sous presse, ou soumis. Ceci a donc orienté notre choix pour présenter les résultats de cette thèse sous forme de 'thèse-articles'. Ce travail ayant pour objet la microphysique du manteau neigeux, une première partie (**chapitre II**) est consacrée à une étude bibliographique sur la neige et sa surface spécifique: Après avoir présenté la structure de la glace, nous expliquons comment se forme la neige dans les nuages et comment elle évolue dans le manteau neigeux. Puis, nous présentons le principe du modèle d'adsorption BET que nous avons utilisé pour les mesures de surface spécifique. Un dernier paragraphe reprend les différents travaux déjà effectués sur l'étude de la surface spécifique de la neige.

Le **chapitre III** est consacré aux résultats et à leur discussion. Six articles y sont regroupés. Une introduction à ce chapitre présente le contenu de ces différents articles ainsi que les objectifs

auxquels ils tentent de répondre. Nous orientons aussi le lecteur dans la ‘découverte’ de ce mémoire afin de limiter les redondances notamment lors de la description des sites, ou de la méthode expérimentale utilisée. L’ordre de présentation des différents articles a été choisi dans le but de suivre le mieux possible les différentes étapes de notre travail résumées ci-dessus. Afin de pouvoir se référencer facilement à ces articles, nous les avons numérotés de 1 à 6. Nous terminons par une application atmosphérique où nos résultats ont été utilisés pour interpréter l’évolution du formaldéhyde dans la neige de l’Arctique (Perrier et al., sous presse).

CHAPITRE II

ETUDE BIBLIOGRAPHIQUE

Ce chapitre rappelle la structure de la glace, les mécanismes de formation des cristaux de neige dans les nuages ainsi que l'évolution de leur forme et leur taille dans le manteau neigeux. Puis, le principe du modèle d'adsorption BET utilisé pour les mesures de surface est présenté. Enfin, les différents travaux déjà effectués sur l'étude de la surface spécifique de la neige sont brièvement décrits.

II.1. Structure de la glace.

Nous faisons dans cette section une présentation sur la structure de la glace hexagonale qui compose les cristaux de neige formés dans la troposphère. Nous nous sommes inspirés des travaux de Hobbs (1974), Schmitt (1986), Chaix (1997), et Rey-Hanot (1999) qui proposent une littérature plus détaillée sur la structure de la glace.

II.1.1. Différentes structures cristallines.

La molécule d'eau faite de deux atomes d'hydrogène et d'un atome d'oxygène possède une géométrie non linéaire et un moment dipolaire qui lui permettent de créer en phase condensée, des liaisons hydrogènes avec 4 molécules voisines selon une structure tétraédrique (fig. **II.1.1**). Cette structure se retrouve dans la glace dont elle constitue le motif de base.

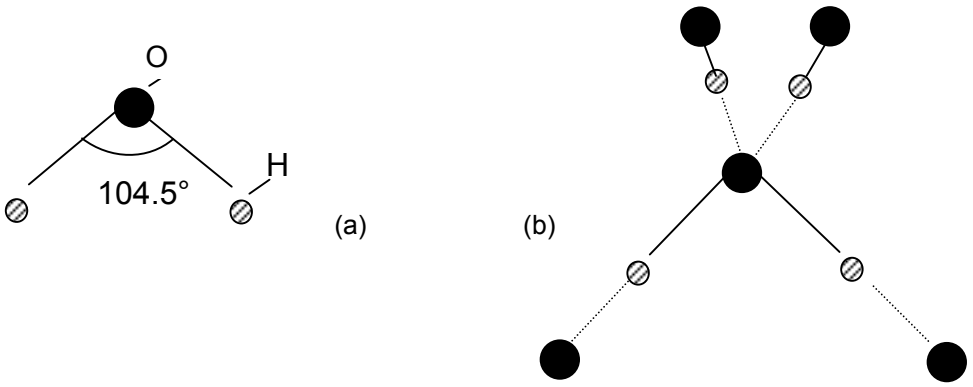

Figure II.1.1: Géométrie de la molécule d'eau. (a) Molécule d'eau isolée en phase gazeuse. (b) Liaisons hydrogènes possibles avec la molécule d'eau en phase condensée.
— liaison de valence, □ □ liaison hydrogène, ● oxygène, ▨ hydrogène.

La glace est connue sous dix formes cristallines différentes et au moins deux formes amorphes. Cependant, la plupart de ces structures ne sont stables que sous très forte pression (> 1 ou 2 kbar) ou à très basse température. Sous pression atmosphérique, seules deux formes cristallines, cubique I_c et hexagonale I_h peuvent exister. La glace cubique est une forme métastable sous des conditions atmosphériques. Cette forme n'a été observée que expérimentalement et peut être obtenue par condensation de vapeur d'eau entre 135 K à 195 K environ (Honjo et al., 1956). Ainsi dans les nuages de la troposphère, aux températures comprises entre -60 et 0°C, la glace cristallise sous sa forme hexagonale I_h (Pruppacher et Klett, 1978).

II.1.2. Structure de la glace hexagonale I_h.

De nombreuses études de la structure en volume de la glace I_h ont été réalisées afin de définir l'arrangement géométrique des atomes d'oxygène (Rinne, 1917 ; Dennison, 1921 ; Bragg, 1922). Chaque atome d'oxygène est entouré de 4 autres atomes d'oxygène selon une coordinence tétraédrique qui confère au réseau de la glace une symétrie hexagonale. Dans cette structure, les molécules sont toutes rassemblées près de plans parallèles, appelés plans de base. La normale aux plans de base est appelé l'axe c, qui est l'axe de symétrie d'ordre le plus élevé. L'arrangement des atomes d'oxygène dans la structure hexagonale est représenté sur la figure **II.1.2**.

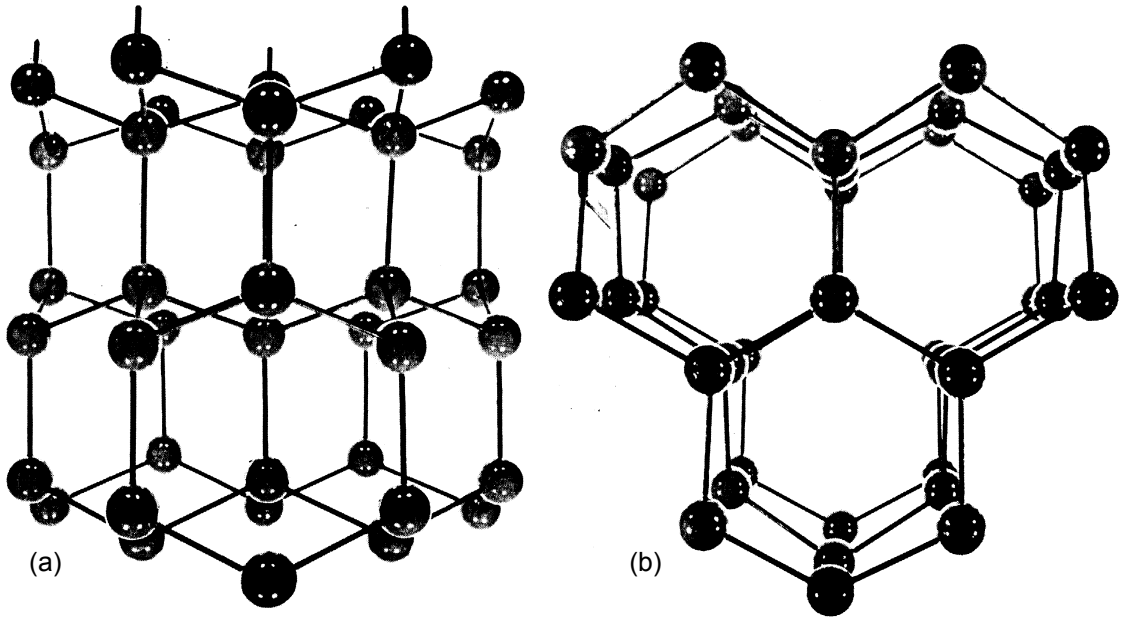

Figure II.1.2: Atomes d'oxygène dans la glace I_h. (a) Vue perpendiculaire à l'axe c. (b) Vue parallèle à l'axe c.

La figure **II.1.3a** représente la maille hexagonale de la glace I_h. Chaque atome d'oxygène disposé sur les huit coins (OPMNQRST) est partagé par 8 mailles adjacentes, chaque atome sur les arêtes de la maille (UVWX) est partagé par 4 mailles, les deux atomes restants (YZ) sont à l'intérieur de la maille. Par conséquent, le nombre total d'atomes d'oxygène (et donc de molécules H_2O) dans la maille est de 4. La figure **II.1.3b** représente le réseau primitif avec les paramètres de maille a_0 et c_0. Ces paramètres de maille varient très peu avec la température, entre 0 et –180°C (La Placa et Post, 1960) et leurs valeurs moyennes, dans ce domaine de température, sont:

a_0 = 4.50 Å

c_0 = 7.34 Å

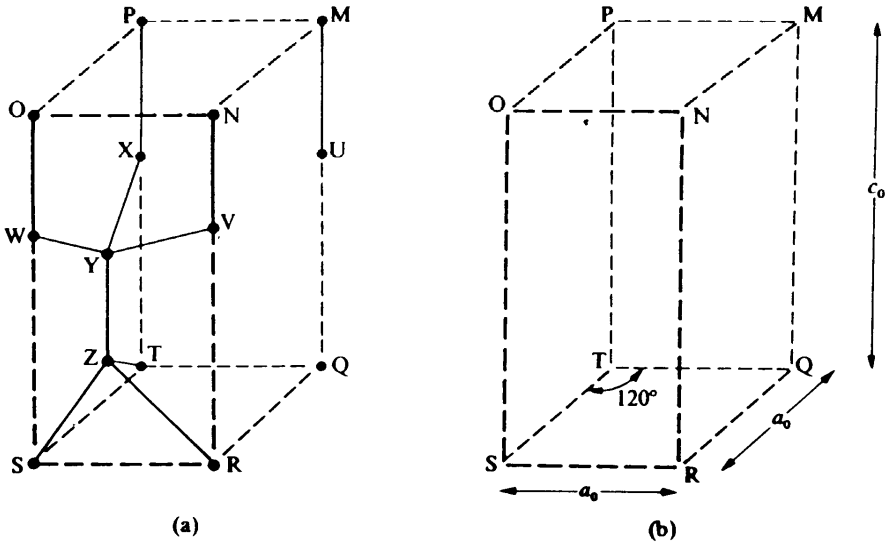

Figure II.1.3: (a) Maille élémentaire de la glace I_h, (b) Réseau primitif de la glace I_h.

Le rapport c_0/a_0 d'une valeur de 1.631 ne varie pas avec la température. Il est très voisin de la valeur $2\times\sqrt{2/3}$ = 1.633 ce qui permet de considérer que la coordination tétraédrique est parfaite et l'empilement moléculaire compact. La distance la plus courte entre deux atomes d'oxygène est de 2.76 Å.

Les atomes d'hydrogène ne sont pas situés à égale distance des deux oxygènes. Bernal et Fowler (1933) suggérèrent qu'ils soient situés à 1 et 1.76 Å des deux atomes d'oxygène les environnant. L'arrangement dans le cristal complet est tel que chaque atome d'oxygène a deux atomes d'hydrogène à environ 1 Å de lui. L'angle entre deux liaisons covalentes est de 109° contre 104°5 dans la phase vapeur et les différents éléments de symétrie de la glace I_h sont ceux du groupe d'espace $P6_3/mmc$ (Barnes, 1929).

Pauling (1935), considérant les propriétés diélectriques de la glace I_h étudiées par Debye (1929), indiqua que les atomes d'hydrogène pouvaient prendre n'importe quel arrangement proposé par Bernal et Fowler (fig. **II.1.4)**.

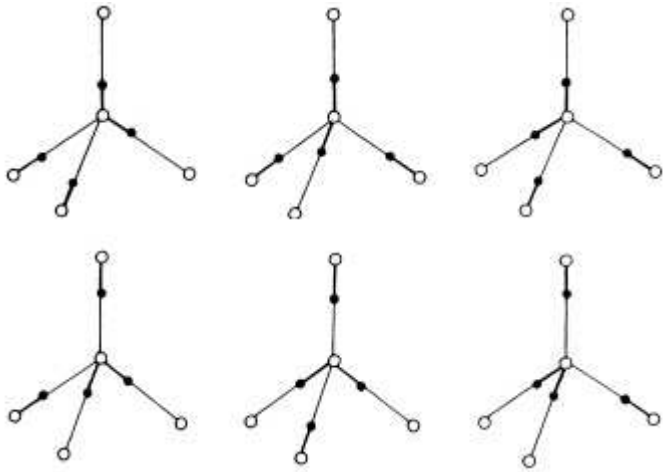

Figure II.1.4 : Les six arrangements possibles des atomes d'hydrogène sur les quatre liaisons autour de chaque oxygène dans la glace I_h (d'après Hobbs, 1974). o: oxygène, ●: hydrogène

Il proposa alors un modèle statistique plus précis pour la glace I_h, basé sur les règles suivantes:

(i) Chaque atome d'oxygène est lié de façon covalente à deux atomes d'hydrogène, chacun à une distance d'environ 0.95 Å, formant ainsi une molécule d'eau. Il est également lié par liaisons hydrogène à deux autres H, à des distances de 1.8 Å.
(ii) Chaque molécule d'eau est orientée de telle façon que ses deux hydrogènes soient dirigés approximativement vers deux des quatre oxygènes qui l'entourent tétraédriquement.
(iii) L'orientation des molécules d'eau adjacentes est telle qu'il existe un seul hydrogène entre les deux oxygènes.
(iv) Sous des conditions ordinaires, la glace I_h peut exister dans n'importe quelle configuration, chacune de celle-ci correspondant à une certaine distribution des atomes d'hydrogène par rapport aux atomes d'oxygène.
Les règles énoncées ci-dessus sont appelées "règles de Bernal-Fowler".

II.1.3. Défauts de la structure cristalline I_h

Les cristaux parfaits formés pas la répétition périodique d'une maille élémentaire, se rencontrent très rarement. Un cristal de glace réel comporte un ensemble de défauts dans son volume qui peuvent affecter certaines propriétés du solide, voir même de la surface car certains défauts peuvent y émerger.

II.1.3.1 Défauts ponctuels.

Le terme "ponctuel" signifie que les défauts sont situés en des points spécifiques du cristal. Leur extension spatiale se limite à une ou deux mailles élémentaires, bien que la déformation élastique produite par ces défauts puisse se propager sur de plus grandes distances. Il existe plusieurs types de défauts ponctuels : moléculaires, ioniques et les défauts de Bjerrum.

Les défauts moléculaires de la glace peuvent se caractériser par une lacune, c'est à dire l'absence d'une molécule d'eau dans le réseau cristallin, ou par la présence d'une molécule supplémentaire située en position interstitielle. Ces défauts peuvent se créer par paire, en déplaçant une molécule d'eau de son site normal à une position interstitielle, mais ils peuvent se former indépendamment. Les molécules d'eau peuvent diffuser dans le réseau de la glace par ces sites vacants ou interstitiels : ce mécanisme est appelé "auto-diffusion". Des observations par topographie de rayons X (Hondoh et al., 1987) ont révélé que le défaut ponctuel majoritaire dans la glace à T > -50°C est le site interstitiel et que l'auto-diffusion des molécules d'eau dans la glace est due à la migration de ces défauts à travers le réseau.

Le désordre des atomes d'hydrogène dans le réseau de la glace hexagonale, et plus particulièrement la violation des règles de Bernal-Fowler, sont responsables de la formation d'autres types de défauts ponctuels : les défauts de Bjerrum (Bjerrum, 1951) et les défauts ioniques. La violation de ces lois conduit à la création de quatre types de défauts décrits sur la figure **II.1.5.**

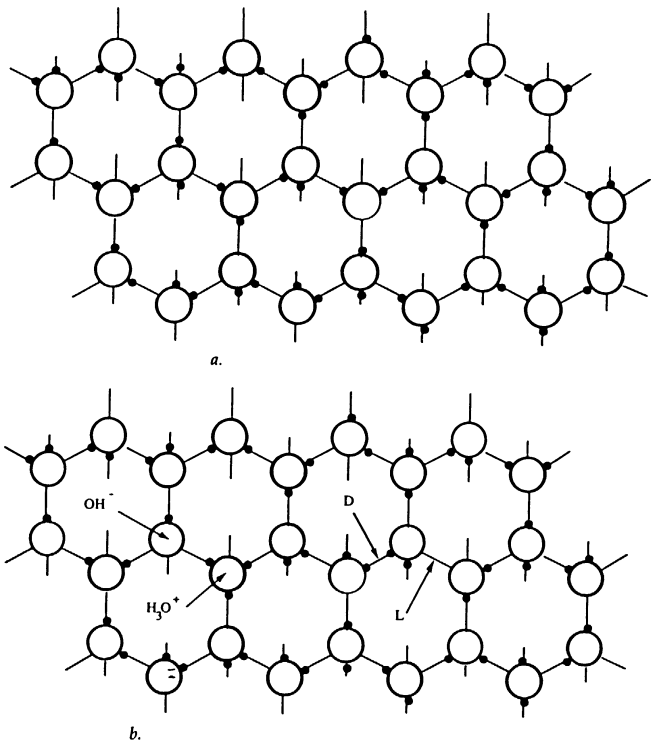

Figure II.1.5 : Structures de la glace I_h. (a) Structure parfaite. (b) Structure avec des ions H_3O^+ et OH^-, ainsi que des défauts de Bjerrum L et D.

Les ions H_3O^+ et OH^- sont formés par glissement d'un proton le long d'une liaison hydrogène, par effet tunnel. La rotation d'une molécule d'eau peut former simultanément un défaut de Bjerrum de type L (liaison non occupée par un H) et un de type D (liaison occupée par deux H). Contrairement au cas précédent, la molécule d'eau n'est pas ionisée et garde son entité moléculaire. Cependant, comme les atomes d'hydrogène dans la molécule d'eau ont une charge électrique positive, il s'ensuit qu'un défaut D est chargé positivement et un défaut L négativement. La charge électrique de ces défauts est faible : un ion H_3O^+ a une charge électrique environ deux fois plus forte qu'un défaut D (Zaretskii et al., 1988). Ces défauts protoniques, une fois formés, peuvent migrer le long du réseau de liaisons hydrogène par sauts de protons.

L'introduction de ces défauts change considérablement les forces existantes entre atomes adjacents, ce qui conduit à la relaxation du réseau autour du défaut et donc à un réarrangement des atomes. La maille du réseau peut alors être déformée car les distances entre atomes ont changé : par exemple, dans un défaut L, la distance O-O est de 3.17 Å au lieu de 2.76 Å dans la structure parfaite (Plummer, 1992).

Les défauts ponctuels de la glace jouent un rôle fondamental dans beaucoup de processus physiques tels que la diffusion (défauts moléculaires), la conductivité électrique (défauts protoniques), l'absorption optique, etc La majorité des défauts ponctuels dans la glace ont une grande mobilité, à des températures supérieures à 100 K.

II.1.3.2. Les dislocations

Les dislocations sont des lignes de défauts dans un cristal: elles sont produites par le glissement d'un plan d'atomes par rapport à un autre, comme sur l'exemple représenté sur la figure **II.1.6**. Dans l'étape intermédiaire présentée sur cette figure, la ligne BC est la limite entre la région qui a glissé ABC et le reste du plan de glissement. Cette ligne BC est une ligne de dislocation ou plus simplement une dislocation. Le vecteur de translation $\vec{b}$ définissant le glissement du plan d'atomes ABC est appelé vecteur de Burgers.

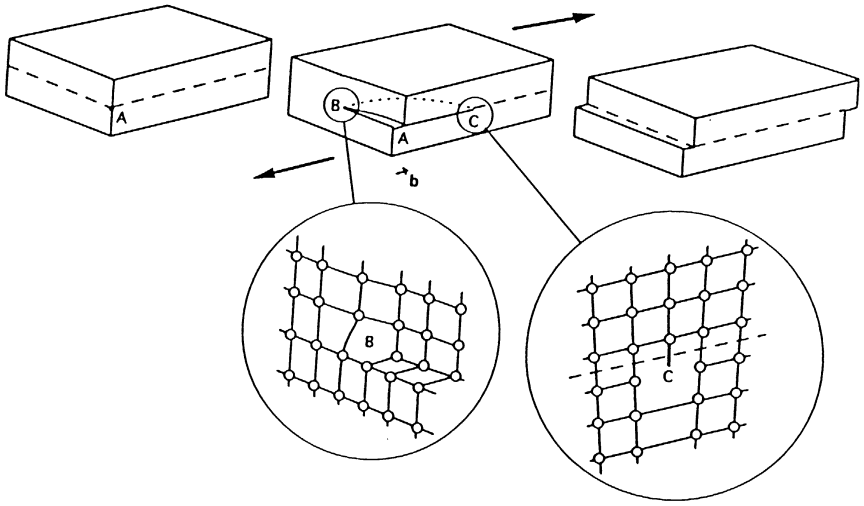

Figure II.1.6: Formation d'une ligne de dislocation BC par glissement d'un plan dans une structure cristalline. La direction et l'amplitude du glissement sont données par le vecteur de Burgers $\vec{b}$ (Petrenko et Whithworth, 1999).

Les agrandissements de la figure **II.1.6** montrent l'arrangement des atomes autour de la dislocation "vis" au point B (dislocation parallèle au vecteur b) et de la dislocation "coin" au point C (dislocation perpendiculaire au vecteur b). En général, une ligne de dislocation possède ces deux composantes. La présence d'une dislocation implique une distorsion élastique de tout le cristal mais celle-ci est plus importante le long de la ligne BC. Lorsqu'une dislocation se déplace le long d'un plan de glissement, les atomes au-dessus de ce plan vont être déplacés d'une distance égale au vecteur de Burgers.

Les dislocations peuvent être incorporées au cristal de glace pendant sa croissance, affectant ainsi la structure de tout le réseau. Par exemple, si une dislocation vis est présente à la surface d'un cristal, celui-ci peut croître en spirale à partir de l'axe de la discontinuité (fig. **II.1.7**).

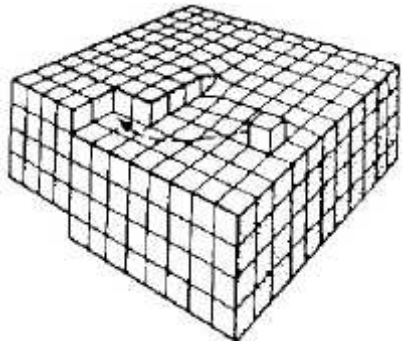

Figure II.1.7: Dislocation vis à la surface d'un cristal, celle-ci va initier la formation d'une spirale de croissance (Pruppacher et Klett, 1978).

La plupart des dislocations dans la glace se situent dans son plan de base (0001) car il se déforme plus facilement (Glen et Perutz, 1954) et les glissements d'autres plans sont beaucoup plus difficiles.

II.1.3.3. Les sous-joints.

A l'intérieur d'un grain ou d'un morceau de glace ne contenant qu'un seul cristal, il existe souvent des sous-joints, à travers lesquels il y a une désorientation du réseau d'une fraction de degré (angle θ). Ces sous-joints sont constitués d'un regroupement de dislocations représenté sur la figure **II.1.8**, espacées d'une distance D = b/θ, où b est l'amplitude du vecteur de Burgers de ces dislocations. Ils peuvent migrer par le glissement de ces dislocations, sous une contrainte mécanique orientée, ceci a été observé dans la glace par Higashi et Sakai (1961).

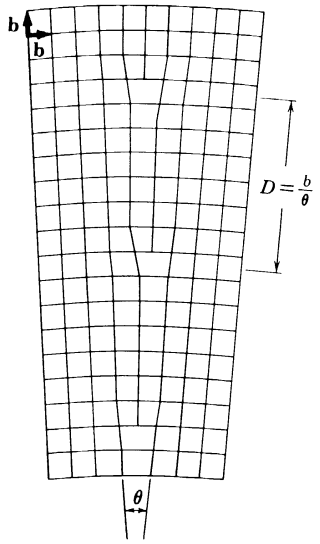

Figure II.1.8: Représentation d'un sous-joint constitué de dislocations régulièrement espacées d'une distance D = b/θ, où b est le module du vecteur de Burgers de ces dislocations et θ la désorientation créée par le sous-joint.

II.1.3.4. Les joints de grains

Il s'agit de défauts de structure propres aux glaces polycristallines : Les joints entre les cristaux individuels (ou "grains") peuvent être considérés comme des défauts plans appelés joints de grain. Ils sont formés de plusieurs formes, tailles et orientations, dépendantes de l'histoire thermique et mécanique de l'échantillon. Pour un cristal recuit, l'énergie de surface est minimisée et les joints sont approximativement plats. Ils peuvent agir comme des sources ou puits de défauts ponctuels et de dislocations, et les impuretés présentes dans la glace ont tendance à s'y concentrer : de fortes concentrations de SO_4^{2-} ont été mesurées aux intersections des joints de grains de la glace d'Antarctique (Mulvaney et al., 1988). Dans le manteau neigeux, des joints de grains sont bien visibles entre deux cristaux agglomérés par frittage ou par des cycles de fusion-regel comme nous le verrons dans le paragraphe **II.3.3.2**.

Il existe donc un grand nombre de défauts dans le réseau de la glace qui peuvent être fonction des conditions de formation ainsi que de l'histoire thermique et mécanique de la glace. Ces défauts vont avoir un rôle pour comprendre le mécanisme de croissance des cristaux de neige dans les nuages, ainsi que le mécanisme d'évolution dans le manteau neigeux, le névé et la glace.

II.1.3. La surface de la glace.

II.1.3.1. Hétérogénéité de la surface de la glace

Cette interface est très importante puisque c'est la partie du cristal de glace où les gaz peuvent venir s'adsorber. La surface de la glace peut présenter une importante hétérogénéité qui va influencer les propriétés d'adsorption des gaz. A l'échelle moléculaire, cette hétérogénéité peut se caractériser par exemple par la présence de marches, ou la présence de pores dont la taille peut varier de 20 à 1000 Å. A l'échelle macroscopique, d'autres défauts tels que des creux ou des cavités sont parfois présents sur les faces cristallographiques.

La surface développée par les cristaux de neige va dépendre de cet état de surface ainsi que de la taille et la forme des cristaux. La porosité apparaît pour des glaces condensées à partir de vapeur d'eau mais nécessite des températures inférieures à 200 K pour être vraiment importante. Comme les cristaux de neige se forment dans les nuages à des températures généralement plus élevées, la présence de pores n'est donc pas envisageable à leur surface.

II.1.3.2. Désordre de la couche de surface à haute température

De nombreuses mesures directes ou indirectes, par différentes techniques, effectuées aux températures proches du point de fusion ont montré des propriétés particulières de la surface de la glace, ce qui a amené à postuler l'existence d'une ''couche quasi-liquide''. Cette couche très désordonnée dont la structure exacte n'est pas encore très bien connue (Petrenko et Withworth, 1999), doit son nom à ses propriétés intermédiaires entre celles de l'eau et celles de la glace.

Selon les techniques utilisées pour l'étudier, ses propriétés sont soit plus proches de celles de l'eau soit plus proches de celles de la glace. La plupart des expériences réalisées montrent l'existence de cette couche au-dessus de -30°C mais cette valeur limite dépend également de la technique utilisée. De plus, des mesures par ellipsométrie (Beaglehole et Nason, 1980) indiquent que son épaisseur qui augmente avec la température, n'est pas la même sur les plans de base que sur les faces prismatiques de la glace.

La couche quasi-liquide est principalement caractérisée par :
- Une grande amplitude de rotation des molécules H_2O proche de l'eau liquide. Celle-ci a été détectée par des mesures RMN (Mizuno et Hanafusa, 1987).
- Une grande amplitude de vibration thermique des atomes d'oxygène, mesurée par canalisation protonique (Golecki et Jaccard, 1977).
- Une densité proche de celle de l'eau, mesurée par ellipsométrie (Furukawa et al., 1987).
- Une importante concentration en défauts ioniques et de Bjerrum, qui a pu être révélée par la mesure de la conductivité électrique (Petrenko et Withworth, 1999). Cela peut correspondre à un état de surface où toutes les molécules sont polarisées et mobiles.
- Une orientation des protons vers l'extérieur pour une grande partie des molécules d'eau, ce qui induit une polarisation positive de la surface. Cette caractéristique a été déterminée par une étude théorique (Fletcher, 1968).

Récemment, Girardet et Toubin (2001) ont effectué des simulations de dynamique moléculaire afin de déterminer la structure et les propriétés dynamiques d'un film de glace. Le film de glace étudié consiste en 6 bicouches de glace 'mobiles' fixées sur 2 bicouches de glace 'fixes'. La figure **II.1.9** illustre les résultats obtenus à 190, 235 et 270 K. Elle montre le désordre de la couche de surface qui apparaît à 235 K, puis qui se propage sur plusieurs bi-couches à 270 K en supprimant totalement l'ordre cristallin.

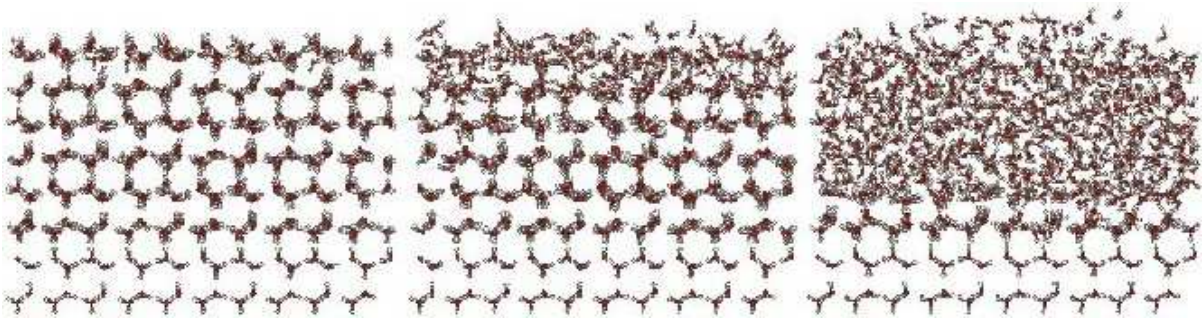

190 K 235 K 270 K

Figure II.1.9: Simulation d'un film de glace constitué de 6 bicouches déposées sur 2 bicouches de glace fixes à températures variables (Girardet et Toubin, 2001).

L'étude d'adsorption d'alcanes sur la glace à différentes températures (Orem et Adamson, 1969) a montré une nette transition vers 238 K des paramètres thermodynamiques d'adsorption : chaleur isostérique q^{st} et entropie différentielle ΔS. Ainsi, au-dessus de 238 K, la glace et l'eau présentent des similitudes dans leur interaction avec le n-hexane. Ceci indique que la capacité et la thermodynamique d'adsorption des gaz à la surface de la glace va être fortement affectée par l'existence de cette couche quasi-liquide. Cependant, une grande incertitude règne sur les propriétés de cette couche, et un comportement de la glace similaire à l'eau comme adsorbant dépend aussi du gaz avec lequel elle interagit et cette similitude n'est pas toujours évidente. A titre d'exemple, Nelson et Knight (1998) ont récemment montré par mesures de sursaturation au-dessus de cristaux de glace, la présence d'une couche désordonnée mais pas celle d'une surface surfondue, et ceci jusqu'à -1°C.

L'adsorption des gaz peut donc dépendre de l'hétérogénéité de surface à l'échelle microscopique et macroscopique, mais aussi du désordre moléculaire de surface qui va affecter leur propriétés d'adsorption.

II.2. Formation de la neige et des cristaux de glace qui la constituent

Nous avons vu que les cristaux de glace qui forment la neige appartiennent à la structure hexagonale I_h. Ces cristaux naissent dans les nuages où les températures rencontrées peuvent être très différentes. Nous allons voir comment se forment ces cristaux et pourquoi ils se présentent sous différents aspects.

II.2.1. Formation de la glace dans les nuages

II.2.1.1. Les nuages de la troposphère

La troposphère est la partie basse de l'atmosphère, qui s'étend du sol jusqu'à 10 à 15 km d'altitude suivant la latitude. Elle contient 85% de la masse atmosphérique totale, ainsi que tous les nuages influençant les conditions météorologiques quotidiennes. Différents types de nuages sont rencontrés en fonction de l'altitude.

Dans la haute troposphère, se trouvent les cirrus, les cirrostratus ainsi que des traînées de condensation d'avions issues de la vapeur d'eau rejetée par les moteurs. Ces nuages ont des températures comprises entre -40 et -60°C et sont constitués uniquement de glace. La quantité de vapeur d'eau qu'ils contiennent est faible et ils ne génèrent pas de précipitation.

A plus basse altitude, dans la moyenne et basse troposphère, les principaux nuages sont les stratus, strato-cumulus, nimbostratus, ainsi que les cumulus et les cumulonimbus qui sont des nuages à développement vertical pouvant atteindre la haute troposphère. Ces nuages ont des températures comprises entre -40 et +10°C et sont à l'origine de la majorité des précipitations que nous observons sous formes de neige, pluie, et grêle.

II.2.1.2. Nucléation de la glace et naissance des cristaux dans les nuages.

La glace dans les nuages peut se former par condensation de vapeur d'eau ou par congélation d'eau liquide. Cependant, ces changements de phase ne sont pas spontanées dans l'atmosphère et sont initiés par des aérosols : les noyaux de condensation initient la naissance des gouttelettes d'eau, et les noyaux glaçogènes sont à l'origine des cristaux de glace. Aux températures faiblement négatives (jusqu'à -20°C), les noyaux glaçogènes actifs formés par des aérosols ne sont pas assez nombreux pour permettre la condensation de toute la vapeur d'eau en excès. Celle-ci condense donc principalement sous forme de gouttelettes liquides dont le diamètre est compris entre 1 et 20 µm (Mason, 1957). Lorsque la température est suffisamment basse, en dessous de -20/-25°C voir -40°C, il y a rupture de surfusion d'un certain nombre de ces gouttelettes qui donnent naissance à de nouveaux noyaux de condensation solides.

Aux températures où les phases solide et liquide coexistent, on parle de nuages mixtes. Comme la pression de vapeur d'eau à l'équilibre au-dessus de la phase liquide est plus élevée qu'au-dessus de la phase solide, il se crée un gradient de vapeur d'eau entre une gouttelette d'eau et un cristal de glace, qui va entraîner l'évaporation des gouttelettes d'eau et la recondensation sur les noyaux

glaçogènes. Ce phénomène appelé effet Bergeron (Bergeron, 1935) va conduire à la croissance d'un cristal de glace, qui va durer jusqu'à la disparition des gouttelettes ou la précipitation des cristaux. Le cristal sera monocristallin s'il est issu d'un noyau glaçogène initié par un aérosol tandis que s'il est issu d'une gouttelette gelée, généralement polycristalline, il sera polycristallin et se développera dans différentes directions autour du noyau de condensation. Ce second type de cristal est important dans les nuages et peut constituer jusqu'à 48% des cristaux observés dans les nuages par une température de -15/-16°C (Auer, 1972).

II.2.2. Formes et mécanisme de croissance des cristaux

II.2.2.1 Observations de cristaux de neige fraîche

Bien que tous les cristaux de glace cristallisent dans la même structure hexagonale I_h, de nombreuses observations ont montré que les cristaux de neige fraîche peuvent se présenter sous une grande variété de formes, ce qui a conduit à plusieurs travaux de classification (Nakaya, 1954 ; Magano et Lee, 1966). A titre d'exemple, différents types de cristaux observés par microscopie optique et microscopie électronique à balayage (MEB) sont reportés respectivement sur les figures **II.2.1**. et **II.2.2**.

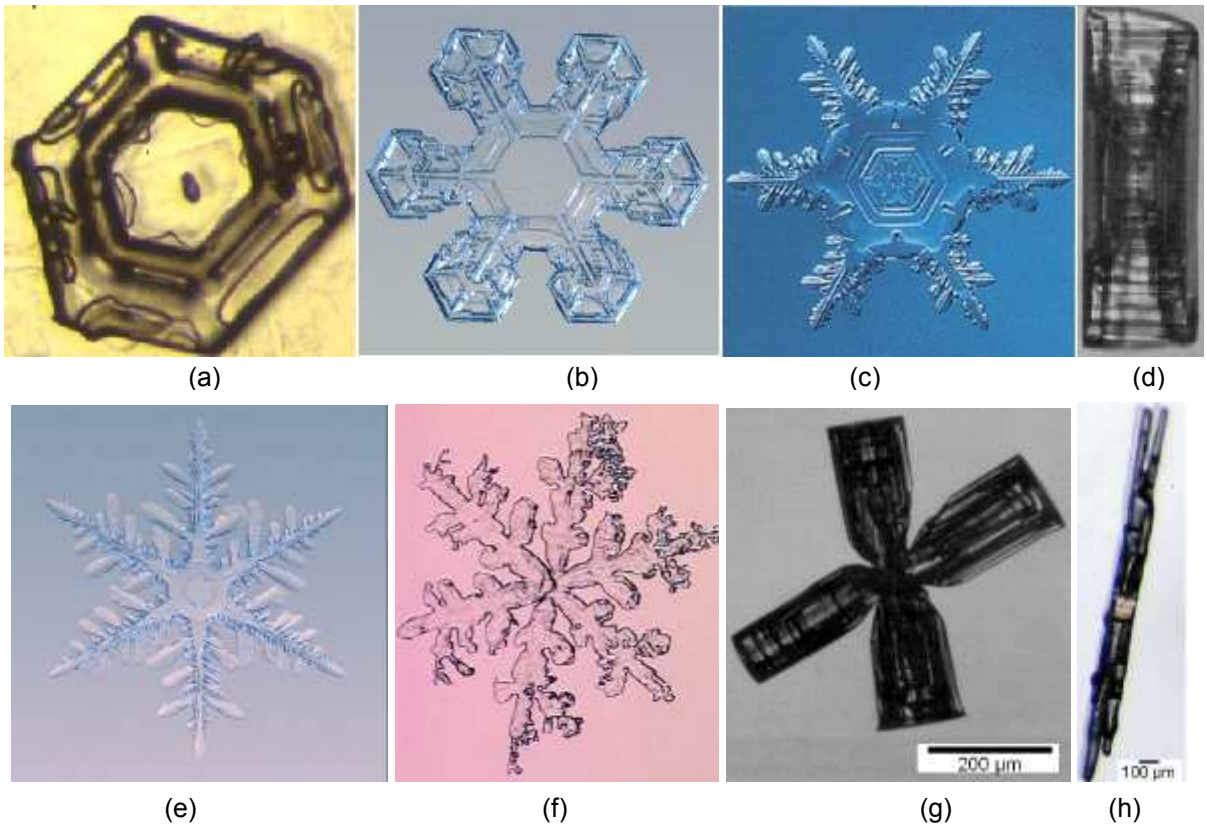

(a) (b) (c) (d)

(e) (f) (g) (h)

Figure II.2.1 : Observations au microscope optique de cristaux de neige prélevés lors de leur précipitation. (a) Plaquette. (b) Plaquette avec extension en étoile (Libbrecht, site web). (c) Plaquette avec extensions dendritiques (Furukawa, 1991). (d) Colonne creuse (Kobayashi et Kurado, 1987). (e) Cristal dendritique. (f) Cristal dendritique légèrement givré. (g) Cristal de 'Diamond Dust' : combinaison de 4 cristaux ayant crû à partir d'une gouttelette gelée polycristalline. (h) Aiguille.

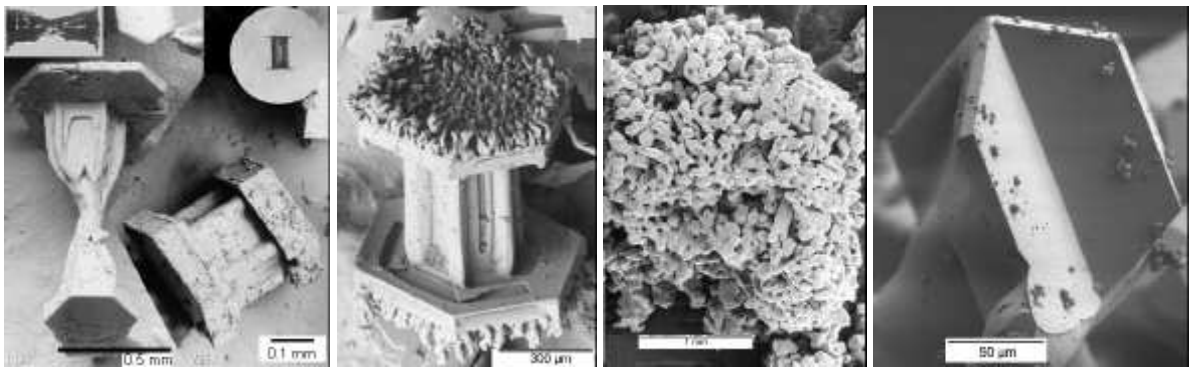

(a) (b) (c) (d)

Figure II.2.2 : Observations au microscope électronique à balayage (MEB) de cristaux de neige prélevés lors de leur précipitation. (a) Cristaux capés avec des plaquettes (Wergin et al., site web). (b) Bouton de manchette (colonne capée par des plaquettes) fortement givré (Wergin et al.). (c) Cristal de neige totalement recouvert par du givre (grésil). (d) Combinaison de plaquettes. Ici, la présence de givre est un artefact du à la condensation de vapeur d'eau atmosphérique lors du transfert dans le MEB.

Ces images suggèrent que la surface spécifique développée par les cristaux va fortement dépendre de leur forme. Il est clair qu'un cristal dendritique (fig. **II.2.1e**) présentant de nombreuses ramifications ou un cristal recouvert de nombreuses microstructures tel que le cristal de la figure **II.2.2b**, auront une surface spécifique plus élevée qu'une simple plaquette (fig**. II.2.1a**).

Les microstructures évoquées précédemment et présentes à la surface de certains cristaux (fig. **II.2.1.f** ; **II.2.2**, **b, c**) sont en fait des gouttelettes surfondues qui ont gelé lors de leur collision avec le cristal. Ce mécanisme est appelé givrage et sa part relative dans la masse totale d'un cristal est très variable : dans les régions polaires, où les températures sont très froides, on peut assister à des 'précipitations de ciel clair ': les cristaux qui les composent, appelés 'Diamond Dust' (fig**. II.2.1.g**), croissent totalement par condensation de vapeur d'eau. Par contre sous nos latitudes, par forte convection dans les nuages, le givrage peut être important et conduire à la formation de neige roulée ou grésil (fig**. II.2.2, c**). En fait, la quantité d'eau liquide sous forme de gouttelettes surfondues, diminue fortement par rupture de surfusion en dessous de -20°C (Pruppacher et Klett, 1978). Ceci explique que le givrage soit uniquement observé dans les nuages chauds que l'on rencontre généralement sous nos latitudes, et où la température est supérieure à –20°C.

Tous les cristaux présentés ici ont une morphologie différente, mais d'un point de vue cristallographique, ils ont tous la même forme de base: le prisme hexagonal avec deux plans de base (0001) et 6 faces prismatiques $(10\bar{1}0)$ (fig. **II.2.3**). D'autres faces existent mais se développent rarement. C'est les cas des faces de type $(10\bar{1}1)$ et $(10\bar{1}2)$ qui donnent des formes pyramidales. La figure **II.2.4** montre un cristal où ce type de face s'est développé.

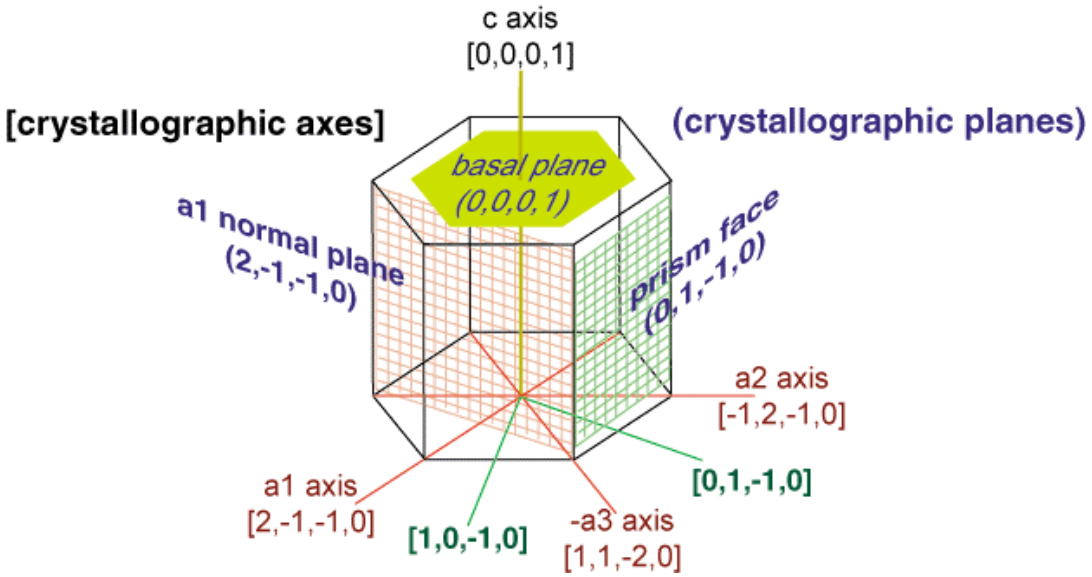

Figure II.2.3: Représentation schématique du motif de base d'un cristal de neige.

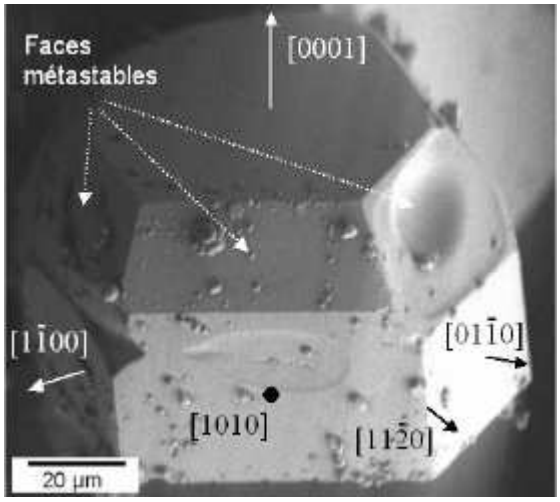

Figure II.2.4: Cristal de neige fraîche observé au MEB. Le plan de base hexagonal et les faces prismatiques sont clairement illustrés. Ce cristal est caractérisé par la présence de faces métastables qui peuvent être observées notamment dans les cristaux de 'Diamond Dust' (Itoo, 1957). La présence de givrage sur certaines faces est ici un artefact du à la condensation de vapeur d'eau atmosphérique lors du transfert dans le MEB.

II.2.2.2. Etude du rôle de la température et de la sursaturation

Afin de comprendre pourquoi les cristaux se présentent sous différentes formes, de nombreux travaux en laboratoire ont été entrepris.

Lamb et Hobb (1971) ont mesuré les vitesses de croissance linéaire du plan de base et du plan prismatique en fonction de la température (fig. **II.2.5**). Les résultats de leur étude montrent qu'entre –20 et –9°C, les plans prismatiques croissent plus vite que les plans de base, puis il y a une transition entre –9 et –6°C, où la croissance selon les plans de base devient la plus rapide. Au-dessus de –6°C, la croissance selon les plans prismatiques redevient la plus rapide. D'autres mesures des coefficients de condensation dont dépendent les vitesses de croissance ont par la suite confirmé ces résultats (Lamb et Scott, 1972a ; Sei et Gonda, 1989). La variation du rapport des vitesses selon les deux

types de plans va déterminer la forme primaire du cristal, c'est à dire une croissance favorisée selon les plans de base ou les plans prismatiques. Il semble donc que c'est la température qui va déterminer ce paramètre.

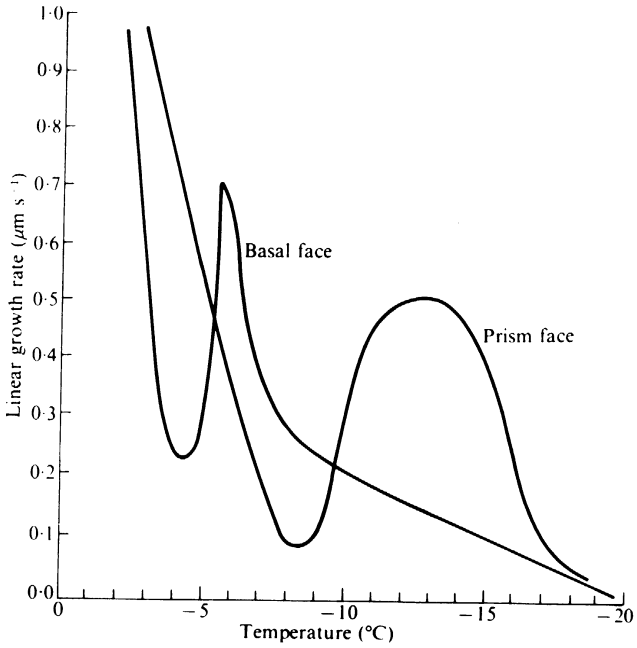

Figure II.2.5: Vitesses de croissance linéaire du plan de base et des faces prismatiques d'un cristal de glace, pour un excès de vapeur d'eau donné ($1{,}3.10^{-5}$ bar), en fonction de la température (d'après Lamb et Hobbs, 1971*).*

D'autres travaux consistant à faire croître des cristaux sous différentes conditions de température et d'humidité ont été entrepris (Hallet et Mason, 1958 ; Kobayashi, 1961 ; Rottner et Vali 1974). L'ensemble des résultats qu'ils ont obtenus a permis de regrouper sur un graphique les différents types de cristaux observés en fonction de la température et la sursaturation. Ces résultats sont présentés sur la figure **II.2.6.**

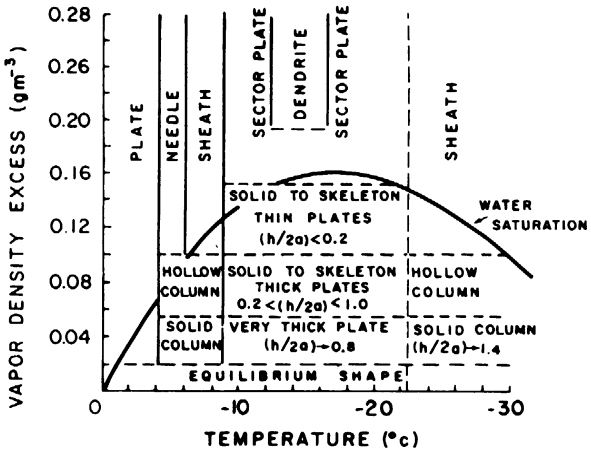

Figure II.2.6 : Variation de la forme des cristaux en fonction de la température et l'excès de vapeur d'eau (Pruppacher et Klett, 1978). (basée sur les observations en laboratoire de Kobayashi (1961) et Rottner et Vali (1974)).

Ils montrent, comme sur la figure **II.2.5**, que la forme primaire des cristaux dépend de la température, avec des transitions observées vers -4, -9 et autour de -22°C. Par exemple à -3°C, la croissance selon les faces prismatiques est favorisée et conduit à la formation de plaquettes alors que vers –6 °C c'est la croissance selon les plans de base qui est dominante, ce qui produit des colonnes. Par contre, la forme secondaire qui définit les détails du cristal, va dépendre de la vitesse de croissance qui est liée à la sursaturation. Ainsi, l'excès de vapeur d'eau va déterminer la transition entre une colonne et une aiguille ou entre une plaquette et une dendrite.

Une grande variété de cristaux existe dans l'atmosphère car un cristal de neige, une fois formé dans un nuage par condensation de vapeur d'eau, va traverser différentes zones où la température et la sursaturation vont changer, avant d'arriver au sol.

La figure **II.2.6** montre que la présence de la phase liquide dans les nuages va imposer une valeur donnée de la sursaturation par rapport à la glace. Cette sursaturation dépendante de la température est maximale vers –12°C (Pruppacher et Klett, 1978) et correspond à une sursaturation d'environ 15% (0.17 g/m^3). Le fort gradient de vapeur existant va provoquer la croissance rapide des cristaux de glace (>1.5µm/s) et conduire à la formation de cristaux dendritiques. Ces cristaux représentés sur la figure **II.2.1e** sont des monocristaux de glace dont les branches principales se sont développées à partir des faces $(11\bar{2}0)$, c'est à dire aux coins des faces prismatiques $(10\bar{1}0)$.

Typiquement, la longueur des prismes et le diamètre des plaquettes sont compris entre 10 µm et 1 mm, avec toutefois un maximum qui peut atteindre quelques millimètres. Les cristaux dendritiques sont les plus gros (moyenne de 2 mm) et les colonnes sont les plus petits (< 1 mm). Quant au grains de grésil qui croissent par accrétion de gouttelettes surfondues, ils peuvent atteindre 1 cm (Pruppacher et Klett, 1978).

II.2.3. Mécanisme de croissance à l'échelle moléculaire

La croissance d'un cristal se produit lorsque des molécules diffusent depuis la phase gaz, entrent en contact avec la surface du cristal puis s'incorporent au réseau cristallin. Bien que la vitesse de croissance soit en partie contrôlée par la diffusion en phase vapeur, c'est le coefficient de condensation, différent d'une face à l'autre, qui détermine la forme du cristal. Le coefficient de condensation représente la fraction de molécules arrivant à la surface d'une face qui s'incorpore au réseau.

L'énergie de liaison d'une molécule étant plus forte sur une marche que sur un plan (Kittel, 1968), la structure cristalline va se développer par propagation de marches atomiques moléculaires (Lamb et Scott, 1972b), qui peuvent être générées par nucléation homogène de nouvelles couches moléculaires ou par des lignes de défauts de surface comme les dislocations vis (Franck, 1949). Le processus de nucléation homogène est illustré sur la figure **II.2.7a**. Il est initié depuis les arêtes des faces cristallines car le taux de nucléation est proportionnel à l'excès de vapeur d'eau qui est plus

élevé aux extrémités des faces cristallines (fig.**II.2.8**). Il est également fortement dépendant d'un terme γ défini comme l'énergie libre d'une marche moléculaire. Ainsi, une faible variation de γ due par exemple à une légère variation de température, peut changer radicalement les vitesses de croissance sur chaque face et expliquer une transition abrupte entre une fine plaquette et une aiguille (Nelson et Knight, 1998).

Dans le cas des dislocations, la propagation des marches est initiée par des lignes de dislocation émergeant sur les faces du cristal. Les molécules viennent ainsi s'adsorber sur le front de la dislocation qui croît en spirale et s'étend sur toute la face cristalline (fig. **II.2.7, b**). De telles figures géométriques ont été observées lors de la croissance de la glace à partir de la phase liquide (Ketcham et Hobbs, 1968).

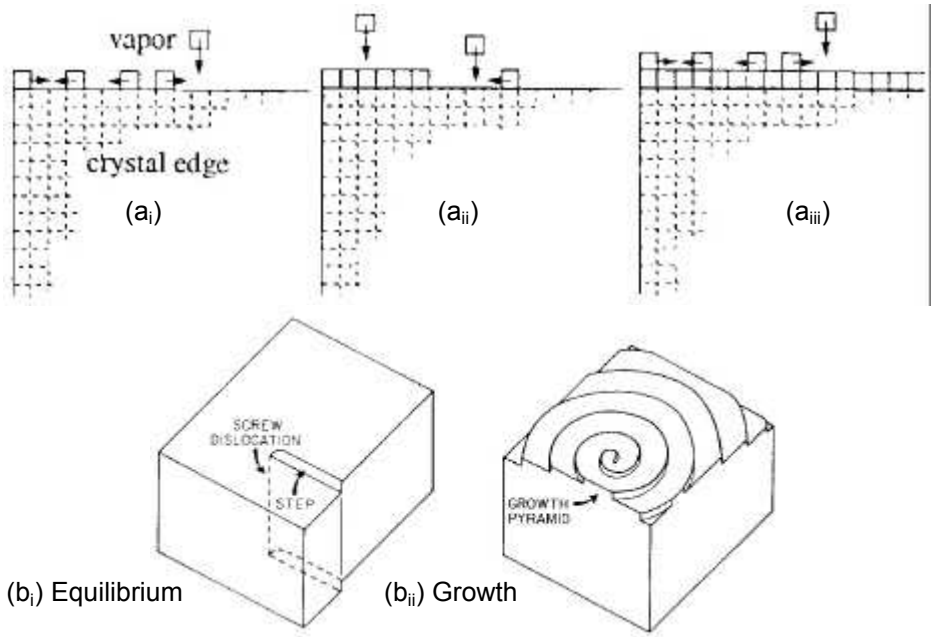

Figure II.2.7 : Mécanisme de croissance des faces cristallines (a) par nucléation homogène (d'après Nelson, 1998). Lorsqu'une marche est nucléée sur le bord d'une face les molécules s'adsorbent et la marche se propage vers le centre de la face (a_i et a_{ii}) ; puis une nouvelle couche peut commencer à se former (a_{iii}).
(b) par croissance en spirale d'une dislocation vis (d'après Lamb et Scott, 1972b).

La mécanisme de croissance en spirale est celui décrit pour la glace dans les livres de physique de la glace et des nuages (Pruppacher et Klett, 1978 ; Hobbs, 1974) car c'est le mécanisme le plus répandu pour les autres type de cristaux (Burton et al., 1951 ; Franck, 1982, 1993). Cependant de nombreuses études indiquent que des cristaux de glace obtenus à partir de la phase vapeur sont souvent sans dislocation ce qui exclut la présence d'une forte densité de ce type de défaut pour la neige (McKnight et Hallet,1968 ; Mizuno, 1978). De plus, à partir de mesures effectuées par Sei et Gonda (1989), il a été montré que le mécanisme de croissance en spirale ne peut pas expliquer simplement la forte anisotropie de croissance lors de la formation de fines plaquettes ou de colonnes contrairement au processus de nucléation homogène (Nelson et Knight, 1998). Il résulte de ces observations que la propagation de marches en spirale n'est probablement pas le mécanisme dominant de la croissance d'un cristal de neige d'autant plus qu'il n'a pas été prouvé que ce mécanisme existe vraiment dans le cas de la neige. La croissance par nucléation homogène de

marche aux arêtes semble donc être le mécanisme dominant pour la croissance des cristaux de neige.

Par fortes sursaturations, des colonnes creuses ou des dendrites peuvent être observées suivant la gamme de température. Quand un cristal est de petite taille, ce sont les effets de surface qui gouvernent la croissance et conduisent à une simple croissance prismatique. Cependant lorsque le cristal croît plus vite, la diffusion joue un rôle plus important : lorsque les faces d'un cristal croissent rapidement, la sursaturation est plus élevée aux extrémités du cristal (fig. **II.2.8**). Quand une nouvelle marche apparaît, elle réduit le champ de capture de la précédente. Par conséquent, si la nucléation est rapide, la croissance des marches précédentes s'arrête. Dans le cas d'une croissance selon l'axe c, les bords de la face croissent plus rapidement que son centre et un creux apparaît (fig. **II.2.8**). Ce phénomène peut être également observé lors d'une croissance des faces prismatiques comme le montre la figure **II.2.9**.

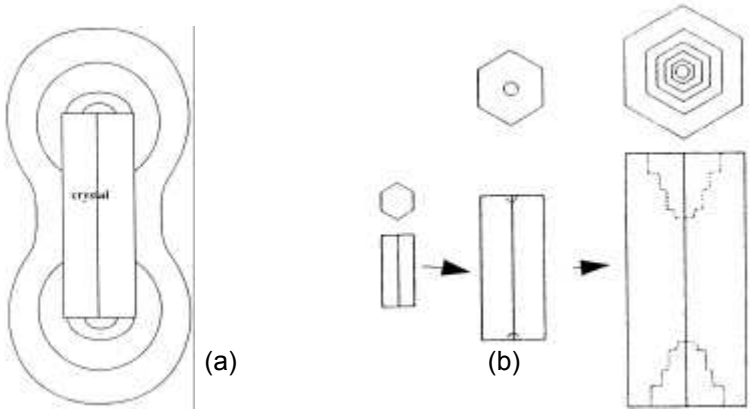

Figure II.2.8: Représentation d'une cristal croissant selon l'axe c par forte sursaturation. (a) Excès de vapeur d'eau dans l'environnement du cristal. (b) Vue d'une colonne dont les faces basales croissent plus lentement en leur centre que sur les cotés (d'après Nelson et Baker, 1996).

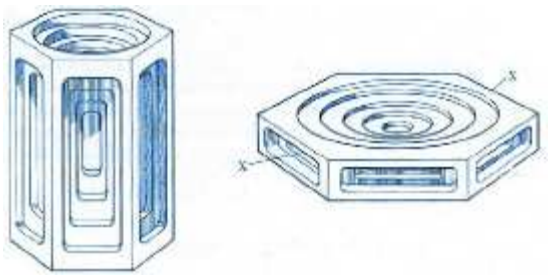

Figure II.2.9 : Représentation d'un prisme et d'une plaquette creusés au centre de leurs faces

Dans le cas de la formation d'un cristal dendritique, le cristal croit initialement comme une simple plaquette. Comme l'environnement des coins des faces devient plus saturé qu'au-dessus du centre des faces prismatiques, les coins croissent plus vite, et une petite pointe se forme. Celle-ci pénètre plus loin dans le milieu saturé en vapeur d'eau. Elle atteint donc des régions où la concentration en vapeur d'eau est plus élevée que sur le reste de la surface. C'est l'instabilité de Mullins-Sekerka (Mullins et Sekerka, 1963). Il en résulte que le cristal tend à évoluer vers des formes compliquées, car elle favorise l'apparition d'irrégularités. Les angles du cristal de départ donnent naissance à des branches, qui à leur tour deviennent instables par le même mécanisme. La formation de cristaux dendritiques est alors favorisée.

II.3. Le manteau neigeux et ses métamorphoses

II.3.1. Le manteau neigeux

Lors de leur dépôt au sol, les cristaux de neige vont former des strates ou couches de neige aux propriétés parfois différentes qui vont venir s'empiler les unes sur les autres pour former un assemblage hétérogène que l'on appelle manteau neigeux (fig. **II.3.1**), et dont l'évolution de l'aspect et des propriétés physiques sont aisément observables. Dans les régions où la température reste basse même l'été, la neige ne disparaît pas totalement et va se transformer lentement en névé puis en glacier ou calotte polaire. En moyenne montagne sous nos latitudes, ou en région côtière dans l'Arctique où les températures estivales sont plus élevées, la couverture neigeuse est saisonnière et disparaît lentement par fusion au printemps ou au début de l'été.

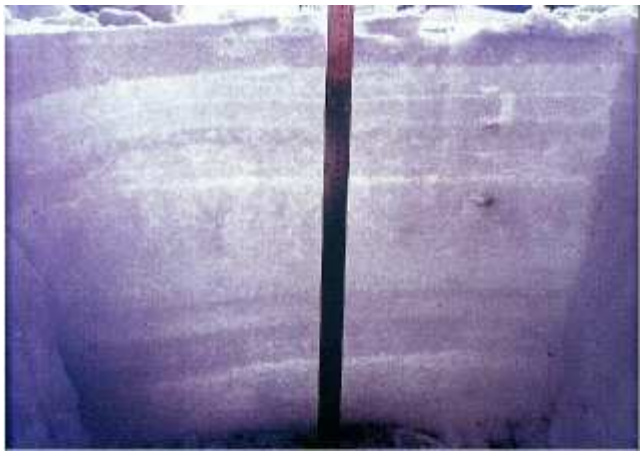

Figure II.3.1 : Coupe vertical du manteau neigeux

Deux particularités du manteau neigeux sont à l'origine de ses propriétés physiques et des transformations qui y sont observées. Tout d'abord, le manteau neigeux est un mélange de glace et d'air où l'air occupe le plus grand volume : 90 % pour une neige fraîche (Judson et Doesken, 2000) et 50 à 75% pour une neige âgée (cf. chap. **III, article 1**). Ceci lui confère des propriétés mécaniques et thermiques très différentes de celles des autres solides (Rey, 1986), comme une mauvaise conductivité thermique à l'origine de gradients de température (cf. § **II.3.3.1**.). Ensuite la glace a une forte tension de vapeur, qui dépend bien sûr de la température. La présence de gradients de température va donc permettre des échanges de matière entre diverses parties du manteau neigeux, qui vont pouvoir provoquer des transformations morphologiques importantes. Deux types d'actions simultanées et interdépendantes vont diriger la métamorphose: une action mécanique et une action thermodynamique.

Les principales étapes de la métamorphose de la neige sont repérées par 6 types de grains auquel un symbole est attribué :

Neige fraîche	+	Particules reconnaissables	/
Grains fins	•	Grains à faces planes	?
Givre de profondeur (gobelets)	?	Grains ronds	○

II.3.2. Action mécanique

L'action mécanique est la première action qui intervient dans la métamorphose de la neige. Elle est généralement rapide et se traduit par une destruction des cristaux de neige fraîche (+) en particules où la forme initiale est encore reconnaissable (/). Elle peut être provoquée par le vent ou par une compression due au poids des couches supérieures. L'efficacité de cette action va dépendre de la force du vent, et de la nature des cristaux : des étoiles plus fragiles y seront plus sensibles que des grains de grésil (Pahaut et Sergent, 1991). Cette destruction est associée à un tassement de la couche et à une augmentation de la densité : jusqu'à 180-200 kg/m^3. Si, la neige est très ventée, elles peut être réduite à l'état de fines particules assimilées aux grains fins (•) avec une densité de l'ordre de 250-350 kg/m^3.

L'échange de vapeur d'eau entre les cristaux contribue également à cette évolution en grain fins. Ces échanges résultent d'une recherche permanente d'équilibre thermodynamique entre les phases solides et gazeuses dans le cas de la neige sèche, auxquelles peut se rajouter la phase liquide pour une neige humide. Le vent et le compactage facilitent l'évolution vers cet équilibre thermodynamique en accélérant les échanges de vapeur d'eau, en réduisant la distance inter-granulaire et en augmentant les points de contact entre les cristaux. Ainsi, l'action mécanique joue un rôle de catalyseur qui favorise et accélère l'action thermodynamique. C'est notamment le cas pour la formation de ponts de glace entre les cristaux qui augmente la cohésion de la neige, et que l'on appelle cohésion de frittage. Le frittage est en effet plus efficace en présence de vent, et explique notamment la formation des corniches et la portance de la neige.

II.3.3. Action thermodynamique

L'action thermodynamique, qui résulte d'une recherche d'équilibre, est une action continue qui dure pendant toute l'existence du manteau neigeux. Les évolutions qui en dépendent seront assez lentes mais pourront être accélérées par des actions mécaniques, comme nous l'avons vu précédemment.

II.3.3.1. Métamorphose de la neige sèche

Dans la neige sèche (absence de phase liquide), les échanges de vapeur d'eau qui vont entraîner des changements morphologiques des cristaux, proviennent de processus de sublimation/condensation de la glace qui ont lieu continuellement dans l'ensemble du manteau neigeux. Ces transferts de matière peuvent se faire au sein d'un même cristal et/ou de grain à grain, et sont dus à des gradients de vapeur d'eau à l'échelle microscopique et macroscopique, résultant d'un gradient de rayon de courbure et de gradients de température.

a) Effet de la courbure des cristaux

A l'échelle du cristal, les transferts de vapeur d'eau résultent de la loi de Kelvin où la pression de vapeur saturante est fonction du rayon de courbure r :

$$\ln\left(\frac{P_{r,T}}{P_{r_\infty,T}}\right) = \frac{2.\gamma.V_L}{R.T} \times \frac{1}{r} \qquad \text{(II.1)}$$

où γ et V_L sont la tension de surface et le volume molaire de la glace, P_{r_∞}, R, T sont la pression de vapeur d'eau au-dessus d'une surface plane, la constante des gaz parfaits, et la température. L'effet du rayon de courbure sur la variation de la pression de vapeur saturante est montré sur la figure **II.3.2**.

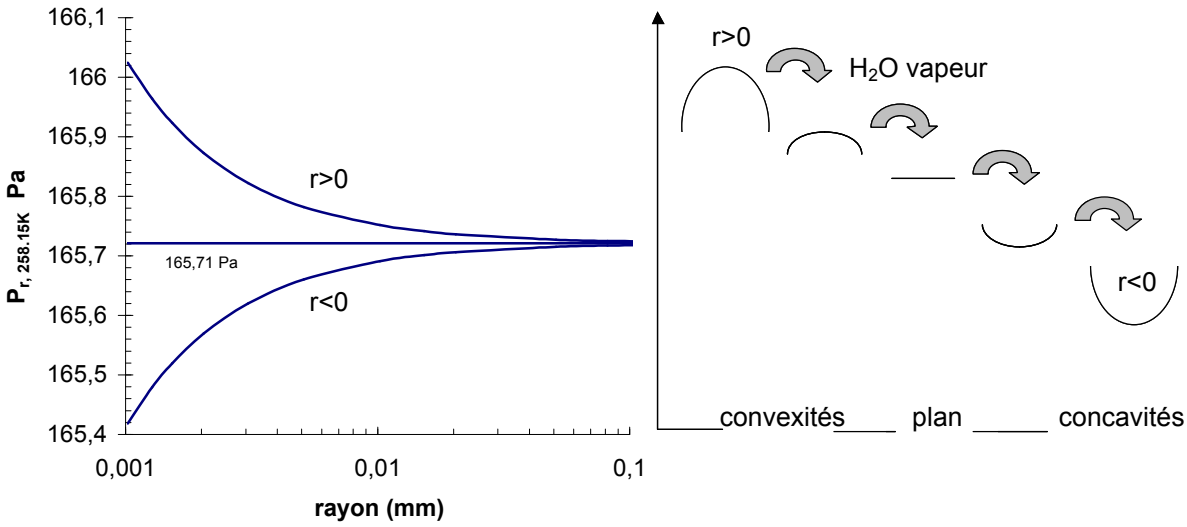

Figure II.3.2: Variation de la vapeur de pression saturante en fonction du rayon de courbure, calculée à –15°C.

Ainsi, une surface à rayon de courbure faible et positif telles que les pointes d'étoiles ou de dendrites, va être le siège d'une sublimation au profit d'une surface concave (r < 0). Ce processus qui tend à faire disparaître les angles vifs et les pointes, à lisser les contours, et à combler les creux, a donc un effet destructif. Il est illustré sur la figure **II.3.3.**

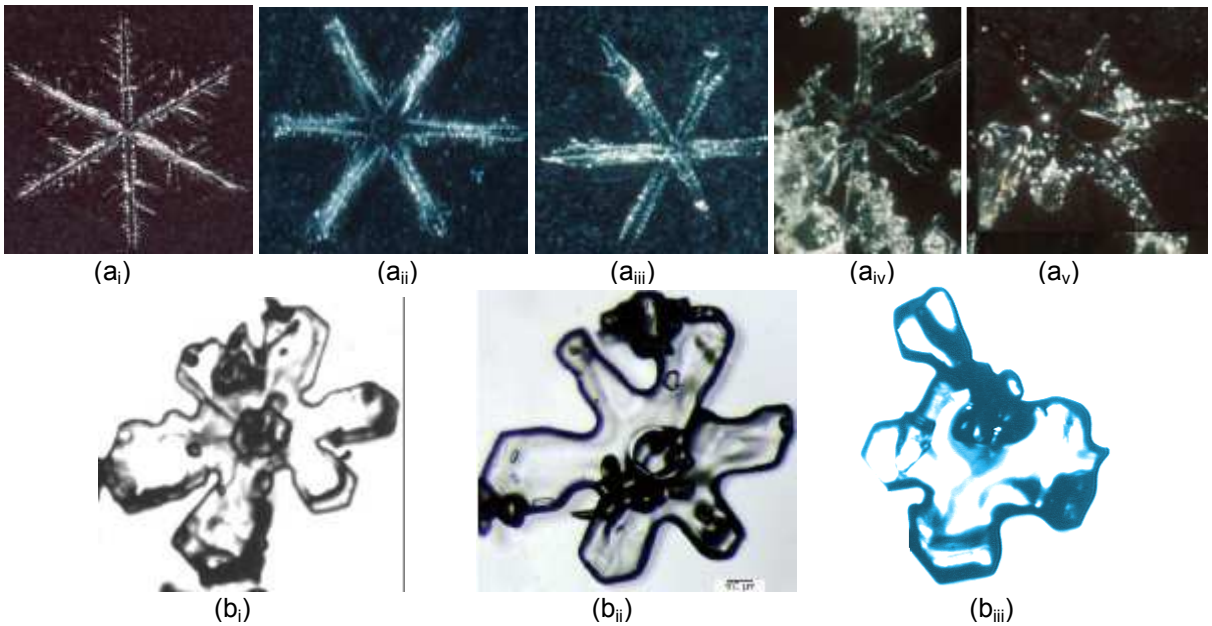

Figure II.3.3 : Métamorphose de la neige due à la loi de Kelvin. a. Transformation de cristaux dendritiques. b. Arrondissement des branches d'une étoile.

b) Effet du gradient de température.

A cause des propriétés isolantes du manteau neigeux, l'onde de froid provenant de sa surface a du mal à pénétrer en profondeur et provoque l'établissement d'un gradient de température vertical qui entraîne des flux de vapeur d'eau entre les grains, modifiant ainsi leur structure.

Afin de comparer l'effet du gradient de température à celui du rayon de courbure, nous avons représenté sur la figure **II.3.4**, les gradients de vapeur d'eau (Pa m^{-1}) résultant de gradients de température (°C/m) rencontrés dans le manteau neigeux, avec ceux résultant de gradients de courbure. Les gradients de vapeur d'eau dus à la courbure des cristaux ont été calculés entre une zone convexe de rayon (r) positif et une surface plane de rayon infini située à 0.1 mm.

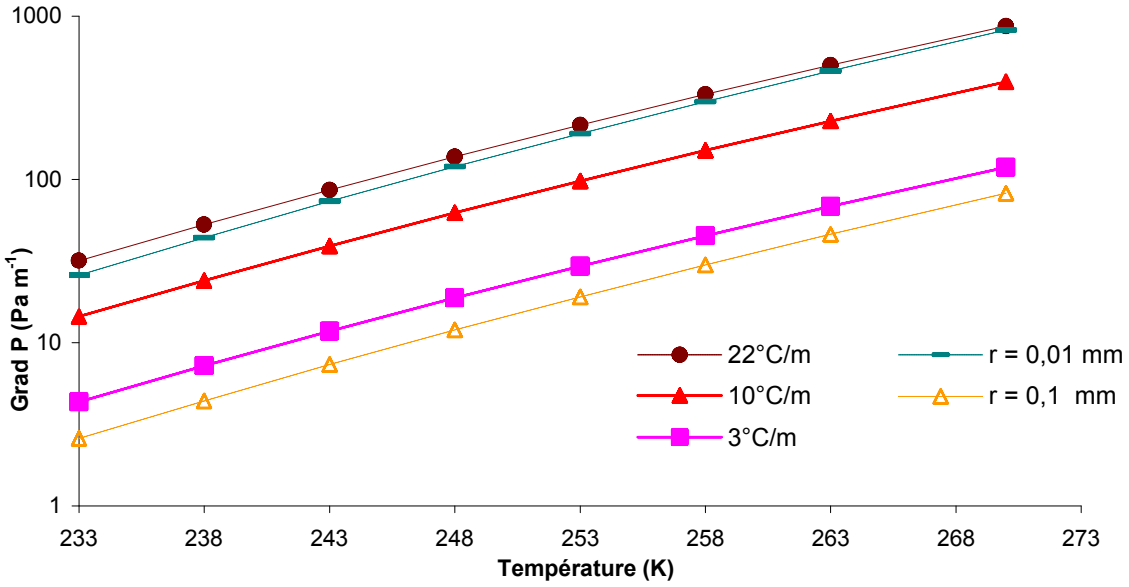

Figure II.3.4 : Evolution du gradient de vapeur d'eau en fonction de la température, résultant de gradients de courbure des cristaux et de gradients de température.

On voit que l'effet du rayon de courbure peut prédominer pour r < 0.01 mm, puis devient négligeable pour r > 0.1 mm. Ainsi, après la rapide disparition des arêtes très vives, l'effet de ce processus sur la métamorphose de la neige sera négligeable. C'est donc le gradient de température qui va être le moteur principal de la métamorphose de la neige (Colbeck, 1986).

Les gradients thermiques sont dus à l'onde de froid qui se propage lentement depuis la surface. Ainsi, la partie supérieure des grains sera la plupart du temps plus froide que sa partie inférieure. Au niveau des points chauds, la sublimation va entraîner un arrondissement (Nelson, 1998). Aux zones de condensation (points froids), une croissance lente va conduire également à des formes arrondies se rapprochant des formes d'équilibres ellipsoïdales (Nelson, 1998). Par contre, si la croissance est rapide, elle va produire des facettes et des arêtes franches (Marbouty, 1980). La vitesse de croissance dépend du gradient de vapeur d'eau et par conséquent du gradient de température. C'est donc la valeur du gradient de température qui va déterminer l'évolution de la forme des cristaux :

(i) Si ce gradient est faible (< 5°C/m), les flux de vapeur d'eau vont être limités. Les cristaux vont évoluer vers des formes arrondies. Après avoir subi une première action mécanique destructive plus

ou moins importante, les aiguilles, plaquettes ou étoiles vont se transformer partiellement (/ •) (fig. **II.3.5**) ou complètement (• •) en grains fins à peu près sphériques d'un diamètre assez uniforme (0.2 à 0.4mm). La transformation de la neige fraîche en grains fins est cependant beaucoup plus lente qu'en présence de vent et pourra prendre plusieurs semaines si le gradient est proche de 0°C/m et si la neige reste froide.

Figure II.3.5 : Cristaux de neige partiellement transformés ou l'on peut reconnaître des branches d'étoiles brisées

(ii) Si le gradient de température est moyen, c'est à dire compris entre 5 et 15 à 20°C/m; les flux de vapeur d'eau vont être plus importants. Les cristaux vont évoluer en grains caractérisés par des facettes à angles vifs (grains à faces planes ?). La croissance de ces cristaux reste limitée et leur diamètre excède rarement 1 mm (fig. **II.3.6**). Cette évolution morphologique peut se faire à partir de neige récente ou de grains fins et va entraîner une perte de cohésion. Tant que les grains ne sont pas trop gros, cette transformation n'est pas irréversible. Si le gradient devient faible, les grains à faces planes perdent leur caractère anguleux et se transforment en grains fins. L'alternance entre des faibles et moyens gradients est fréquente et explique la formation rapide de grains fins.

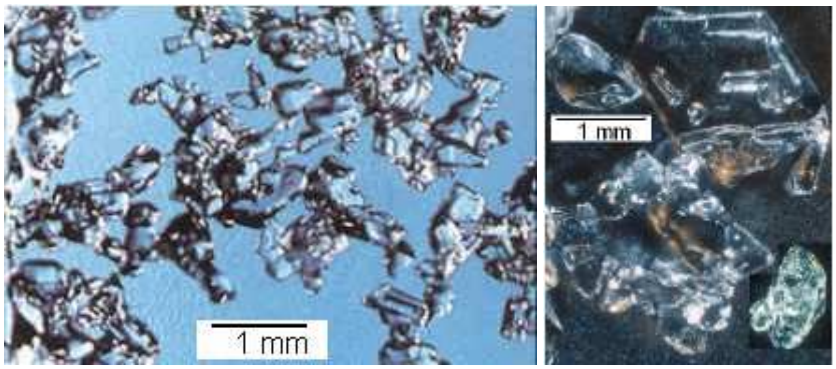

(a) (b)

Figure II.3.6 : Cristaux facettés ayant cru par gradient moyen : a. Grains de taille moyenne pouvant évoluer en grains fins si le gradient diminue. b. Ici les facettes sont beaucoup plus grandes, et le processus de réversibilité en grains fins n'est plus possible.

Si le gradient de température est suffisant (>15°C/m), les cristaux facettés peuvent évoluer vers des cristaux en forme de pyramides striées et creuses appelées gobelets ou givre de profondeur (?) (fig. **II.3.7)**. Ces cristaux se forment par sublimation du sommet d'un cristal, suivi de recondensation importante à la base du cristal situé au-dessus. On obtient donc des cristaux dont la base est très

anguleuse, alors que le sommet est arrondi. Cette évolution morphologique n'est pas réversible et seule la fonte pourra faire disparaître ce type de cristaux qui n'ont aucune cohésion entre eux.

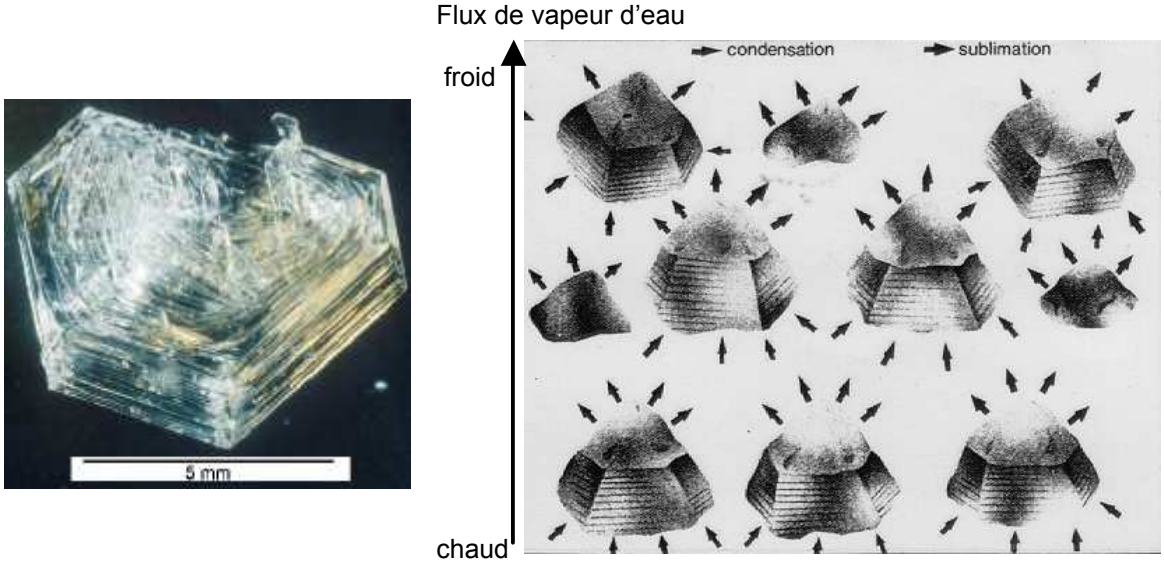

Figure II.3.7 : Mécanisme de croissance de grains anguleux sous l'effet d'un fort gradient de température (> 15°C/m). Les cristaux de givre de profondeur peuvent atteindre plusieurs mm comme le montre la photographie de gauche

La vitesse de croissance de cristaux fortement facettés va dépendre du gradient de température mais aussi de la température moyenne de la couche de neige en évolution. Elle apparaît maximale autour de –5°C (Marbouty, 1980). A plus haute température, le désordre de la couche de surface ('quasi-liquide') des cristaux limiterait la formation des facettes (Colbeck, 1983b).

Le refroidissement radiatif nocturne de la surface du manteau neigeux génère également de forts gradients thermiques qui provoquent la croissance rapide de cristaux anguleux atteignant parfois quelques cm, et dénommés givre de surface (fig. **II.3.8)**.

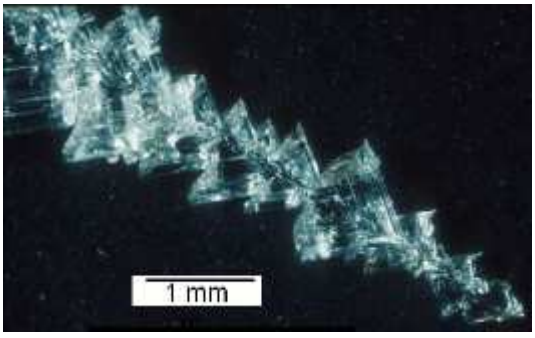

Figure II.3.8 : Cristal de givre de surface formé par condensation de vapeur d'eau atmosphérique sur la surface du manteau neigeux refroidie radiativement.

II.3.3.2. Métamorphose de la neige humide

Une couche de neige peut être rendue humide par fusion due à un apport d'énergie (essentiellement par rayonnement solaire) ou par percolation d'eau provenant de couches supérieures apportée par fusion ou pluie. Dans ce cas, toute la couche est à une température homogène de 0°C. L'humidité de la neige est déterminée en mesurant sa teneur en eau liquide (TEL) volumique ou massique. Les

méthodes utilisées pour déterminer la TEL sont souvent basées sur la mesure de la constante diélectrique de la neige aux fréquences radio, celle-ci étant différente pour l'eau et la glace (Denoth, 1994 ; Lundberg, 1997 et référence incluses).

Si cette TEL est faible, sous l'effet des forces de capillarité, l'eau va se localiser aux points de contact des grains ainsi que dans les zones concaves sous forme de film. Ainsi, la cohésion de capillarité remplace la cohésion de frittage. Suite à un regel, une solidification se produit dans ces zones et la chaleur de solidification dégagée va faire fondre les petits grains environnants. Ainsi, ces derniers disparaissent au profit des plus gros qui croissent et s'arrondissent en ''grains ronds'' (○) (fig. **II.3.9**).

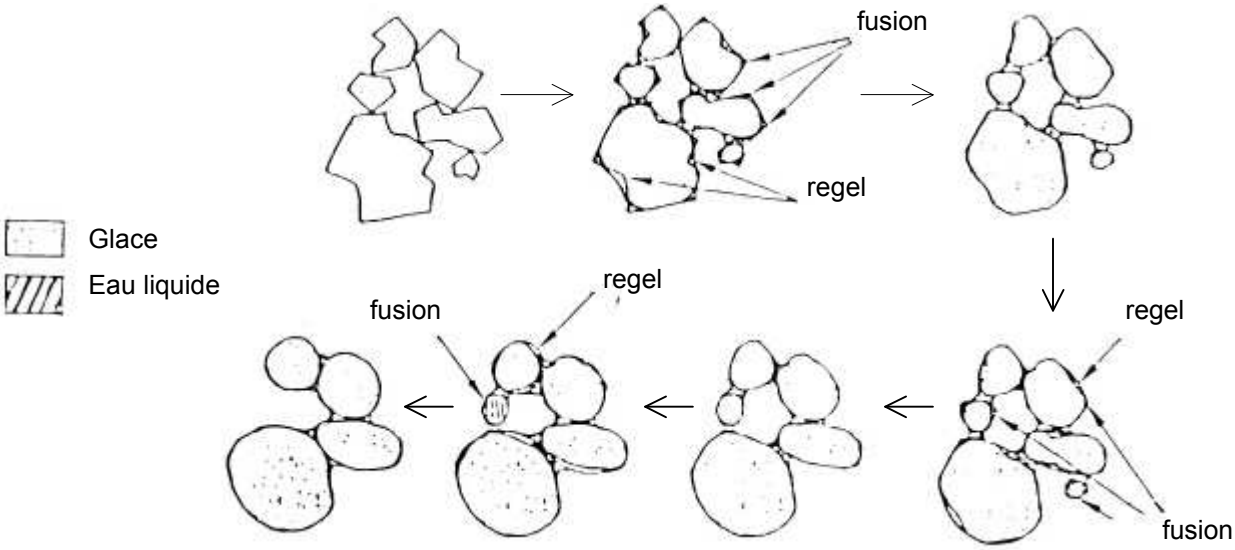

Figure II.3.9 : Mécanisme d'arrondissement des grains dans une neige humide. L'eau se localise dans les zones concaves. Puis l'énergie libérée lors de la solidification fait fondre les plus petits grains et les zones convexes des cristaux.

Ces grains ronds se groupent rapidement en agglomérats de plusieurs mm mais il est encore possible de distinguer chaque grain bien arrondi comme le montre la **figure II.3.10**. La TEL est en fait le moteur de cette métamorphose et elle sera d'autant rapide que la TEL sera élevée (Brun, 1989).

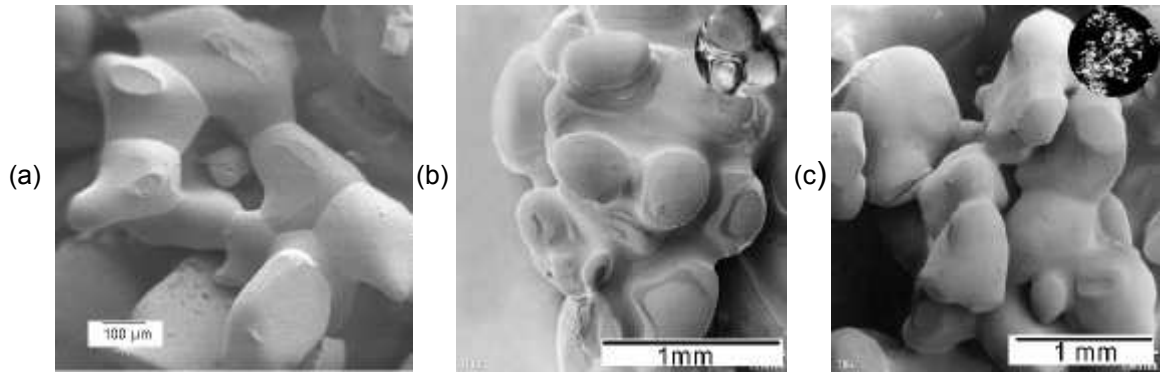

Figure II.3.10 : Observations au MEB d'échantillons de neige humide. (a) Début d'arrondissement de grains dans une neige faiblement humide. Leurs agglomérations mettent en évidence les joints de grain mentionnés dans le paragraphe II.1.3.4. (b) Echantillon de neige avec une faible TEL : on peut distinguer les formes sphériques des grains. (c) Echantillon de neige mouillée. La teneur en eau est importante et la forme arrondie n'est plus distinguable.

Si la TEL est importante (> 8-10% en volume), l'eau peut percoler vers le bas et peut saturer une couche de neige. Le refroidissement nocturne va entraîner la formation d'une solide couche de regel dont l'épaisseur peut varier de 1-2 cm à 30 cm si toute la couche a été saturée en eau liquide. Cette métamorphose est donc l'étape ultime avant la fonte et la disparition du manteau neigeux. L'aspect d'une telle couche se présente sous forme de gros agglomérats ou les grains ronds ne sont plus distinguables.

On voit donc que l'effet important de deux métamorphoses, de neige sèche et neige humide, est de faire grossir les cristaux et de détruire les petites particules. On peut donc déjà s'attendre à observer dans notre étude une diminution de la surface spécifique de la neige dans le manteau neigeux car celle-ci est inversement proportionnelle à la taille des cristaux.

II.4.Théorie de l'adsorption

II.4.1. Généralités

Le terme "adsorption" a été introduit par Kayser (1881) pour désigner la condensation de gaz sur des surfaces libres, en opposition avec l'absorption où les molécules de gaz pénètrent dans la masse du solide. L'adsorption se produit grâce aux forces qui existent entre le solide et les molécules du gaz. Ces forces sont de deux types (Israelachvili, 1985): physiques ou chimiques et elles donnent lieu à la physisorption ou à la chimisorption, respectivement.

La physisorption résulte de l'établissement de forces de Van der Waals entre les molécules de gaz et le solide. Ces forces sont dues à la fluctuation rapide de la densité électronique créant simultanément des forces de répulsion (London, 1930) et d'attraction autour des atomes. L'énergie mise en jeu est de l'ordre de quelques dizaines de KJ/mol. La chimisorption résulte de la création d'une liaison chimique entre la molécule de gaz et le solide (quelques centaines de KJ/mol). L'adsorption d'un gaz sur un solide est exothermique (enthalpie $\Delta H<0$) car il y a établissement d'interactions globalement attractives qui libèrent de l'énergie.

La quantité de gaz adsorbée sur un solide dépend : de la température, de la pression du gaz P, de la nature du solide et du gaz, et de la surface accessible au gaz.

Les études d'adsorption de gaz sur des surfaces visent à quantifier l'effet de ces différents paramètres sur la quantité adsorbée. La représentation des résultats de ces études peut prendre plusieurs formes, dont la plus courante est sans doute l'isotherme d'adsorption (Gregg et Sing, 1982).

II.4.2. Isotherme d'adsorption

Une isotherme d'adsorption représente la quantité de gaz adsorbé N_{ads}, en fonction de la pression partielle P/P_0 à température constante, ou bien la fraction de la surface du solide θ recouverte par le gaz à l'équilibre.

$$N_{ads} = f(P)_T \quad \text{ou} \quad \theta = f(P)_T \qquad \text{(II.2)}$$

Brunauer, Deming, Deming et Teller (1940) ont établi une classification des cinq types d'isothermes rencontrés, de I à V (B.D.D.T.), auxquels on a ultérieurement ajouté un type particulier, numéroté VI (fig. II.4.1).

Les isothermes de type II et III sont caractéristiques de l'adsorption sur des solides non poreux. Les types IV et V comportent une boucle d'hystérésis, c'est à dire que les courbes obtenues en étudiant l'adsorption par recouvrement croissant sont différentes de celles obtenues par recouvrement décroissant. Elles apparaissent pour des solides mésoporeux (taille des pores comprise entre 25 et 500 Å) alors que l'adsorption sur des solides microporeux (taille des pores inférieure à 25 Å) se traduit par des isothermes de type I; l'isotherme de type VI en escalier reste un cas particulier: elle est obtenue quand un grand nombre de sites d'adsorption ont la même énergie. C'est le cas de l'adsorption de H_2O sur MgO (Ferry et al., 1996).

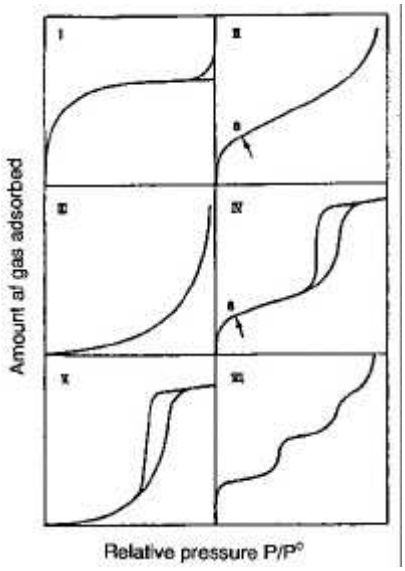

Figure II.4.1 : Les six types d'isotherme d'adsorption d'après la classification B.D.D.T.

Les boucles d'hystérésis dans les isothermes de type IV ou V rendent compte de l'existence d'une condensation capillaire dans les pores de l'adsorbant. La différence de forme entre les isothermes de type II et IV, d'une part, et celle de type III et V, d'autre part, provient de l'intensité des interactions gaz-solide (forte et faible énergie d'adsorption, respectivement).

Pour chaque couple gaz-solide étudié, l'obtention d'une isotherme d'adsorption va ainsi nous permettre d'obtenir des informations sur l'interaction gaz-solide et sur la microstructure du solide. De plus, la mise en équation des isothermes va permettre d'atteindre des grandeurs thermodynamiques ainsi que la surface spécifique développée par le solide.

II.4.3 Modèle d'adsorption sur les solides non poreux

Nous verrons dans la partie résultat que l'adsorption du méthane sur la neige se caractérise par une isotherme de type II (cf. chap. **III**, **article 1**.). Nous allons donc présenter la mise en équation de ce type d'isotherme qui permet d'obtenir la surface spécifique mais aussi l'énergie moyenne d'adsorption de la première monocouche (θ=1).

Il existe plusieurs modèles pour décrire l'adsorption de gaz sur les solides. Langmuir (1916) a proposé un modèle cinétique de processus d'adsorption dans lequel chaque molécule s'adsorbe sur un site bien défini avec une énergie indépendante du recouvrement. Dans ce modèle, Langmuir a considéré que le taux de recouvrement ne pouvait excéder l'unité, soit une monocouche. Plus tard, le phénomène d'adsorption étendu aux couches supérieures (soit $\theta > 1$) a été admis comme un cas plus général et le recouvrement monocouche s'est révélé comme un cas particulier.

Brunauer, Emmett et Teller (1938) ont proposé un modèle multicouche (appelé B.E.T.) qui est une extension du modèle de Langmuir où chaque molécule adsorbée est un site d'adsorption pour la molécule de la couche suivante.

II.4.3.1. Le modèle d'adsorption multicouche B.E.T.

Dans ce modèle, on suppose que :

- la surface de l'adsorbant est divisée en fractions S_0, S_1, S_2,□ , S_i couvertes par 0, 1, 2,□ , i couches de molécules adsorbées représentées sur la figure **II.4.2**.
- à tout moment, il y a un équilibre d'adsorption entre la couche d'ordre (i-1) et la couche d'ordre (i).

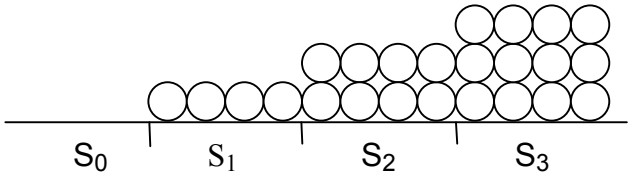

Figure II.4.2: Représentation de l'interface gaz-solide dans le modèle BET. La surface du solide peut être divisée en fraction S_i.

Les équilibres d'adsorption-désorption entre les couches successives peuvent s'écrire:

$$b_i \times P \times S_{i-1} = a_i \times S_i \times \exp\left(-\frac{q_i}{RT}\right) \qquad \text{(II.3)}$$

où b_i $a_i.\exp(-q_i/RT)$ sont des constantes, q_i est la chaleur d'adsorption de la couche i.

Dans une description rigoureuse de l'adsorption physique, il faudrait tenir compte de la décroissance progressive de l'énergie d'adsorption q_i à mesure que l'on s'éloigne de la surface. L'hypothèse simplificatrice du modèle BET est de ne considérer que deux valeurs pour q_i: q_1 pour les molécules de la première couche, en interaction directe avec la surface, et q_L, la chaleur de liquéfaction, pour les molécules dans les couches supérieures.

Après un traitement mathématique, on obtient la forme définitive de l'équation de l'isotherme d'adsorption dans le modèle BET:

$$\theta = \frac{N_{ads}}{N_m} = \frac{C \cdot (P/P_o)}{(1-P/P_o)(1-P/P_o + C \cdot P/P_o)} \qquad \text{(II.4)}$$

L'équation (II.4) est appelée l'équation BET, la constante C (dont la signification est discutée dans le paragraphe suivant) est appelée constante BET. N_{ads} et N_m sont respectivement le nombre de molécules adsorbées, et le nombre de molécules nécessaires pour former une monocouche, P/P_0 est la pression relative avec P_0 la pression de vapeur saturante de l'adsorbat (gaz qui s'adsorbe) à température considérée.

II.4.3.2. Applications du modèle BET

L'équation (II.4) est à la base de la méthode la plus classique de mesure de surface spécifique. Elle peut se mettre sous la forme:

$$Y = \frac{P/P_o}{N_{ads} \cdot (1 - P/P_o)} = \frac{1}{N_m \cdot C} + \frac{C-1}{N_m \cdot C} \times \frac{P}{P_o} \qquad \text{(II.5)}$$

En traçant Y en fonction de P/P_o, on obtient une droite, pour une certaine gamme de pression relative ($0.05 < P/P_o < 0.35$) :

$$\text{de pente: } A = \frac{C-1}{N_m \cdot C} \qquad \text{et d'ordonnée à l'origine: } B = \frac{1}{N_m \cdot C}$$

A partir de ces données, on peut calculer N_m, le nombre de molécules adsorbées dans une monocouche, appelée également capacité monocouche, et la constante BET C:

$$N_m = \frac{1}{A + B} \qquad \text{(II.6)}$$

et

$$C = \frac{1}{N_m \cdot B} = \frac{A + B}{B} \qquad \text{(II.7)}$$

A partir de la valeur de N_m, et connaissant la surface d'une molécule d'adsorbat σ_o, on peut atteindre la surface totale du solide S:

$$S = N_m \times s_o \qquad \text{(II.8)}$$

D'après le modèle BET:

$$C = \frac{a \cdot b_1}{b \cdot a_1} \times \exp\left(\frac{q_1 - q_L}{RT}\right) \qquad \text{(II.9)}$$

On considère en général que le rapport $a.b_1/b.a_1$ est proche de 1. Dans ce cas, on peut écrire:

$$C = \exp\left(\frac{q_1 - q_L}{RT}\right) \qquad \text{(II.10)}$$

La constante BET nous permet donc d'accéder directement à la chaleur nette d'adsorption ΔQ. Elle est définie par: $\Delta Q = q_1 - q_L = RT \ln C$ (J/mol) (II.11)

où q_1 est la chaleur moyenne d'adsorption de la 1ère couche et q_L est la chaleur de liquéfaction du gaz. Cette énergie est obtenue à partir des données expérimentales dans un domaine de pression relative restreint qui correspond au domaine de formation de la monocouche.

Plus la valeur de C est grande, plus la distinction entre l'adsorption de la première couche et la condensation des nombreuses couches suivantes est marquée. Dans l'isotherme, cette distinction se marque par l'inflexion qui apparaît sur la figure II.4.3.

Le calcul montre que pour $C > 2$, on a une isotherme de type II ou IV et une valeur de $C < 2$ conduit à une isotherme de type III ou V. Cette constatation peut être interprétée de la manière suivante:

Lorsque C est supérieur à 2, la théorie rend compte des isothermes de type II où $q_1 >> q_L$. Les couches supérieures à la première ne se remplissent que lorsque la première monocouche est complète. La courbure de l'isotherme devient plus prononcée lorsque C augmente.

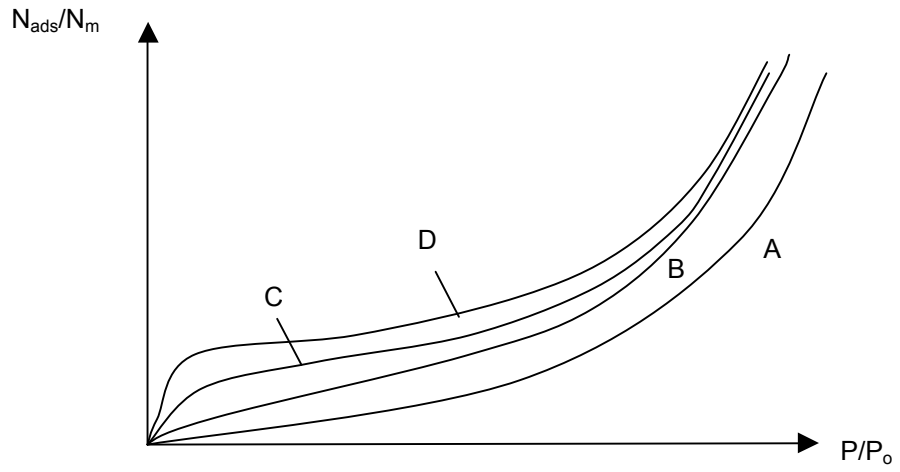

Figure II.4.3: Influence de la valeur de la constante C sur la forme de l'isotherme d'adsorption. (A): C=1; (B): C=10; (C): C=100 et (D): C=1000.

Si C < 2, c'est à dire que $q_1 < q_L$, la surface du solide présente peu d'affinité pour le gaz et la courbure de l'isotherme disparaît.

II.4.3.3. Critique du modèle BET

On a constaté dans la littérature que la théorie BET réussissait à rendre compte d'une variété considérable de situations à partir d'un modèle moléculaire simple. Néanmoins, le modèle présente certaines contradictions internes (*Gregg et Sing,* 1982). D'une part, les couches adsorbées, autres que la première, sont supposées avoir des caractéristiques énergétiques très proches de celles du liquide ($q_{i>1} = q_L$). D'autre part, le modèle postule une adsorption localisée dans laquelle les molécules peuvent s'empiler les unes sur les autres en formant des "gratte-ciel" moléculaires (ce qui revient à admettre que la tension superficielle est nulle). Ces deux hypothèses sont évidemment incompatibles. Fondamentalement, il y a deux améliorations importantes à apporter à ce modèle:

il devrait tenir compte d'une décroissance progressive de la chaleur d'adsorption ($q_1 > q_2 > q_3 > \square . > q_L$).

- les interactions latérales entre molécules adsorbées ne peuvent être négligées.

Les hypothèses simplificatrices de ce modèle conduisent à une surestimation des quantités adsorbées au-delà de la monocouche et à des déviations possibles dans les valeurs de ΔQ et de S. Le modèle BET reste néanmoins le plus utilisé dans le cas d'une physisorption et dans les calculs de surface spécifique.

II.5. Bibliographie sur la surface spécifique de la neige.

Nous avons vu dans l'introduction que la surface spécifique (SS) de la neige était un paramètre crucial pour comprendre et quantifier les échanges entre le manteau neigeux et l'atmosphère. Paradoxalement, son étude a suscité peu d'intérêt avant notre travail puisque à l'exception de la publication de Narita (1971), seules des mesures isolées ont été effectuées avant 1998. L'article de Narita a été rédigé en japonais et seul le résumé est en anglais. Ceci explique probablement le fait qu'il soit rarement mentionné dans les travaux récents discutant de la SS de la neige (Hoff et al., 1998 ; Fassnacht et al., 1999 ; Hanot et Dominé, 1999), et ceux traitant de l'adsorption de gaz à la surface de la neige (Hoff et al., 1995 ; Wania, 1997)

Nous présentons dans cette section les différentes valeurs de SS de la neige qui ont été obtenues avant notre travail ainsi que les méthodes utilisées. La validité de ces résultats sera commentée dans le chapitre **III** (cf. **article 1**).

II.5.1. Méthodes expérimentales.

Trois méthodes principales sont connues pour déterminer la surface spécifique d'échantillons de neige :

(i) la méthode d'adsorption de gaz**,** généralement à 77 K, qui est similaire à l'adsorption de gaz traces à la surface des cristaux dans le manteau neigeux. Cette méthode apparaît comme la plus pertinente en ce qui concerne l'étude des échanges de gaz entre le manteau neigeux et l'atmosphère puisqu'elle détermine la surface accessible aux gaz. C'est l'une des deux méthodes expérimentales que nous avons utilisées dans ce travail ; elle est détaillée dans le chapitre **III** (cf. **article 1**).

(ii) La stéréologie : Elle consiste à analyser des images 2D de coupes transversales d'échantillons de neige de 2 à 3 cm de coté. Cette méthode nécessite de verser dans l'échantillon un liquide insoluble tel que le diethyl-orthophtalate (phtalate, T_{fusion} -5°C,) ou l'aniline, ainsi qu'un colorant généralement de couleur bleu qui remplissent l'espace poreux de l'échantillon par capillarité. L'ensemble est ensuite solidifié par refroidissement jusqu'à -40°C afin de renforcer la structure de l'échantillon. Puis, celui-ci est découpé par microtomage en plans parallèles (quelques dizaines de µm d'épaisseur) qui sont photographiés. Ensuite, une méthode d'analyse d'images appropriée permet de déterminer la surface occupée par la glace sur chaque photographie et de déduire la surface spécifique de l'échantillon (Narita, 1971 ; Perla, 1986).

(iii) Une troisième méthode est l'analyse d'images de cristaux isolés obtenues par microscopie optique. Elle consiste à déterminer les dimensions des cristaux de neige à partir desquels on déduit la surface qu'ils développent, leur volume et ainsi leur surface spécifique. Cette méthode a également été utilisée dans notre travail (cf. chap. **III, article 2**), et récemment par Fassnacht et al. (1999), qui se sont aidés d'un logiciel d'analyse d'images.

II.5.2. Résultats des travaux précédents.

La première valeur de surface spécifique de la neige a été proposée par Adamson et al. (1967). En utilisant l'adsorption de l'azote à 77 K, ils ont obtenu des valeurs de 2000 cm^2/g pour un échantillon de neige fraîche prélevé lors d'un blizzard au Mont Gorgonio (2400 mètres d'altitude) près de Los Angeles, et de 13 000 cm^2/g pour un échantillon collecté près de Denver, 4 jours après sa chute. Avec une méthode similaire, Jellinek and Ibrahim (1967) ont reporté une valeur bien plus élevée de 77 700 cm^2/g pour un échantillon de neige d'origine non spécifiée.

Rey (1995) en utilisant l'adsorption de méthane à 77 K, a obtenu pour une neige fraîche récoltée pendant la chute, à Grenoble par une température de -1.5°C, une valeur de 640 cm^2/g. Par cette même méthode, Chaix et al. (1996) ont obtenu 570 cm^2/g pour une neige tombante prélevée à Grenoble par une température de -2°C. Récemment, Hoff et al. (1998) ont obtenu par adsorption d'azote à 77 K des valeurs comprises entre 600 et 3700 m^2/g pour six échantillons de neige collectée quelques heures après leur chute.

En utilisant la stéréologie, Narita (1971) a déterminé la surface spécifique de nombreux types de neige, sans toute fois étudier de neige tombante. Il a répertorié une centaine de valeurs de surface spécifique dans un graphe de la surface spécifique en fonction de la densité, qui indiquent des valeurs comprises entre 60 et 750 cm^2/g pour des masses volumiques inférieures à 0.55 g/cm^3.

D'autres valeurs, estimées à partir de paramètres géométriques, s'étendent sur un intervalle assez grand. Par exemple, Hoff et al. (1998) ont estimé des valeurs comprises entre 300 et 8000 cm^2/g et centrées vers 1000 cm^2/g, à partir de dimensions de cristaux de neige mesurés par Hobbs (1974) et Pruppacher et Klett (1978) en microscopie optique. Ils ont également estimé que la présence de microstructures dues au givrage et détectées en microscopie électronique à balayage (MEB) (Wergin et al., 1995) pourrait augmenter la SS de la neige jusqu'à 10 000 cm^2/g. Plus récemment, par analyse d'image, en utilisant des relations géométriques entre la taille des cristaux et leurs épaisseurs (Pruppacher et Klett, 1978 ; Auer and Veal, 1970) et des distributions de taille de cristaux, Fassnacht et al. (1999) ont déterminé la surface spécifique de 50 cristaux de neige fraîche dendritiques photographiés par Bentley et Humphries (1931), et différenciés selon la classification de Magano et Lee (1966). Pour des cristaux non givrés, ils ont obtenu une SS moyenne de 1820 cm^2/g avec des valeurs comprises entre 900 et 3300 cm^2/g.

Avec une quatrième méthode, Granberg (1985) a proposé un estimation de la surface spécifique d'échantillons de neige en étudiant la distribution en taille des cristaux à l'aide de tamis. Il a étudié le profil de différentes couvertures neigeuses (50-100 cm d'épaisseur) en Février 1983 et 1984 près de Schefferville, Québec. La SS a été déterminée en calculant la surface développée par des sphères de taille identique à celles des cristaux, qu'il a multiplié par un facteur constant de 1,5 pour tenir compte de la non-sphéricité. Il a obtenu des valeurs comprises entre 60 cm^2/g pour des couches de neige profondes et 200 cm^2/g près de la surface.

La seule étude traitant de la surface spécifique d'une couche de neige et de son évolution a été effectuée par Hanot et Dominé (1999). Comme cela a été dit dans l'introduction, cette étude a été

l'élément initiateur de notre travail puisque les résultats qu'ils ont obtenus ont montré le potentiel du manteau neigeux pour stocker des gaz traces et les échanger avec l'atmosphère. En effet, en utilisant la méthode d'adsorption de méthane (CH_4), ils ont mesuré des SS comprises entre 22 500 et 2 500 cm^2/g et observé une décroissance de la SS avec le temps. Ainsi, ils ont montré qu'une couche de neige de 1 m d'épaisseur pouvait séquestrer par adsorption presque la totalité d'un gaz trace adsorbable comme l'acétone, contenu dans une colonne d'air de 300 m de hauteur. Suite à une décroissance de la SS, une importante fraction de ce gaz pouvait être relarguée vers l'atmosphère, augmentant ainsi considérablement sa pression partielle.

Ces différents résultats montrent que la surface spécifique de la neige présente une grande variabilité avec des valeurs comprises entre 77 700 et 60 cm^2/g. Une surface spécifique de 77000 cm^2/g correspond à des sphères de 0.84 µm de diamètre, ce qui semble très petit au vu des nombreuses observations microscopiques de cristaux de neige. Une méthode précise et fiable apparaît donc comme indispensable pour mesurer la SS des divers types de neige, et évaluer précisément l'impact de la couverture neigeuse sur la chimie atmosphérique.

CHAPITRE III

RESULTATS et DISCUSSION

Ce chapitre est consacré aux résultats obtenus durant notre étude. Ils sont présentés sous forme de 6 articles. Nous faisons d'abord une introduction, où nous présentons les différents objectifs de ce travail et en indiquant quel(s) article(s) tente(nt) d'y répondre. Puis, les articles sont proposés tels qu'ils ont été soumis dans les journaux. Ensuite un résumé reprend les points importants de chaque article. Nous finissons par une application atmosphérique où nos données ont été utilisées pour interpréter l'évolution du formaldéhyde dans la neige de l'Arctique (Perrier et al., sous presse).

III.1. Présentation des articles et des différents objectifs de cette étude

Les titres des 6 articles présentés dans ce chapitre sont indiqués ici. Afin de pouvoir s'y référer facilement, nous les avons numérotés de 1 à 6:

1 **Measurement of the specific surface area of 176 snow samples using methane adsorption at 77 K**, *Journal of Geophysical Research*, soumis le 29 Juin 2001, accepté le 04 Février 2002.

2 **Specific surface area of snow samples determined by CH_4 adsorption at 77 K, and estimated by optical microscopy and scanning electron microscopy**, *Environmental. Science and Technology., 35*, 771-780., 2001.

3 **Structure, microphysics, and surface area of the Arctic snowpack near Alert during the ALERT 2000 campaign**, *Atmospheric. Environment*, soumis le 07 Juin 2001, accepté le 01 Décembre 2001.

4 **Evolution of the specific surface area and of crystal morphology of Arctic fresh snow during the ALERT 2000 campaign**, *Atmospheric Environment*, soumis le 07 Juin 2001, accepté le 07 Décembre 2001

5 **Evolution of the specific surface area of surface snow layers**, *Journal of Geophysical Research*, soumis le 02 Octobre 2001.

6 **Evolution of crystal shapes and of the specific surface area of a snowfall determined by scanning electron microscopy and CH_4 adsorption**. Sera soumis prochainement.

La présentation de ce mémoire sous forme de thèse-articles implique certaines redondances inévitables. Ainsi, les premières parties des introductions qui présentent le contexte scientifique ont de nombreuses similitudes. De même, les sites de prélèvement et la méthode d'adsorption sont décrits plusieurs fois. Nous conseillons donc au lecteur de pas lire tous les articles en entier : en ce qui concerne la **méthode d'adsorption de méthane** et son protocole expérimental, une description

détaillée est faite dans l'**article 1**; il n'est donc pas utile de relire son principe dans les autres articles. **Les sites de prélèvement** sont décrits dans la plupart des articles mais nous suggérons de lire la description de l'**article 5** où ils sont tous présentés. Une présentation plus détaillée du site d'Alert (campagne ALERT 2000) est faite dans l'**article 3**. Cet article décrit aussi la **méthode d'échantillonnage** et il n'est pas nécessaire de relire sa description dans les autres articles.

III.1.1. Méthodes expérimentales

Le premier objectif de cette étude était d'avoir une méthode précise et fiable pour déterminer la surface spécifique (SS) de la neige. La méthode d'adsorption de méthane à la température de l'azote liquide (77 K), qui était déjà utilisée au laboratoire (Hanot et Dominé, 1999), était considérée comme la méthode de référence car elle permet de mesurer la surface accessible aux gaz. Bien que le principe de cette méthode soit simple, l'obtention de résultas fiables et reproductibles est délicate car la neige a une surface spécifique faible comparée à d'autres matériaux, et ne dépasse pas 1500 cm^2/g. Ainsi, des artefacts et certaines sources d'erreurs peuvent modifier fortement les mesures de surface spécifique et par conséquent fausser les résultats obtenus. Nous avons donc élaboré un protocole expérimental afin de limiter le risque d'erreur, et de disposer d'une méthode fiable et précise. Ce travail est décrit dans l**'article 1**. Les différents artefacts qui peuvent être rencontrés y sont mentionnés, et un test de fiabilité est également proposé.

Bien que la méthode d'adsorption semble la plus pertinente en ce qui concerne l'étude des échanges de gaz entre le manteau neigeux et l'atmosphère, cette méthode est délicate mais est aussi assez longue : elle nécessite plusieurs heures pour obtenir une mesure de SS. De plus, elle nécessite l'utilisation d'azote liquide qui n'est pas toujours disponible lors de campagne de terrain aux hautes latitudes. Nous avons alors tenté de savoir si l'on pouvait estimer avec une précision suffisante la SS de la neige par une méthode plus rapide et plus simple que la méthode d'adsorption. Nous avons alors comparé la méthode d'adsorption à deux méthodes d'analyse d'images de cristaux isolés obtenues par microscopie optique et par microscopie électronique à balayage (MEB). **L'article 2** a été consacré à ce travail. Quatre échantillons de différents types de neige ont été étudiés par microscopie optique afin d'estimer leur SS. Les résultats obtenus ont été comparés à la méthode d'adsorption considérée comme la plus fiable. Des images obtenues en microscopie électronique à balayage pour deux des quatre échantillons ont également été utilisées pour estimer la SS. Les résultats obtenus indiquent qu'il est possible de déterminer la SS avec ces deux techniques, mais leur précision reste insuffisante comparée à la méthode d'adsorption.

III.1.2. La surface spécifique de la neige

La première question que l'on peut se poser dans cette étude sur la microphysique de la neige, est savoir quelle est la surface spécifique de la neige et quel est son rapport avec son aspect. Les **articles 1** et **2** tentent de répondre à cette question.

Dans l'**article 1**, après avoir décrit le protocole expérimental de la méthode d'adsorption, nous présentons une compilation de tous nos résultats obtenus dans les Alpes et l'Arctique. L'ensemble de nos données, soit 176 mesures de SS, sont regroupées en 14 catégories en fonction du type de neige et de son âge. La SS moyenne de chaque type de neige ainsi que l'écart type ont été mesurés afin de déterminer si une corrélation existe entre un type de neige et sa SS. Pour 13 catégories, nous avons également étudié la corrélation entre la SS de la neige et sa densité. Nos données nous permettent ainsi de proposer une estimation de la SS de la neige dans un intervalle de confiance comprise ente 25 et 40 % suivant le type de neige observé. De plus, dans cet article, nous commentons la précision des différentes méthodes utilisées pour déterminer la SS de la neige, et discutons la validité des mesures de SS obtenues avant notre travail.

Dans, l'**article 2**, où nous avons essayé d'estimer la SS de la neige par deux techniques différentes de la méthode d'adsorption, les photographies de cristaux de neige montrent qu'elles sont utiles dans la compréhension de la SS, et ceci notamment par la microscopie électronique à balayage qui donne un aperçu 3D des cristaux. Il en ressort que la SS de la neige et son évolution, déterminée par adsorption, peut être mieux interprétée si elle est couplée à une méthode d'analyse visuelle appropriée.

On peut s'interroger sur l'impact attendu des processus d'adsorption/désorption sur la chimie atmosphérique. La réponse à une telle question nécessite de connaître quelle est la surface totale développée par le manteau neigeux. La détermination de cette surface totale est notamment proposée dans l'**article 3**. Dans cet article, le principal objectif est de fournir des données permettant de quantifier les processus de surface ayant lieu dans le manteau neigeux, tels que l'adsorption/désorption de composés chimiques, ou les réactions hétérogènes. Ce travail a été effectué à partir des données obtenues à Alert (82°30'N, 62°20'W, Ile d'Ellesmere, Canada) lors de la campagne de terrain ALERT 2000, dont le but était d'étudier l'impact du manteau neigeux sur la chimie de la basse troposphère. La SS et la densité des différentes couches de neige composant le manteau neigeux y ont été étudiées à Alert en février et avril 2000. Ainsi, nous avons pu déterminer la surface totale développée par le manteau neigeux et son évolution au cours du temps. Les données obtenues ont été utilisées pour estimer l'impact potentiel du manteau neigeux sur la chimie atmosphérique. La capacité du manteau neigeux à stocker des gaz traces adsorbés à la surface des cristaux de neige a été déterminée, et le relargage de gaz traces, résultant de la métamorphose du manteau neigeux est également discuté. L'acétone, qui s'adsorbe de manière importante à la surface de la glace, et dont les isothermes d'adsorption ont été mesurées vers 200 K (Rey-Hanot, 1999), a été choisie comme exemple.

Le troisième point essentiel de cette étude est de déterminer quelle est la vitesse d'évolution de la SS de la neige, en particulier pour les neiges récentes et quel sont les mécanismes responsables de cette évolution. Les **articles 4, 5,** et **6** tentent d'apporter des réponses à cette question. Dans l'**article 4**, nous présentons l'étude de la SS et son évolution pour les couches de neige fraîche observées lors de la campagne ALERT 2000. Les couches de neige fraîche situées à la surface du manteau neigeux ont le plus grand potentiel d'interaction avec l'atmosphère et ont aussi un plus grand potentiel d'évolution que les couches de neige plus âgées situées en profondeur, c'est pourquoi nous les avons étudiées en détail. Afin d'interpréter du mieux possible la SS de la neige et son évolution, de nombreuses photographies de cristaux ont été faites pour les nombreux échantillons prélevés. A Alert, la SS de 5 couches de neige fraîche ont été mesurées et l'évolution de 4 d'entre elles a pu être suivie. La décroissance de la SS observée pour chacune d'elle, a été interprétée en suivant les changements morphologiques des cristaux à l'aide de macrophotographies. Dans l'**article 4**, une application atmosphérique montre l'impact des couches de neige de surface sur la répartition d'un gaz trace adsorbable entre l'air et la neige.

Dans l'**article 5**, nous comparons l'évolution de la SS des différentes couches de neige de surface que nous avons étudiées dans les Alpes et l'Arctique. Les 8 couches de neige récente étudiées nous ont permis de proposer une paramétrisation préliminaire de la vitesse d'évolution de la SS de la neige fraîche en fonction de la température. Finalement, l'**article 6** utilise des observations au MEB pour relier le détail des transformations morphologiques au métamorphisme et à la décroissance de la SS.

III.2. Measurement of the specific surface area of 176 snow samples using methane adsorption at 77 K.

La première partie de cet article est consacrée à une description détaillée de la méthode d'adsorption utilisée pour déterminer la surface spécifique de la neige. Bien que le principe de cette méthode soit simple, la mesure de la surface spécifique de la neige reste délicate, et de possibles artefacts peuvent fausser les résultats obtenus. Il nous a donc semblé nécessaire de proposer un protocole expérimental qui permette d'utiliser cette méthode en évitant les possibles sources d'erreur afin d'obtenir des résultats précis et fiables.

Dans la seconde partie, nous présentons une compilation de toutes nos mesures de SS. Celles-ci sont regroupées en 14 catégories en fonction de leur âge et du type de neige. Une corrélation a été observée, et nos données nous permettent de proposer une estimation de la surface spécifique. Une corrélation entre la surface spécifique et la densité de la neige a également été obtenue.

Measurement of the Specific Surface Area of 176 Snow Samples Using Methane Adsorption at 77 K

Loïc Legagneux, Axel Cabanes and Florent Dominé*

CNRS, Laboratoire de Glaciologie et Géophysique de l'Environnement, BP 96, 38402 St Martin d'Hères cedex, France

*Phone: (33) 476 82 42 69; fax: (33) 476 82 42 01; e-mail : florent@glaciog.ujf-grenoble.fr

Abstract

To help quantify exchanges between the atmosphere and the snow cover, we have measured the specific surface area (SSA) of 176 snow samples taken from the seasonal snowpack in the Alps, Svalbard, and the Canadian high Arctic around Alert. A volumetric method was used, and the adsorption isotherm of CH_4 on snow at 77 K was recorded. The data were analyzed by the BET method to yield SSA and ΔQ_{CH4}, the mean heat of adsorption of the first CH_4 monolayer. SSA values obtained were between 100 and 1580 cm^2/g. The reproducibility of the method is estimated at 6%, and the accuracy at 12%. We propose that ΔQ_{CH4} = 2240 $\pm$ 200 J/mol should be used as a criterion of reliability of the measurement. The method is described in detail to promote its use. Aged snow samples have lower SSA than fresh ones. The lowest values were found for faceted crystals and depth hoar, and the highest values for fresh rimed dendritic snow. A method that field investigators can use to estimate SSA from a visual examination of the snow and from a density measurement is suggested. Snow samples are classified into 14 types based on snow age and crystal shapes. Within each type, a density vs. SSA correlation is determined. Our data indicate that, depending on snow type, SSA can then be estimated within 25 to 40 % at the 1σ confidence level with the method proposed. Preliminary data suggest that SSA spatial variability of a given snow layer is low (<5%), but metamorphism can increase it.

Index terms: 1863: Snow and Ice; 3947: Surfaces and interfaces; 0399: General or miscellaneous; 0320: Cloud physics and chemistry

Submitted, JGR, 29 June 2001

Revised, 19 November 2001

Introduction

Some aspects of atmospheric chemistry above snow-covered surfaces are not well understood. Among these aspects is springtime ozone depletion (Barrie et al., 1988). Despite years of investigation, modeling this complex chemistry remains uncertain and the actual role of the snowpack still has to be elucidated (Michalowski et al., 2000). Recently, the interest in studying the impact of the snowpack on the chemical composition of the lower troposphere has increased, because new observations have shown that significant exchanges of reactive trace gases were taking place between the snow and the overlying air. Formaldehyde has been observed to come out of the snowpack in Greenland and in the Canadian high Arctic (Hutterli et al., 1999; Sumner and Shepson, 1999). Fluxes of acetaldehyde and acetone coming out of the seasonal snow cover in Michigan were measured by Couch et al. (2000). Various nitrogen oxides were also observed to be exchanged between the snow and the atmosphere in Greenland and Antarctica (Dibb et al., 1998; Honrath et al., 1999; Weller et al, 1999). Ozone was found to be destroyed in snow (Peterson and Honrath, 2000). Snow chamber experiments, where air of controlled composition was passed through snow, confirmed that emission of carbonyls and nitrogen oxides by snow was taking place (Couch et al., 2000, Honrath et al., 2000).

Thus, because snow can cover up to 50% of land masses in the northern hemisphere (Robinson et al. 1993, Frei and Robinson, 1998), the impact that this ground cover may have on the chemical composition of the lower troposphere is potentially very important on a global scale. The main reason why an accurate and reliable model of atmospheric chemistry in the presence of a snow cover does not exist is because the processes involved are not understood (Michalowski et al., 2000). These processes include adsorption/desorption from the snow surface, that have been invoked to explain formaldehyde emission (Hutterli et al., 1999), photolysis of a dissolved precursor that has been postulated as the source of NO_x coming out of the snow (Honrath et al., 1999; Weller et al, 1999), and which has been confirmed by laboratory experiments (Honrath et al., 2000), co-condensation of trace gases with water vapor, with subsequent sublimation of the solid solution formed (Weller et al., 1999) and solid state diffusion in and out of ice crystals (Dominé and Thibert, 1996; Thibert and Dominé, 1998).

Determining which process is predominant requires the quantification of each one of them, which will necessitate many careful studies. The purpose of this study is to help quantify adsorption/desorption processes and the rates of heterogeneous reactions by reporting data that will aid in evaluating the surface area (SA) of a given volume of snow. By surface area we mean, following Gregg and Sing (1982) the area of snow that is accessible to gases, and this area is expressed in m^2, or cm^2 for small values. The SA of snow is evaluated from the measurement of the specific surface area (SSA) of snow samples, i.e. the SA of the sample divided by its mass, and this is expressed in m^2/g, or rather in cm^2/g as values of SSA for snow have been found to be small. The product of the density, SSA, and volume of the snow under consideration yields the SA of the snow. Values of snow SA, together with the knowledge of the adsorption isotherms of the atmospheric trace gas of interest on ice, can be used to quantify the amounts of trace gases adsorbed on ice, and the rates of heterogeneous reactions.

The method used here to measure snow SSA is CH_4 adsorption at 77 K. The principle and merits of this method have been briefly described in previous publications (Hanot and Dominé, 1999, Dominé et

al., 2000 and 2001), and we believe that it can yield reliable and reproducible results, and that it is perhaps one of the fastest methods to obtain SSA values. Although the principle of the method is simple, performing reliable measurements is delicate, and we wish to report here a detailed protocol, propose selected values of parameters that could *a priori* be chosen somewhat arbitrarily in data analysis, suggest reliability tests and mention commonly encountered artifacts, so that other authors can use this method to obtain results that can be inter-compared with ours.

Another objective of this work is to report the results of 176 snow SSA measurements, performed in the Alps and in the Arctic, and to attempt to find a correlation between snow types and SSA values, so that the values reported here can be used to estimate the SA of snow encountered in field studies.

Experimental methods

Principle of the method

To determine snow SSA, the adsorption isotherm of CH_4 on the snow sample, is measured at liquid nitrogen temperature (77.15 K at atmospheric pressure), using a volumetric method (Gregg and Sing, 1982). The isotherm is then analyzed using a BET method (Brunauer et al., 1938) to obtain the SA of the sample and the net heat of adsorption of CH_4 on ice, ΔQ_{CH4}.

Most SA measurements using the volumetric method have dealt with materials of high SSA and used N_2 as the adsorbent (Gregg and Sing, 1982). The use of a commercial apparatus designed for high SSA materials to measure snow SSA, has been attempted by Hoff et al. (1998), but as mentioned in Hanot and Dominé (1999), numerous artifacts were encountered in that study, resulting in large errors. Because snow samples used here had a SA of only about 1 m^2, modifications had to be made to the conventional volumetric apparatus. The apparatus used and the protocol followed have been briefly described in Chaix et al. (1996), and in Hanot and Dominé (1999), and will be discussed in more detail here. The apparatus is shown in Figure 1.

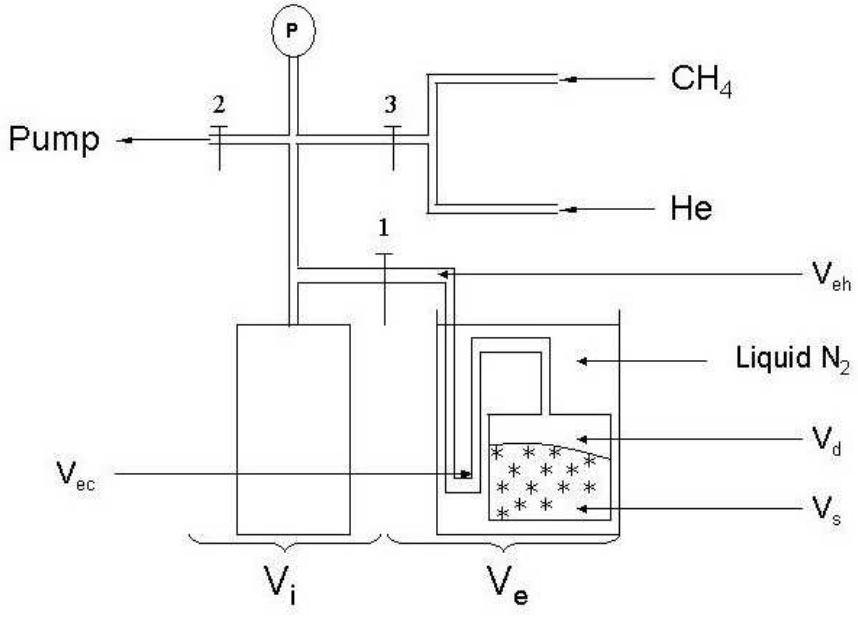

Figure 1 : Experimental setup. The introduction volume V_i is delimited by valves 1 to 3 and is at room temperature. The expansion volume V_e consists of V_{eh} at ambient temperature and V_{ec} at 77 K. V_{ec} is subdivided into the snow volume V_s and the dead volume V_d. P is the manometer.

It consists of an introduction volume V_i kept at room temperature and connected to a capacitance manometer (MKS Baratron, 10 Torr full scale) and to an expansion volume V_e that contains the snow sample and is immersed in liquid N_2.

The adsorption isotherm is recorded as follows. A given pressure of CH_4, P'_1, is introduced into V_i. Knowing V_i and P'_1, the number of molecules of CH_4 in V_i, N'_1, is calculated using the ideal gas equation. The valve between V_i and V_e is then opened. The CH_4 pressure drops due to expansion and adsorption. The new pressure, P''_1, is used to calculate N''_1, the number of CH_4 molecules still in the gas phase. The number of adsorbed molecules after this first CH_4 increment is then $N_{ads1} = N'_1 - N''_1$. Further increments are added and the total number of molecules adsorbed after the addition of n increments of CH_4 is :

$$N_{ntads} = \left(\frac{V_i}{R \cdot T_h} \times \sum_1^n (P'_k - P''_k) - \frac{P''_n}{R} \times \left(\frac{V_{eh}}{T_h} + \frac{V_d}{T_c} \right) \right) \times A \qquad (1)$$

where R, A, T_h, T_c, are respectively the ideal gas constant, the Avogadro number, the ambient and liquid nitrogen temperature. V_{eh} is the part of the expansion volume that is at room temperature, and V_d is the dead volume (see figure 1 for details). P'_k and P''_k are the pressures before and after expansion of gas increment k.

The adsorption isotherm can then be plotted, and an example is shown in Figure 2. The adsorption isotherm is of type II in the classification of Brunauer et al. (1940) and lends itself to the BET treatment (Brunauer et al., 1938).

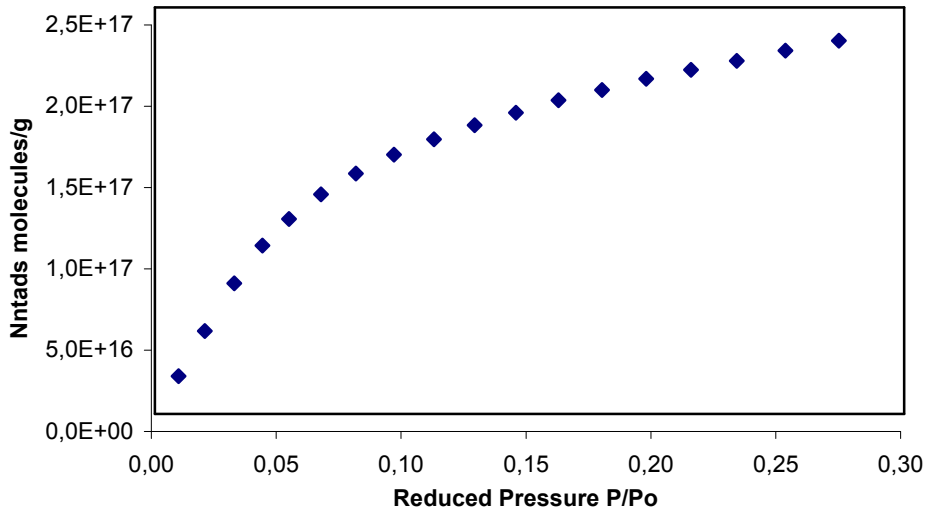

Figure 2: Example of an adsorption isotherm of CH_4 on snow. The number of molecules adsorbed per gram of snow, N_{ntads}, is plotted as a function of the reduced CH_4 pressure, P/P_0, where P_0 is the saturating vapor pressure at liquid nitrogen temperature.

Briefly, a function $Y=f(P_{CH4}/P_0)$ is plotted where P_0 is the saturating vapor pressure of CH_4 at liquid nitrogen temperature. The plot of Y yields a linear portion, whose slope S and intercept I, yield the

monolayer capacity of the sample, $N_m=1/(S+I)$, and the so-called BET constant, $C=(S+I)/I$. The SA of the sample is then deduced as $SA=N_m*\sigma_m$ where $\sigma_m=19.18\ 10^{-20}$ m^2 (Chaix et al., 1996) is the molecular cross sectional surface area of CH_4 on ice. The net heat of adsorption of CH_4 on snow, ΔQ_{CH4}, i.e. the mean heat of adsorption of the first CH_4 monolayer, can also be derived from $\Delta Q_{CH4}=RT*\ln(C)$ where R is the gas constant.The mass of the snow sample is then determined by weighing, and the SSA is obtained as the ratio of SA over mass. The BET transform of the isotherm of Figure 2 is shown in Figure 3. The linear part is roughly in the relative pressure P/P_0 region 0.07 to 0.22.

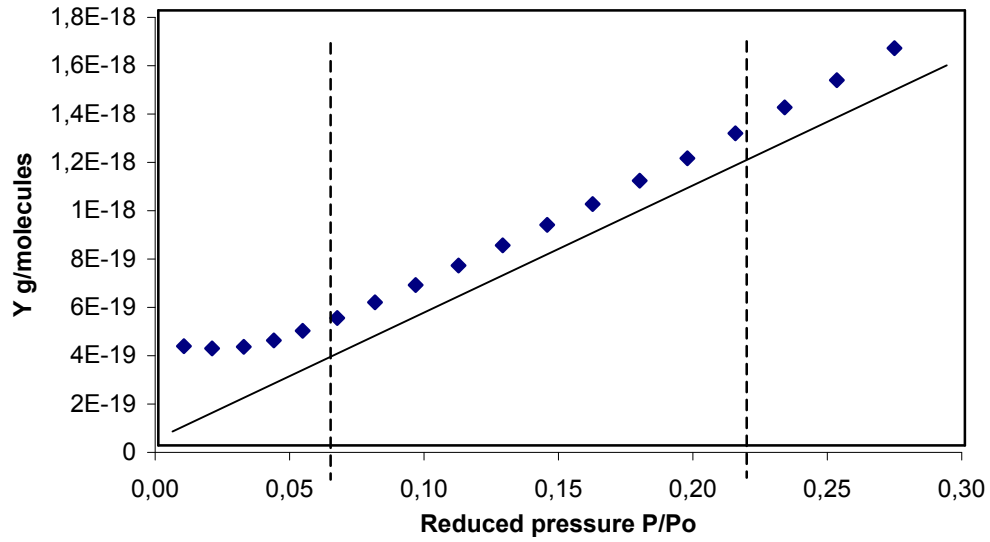

Figure 3: BET transform of the isotherm of Figure 2. A linear portion can be seen. The least square fit in the P/P_0 region 0.07 to 0.22 is shown, and has been used to obtain the snow sample SA and ΔQ_{CH4}. The ordinate Y is the BET transform.

Apparatus and data treatment optimization

Measuring small SA values required changes to the standard volumetric equipment. First of all, CH_4 was used as the adsorbent rather than N_2 for 5 main reasons. (i) Its low saturating vapor pressure, $P_0=1294$ Pa justifies the use of the ideal gas equation without any correction. (ii) Low pressures minimize the amount of CH_4 used, which is an advantage for field campaigns in remote areas. (iii) The low P_0 means that smaller amounts of CH_4 than N_2 need to be introduced into V_e, thus reducing the risk of snow annealing by expansion of a warm gas. (iv) The low P_0 also means that relative pressure changes will be greater than for N_2, which will improve the accuracy of the measurements. This aspect was found to be crucial to obtain quality measurements. (v) Methane is a spherical molecule that has neither a dipole nor a quadrupole moment, in agreement with the approximations of the BET theory (Brunauer et al., 1938).

Another important aspect is the ratio V_i/V_e, which must be chosen adequately to optimize data quality. Two opposite effects come into play to determine the optimum ratio. (i) if V_i is too high, expanding the gas from V_i to V_e will not change the pressure enough to produce a detectable effect on the manometer. This loss of sensitivity will also increase the impact of the manometer thermal drift: a drift of one unit will represent a larger proportion of the pressure change, which will decrease data reliability. (ii) if V_i is instead too small, reaching the pressure required to use the BET treatment would

necessitate more increments. Since errors caused by each increment add up, a small V_i will increase the uncertainty.

Determining the optimum ratio by considering equations is not simple. Moreover, the optimum is different for each snow sample, as what actually comes into play is not V_e, but the dead volume $V_d=V_e-V_s$, where V_s is the snow volume, and V_d varies with each snow sample. The expansion ratio P'/P'' during adsorption also comes into play and varies with each snow sample as it depends on sample SA. Empirically, we observed that using V_i/V_e between 0.5 and 2 gave good quality data. The apparatus used to obtain most of the data presented here used V_i= 287.3 cm^3 and V_e=263.3 cm^3, and the volumes were connected by a tubing with a 4 mm inner diameter, which is sufficiently large to avoid thermal transpiration problems, as detailed in the next section.

The use of the BET treatment requires the selection of a linear P/P_0 range in the BET transform (Figure 3). This selection, and the number of data points obtained in this portion of the isotherm are somewhat arbitrary. Both SA and ΔQ_{CH4} were slightly affected by the selection of the linear range. It is essential to propose a range that is common to all experimentalists to facilitate intercomparisons and to allow a test of the reliability of the measurements. Moreover, Dominé et al. (2000) proposed that the value of ΔQ_{CH4} could be used to test the reliability of SA measurements. If this test is to be reliable, then arbitrary choices that cause variations in ΔQ_{CH4} must be minimized.

By searching the optimum correlation coefficient of the least squares fit of the BET transform, it appeared that the best range for P/P_0 was 0.07 to 0.22. The number of data points within this range is also important. It has to be sufficient to obtain a reliable fit, but since errors add up at each data point, there is also an optimum number. Using 9 data points within this P/P_0 range was found to be a good compromise and we recommend using this number. Under those conditions, 176 measurements done by 2 different experimentalists yielded $\Delta Q_{CH4} \pm \sigma$ = 2240 $\pm$ 100 J/mol. We then recommend $\Delta Q_{CH4} \pm \sigma$ = 2240 $\pm$ 200 J/mol as a test of measurement reliability. Shifting the P/P_0 range by 0.02 induced about 3% changes in ΔQ and 2% changes in SSA. Dominé et al (2000), based on a limited data set, had temporarily proposed ΔQ_{CH4} = 2100 $\pm$ 150 J/mol. The new recommendation is consistent with the previous one, but is based on a much larger data set.

Common artifacts and sources of errors

Artifacts and large sources of error can be encountered at several stages of SSA measurements with the present method. These include the formation of amorphous ice of very high surface area during sample cooling, snow annealing by rapid injection of warm gas, perturbation of the snow during sampling, errors in temperature measurements or temperature instabilities, errors in pressure measurements, and errors in the determination of the dead volume above the snow. These are detailed below.

Amorphous ice formed at 77 K is micro-porous and can have a SSA of several hundred m^2/g (Mayer and Pletzer, 1987). Because our snow samples had SA around 1 m^2, even the formation of a small fraction of a gram of amorphous ice can considerably increase the SA of the sample. SSA values found were between 100 and 1580 cm^2/g. Values above about 5000 cm^2/g should in general be

considered suspect and a desorption isotherm should then be measured to check for the presence of porosity. For example, the snow used to obtain the hysteresis loop of Figure 4 was aged hard wind-packed snow, with an expected SSA around 200 cm^2/g. The SSA found was 20 800 cm^2/g, which led us to measure desorption. An examination of the snow under a microscope is another method to check the validity of a very high SSA (Dominé et al., 2001).

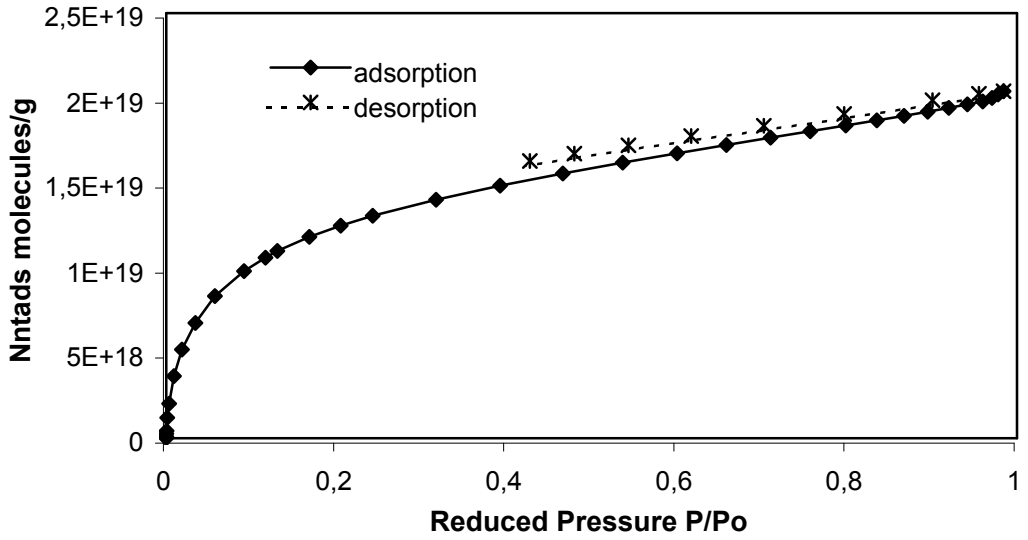

Figure 4: Hysteresys loop on an adsorption isotherm, revealing the presence of microporous ice formed during the cooling of a snow sample under a low gas pressure.

Micro-porous ice could be formed by the condensation of the water vapor in equilibrium with the snow in the container. However, simple calculations show that the amount of water vapor present in the expansion volume is much too small to yield detectable amounts of microporous ice. On the contrary, when the container with the snow sample is immersed in liquid nitrogen, large temperature gradients are established, that produce water vapor gradients and fluxes. To avoid amorphous ice formation water vapor fluxes must be limited (Kouchi et al., 1994), and the snow sample must be cooled under a total pressure of about one atmosphere. The water vapor flux is proportional to the diffusion coefficient of water vapor in the gas filling the container, and this is inversely proportional to the total pressure. Keeping the snow under atmospheric pressure during cooling was found to be sufficient to prevent the formation of detectable amounts of microporous ice. The fact that optical and electron microscopy images of the snow yielded reasonable estimates of the SSA measured by CH_4 adsorption (Dominé et al., 2001) also supports the fact that microporous ice formation can indeed be prevented by following this simple protocol.

In our system, V_i is at room temperature rather than at 77K to minimize liquid N_2 consumption during field experiments. Repeated injections of warm gas during adsorption measurements could anneal the snow and reduce its SSA. This was avoided by inserting a U-shaped tubing, that was immersed in liquid N_2, between V_i and V_e (see Figure 1). The efficiency of this procedure was checked by measuring several consecutive isotherms, and observing no changes in SSA.

Sampling can perturb Snow. Appropriate sampling must preserve the structure of snow. Breaking fresh snow crystals, creating new contacts between snow grains by packing, and creating new surfaces by loosening up sintered grains must be avoided. For example, hard dense snow has to be

broken into pieces to be inserted into the container. The maximum impact of breaking up hard snow on its SSA was measured. A very hard wind-packed snow layer with a density of 0.48, near the surface of the Arctic snowpack, was used. The snow was sampled in 2 ways: (i) the container was filled by loosening up grains from the vertical face of a pit dug in this snow layer. (ii) large chunks, of at least 2 cm^3 were broken up and inserted into the container; any small grains that may have inadvertently been placed in the container were removed by placing the container upside down. The first sampling method yielded a SSA of 312 cm^2/g, while the second one yielded 147 cm^2/g, showing that great care must be taken while sampling. No tests have been performed to evaluate the effect of packing fresh snow into a container on its SSA, but we checked on several occasions that density increases of fresh snow due to careful sampling were less than 10 %, and we then suggest that careful sampling of fresh snow can minimize the creation of extra contacts between snow crystals.

Drifts in the manometer gain can cause a systematic error in the pressure measurement. An ambient temperature different from that at which the manometer was calibrated can cause such drifts. We tested the effect of a systematic pressure error of the type given in eq. (2) on SSA and ΔQ_{CH4}.

$$P_{Measured} = (1+\alpha) \times P_{real} \qquad (2)$$

Table 1 shows the effect of systematic errors of 0.5% and 2% on the manometer reading, caused by gain drift.

Table 1: Simulated impact of variations in the manometer gain on SSA and ΔQ_{CH4}. α is defined in eq.(2).

α	SSA=125 cm²/g		SSA =400 cm²/g		SSA =800 cm²/g	
	$\Delta(\Delta Q)$	Δ SSA	$\Delta(\Delta Q)$	Δ SSA	$\Delta(\Delta Q)$	Δ SSA
α = 0.5%	-0.05%	0.3%	-0.01%	0.3%	0.01%	0.3%
α = 2%	-0.1%	1.3%	-0.03%	1.2%	0.04%	1.3%

The test was performed on snow samples of low to moderately high SSA. Table 1 shows that even large systematic pressure errors result in errors on SSA that are 1.3 % at the most.

As our method relies on pressure measurements and molar budgets using the ideal gas equation, errors caused by temperature measurements need to be investigated. A sensitivity analysis showed that a 1.5°C error on the ambient temperature resulted in a 0.5% error on the SSA and no detectable error on ΔQ_{CH4}. Random temperature variations during the isotherm measurement, or temperature variations between the measurements of the dead volume and the isotherm can also cause errors that will be greater for samples with low SA. Using a sensitivity analysis, it was found that variations of 0.3°C between the measurement of the dead volume and of the isotherm caused errors on SSA of 0.7 % for an SA of 1.9 m^2, and caused an error of 2.5% for a SA of 0.64 m^2. Errors about half as large were observed on ΔQ_{CH4}. It is then clear that a stable temperature is crucial, while an accurate measurement of ambient temperature is much less important. We recommend maintaining the temperature constant within $\pm$ 0.3 K for accurate measurements. Using a thermostated manometer caused more problems than it solved, because it produced temperature gradients in the line connecting V_i to the manometer, and an accurate molar budget was then difficult to perform.

Temperature gradients exist in the tubing connecting V_i and V_e, and this can result in an error in the molar budget, as detailed in Dominé et al. (2000). In the present system, this tubing had an inner diameter of 4 mm. Thus, the volume where a temperature gradient is present was only about 1 cm^3, while the total volume was 600 cm^3, and the error caused by this transition volume is negligible. Thermal transpiration has negligible effects here, as detailed in Dominé et al. (2000). The mean free path of CH_4 at 0.1 Torr is about 0.45 mm at 298 K, and half as much at 77 K, and this is much smaller than the tubing diameter.

V_d is measured by expanding helium from V_i to V_i+V_d. Helium does not adsorb on ice at 77 K (Haas et al., 1971). Consecutive measurements of V_d usually yielded increasing values that stabilized after 2 or 3 operations. During the first measurement, pressure P' before expansion stabilized fast, within 10 seconds, whereas pressure P" after expansion sometimes kept decreasing for 10 minutes. This effect could be caused by : (i) helium diffusion into the ice lattice (Klinger and Ocampo, 1983); (ii) the presence of small amounts of water vapor inside the part of the expansion volume at room temperature V_{eh} ; (iii) too short thermalization times. The first cause (i) had to be discarded. Using the data of Haas et al. (1971), we found that the pressure decrease due to diffusion should be $5x10^{-5}$ Pa at the most, which is well below the manometer detection limit. Cause (ii) could be caused by snow being entrained during the evacuation of V_e. The snow that would be in V_{eh} would then melt. Its evaporation would increase the pressure. This pressure increase would be reduced with time because of cryo-pumping. The amount of water would decrease at each measurement of V_d, thus resulting in increasing measured values. Careful and slow evacuation of V_e can suppress this problem. Careful tests showed that perfect thermalization is in fact quite slow, and we conclude that the main cause is (iii), though (ii) could occasionally enhance the problem in the case of very light snow.

An accurate measurement of V_d is crucial. Figures 5 and 6 show the simulated impacts of errors on V_d on the measured values of SA and ΔQ_{CH4}.

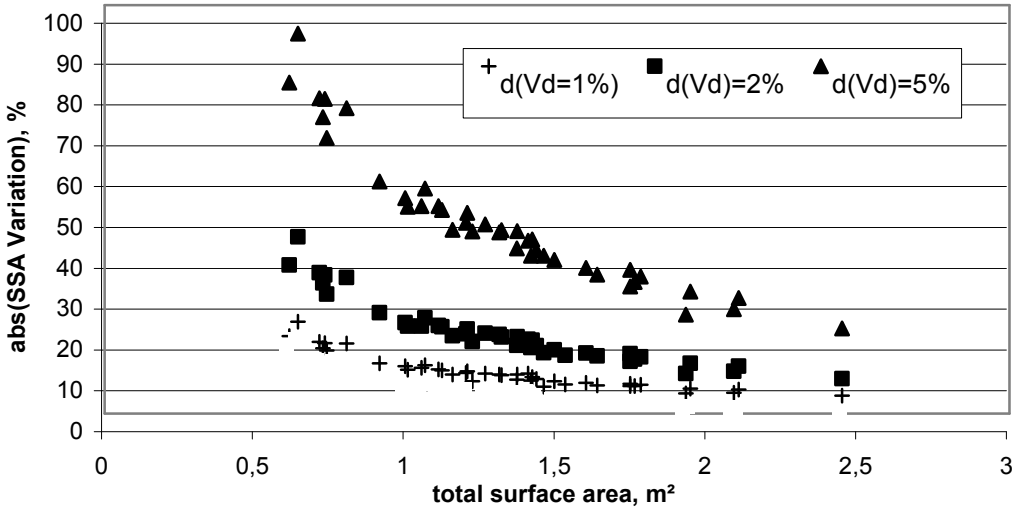

Figure 5: Sensitivity of the SSA value on the error on the dead volume V_d, vs. sample surface area. A positive error on V_d leads to a negative error on SSA.

This was done by changing the value of V_d used in the calculations. Since most SA values were around 1 m^2, it appears that errors on V_d are amplified at least tenfold in the final SA and ΔQ_{CH4}

determination. In most of our measurements, the standard deviation on V_d was 0.1% or better. Therefore, the uncertainty on SA and ΔQ_{CH4} caused by errors on V_d were usually around 1%.

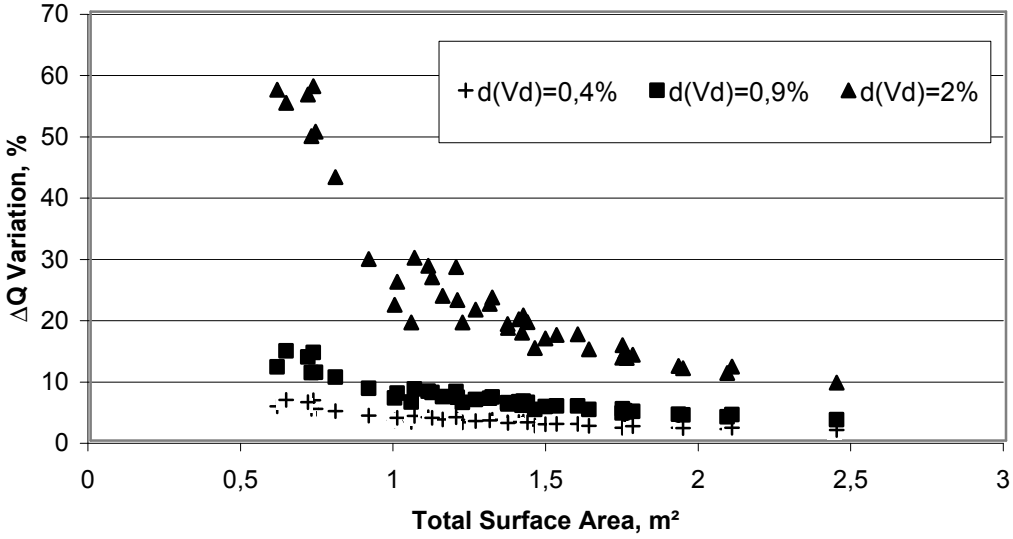

Figure 6: Sensitivity of the ΔQ_{CH4} value on the error on the dead volume V_d, vs. sample surface area.

The importance of an accurate measurement of V_d is illustrated by the work of Hoff et al. (1998). Those authors used a commercial volumetric apparatus to measure the SSA of fresh snow samples using N_2 adsorption. They had difficulties to measure directly V_d and estimated it using 2 different methods. In both methods, they had to neglect the closed porosity of the snow. It is well known that snow crystals almost always contain air bubbles that reduce the density (see e.g. Dominé et al., 2001). Thus, Hoff et al. (1998) overestimated V_d, which should introduce a bias in the ΔQ value. The sign of this bias depends on the experimental setup. This apparently significantly affected their ΔQ_{N2} values, which are systematically much lower than the recommended value ΔQ_{N2}=2700 J/mol (Dominé et al., 2000). Note that measurement inaccuracies are enhanced by the use of N_2 rather than CH_4, as detailed above.

To conclude on the measurement of V_d, we found that the most reliable method was to perform repeated measurements until a stable V_d value was obtained. It is crucial that the ambient temperature remains stable during the measurement of both V_d and the adsorption isotherm.

Reproducibility and accuracy

Tests were conducted on snow sampled at Les deux Alpes, about 50 km E-SE of Grenoble to determine the reproducibility of our method. Results are presented in Table 2.

Table 2 : Summary of reproducibility tests.

Experimentalist	Sample	Mass	V_d	ΔQ	SSA	Total SA
		g	cm^3	J/mol	cm^2/g	m^2
1			212.2	2294	240	0.989
2			212.8	2276	240	0.989
2			212.6	2274	238	0.981
2	1	41.2	212.7	2200	235	0.968
2			213.0	2244	233	0.960
2			212.7	2207	239	0.985
2			212.6	2265	235	0.968
1			225.7	2278	261	0.934
2			225.9	2232	266	0.952
1			225.7	2276	257	0.920
1	2	35.8	225.6	2305	256	0.916
1			225.6	2285	263	0.942
1			225.5	2247	264	0.945
1		26.9	228.4	2362	307	0.826
2	3		228.4	2248	311	0.837
1		28.1	233.6	2345	327	0.919
2	4		234.5	2306	317	0.891
1		48.1	206.6	2329	266	1.279
2	5		207.1	2331	256	1.231
1		26.5	236.0	2289	326	0.864
2	6		237.0	2317	307	0.814
1		39.2	214.4	2286	269	1.054
2	7		215.5	2298	255	1.000

Three points were investigated.

1) The repeatability of a measurement performed by a given experimentalist on a given sample. Experimentalist 1 performed 5 measurements on sample 2, and obtained a standard deviation σ=1.2% on the SSA. Experimentalist 2 performed 6 measurements on sample 1, and obtained σ=1.4%. Repeatability is then 2σ= 2.8% or better.

2) The reproducibility of the measurement performed by two different experimentalists on the same sample. 7 samples were analyzed successively by each of the 2 experimentalists yielding a reproducibility of 2σ=6.3%. We derived the reproducibility 2σ as:

$$2\times\sigma = 2\times\sqrt{\left(\frac{1}{7}\times\sum_{k=1}^{7}\left(\left(\frac{\Delta SSA}{SSA}\right)_m-\left(\frac{\Delta SSA}{SSA}\right)_k\right)^2\right)} \qquad (3)$$

where $(\Delta SSA/SSA)_k$ is the difference between the values obtained by both experimentalists for sample k, and $(\Delta SSA/SSA)_m$ is the mean of all $(\Delta SSA/SSA)_k$ value, and is 2.3%.
These results call two comments: (i) There is a positive correlation between the difference in V_d and the difference in SSA measured by both experimentalists, which confirms that an accurate determination of V_d is critical to obtain reliable results. (ii) For these measurements, special care was taken to always select the same P/P_0 range, with the same number of points, and to follow the various recommendations made above as closely as possible. The value of ΔQ_{CH4} obtained from this data set is 2280 ± 40 J/mol, in agreement with our current recommendation. The low standard deviation supports the importance of our previous recommendations, and the slightly higher value may actually be closer to the real value, but this should be confirmed by more measurements.

To evaluate the total uncertainty on our SSA measurements, the contribution of systematic errors that are inherent to the BET method must also be included. The method accuracy is limited by the knowledge of the molecular surface area, by the choice of the BET linear part, and by the approximations of the BET theory, which include: (i) all the adsorbed layers but the first one are equivalent, (ii) the molecular surface area a_m does not depend on the adsorbent/adsorbate and adsorbate/adsorbate interactions. Following Gregg and Sing (1982), we estimate the systematic uncertainty at about 10%, even though some tests on well characterized solids showed that in some cases, systematic errors as low as 2% could be obtained.

The overall uncertainty on the SSA for a given sample is then:

$$\textit{Total uncertainty} = \sqrt{\left(\textit{Reproducibility}^2 + \textit{Systematic error}^2\right)} = 12\% \qquad (4)$$

Density measurements

Density was measured as often as possible to investigate SSA-density correlations. In most cases, this was done by weighing snow samples whose volumes were known by the use of a calbrated sampling volume. In this case, the accuracy is 5 to 10%, depending on the snow type. For thin surface layers (i.e. less than 5 mm) resting on hard wind packed layers, as often encountered in the Arctic, 400 cm^2 of snow were scraped and weighted, after the thickness had been measured in about 10

spots within the 400 cm^2 sampled (Dominé et al., submitted). The accuracy is then estimated at 15 to 20 %. For very irregular or very thin layers, density could not be measured. Upper limits of density were nevertheless obtained in some of these cases by scraping snow into a calibrated volume.

Results

Measured values of snow SSA

The SSA of 176 snow samples were measured. 85 were collected in the French Alps between 1998 and 2001, 58 were collected near Alert, Canadian Arctic, during the ALERT2000 campaign in February and April 2000, and 33 were collected in Ny-Alesund, Svalbard, during the NICE campaign in April-May 2001. Not all snow types were encountered. Our purpose here will be to present our data in such a way that it can help scientists to estimate, within a factor of 2 or better, the SSA of snow observed in the field. To that end, empirical correlations will be used. The 2 correlations used will be between SSA and snow types, and between SSA and density.

Snow samples were first classified according to their age. This is justified by the observation that SSA almost always decreased with time. Then, snow samples of a given age range were further subdivided according to crystal shapes. Table 3 shows SSA values obtained for the snow types studied. Figure 7 shows photomacrographs of most snow types.

The nomenclature of Table 3, and the classification used call several comments. Classifications of snow crystals have already been proposed by Sommerfeld and LaChapelle (1970) and by Colbeck (1986) among others, and these should in principle be respected. However, we had difficulties applying them to our problem. For example, Type I of Colbeck (1986) is “precipitation” and is not very detailed, while we found that dendritic snow had often higher SSA than plates or needles, and there is clearly a need for us to separate these 2 types. Also, we believe that it is often easier to use a classification that does not require the knowledge of the metamorphic history of the snow. The snow types chosen are therefore based on a cursory visual examination of the snow in the field, with the help of a magnifying glass. We then propose a classification with 14 types, illustrated by pictures shown in Figures 7. This classification is in no way meant to be substituted to existing ones. First of all, it is not complete, as not all snow types were encountered, and second it is intended to be applied to our purpose, i.e. the rapid estimation, in the field, of the SSA of observed snow samples.

The first classification criterion is the age of the snow. Freshly fallen snow is snow sampled within 24 hours of its fall, and usually much less. Freshly fallen snow was subdivided into dendritic snow, columns and bullet combinations as often observed in the arctic under cold (< -25°C) conditions, plates, columns and needles, observed in the Alps and the Arctic under moderate temperature conditions, and wet snow, i.e. snow falling when the air temperature was >0°C. This last type includes all shapes, and this is justified by the assumption that melting removes rapidly all small structures, that are expected to explain a large part of SSA variations from one type to the other. It was usually not simple to optically distinguish wet fresh snow from dry fresh snow, and the criterion actually used is the air temperature. This appears meaningful, however, as this type has the lowest mean SSA value.

These 4 types are numbered F1 to F4 (F stands for fresh). Except for the wet character, a visual determination of these types is usually trivial. Dendritic snow in most cases had some observable rime, but no classification according to the degree of riming was attempted, as this is difficult to evaluate accurately. Cold Arctic columns and bullets never had rime. Small plates, needles and columns usually had little or no rime. One precipitation in Svalbard consisted of heavily rimed needles, that fell at T>0°C, and had a SSA of 672 cm^2/g. Another one consisted of a mixture of rimed stellar crystals and columns and had a SSA of 853 cm^2/g.

The second group is snow with recognizable particles. It refers to snow still near the surface that is more than one day old, and that usually already shows signs of metamorphism, such as rounding of

Table 3. SSA values of 176 snow samples classified into 14 types

Type group	Type	SSA cm^2/g	Mean SSA $\pm \sigma_{SSA}$	Type code	Figure
Freshly fallen Snow	Dendritic, from lightly rimed to graupel (Arctic, Alps)	1527; 1300; 1070; 1028; 1022; 730; 690; 666; 627	962 ± 310	F1	7a
	Columns, bullet combinations (Arctic,T<-25°C)	1460; 802; 779; 770	953 ± 340	F2	7a
	Plates, needles and columns (Alps, Arctic)	1580; 853; 840; 800; 780; 714; 700; 650; 640; 630; 620; 610; 600; 600; 600; 560; 530; 500; 470; 440; 430; 430; 400; 400; 360	629 ± 240	F3	7a
	Air Temperature Above 0°C (Alps, Arctic)	672; 594; 489; 400	539 ± 120	F4	n.t.*
Snow with recognizable particles	Dendritic, Variably rimed (Alps, Arctic)	1015; 579; 575; 540; 470; 456; 435; 410; 400; 329; 257	497 ± 200	R1	7a
	Columns, bullet combinations (Arctic)	770; 760; 725; 690; 690; 680; 608; 600; 570; 560; 550; 535; 530; 500; 460; 452; 444; 439; 408; 405; 404; 357; 341; 341; 326	526 ± 140	R2	7b
	Plates, needles and columns (Alps, Arctic)	670; 607; 600; 560; 500; 499; 495; 470; 450; 430; 420; 391; 376; 374; 370; 350; 340; 324; 322; 322; 317; 313; 309; 300; 290; 290; 288; 280; 270; 262; 261; 261; 257; 237; 180	373 ± 120	R3	7b
	Wet snow (Alps)	550; 290	420 ± 180	R4	n.a.§
Aged snow, no more recognizable particles	Mostly rounded grains (Alps, Arctic)	400; 380; 370; 280; 270; 270; 263; 252; 240; 216; 187; 168; 150; 150; 146	249 ± 80	A1	7b
	Mostly facetted crystals (Alps, Arctic)	231; 174; 170; 168; 161; 161; 146; 136; 134; 130; 127; 116; 113; 106; 101; 100	151 ± 50	A2	7b
	Depth hoar (Arctic)	240; 200; 175; 171; 160; 150; 132; 123; 113	163 ± 40	A3	7b
	Melt-freeze layer or sun crust (Alps)	300; 290; 270; 270; 260; 260; 250; 240; 240; 225; 220; 180; 134; 118	233 ± 50	A4	7b
Surface hoar (Arctic)		590; 354; 316; 315	394 ± 130	S1	7a
Airborne or recently wind-blown (Alps, Arctic)		650; 473; 408	510 ± 130	W1	n.t.*

*n.t. Snow crystals of these types can have any shape. No typical picture exists.
§n.a. Photograph not available.

edges or the disappearance of microstructure (Cabanes et al., in press). Under cold weather, snow that is up to 20 days old can sometimes still belong to this group. Types are the same as in the case of fresh snow, and are numbered R1 to R4 (R stands for recent, or recognizable).

The third group is aged snow without recognizable particles. It refers to very metamorphosed snow that can be in very deep layers or near the surface, and where the initial precipitation type cannot be recognized. Types are based on crystals shape, which are determined by metamorphic history. Depth hoar is the result of high temperature gradient metamorphism (Marbouty, 1980) and consists of large faceted crystals, with at least some of them cup-shaped and hollow. The density of this type was always <0.25. Faceted crystals are produced by metamorphism of lower temperature gradient, and usually form in snow with density >0.25, that is too high to allow depth hoar formation. Facets are clearly visible, but rounded edges were almost always present, and often formed a large fraction of the visible shapes. This type contains very few or no hollow shapes. Snow with rounded grains show a predominance of rounded shapes, but facets were almost always present, so that the border between these latter 2 types is not well defined and will certainly depend on the observer. Table 3 clearly shows, however, that faceted crystals have lower SSA than rounded grains. In the Arctic, snow with rounded grains had usually been hard wind-packed, grains were highly sintered and formed hard layers, sometimes so hard that even a pencil could not penetrate them. In the Alps, such snow could also be formed by low temperature gradient metamorphism over extended periods. Finally, aged snow samples that had been subjected to melting episodes were sampled in the Alps. These 4 aged snow sub-types are numbered A1 to A4 (A stands for aged).

Surface hoar has been classified separately (type S1, S standing for surface). It consists of readily recognizable particles that in the cases studied, formed continuously, and is therefore composed of both recent crystals and older ones. No buried surface hoar was studied. The sample with SSA=590 cm^2/g was actually hoar frost growing at Alert on antenna guy wires in February, about 2 m above the ground (Cabanes et al., in press). Surface hoar was forming at the same time, but much slower and could not be sampled separately from surface snow. Photomacrographs suggest that hoar frost and surface hoar were similar in structure, and the evolution in SSA of surface snow appears consistent with the suggestion that hoar frost and surface hoar had similar SSA (Cabanes et al., in press), but we are not entirely certain that this similarity is real. The other 3 surface hoar samples came from April arctic campaigns, and consisted of long feather-shaped crystals, as shown in figure 7. Surface hoar formed by large clusters of hexagonal, hollow crystals were observed in the Alps, but are not discussed here. Feather-shaped surface hoar is numbered S1, thus leaving room for additional types.

The last type consists of snow being wind-blown, or very recently deposited by wind. The sample with SSA=650 cm^2/g was sampled in February at Alert while airborne, and this was done by placing a container on the snow surface, with its opening facing the wind, and letting the wind fill the container. This sample consisted of a mixture of many layers. A small fraction of the crystals could be recognized as rounded and broken surface hoar, columns, and bullets. The other samples were taken after being deposited by wind, but before efficient sintering had taken place. This type is numbered W1, W standing for wind.

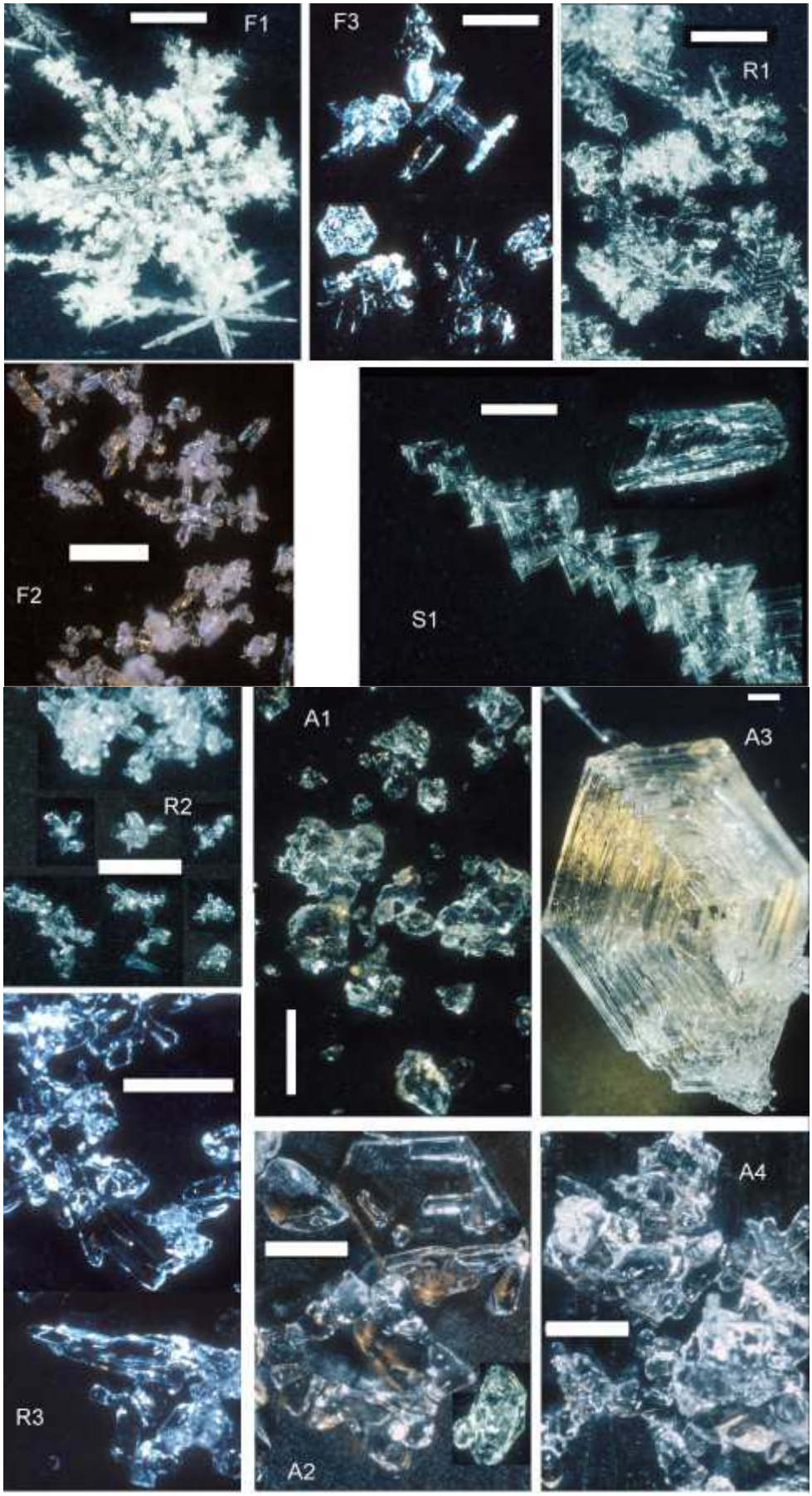

Figure 7: Photomacrographs of snow crystals representative of different snow types. All scale bars: 1mm.

Table 3 clearly shows that there is a correlation between snow type and SSA, and confirms our revious statement that SSA almost always decrease with time. Table 3 also shows that standard deviations are usually in the 25 to 40% range, and show no trend with snow age, so that metamorphism does not seem to have a homogeneizing effect. Density can also be used to facilitate the estimation of SSA. A correlation between SSA and density has already been proposed by Narita (1971), who used stereological methods to measure SSA. However, his method was applicable mainly to aged snow, and very few data for fresh snow were presented. Figure 8 shows SSA vs. density plots for each snow type, except for surface hoar (type S1), whose density could never be measured. Density was not measured in all cases. Usually, this was because layers were too thin, but sometimes approaching polar bears suggested that measuring density was not all that important after all.

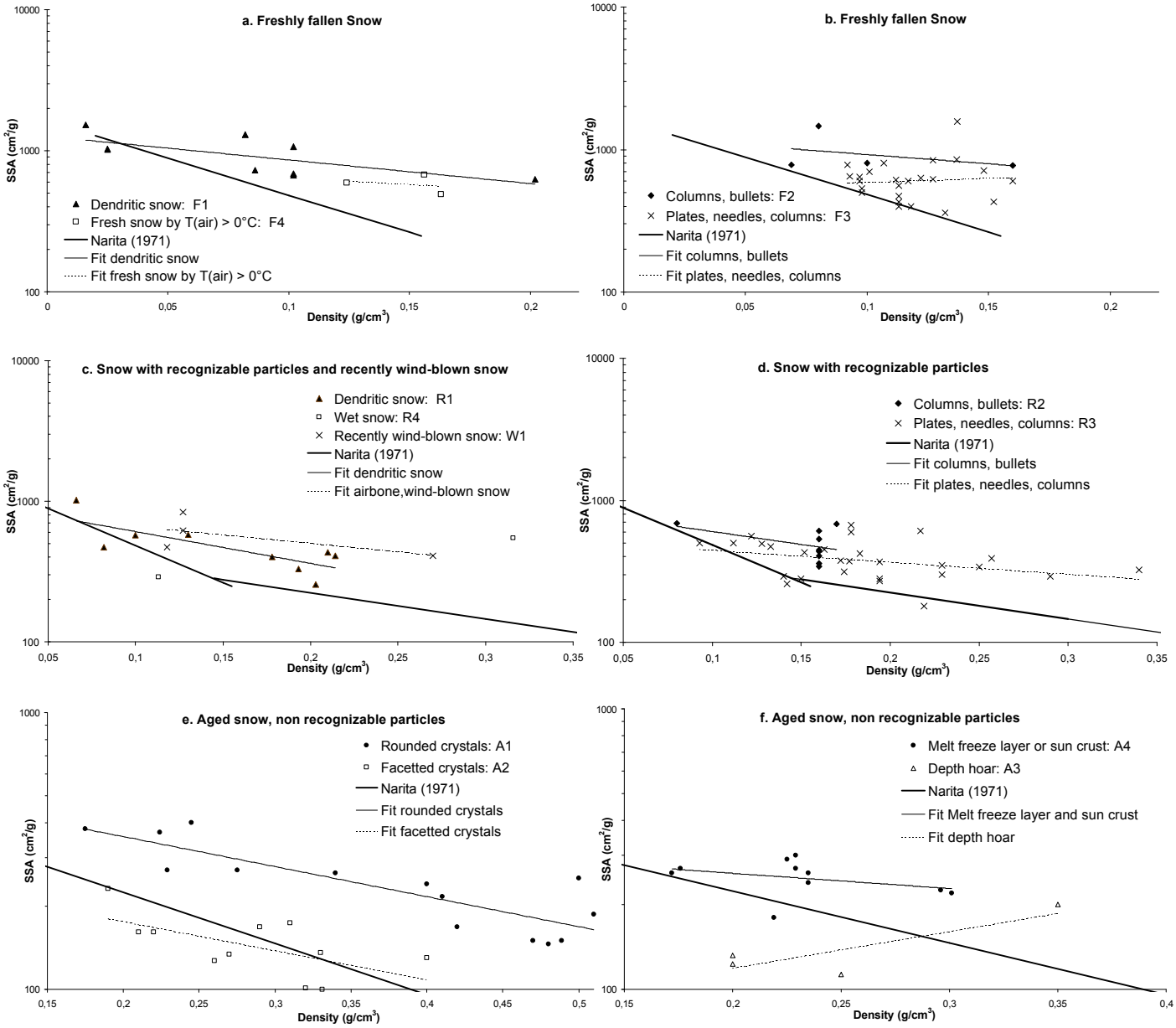

Figure 8: SSA - density correlations for the snow types of Table 3, except for surface hoar, whose density was not measured.

Least square fits obtained for each snow types yielded equations (5) to (17), where d is density and where the correlation coefficient has been added (Table 4).

Table 4: Correlation between SSA and density according to snow type.

Snow Type	List square fit	Correlation coefficient	Equation N°
F1:	ln SSA = - 3.850 d + 7.141	R^2=0.484	(5)
F2:	ln SSA = -2.978 d + 7.124	R^2=0.150	(6)
F3:	ln SSA = + 1.263 d + 6.274	R^2=0.0058	(7)
F4:	ln SSA = - 2.260 d + 6.697	R^2= 0.0086	(8)
R1 :	ln SSA = - 5.199 d + 6.930	R^2=0.614	(9)
R2 :	ln SSA = - 4.188 d + 6.820	R^2=0.184	(10)
R3 :	ln SSA = - 1.941 d + 6.295	R^2=0.122	(11)
R4:	ln SSA = + 3.153 d + 5.314	R^2=1 (only 2 points)	(12)
A1:	ln SSA = - 2.497 d + 6.376	R^2=0.721	(13)
A2:	ln SSA = - 2.421 d + 5.655	R^2=0.380	(14)
A3:	ln SSA = + 3.005 d +4.1789	R^2=0.703	(15)
A4:	ln SSA = - 1.249 d + 5.807	R^2=0.119	(16)
W1:	ln SSA = - 2.774 d + 6.779	R^2=0.407	(17)

Regarding fresh snow (types F1 to F4) only types F1 (dendritic snow) and F3 (plates, columns, needles) have sufficient data for the correlations to be meaningful. For type F1, there is a reasonable correlation coefficient, 0.484, and using figure 8a can lead to the estimation of the SSA of dendritic snow, knowing its density, within about 25% at the 1σ level. This relationship could be strengthened with more data, however. For type F3 (plates, needles, columns) there is no correlation between density and SSA, and Table 3 only can be used to determine SSA, within 38% at the 1σ level. Similarly, for types F2 and F4, only the use of Table 3 is possible, but there are clearly too few data to suggest a level of confidence.

Equations (9) to (11) show a weak decreasing trend of SSA with density for types R1 to R3. R4 obviously has insufficient data. The decreasing trend is visually clear for types with the most data points: dendritic snow, and plates and columns. Using the plots of Figure 8c and 8d can then lead to a more accurate value than just using table 3, and an estimation within 25 to 35 % at the 1σ level appears possible.

Equations (13) for type A1 and (14) for type A2 indicate a significant correlation for rounded and faceted grains, and using Figures 8e and 8f will lead to an estimation within 20 to 30% at the 1σ level. For depth hoar (eq. 15), there is insufficient data for a meaningful correlation and we recommend using Table 3, with a 25% uncertainty at the 1σ level. For melt-freeze layers and sun crusts, measuring density is often delicate, as these layers are often thin. Insufficient data in Figure 8 lead to a poor correlation, and we recommend using Table 3, with a 25% uncertainty at the 1σ level. For surface hoar, note that the 3 values obtained in the springtime in the Arctic are within about 10% of each other, while the winter hoar frost value is much higher. Finally, both values obtained for recently wind blown snow are lower than that of the airborne snow, possibly because contact between grains and the start of the sintering process had decreased SSA, but data are too few and this is speculative.

Spatial variability of snow SSA

Since one of the objectives of the present work is to allow the derivation of snow SSA for use in atmospheric modeling, it is crucial to test whether measurements performed at one location are representative of larger areas. Only limited data are presented to address this question, and the answer appears different for fresh snow and for snow that has undergone metamorphism.

A preliminary test of spatial variability was made at Col de Porte (French Alps, just north of Grenoble). We collected two samples consisting of unsintered rounded grains 1 cm under the surface of the snowpack and separated by 1 m horizontally. The measurement of their SSA was repeated by the same experimentalist three times for one sample and twice for the other one. Results indicate that the difference between both samples was 3.6%. Considering a repeatability of about 2.8%, and using an equation similar to (4), we deduce that the actual SSA difference was about 2%.

Another test was done at Alert, where we monitored the SSA evolution of a snow layer that precipitated on 3 February 2000 (Cabanes et al., in press) and that consisted of columns and bullet combinations. Sampling was done at 2 sites during 17 days: on land, and on the sea ice, about 7 km away. No simultaneous sampling was done at both sites. However, a plot of SSA vs. time show that the 2 data points obtained on the sea ice fall almost exactly on the curve drawn with the 6 data points obtained on land (Cabanes et al., in press), from which we infer that, for this fresh snow layer, the difference in SSA measured at both sites was less than 5%. Since the repeatability is 2.8%, the actual difference in SSA in this snow layer, between 2 sites 7 km apart was less than 4%.

A last test was performed with snow from Les deux Alpes. We used the 7 snow samples described in the table 2, that came from a layer 3 cm under the surface, that had been wind-blown two days before. Samples were taken from spots about 1 m apart. Two experimentalists measured the SSA of each sample, and the sample SSA is given as the mean value. For the whole layer, $SSA_{layer} = 281 \pm 34$ cm²/g. The spatial reproducibility is then equal to $2\sigma=24\%$ for this layer, which is only reduced to 23% if the reproducibility is taken into account. This high value may be explained by the fact that the samples were taken on an exposed slope where strong winds up to 100 km/h had blown two days ago. Local variations in wind effects, which include wind speed and accumulation, may therefore have resulted in different metamorphic scenarios for 2 adjacent spots, and this would have been enhanced by the high temperatures, that remained close to 0°C during that period.

From these preliminary data, we suggest that the spatial variability of fresh undisturbed snow is low, so that SSA spatial variations <5% can probably be expected, while metamorphism, including wind-induced effects, can lead to much larger spatial variations. Of course, it is clear that more extensive studies using larger data sets are needed before these numbers can be confirmed.

Discussion

Comparison with other methods and previous work

Numerous methods can be used to measure snow SSA. Among these are stereology, grains sieving, image analysis, and the adsorption of gases other than CH_4.

Narita (1971) used stereology to measure snow SSA. Only his abstract is in English, and only some of the details, that are in Japanese, could be translated. He apparently studied various types of snow and plotted 113 values in a density-SSA diagram similar to ours. He divided his data into 3 groups according to their density: $d<0.15$, $0.15<d<0.55$, and $0.55<d<0.83$, and performed distinct fits for these 3 regions, with apparently reasonable correlation coefficients, although he had only 8 points for $d<0.15$. As we have no data for $d>0.55$, only 2 of his fits are reported in figure 8. In general, his fits

indicate lower SSA values than ours, especially for fresh snow. Three possible reasons stand out: 1/ Fresh snow of low density sampled by Narita (1971) was already a few days old and is not of type F1 nor of type R1. 2/ his method is not sensitive to small structures. Indeed his optical technique makes it difficult to take into account structures in the size range of 10 µm or smaller, while CH_4 adsorption will detect even molecular-size structures. Hence it is not surprising to note that the higher the SSA, the greater the difference between his fits and ours. 3/ accurate stereological measurements require isotropy of particle location and orientation (Davis et al., 1987), which is not true for surface hoar and depth hoar, and possibly also for some fresh snow types. We then suggest that for the snow types studied here, stereology will tend to underestimate SSA. A comparison using the same samples is necessary to confirm this suggestion. Stereology may be efficient to measure low SSA values, in deep firn and very dense snow, where isotropy is expected. Furthermore, such samples would have no microstructures, as these are eliminated by metamorphism, and the systematic error that they probably cause would then not exist. Narita (1971) reports 15% uncertainty for every snow type he studied. Most of our samples had a total SA around 1 m^2. For such samples, our reproducibility is 6% and our accuracy is 12 %. We estimate that this remains essentially true for samples with total SA around 0.75 m^2. For lower total SA, the accuracy will be reduced. Narita reports SSA values as low as 7 cm^2/g, obtained when d=0.7. In our system, such a sample would have a total SA of 0.12 m^2. Although CH_4 adsorption would definitely be detected, our accuracy would be 50%, at best. CH_4 adsorption and stereology may then be complementary techniques, to be used on different snow samples.

Granberg (1985) used grain sieving to evaluate the SSA of snow samples in Quebec. Crystals were equated to spheres of equivalent radius and SSA was multiplied by 1.5 to account for non-sphericity. He obtained low SSA values between 60 cm²/g in deep snow and 200 cm²/g close to the surface. In the absence of more details on the snow studied by Granberg (1985), we cannot make any comparison with our data. However, his results do seem much lower than ours, most likely because this simple method cannot take into account microstructures.

The potential of image analysis to determine SSA had been discussed at length by Dominé et al. (2001), and has also been attempted by Fassnacht et al. (1999). A major problem with that technique is that it is extremely tedious and time consuming, even if sophisticated softwares are used. One SSA measurement using CH_4 adsorption takes 3 hours with an accuracy of 12%, while selecting and analyzing a representative number of pictures of one snow sample is much longer, and only results in an accuracy of 30 to 50%. By comparison, a moderately trained eye can obtain SSA estimates with the same 30 to 50% accuracy using the data presented in Table 3 and Figure 8, and this will be rapid.

Previous authors have measured the SSA of a few snow samples using N_2 adsorption. Adamson et al. (1967) obtained 13 000 and about 2000 cm^2/g for 2 snow samples. The ΔQ_{N2} values obtained were zero or negative. According to Dominé et al. (2000) a ΔQ_{N2} value around 2700 J/mol is a necessary condition for a reliable measurement, and these results have to be questioned. The very high values obtained also suggest that the formation of amorphous ice of high surface area may have taken place during sample cooling. Similarly, Jellinek and Ibrahim (1967) obtained 77 700 cm^2/g and ΔQ_{N2} = 605 J/mol for one unspecified snow sample. For the same reasons as above, this high value is certainly unreliable and perturbed by amorphous ice formation. Such a formidable value, equivalent to that of

ice spheres less than 1 µm in diameter, appears impossible for snow. Hoff et al. (1998) measured the SSA of 6 snow samples and obtained values in the range 600 to 3700 cm^2/g, with ΔQ_{N2} values in the range 1334-2483 J/mol, mostly much lower than the recommended value of 2700 J/mol. A low value of ΔQ_{N2} leads to an overestimate of SSA, and this may explain why they obtained values higher than the highest one found in this study.

CH_4 adsorption has been used by Chaix et al. (1996) and Hanot and Dominé (1999). Chaix et al. obtained one value of 570 cm^2/g for fresh snow sampled under an air temperature of –2°C. This appears consistent with Type F3 snow, even though their ΔQ_{CH4} value was a bit low, 1919 J/mol. Hanot and Dominé (1999) studied the evolution of the SSA of a snow layer and of surface hoar and found values in the range 22 500 to 2 500 cm^2/g, with a mean ΔQ_{CH4} value of 2195 J/mol, i.e. within the range recommended here. Their values appear very high, and formation of amorphous ice during sample cooling is a clear possibility. It is troubling, however, that if such an artifact took place, it is reproducible. Two measurements on 2 distinct surface hoar samples yielded similar values: 2 500 and 2 600 cm^2/g. Moreover, SSA variations show the expected trends, that have been confirmed in subsequent studies (Cabanes et al., in press), i.e. they decrease with time. Microstructures in the 3 µm size range are necessary to explain the high values encountered. Such small structures have been observed by Wergin et al. (1995), but it is difficult to imagine that they could make up most of a snow sample. Hanot and Dominé did not take photomacrographs of their samples to support their high values. They did not either perform desorption measurement, to test for the presence of a hysteresis loop, as shown in Figure 4. In this study, we obtained values greater than 10 000 cm^2/g twice. Each time, a hysteresis loop was detected and we realized that a leak in one of the valves had caused the evacuation of our container before the snow was cooled, and that caused amorphous ice formation. Our preferred conclusion on the data of Hanot and Dominé is then that amorphous ice formation probably took place. We cannot explain why their results are reproducible and the observed trends make sense. Perhaps the procedure followed was always identical, and amorphous ice formation acted as an amplification of SSA. Indeed, the flux of water vapor that will form amorphous ice is, to a first approximation, proportional to SSA. Of course, we are not certain that those values are not valid, but a positive confirmation of the existence of snow with such high SSA will require new measurements, whose reliability should be confirmed by the absence of a hysteresis loop, and by adequate photographs.

Potential impact on atmospheric chemistry

The impact on atmospheric chemistry of adsorption/desorption process on snow surfaces has already been discussed in previous studies (Hanot and Dominé, 1999; Dominé et al., in press; Cabanes et al., in press). Briefly, the total surface area (TSA) of the seasonal snow pack is a few thousands of m^2 per m^2 of ground. At Alert, TSA values between 1160 and 3710 (dimensionless) were determined. In Svalbard near Ny-Alesund, values between 1610 for very wind-blown coastal areas and 7600 in the upper part of the ablation zone of glaciers were estimated, as detailed in future publications. In the Alps, TSA values can be even higher. In the spring of 2001, the seasonal snow thickness at 3000 m elevation was 3.5 m. Using a mean density of 0.3 and a mean SSA of 250 cm^2/g, the TSA was then 26 200. These values are sufficient to lead to the important sequestration of trace gases that have a

moderate affinity for the ice surface, such as acetone (Dominé et al., in press), and the snow pack may then affect the atmospheric mixing ratios of a wide range of species.

Conclusion

We have measured the SSA of 176 snow samples and found values between 100 and 1580 cm^2/g. Snow samples were classified by age and by crystal shapes to define 14 snow types, and correlations were found between type and SSA. Using these correlations allows the estimation of the SSA of snow observed in the field within 40 % or better at the 1σ level, although more data for some snow types are needed to confirm some values. Correlations were also found between SSA and density for most snow types where sufficient data exist. Using these correlations together with the classification proposed reduces the uncertainty in SSA estimation. More measurements are required to improve our ability to estimate snow SSA, as some snow types have not been sufficiently sampled. This is the case for cold arctic precipitation and surface hoar, for fresh or recent wet snow, and for recently wind-blown snow. The method proposed here appears reproducible (6%) and accurate (12%) and is more rapid than image analysis. We argue that for snow with SSA greater than about 100 cm^2/g, which includes all the seasonal snow samples studied here, our method may be more accurate than stereology, because it detects the tiniest details. For older snow with lower SSA, and whose small structures have been removed by metamorphism, it seems likely that the accuracy of our method will deteriorate to 50% or worse, and stereology may then be interesting. A comparison of both methods on the same samples is necessary to confirm these suggestions.

Acknowledgements

The Alpine part of this work was funded by Programme National de Chimie Atmosphérique (PNCA) of CNRS. The Arctic part was funded by the French Polar Institute (IFRTP). Numerous people assisted us for snow sampling or provided logistical support. Among these, we particularly thank Olivier Brissaud for help in the Alps, Alan Galland and Armand Gaudenzi for help at Alert, and Roberto Sparapani, Andrea Felici, and Stefano Poli for work in Svalbard. This work is an extension of the studies initiated with Laurent Chaix and Laurence Hanot. Encouragements by Leonard Barrie were critical to the continuation of these measurements.

References

Adamson, A.W., Dormant, L.M., and Orem, M.,. Physical adsorption of vapors on ice. I-Nitrogen. *J. Colloid Interface Sci.* 25, 206-217, 1967

Albert, M.R., Grannas, A.M., Bottenheim, J.W.,. Shepson, P.B., and Perron, F.E. Jr. Processes and Properties of Snow-Air Transfer in the High Arctic with Application to Interstitial Ozone at Alert, Canada. *Atmos. Environm.*, submitted, 2001.

Barrie, L.A., Bottenheim, J.W., Schnell, P.J., Crutzen, P.J. and Rasmussen, R.A. Ozone destruction and photochemical reactions at polar sunrise in the lower Arctic atmosphere, *Nature*, 334, 138-141, 1988.

Brunauer, S., Emmet, P.H. and Teller, E., Adsorption of gases in multimolecular layers. *J. Am. Chem. Soc.* 60, 309-319, 1938.

Brunauer, S., Deming, S., Deming, W.S. and Teller, E.,. *J. Am. Chem. Soc*., 62, 1723, 1940.

Cabanes, A., Legagneux, L., and Dominé, F., Evolution of the specific surface area and of crystal morphology of fresh snow near Alert during ALERT 2000 campaign, *Atmos. Environm.*, in press, 2001.

Chaix, L., Ocampo, J. and Dominé, F. Adsorption of CH_4 on laboratory-made crushed ice and on natural snow at 77K. Atmospheric implications. *Comptes Rendus Acad. Sciences,* 322, série II, 609-616, 1996.

Colbeck, S.C., Classification of seasonal snow cover crystals, *Water Ressources Res.* 22, 59S-70S, 1986.

Couch, T.L.; Sumner, A.-L.; Dassau, T.M.; Shepson, P.B. and Honrath, R.E., An Investigation of the Interaction of Carbonyl Compounds with the Snowpack, *Geophys. Res. Lett.*, 27, 2241-2244, 2000.

Davis, R.E., Dozier, J., Perla, R., Measurement of snow grain properties, *Seasonal Snowcovers*, NATO ASI series C211, 63-74,1987.

Dibb, J., et al., Air-snow exchange of HNO_3 and NOy at Summit, Greenland. *J. Geophys. Res.*, 103, 3475-3486, 1998.

Dominé, F, Chaix, L. and Hanot, L., Reanalysis and new measurements of N_2 and CH_4 adsorption on ice and snow. *J. Colloid. Interf. Sci.*, 227, 104-110, 2000.

Dominé, F., Cabanes, A., Taillandier A.-S. and Legagneux., L., Specific surface area of snow samples determined by CH_4 adsorption at 77 K, and estimated by optical microscopy and scanning electron microscopy. *Environ. Sci. Technol. 35*, 771-780, 2001.

Dominé, F., Cabanes, A., and Legagneux, L., Structure, microphysics, and surface area of the Arctic snowpack near Alert during the ALERT 2000 campaign. *Atmos. Environm.*, in press, 2001.

Dominé, F. and Thibert, E., Mechanism of incorporation of trace gases in ice grown from the gas phase, *Geophys. Res. Lett.*, 23, 3627-3630, 1996.

Fassnacht, S.R. ; Innes, J. ; Kouwen, N. and Soulis, E.D., The specific surface area of fresh dendritic snow crystals. *Hydrol. Process.* 13, 2945-2962, 1999.

Frei, A., and D. A. Robinson, Evaluation of snow extent and its variability in the Atmospheric Model Intercomparison Project. *J. Geophys. Res.*, 103, 8859-8871, 1998.

Granberg, H.B., Distribution of grain sizes and internal surface area and their role in snow chemistry in a sub-arctic snow cover, *Annals of glaciology*, 7, 149-152, 1985.

Gregg, S.J., Sing, K.S.W.,. Adsorption, surface area and porosity. Academic Press, London, 1982.

Haas, J., Bullemer, B., and Kahane, A., Diffusion de l'Hélium dans la glace monocristalline, *Solid State Comm*., 9, 2033, 1971.

Hanot, L., and Dominé, F. Evolution of the surface area of a snow layer. *Environ. Sci. Technol*. 33, 4250-4255, 1999.

Hoff, J. T., Mackay, D., Jia, C.Q., and Wania, F., Measurement of the specific surface area of snow using the nitrogen adsorption technique, *Environ. Sci. Technol*., 32, 58-62, 1998.

Honrath, R.E., Peterson, M.C., Guo, S., Dibb, J.E., Shepson, P.B. and Campbell, B., Evidence of NO_x production within or upon ice particles in the Greenland snowpack. *Geophys. Res. Lett.*, 26 695-698, 1999.

Honrath, R.E., Peterson, M.C., Dzobiak, M.P., Dibb, J.E., Arsenault, M.A.; Green, S.A. Release of NO_x from sunlight-irradiated Midlatitude Snow. *Geophys. Res. Lett.*, 27 2237-2240, 2000.

Hutterli, M. A., Rothlisberger, R., and Bales, R. C., Atmosphere-to-snow-to-firn transfer studies of HCHO at Summit, Greenland, *Geophys. Res. Lett., 26*, 1691-1694, 1999.

Haas, J., Bullemer, B., and Kahane, A., Diffusion de l'Hélium dans la glace monocristalline, *Solid State Comm*., 9, 2033, 1971.

Jellinek, K., and Ibrahim, S., Sintering of powdered ice. *J. Colloid Interface Sci.,* 25, 245-254, 1967.

Klinger, J., Ocampo, J., Apparent solubility of Helium in snow and ice, *J. Phys. Chem*., 87, 4114, 1983.

Kouchi, A., et al., Conditions for condensation and preservation of amorphous ice and astrophysical ices, *Astron. Astrophys*., 290, 1009-1018, 1994.

Marbouty, D. An experimental study of temperature gradient metamorphism ; *J. Glaciol*. 26, 303-312, 1980.

Mayer, E. and Pletzer, R. Amorphous ice. A microporous solid : astrophysical implications. J. Phys. 48, C1-581-C1-586, 1987.

Michalowski, B.A., Francisco, J.S., Li, S.-M., Barrie, L., Bottenheim, J.W. and Shepson, P. A computer model study of multiphase chemistry in the arctic boundary layer during polar sunrise. *J. Geophys. Res., 105*, 15131-15145, 2000.

Narita, H. Specific surface of deposited snow II, *Low Temp. Sci.* A29, 69-81, 1971.

Peterson, M.C., and Honrath, R.E. Observations of rapid photochemical destruction of ozone in snowpack interstitial air. *Geophys. Res. Lett*. *28*, 511-514, 2000.

Robinson, D. A., K. F. Dewey, and R. R. Heim, Jr. Global snow cover monitoring: an update. Bull. Amer. Meteor. Soc. 74, 1689-1696, 1993.

Sumner, A.L. and Shepson, P.B. Snowpack production of formaldehyde and its effect on the Arctic troposphere. *Nature*, 398, 230-233, 1999.

Thibert, E., and F. Dominé Thermodynamics and kinetics of the solid solution of HNO_3 in ice. *J. Phys. Chem. B*. 102, 4432-4439, 1998.

Weller, R.; Minikin, A.; König-Langlo, G.; Schrems, O.; Jones, A.E.; Wolff, E.W.; and Anderson, P.S. Investigating possible causes of the observed diurnal variability in Antarctic NOy. *Geophys. Res. Lett*. 26, 601-604, 1999.

III.3. Specific surface area of snow samples determined by CH_4 adsorption at 77 K, and estimated by optical microscopy and scanning electron microscopy

La méthode d'adsorption permet de déterminer la SS de la neige avec une bonne précision, cependant elle prend du temps et nécessite l'utilisation de l'azote liquide. Ici, nous avons tenté d'estimer la SS avec deux méthodes d'analyse d'images de cristaux isolés. L'objectif étant de savoir si la SS peut être estimée avec une précision suffisante et de manière plus simple qu'avec la méthode d'adsorption. Les résultats obtenus montrent que ces méthodes permettent d'avoir une estimation correcte de la surface spécifique, cependant leur précision n'est pas aussi bonne que la méthode d'adsorption. L'analyse d'image est toute fois très utile dans l'interprétation de la SS et de son évolution.

Ainsi, de nombreuses images de cristaux obtenues par macrophotographies ou microscopie électronique à balayage (MEB) ont été utilisées par la suite afin d'améliorer notre compréhension de la SS.

Environ. Sci. Technol. **2001**, *35,* 771−780

Specific Surface Area of Snow Samples Determined by CH_4 Adsorption at 77 K and Estimated by Optical Microscopy and Scanning Electron Microscopy

FLORENT DOMINÉ,* AXEL CABANES, ANNE-SOPHIE TAILLANDIER, AND LOÏC LEGAGNEUX

CNRS, Laboratoire de Glaciologie et Géophysique de l'Environnement, BP 96, 38402 St. Martin d'Hères Cedex, France

Snow is a divided medium that can adsorb atmospheric trace gases. Evaluating the impact of the snow cover on atmospheric chemistry therefore requires the knowledge of the specific surface area (SSA) of snow. This paper compares the results of three methods used to measure or estimate the SSA of four snow samples: CH_4 adsorption at 77 K, optical microscopy (OM), and scanning electron microscopy (SEM, used only on two samples). Within error bars, CH_4 adsorption and OM yield similar results on three of the four snow samples. Values for the 4th sample are within a factor of 2. For both samples where CH_4 adsorption, OM, and SEM are used, all three methods yield similar results, but CH_4 adsorption always has a better accuracy and a much better precision. Thus, despite its ease of use, estimates from OM images are often not accurate enough to monitor the evolution of snow SSA. The main sources of error in the OM method are the difficulty to determine snow crystal thicknesses and to take into account the topography of the snow crystal surface. The combination of CH_4 adsorption and OM or SEM can provide useful information on the evolution of both the SSA and the shape of snow crystals. This will be useful to evaluate the respective contributions of adsorption/desorption and sublimation/condensation processes to the impact of the snow cover on atmospheric chemistry.

Introduction

Snow can cover up to 50% of land masses (*1*), and the impact that this highly divided surface cover may have on atmospheric chemistry has been the subject of several recent studies (*2*−*5*). Gas-phase measurements above and within the snowpack have indicated that snow can exchange gaseous species such as formaldehyde (*2*, *3*), acetaldehyde and acetone (*4*), NO_x (*5*, *6*), and HNO_3 (*6*) with the atmosphere. The mechanisms of exchange are still unclear but may include adsorption/desorption from the snow surface (*2*−*4*), photolysis of a dissolved precursor (*5*, *6*), co-condensation of the trace gas with water vapor with subsequent sublimation of the solid solution formed (*6*), and solid-state diffusion in and out of ice crystals (*7*, *8*).

Evaluating the contribution of adsorption/desorption to the above observations requires the knowledge of the surface area (SA) of snow. By surface area, we mean, following Gregg and Sing (*9*), the area of the snow sample considered that is accessible to gases. This area is expressed in m^2 or cm^2 for small values. By specific surface area (SSA), we mean the surface area of a given mass of snow. This is expressed in m^2/g or here in cm^2/g as values of SSA for snow are often small. The determination of the SSA of a snow sample thus requires the knowledge of its mass.

Several methods can be used to measure the SSA of snow. Among the most relevant ones is the adsorption of gases, often at 77 K, as this process is similar to the adsorption of atmospheric gases, the topic of interest here. The use of this method to measure snow SSA has been detailed earlier (*10*). Recent uses include those by Hoff et al. (*11*), who used N_2 adsorption at 77 K to measure the SSA of six snow samples, and by Chaix et al. (*12*) and Hanot and Dominé (*10*), who used CH_4 adsorption at 77 K to measure the SSA of a snow sample and the evolution of the SSA of a snow layer, respectively.

The disadvantage of these adsorption methods is that they require liquid nitrogen (N_2(l)), which is not always available for field studies in remote regions such as the Arctic and Antarctic. Alternative methods include stereology, which requires making serial sections of snow samples that have been previously reinforced by soaking into a liquid that is allowed to solidify and whose images must be analyzed using an appropriate method (*13*−*15*). Using a similar principle, another technology is X-ray tomography (*16*), which can have a resolution of 10 μm if synchrotron radiation is used. The simplest method is probably to analyze optical microscopy (OM) images that allow the determination of some or all the dimensions of snow crystals from which their mass and SA, and hence their SSA, can be obtained.

OM can readily be transported anywhere, but its reliability needs to be evaluated as it only provides SSA estimates rather than actual measurements. Several causes of errors can be anticipated: (i) The determination of SSA values representative of snow layers requires the study of many crystals or grains selected without bias. (ii) Microstructures may not be visible. Hanot and Dominé (*10*) invoked microstructures of about 3 μm to explain the high SSA of some of their snow samples. Such small microstructures, observed by Wergin et al. (*17*) using scanning electron microscopy (SEM), can increase SSA manyfolds and are difficult to see with OM. (iii) It is difficult to evaluate the SA of snow crystals having complex shapes. For example, determining the perimeter of dendritic crystals is difficult even if complex image analysis techniques are used, and this is a lengthy procedure (*18*) that reduces the advantage of OM. (iv) It may be difficult to measure all the dimensions of a snow crystal and therefore its mass: determining the thickness of a dendritic crystal is difficult as it has to stand on its side. Also, the volume of air bubbles reduces the ice mass in an often unknown manner (*19*).

The purpose of this paper is to test whether OM can be used to estimate the SSA of snow samples in replacement of the gas adsorption technique. Four samples of different snow types were studied, and attempts to estimate their SSA by OM were made. The values obtained were compared to those obtained by CH_4 adsorption, which is considered to be more reliable because the application of these measurements is to quantify the capacity of snow to adsorb gases. SEM images of two of the four samples have also been obtained to provide SSA estimates and to test for the presence of structures not

* Corresponding author phone: (33) 476 82 42 69; fax: (33) 476 82 42 01; e-mail: florent@glaciog.ujf-grenoble.fr.

10.1021/es001168n CCC: $20.00
Published on Web 01/17/2001

TABLE 1. Snow Samples Characteristics

sample no.	date sampled and location	date of snow fall	snow temp (°C)	depth of sample (cm)	snow density (g cm^{-3})	snow type
1	Jan 13, 1999, Alps	Jan 13, 1999	−4	2	0.086	heavily rimed dendrites, graupel
2	Mar 4, 1999, Alps	Mar 4, 1999	−0.4	8	0.10	small plates and needles
3	Apr 14, 2000, Arctic	Apr 13−14, 2000	−27	surface	<0.07	diamond dust: columns and combinations of bullets
4	Apr 18, 2000, Arctic	fall 1999	−26.5	32	0.20	depth hoar: large faceted crystals

observable by OM that could explain possible differences between values obtained by OM and CH_4 adsorption.

Experimental Methods

The four snow samples studied were as follows: (i) Fresh snow consisting of heavily rimed dendritic crystals and graupel. (ii) Fresh snow consisting of small plates and columns. Both these samples were taken in the winter of 1999 at Col de Porte, near Grenoble, in the French Alps. Sampling site and methods have been described earlier (*10*). (iii) Fresh snow consisting of columns and combination of bullets that fell under essentially clear sky conditions. Such snow is often called diamond dust. (iv) Large-faceted crystals, often cup-shaped, taken at the bottom of the snowpack. Such snow is called depth hoar. These last two samples were taken near Alert, on the north coast of Ellesmere Island, in the Canadian Arctic (82°30′ N, 62°20′ W), in April 2000 during Polar Sunrise Experiment 2000. Details on the samples are shown in Table 1.

SA was determined by measuring the adsorption isotherm of CH_4 on snow at N_2(l) temperature (77.15 K) by a volumetric method described previously (*10*, *12*). The principle is to measure the number of CH_4 molecules that can be accommodated on the snow surface and, knowing the cross sectional surface area of a CH_4 molecule, to determine snow SA by BET analysis. CH_4 was preferred to N_2, as its saturating vapor pressure is 12.77 mbar, making real gas corrections unnecessary. To obtain the SSA, the mass of snow was determined by weighing the snow container with and without the snow. Snow samples weighed 18−60 g, so that at least hundreds to thousands of snow crystals made up the sample, which is considered representative of the snow layer.

Repeated CH_4 adsorption measurements on the same snow sample indicate a reproducibility better than 5% (usually within 2%). SSA measurements on snow samples taken from the same layer, but a few meters away, showed variations smaller that 5% (usually within 3%). This will be detailed in a future paper (*20*). There are also systematic errors intrinsic to the BET method (*9*) that are estimated to result in a 10% uncertainty. The absolute accuracy of our method is then 15%.

Optical images of the alpine snow were obtained using a Leica MZ6 optical microscope, with magnifications up to 30, located in a cold room at −15 °C. Snow crystals were placed on a glass plate, and pictures were taken using transmitted light. Alpine samples were also studied by SEM. In the cold room, snow crystals were placed on a SEM sample holder using a methyl cellulose solution and then stored in N_2(l). The samples were then sputtered with gold in the N_2(l)-cooled chamber of a SP2000 Emscope instrument. The sample holders, mounted on a metal support near N_2(l) temperature, were then transferred under a dry Ar atmosphere into the vacuum chamber of a JEOL 35 CF SEM operated at magnifications up to 300 with an accelerating voltage of 10 kV. The N_2(l)-cooled stage of this SEM cannot be rotated. During transfer from the N_2(l) to the sputtering chamber, a slight contamination from atmospheric air sometimes resulted in the condensation of small amorphous ice particles on the snow crystals that could be observed on SEM images but were not included in the SA estimations.

Optical images of Arctic snow were obtained using a macro lens and bellows mounted on a Reflex camera. The maximum magnification (size of the crystal on the film/its real size) was 6.2. A flash was used to allow the pictures to be taken at f16, the minimum aperture of the lens. The pictures were taken immediately after sampling in a nonthermostated room whose temperature was −20 to −15 °C.

The surface areas of individual snow crystals were estimated by approximating their shapes with simple geometric shapes, such as hexagonal columns, parallelepipeds, or cylinders. The surface area (SA) and volume (V) of each shape was calculated, and the SSA of a set of crystals was

$$\mathrm{SSA} = \frac{\sum_i \mathrm{SA}_i}{\rho \sum_i V_i} \tag{1}$$

where ρ is the volumic mass of ice. The error on SSA was obtained by differentiating the Ln of eq 1:

$$\frac{\mathrm{d}\,\mathrm{SSA}}{\mathrm{SSA}} = -\frac{\mathrm{d}\rho}{\rho} + \frac{\mathrm{d}\sum_i \mathrm{SA}_i}{\sum_i \mathrm{SA}_i} - \frac{\mathrm{d}\sum_i \mathrm{V}_i}{\sum_i \mathrm{V}_i} \tag{2}$$

The next step requires hypotheses on the shapes of snow crystals. We illustrate our method with the example of hexagonal columns of diameter (from corner to corner) D and length L. Expressing SA and V as a function of D and L gives the relative error on SSA (δSSA) as a function of the relative errors δD, δL, and $\delta\rho$, assumed identical for all crystals:

$$\delta\mathrm{SSA} = \delta\rho + \delta D \left| \frac{\sum_i \left(\frac{3\sqrt{3}}{2} D_i^2 + 3 L_i D_i \right)}{\sum_i 3 D_i \left(\frac{\sqrt{3}}{4} D_i + L_i \right)} - 2 \right| + \delta L \left| \frac{3 \sum_i D_i L_i}{\sum_i 3 D_i \left(\frac{\sqrt{3}}{4} D_i + L_i \right)} - 1 \right| \tag{3}$$

Equation 3, where two vertical bars means absolute value, gives the analytical error. Equations 1−3 indicate that errors on dimensions will affect both SA and V and that the resulting errors on SA and V will partially cancel out, with an efficiency that will depend on crystal shape.

The small number of crystals studied for each sample also causes a representativity error, which has been evaluated

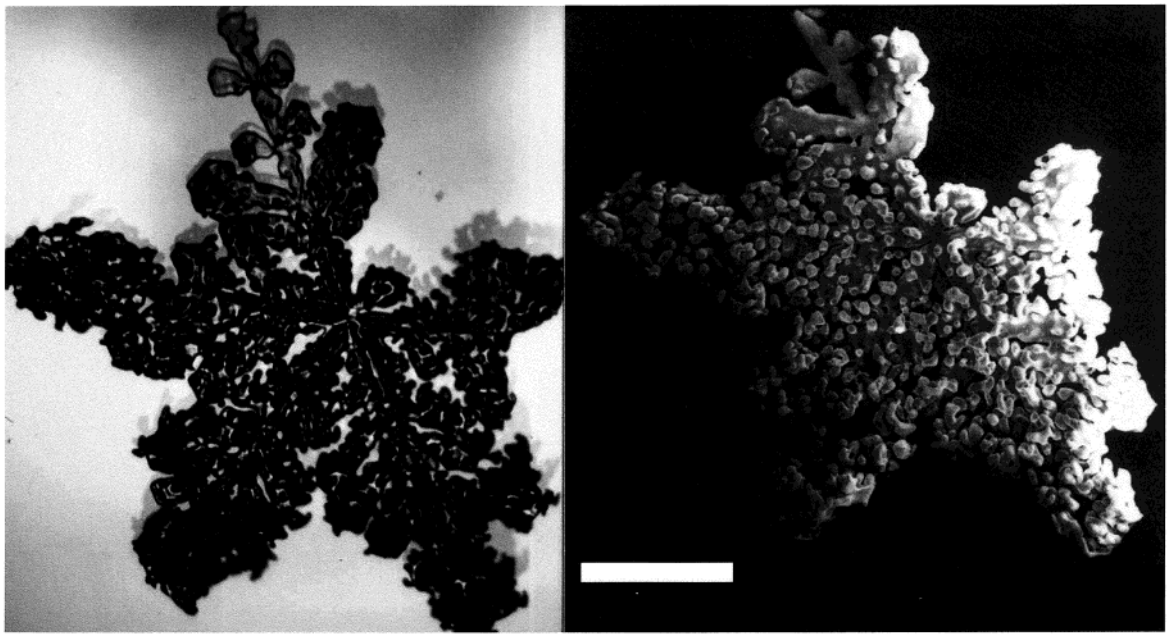

FIGURE 1. Photographs of a heavily rimed dendritic snow crystal, using optical microscopy (left) and scanning electron microscopy (right). Scale bar: 1 mm.

TABLE 2. Comparison of Snow Surface Areas Measured by CH_4 Adsorption and Estimated by Optical and SEM Images[a]

sample no.	snow type	SSA measured by CH_4 adsorption ($cm^2\ g^{-1}$)	SSA estimated by optical images ($cm^2\ g^{-1}$)	SSA estimated by SEM images ($cm^2\ g^{-1}$)
1	heavily rimed dendrites, graupel	730 ± 100	710 ± 200	730 ± 180
2	small plates and needles	700 ± 100	570 ± 180	490 ± 280
3	diamond dust: columns and combination of bullets	840 ± 100	420 ± 220	no images available
4	depth hoar: large faceted crystals	120 ± 20	130 ± 55	no images available

[a] Errors are at the 95% confidence level.

using Student's distribution law. The total error was taken as the square root of the sum of the squares of the analytical and representativity errors. This assumes a random analytical error and no bias in crystal selection. An unintentional bias is likely because crystals with shapes too complex for SSA estimation were not studied. The representativity error was doubled to account for this.

Results

SSA values measured by CH_4 adsorption and estimated from micrographs are reported in Table 2. The estimation of SSA values by OM and SEM are detailed below.

Sample 1. Sample 1 consisted mostly of heavily rimed dentritic crystals and graupel particles and of a few lightly rimed crystals. On the same crystal, some dendrites could be totally rime-free, while others were heavily rimed. Figure 1 shows pictures of the same heavily rimed dendritic crystal taken by both OM and SEM (small parts broke off during handling for SEM). Figure 2 shows the SEM picture of a graupel particle and OM pictures of very heavily rimed stellar and dendritic crystals. These and eight other OM pictures were used to attempt to estimate the mass and SA from crystals geometry from which SSA was derived.

One difficulty is that we could not obtain an accurate measurement of the thickness of the dendritic crystals because no rotatable stage was available. Attempts to handle the crystals by hand in the OM studies did not yield satisfactory results. Pruppacher and Klett (*19*) proposed the relationship (R1) to derive the crystal thickness h from its diameter d:

$$h\ (\mathrm{cm}) = 9.022 \times 10^{-3}\ d^{0.377}\ (\mathrm{cm}) \qquad \text{(R1)}$$

For example, from the OM image of Figure 1, the crystal has a diameter $d = 4.3$ mm from which we infer a thickness $h = 66\ \mu$m for the vapor-grown part of the crystal.

The SSA of the vapor-grown part and of the rime were estimated separately. Estimating the SSA of a dendritic crystal is very tedious. Image analysis softwares can in principle be used (*18*), but they cannot readily be applied to our case as the perimeter is partially hidden by rime. Furthermore, the use and validation of such softwares are complex procedures that are beyond the scope of this paper. A manual method was therefore followed. The shape of each subdendrite was approximated as one or two polygons to estimate the SA of the basal and prism faces. The volume of a crystal was estimated as the sum of the volumes of such polygons. The variability of the thickness of dendritic crystals (*18*) was neglected. An ice density of 0.9 g/cm^3 was used to obtain the mass. The density of pure ice is 0.917 at 0 °C, but air inclusions are often present in snow crystals. Ten crystals, whose perimeters were only moderately perturbed by rime, were studied yielding SSA values in the range of 155−250 cm^2/g, with a sample value of 210 cm^2/g. SEM pictures did not reveal significant new details of the vapor-grown part to justify a different estimate.

Rime drops appear quite different on OM and SEM pictures. On SEM pictures (Figures 1 and 2), it is obvious that

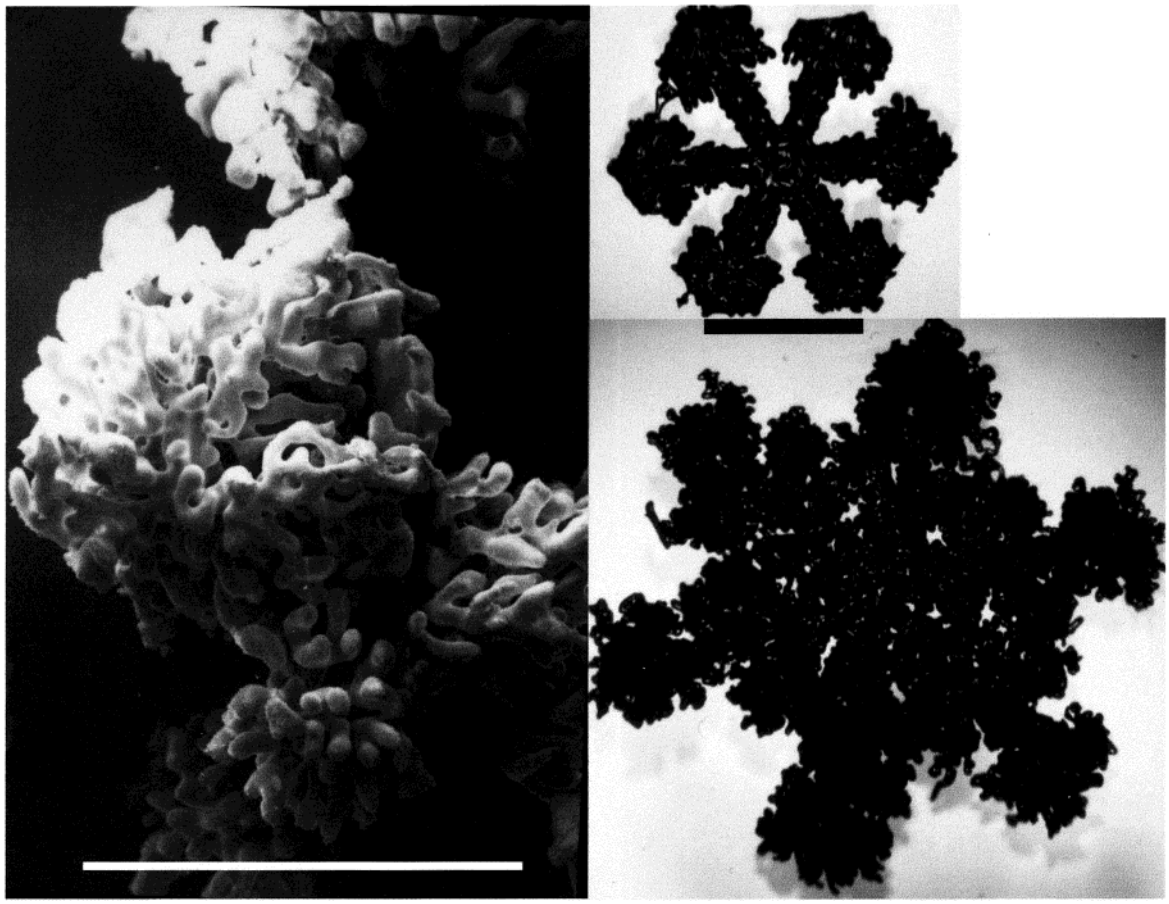

FIGURE 2. Scanning electron microscope photograph of a graupel particle (left) and optical microscopy pictures of very heavily rimed stellar and dendritic snow crystals. Scale bars: 1 mm. The scale is the same for both optical images.

droplets are not spherical but can instead be approximated as a cylinder capped by a half sphere. On our OM pictures, it is difficult to distinguish individual rime drops and to estimate their dimensions if the crystals are heavily rimed. This difficulty has been stressed by Wergin et al. (*21*), who compared video (i.e., optical) and SEM pictures of rimed crystals. Pruppacher and Klett (*19*) also show an OM picture of a graupel particle where the detailed structure visible in Figure 2 is not apparent.

The shape and size of droplets can nevertheless be seen by OM when they are on the side of the crystal. The diameter of rime drops were estimated independently with the OM and SEM pictures. For example, using Figure 1, mean droplet diameters of 48 and 59 μm were obtained from the OM and SEM pictures, respectively. According to our half-sphere on a cylinder shape approximation, mean cylinder heights were 80 and 100 μm for the OM and SEM pictures. We estimate that the SSA of rime drops in Figure 1 is 970 and 790 cm^2/g as determined by OM and SEM, respectively. Six crystals were studied by OM to yield an overall rime drop SSA values of 1110 cm^2/g. The range for individual rime drops was 650−1600 cm^2/g, and these values showed no major variations from one crystal to another. Five crystals were studied by SEM, yielding a value of 950 cm^2/g (range 600−1500).

To obtain the SSA of the snow sample, the proportion of the snow mass present as rime must be estimated. Obviously, SEM shows more useful data to estimate this proportion. For example, OM does not show whether there are one or two layers of rime drops, while SEM does show that. It is thus easy to underestimate the proportion of rime using OM, and our estimates of rime proportion are 55% using OM and 70% using SEM, which lead to overall SSA estimates of 710 and 730 cm^2/g by OM and SEM, respectively.

The analytical error for the vapor-grown part was evaluated using an equation similar to eq 3 but derived for a parallelepiped of length, width, and height (= thickness) L, W, H, and volumic mass ρ. Relative errors used were $\delta L = \delta W = 10\%$ to take into account shape approximations, $\delta H = 40\%$ to take into account the error due to R1, and $\delta\rho = 5\%$, from which a global error of 39% was obtained. The representativity error had little impact, and the SSA of the vapor grown part is then 210 ± 90 cm^2/g.

For the rime drops, the errors for OM are 20% for diameter (taking into account shape approximations), 15% for height, and 5% for ρ to result in a 24% error, i.e., 270 cm^2/g, while the error on representativity was 122 cm^2/g, resulting in a total error of 290 cm^2/g. Using SEM, the errors are 15% for diameter, 10% for height, and $\delta\rho = 5\%$, leading to a 19% analytical error, i.e., 180 cm^2/g. With representativity, the error is 220 cm^2/g.

The values and error bars are then $SSA_{OM} = 710 \pm 200$ cm^2/g and $SSA_{SEM} = 730 \pm 180$ cm^2/g, in good agreement with $SSA_{CH_4} = 730 \pm 100$ cm^2/g (Table 2). All error bars are at the 95% confidence level.

Sample 2. OM and SEM images of sample 2 are shown in Figures 3 and 4. Most of the snow sample mass (estimated at 85%) consisted of plates, but needles often regrouped as bunches were also present. OM pictures do not allow the determination of the plates thicknesses. The two pristine plates of Figure 3 have diameters (from corner to corner) of 860 and 1150 μm. Using R2 for plates (*19*):

$$h\ (\mathrm{cm}) = 1.41 \times 10^{-2}\, d^{0.474}\ (\mathrm{cm}) \qquad \text{(R2)}$$

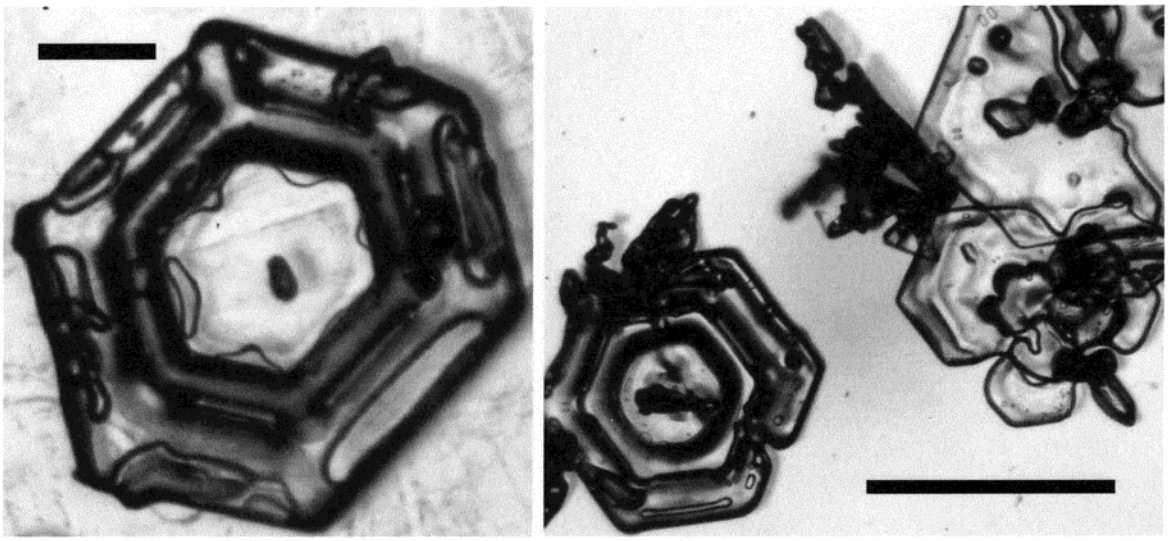

FIGURE 3. Optical microscopy pictures of ice crystals from sample 2. Scale bars: left: 200 μm, right: 1 mm.

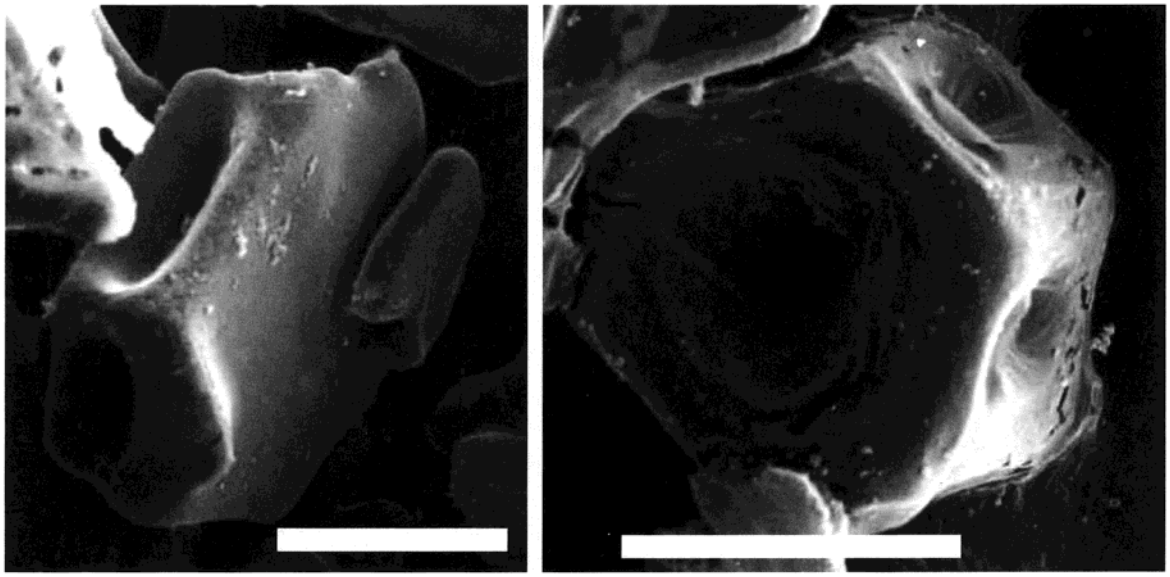

FIGURE 4. Scanning electron microscopy pictures of ice crystals from sample 2. Scale bars: 200 μm.

these plates thicknesses should be 44 and 51 μm. Assuming that these plates have simple prismatic shapes, with flat (0001) and (10$\bar{1}$0) crystal faces, their surface areas and volumes can be deduced. Air inclusions can be seen in transmitted light, and we use a density value of 0.85. We then estimate that these two pristine plates have SSAs of 600 and 510 cm^2/g. Figure 3 reveals however that these plates are not perfect prisms and that structures are present, even though their exact nature is difficult to determine. Plates as small as 300 μm in diameter were also seen. According to R2, they should have $h = 27$ μm and therefore SSA = 1060 cm^2/g. A typical needle of this sample had $h = 330$ μm and $d = 55$ μm, yielding SSA = 1060 cm^2/g if the needle is a perfect prism and is not hollow.

A total of 26 plates and 6 needles were studied, yielding a SSA value of 570 cm^2/g. For plates, the error on h is large, as suggested by the scatter on R2 and confirmed by SEM observations detailed below and is estimated at 100%, while errors on diameter and volumic mass are 15% and 5%, leading to a 33% analytical error. We confirmed by doubling the thicknesses of plates on our spreadsheet that SSA for plates was not very sensitive to thickness. For needles, the error on length and diameter are 15%, taking into account shape approximations but not hollows, and the error on volumic mass is 5%, leading to a 20% error. The error on representativity is small, and we obtain 570 $\pm$ 180 cm^2/g for the SSA of sample 2 estimated by OM pictures (Table 2).

Figure 4 shows a SEM picture of a plate about 300 μm in diameter (at right). Assuming the top surface is tilted 30° relative to horizontal, the thickness of the plate is estimated at 135 μm, while R2 would give $h = 26$ μm. Assuming again that the plate is a perfect prism, its SSA is 360 cm^2/g. Similarly, assuming the plate at left in Figure 4 is tilted 60° relative to horizontal, $d = 460$ μm, $h = 105$ μm, and SSA = 340 cm^2/g. Again, predicting h from R2 yields $h = 34$ μm. Figure 4 clearly shows that the plates are not perfect prisms and that faces are hollowed out in a variable manner. From our pictures, such features are expected to reduce on average the mass by about 15% and to increase the area by the same amount, thus increasing SSA by 32% so that the plates of Figure 4 would have SSAs of 470 and 450 cm^2/g. The small spheres visible on crystal surfaces are amorphous ice formed by the condensation of atmospheric water vapor during sample transfer. They were not considered in SSA estimates.

The SEM pictures of needles obtained were not very good, but they showed that needles were hollow with the internal surface accessible to gases, as also visible on other SEM pictures (*17*). If a needle 330 μm long and 55 μm in diameter has a hollow shaped as a 20 μm diameter cylinder, it increases its SA by 34% and decreases its mass by 19%, resulting in a SSA increase of 60% to 1700 cm^2/g. Using data from six plates and three needles and taking into account the hollow shapes, we obtain a sample SSA value obtained from SEM pictures of 490 cm^2/g.

The error analysis for the SEM pictures uses the same contributions as for OM, except the error on plate thickness, which is 30%, but the improved analytical error is compensated by a large representativity error due to the smaller number of crystals leading to $SSA_{SEM} = 490 \pm 280$ cm^2/g close to $SSA_{OM} = 570 \pm 170$ cm^2/g but somewhat different from although compatible with $SSA_{CH_4} = 700 \pm 100$ cm^2/g (Table 2).

Sample 3. The thickness of this diamond dust layer was 1−2 mm. Sampling was done on a plastic sheet that had been laid out to avoid sampling the underlying snow layer, which fell a day earlier. The thickness of this thin layer, which seemed somewhat spacially variable, could not be measured with an accuracy sufficient to obtain a reliable density value. By filling and weighing a container with snow, we measured a density of 0.07 g/cm^3, which must be considered an upper limit because of the inevitable packing during the filling procedure. This snow consisted (Figure 5) of small columns and combination of bullets whose largest dimension was in all cases <1 mm and sometimes even <0.1 mm. The surface areas of 33 columns or bullets was estimated from their diameters and lengths, taking into account their hexagonal shapes and assuming that they were not hollow. SSAs of single crystals ranged from 290 to 1500 cm^2/g (σ = 340 cm^2/g) to yield a value of 420 cm^2/g for the sample.

Sources of uncertainties on this OM estimation are 15% for crystal length and diameter, with these two errors including shape approximations except the possible existence of hollows, and 5% for volumic mass, leading to a 20% error. The representativity error is dominant here because of the large standard deviation in crystals SSA, and we obtain $SSA_{OM} = 420 \pm 220$ cm^2/g, a factor of 2 lower than $SSA_{CH_4} = 840$ $cm^2/g \pm 100$ (Table 2).

Sample 4. OM images of the large and faceted crystals from the depth hoar sample are shown in Figures 6 and 7. About 30% of the crystals were pristine and mostly cup-shaped (Figure 6). Most other crystals were clusters of faceted crystals of random shapes, as shown in Figure 7 (top). A few crystals had a 4-fold symmetry rather than the usual 6-fold symmetry because of the preferential growth of prism faces, while the growth of basal faces results in hexagonal shapes. These four-sided crystals were either cup-shaped or had a hollow column shape, as in Figure 7 (bottom). Some crystals were very complex in shape: two cup-shaped crystals with hexagonal symmetry had formed on the basal faces of a seed crystal, while six cup-shaped crystals with square symmetry had formed on the prism faces.

The SSA of cup- or hollow column-shaped ice crystals is given by R3:

$$SSA = 2/h\rho \qquad \text{(R3)}$$

where h is the thickness of the wall of the cup or hollow column and ρ is the density of the ice. This assumes that the length and diameter of the crystal are much greater than the wall thickness, which is the case in Figures 6 and 7 and other pictures not shown here. R3 still holds if the wall is not flat and is shaped like a flight of stairs as long as h remains constant. Ten crystals whose wall thicknesses were visible were studied. Thicknesses were in the range of 120−300 μm. Using $\rho = 0.9$, this leads to a range of SSA values of 74−178 cm^2/g, with a sample value of 130 cm^2/g.

Sources of uncertainties on this OM estimate are 30% for crystal thickness, which includes an estimate for shape approximations, no error on other dimensions as they are not used in SSA estimates, and 5% for volumic mass, leading to a 35% error. Adding the error for representativity leads to $SSA_{OM} = 130 \pm 55$ cm^2/g, in excellent agreement with $SSA_{CH_4} = 120 \pm 20$ cm^2/g (Table 2).

Discussion

The subjects requiring discussion are the relative merits of CH_4 adsorption, OM and SEM in obtaining reliable SSA values, and some implications for snow microphysics of the data obtained here.

Reliable SSA values are needed to treat the impact of the snow cover in atmospheric chemistry models. Diffusion in a porous medium may be slow and could reduce the actual SA accessible to atmospheric gases. This is not our concern here: that can be addressed independently in models. Similarly, the adsorption mechanism of CH_4 at 77 K and of atmospheric gases at 240−273 K may be different, but this can be treated independently in models, as we are here concerned with the SA potentially accessible to atmospheric gases. Thus, since CH_4 adsorption measures the surface area accessible to a gas, the value given by this method is identical or very close to the value accessible to atmospheric gases. In particular, it will be sensitive to micronic or submicronic structures that are relevant to the adsorption of atmospheric gases and that will be invisible by OM, stereology, or X-ray tomography. Such small structures may exist in ice despite the presence of a disordered surface layer. They have been observed by SEM (Figures 8 and 9 in ref *17*), and according to recent atomic force microscopy measurements (*22*), the disordered layer has a thickness of 32 nm at −1 °C, decreasing to 11 nm at −10 °C. Thus, it is not thick enough to smooth out submicron structures. Errors would appear if the size of snow structures were of the same order of magnitude as the size of the adsorbing molecule, as the accessible surface area would be molecular size-dependent. Such nanostructures appear incompatible with the disordered nature of the ice surface (*22*) and its dynamics (*23*) at tropospheric temperatures.

A possible artifact of the CH_4 adsorption method is the SA modification upon cooling. The comparison of OM and SEM pictures show no indication of that, as the SEM pictures are taken near 77 K. The only modification observed on SEM pictures is the condensation of atmospheric water vapor that forms amorphous ice spheres. Considering our adsorption experimental protocol, the amount of amorphous ice that could condense during snow cooling is too small to have a detectable effect, even if this amorphous ice had a SSA of 100 m^2/g.

Because samples used for CH_4 adsorption consist of hundreds or thousands of crystals (samples consisted of 18−60 g), errors due to nonrepresentativity are negligible. We estimate that sample 3 contained 7 million crystals! By comparison, we evaluate for sample 3 using Student's distribution law that 125 crystals should be studied to have a representativity error lower than 10%, which would be very time-consuming. The adsorption method also appears to be accurate. On an absolute basis, the uncertainty is 15%, but the precision is 5%, which is very interesting when small evolutions of the SA of snow layers are investigated. Its disadvantages are as follows: (i) the mandatory use of liquid nitrogen; (ii) it is time-consuming, as one measurement takes 3−4 h; and (iii) it does not give any information on the shape of snow crystals.

OM clearly does not have the accuracy of CH_4 adsorption. The reasonable agreement between the values obtained by

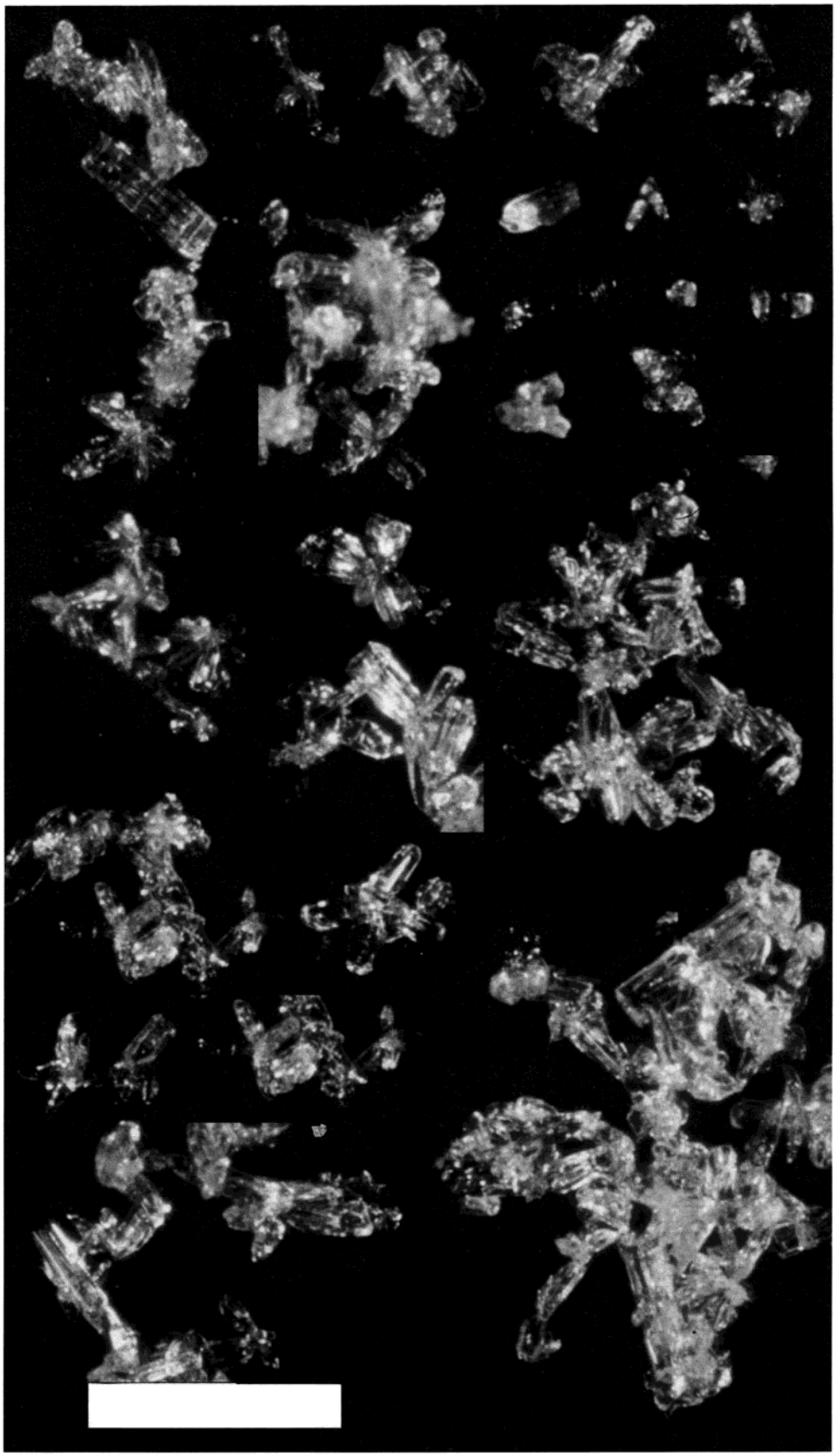

FIGURE 5. Composite optical microscopy picture of diamond dust crystals from sample 3. Scale bar: 1 mm.

CH_4 adsorption and OM for three samples (Table 2) can be misleading. The fairly good agreement for sample 2 is due to two errors canceling out each other: the underestimation of the thickness of the plates leads to an overestimate of SA that is in part compensated by not accounting for complex shapes. The poor agreement between CH_4 adsorption and

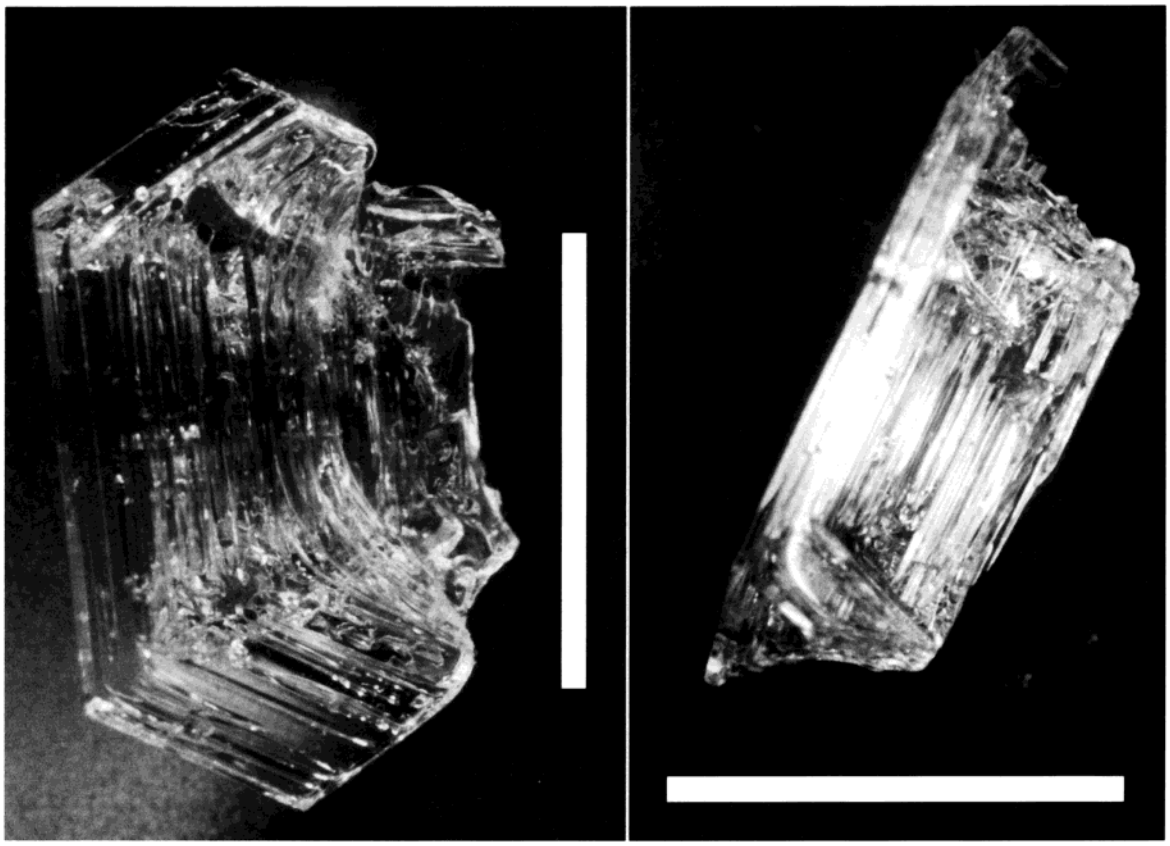

FIGURE 6. Optical microscopy pictures of a cup-shaped depth hoar crystal from sample 4. The same crystal is shown from two different angles. The hexagonal symmetry is clearly visible, showing preferential growth along the *c* axis. Scale bars: 5 mm.

OM for sample 3 is probably caused by hollows in the bullets and columns. These hollows would increase SSA by about 60%, thus bringing both values into acceptable agreement (840 vs 670 cm^2/g). Some crystals of Figure 5 indeed look hollow, and this would be consistent with observations by other authors (*17*, *24*), but higher magnification pictures are needed to see more details.

The main sources of uncertainties of OM have been listed in the Introduction, and the largest ones are the difficulty to determine all dimensions of a crystal, three-dimensional shapes, and surface rugosity. Regarding rugosity, dendritic crystals can have up to nine thickness levels (*18*), and taking those into account could yield a SSA value up to twice that obtained using a constant thickness. The use of relationships to determine crystal thicknesses is not adequate: the discussion of the dimensions of the crystals of Figure 4 shows that actual and predicted thicknesses differ by a factor of up to 5. The only way around this difficulty would be to have a 2-axis orientable stage and to use reflected light. This is in principle possible, but such a setup was not available to us.

Taking into account complex crystal shapes thus appears very difficult with OM as the only tool. Seeing the complex shapes of graupel particles does not appear possible with OM as stressed by Wergin et al. (*21*) and suggested by the photographs of Pruppacher and Klett (*19*). The existence of ridges, hollows, air inclusions, and other structures may be observed with OM using reflected or transmitted light, depending on what is sought, but elaborate setups are required to see such details on small crystals such as diamond dust. In any case, an estimate of the thicknesses will often be difficult, even if stereophotomicrography is used (*24*), and solving these difficulties will make the estimation of one SSA value much more time-consuming than using CH_4 adsorption.

Our conclusion on the merits of OM is that, even using a more sophisticated OM setup than that used here, it does not appear possible to reach the accuracy of adsorption methods. Thus, even though OM appears capable of yielding useful estimates of SSA, monitoring with precision the evolution of the SA of a snow layer does not appear possible with OM. Gross errors in SSA estimates can also be expected if micron-size microstructures are present (*10*, *17*). OM can however be envisaged as a complement to adsorption methods because it allows the monitoring of shape evolution. In particular, it will help evaluate snow sublimation or condensation, which will be necessary to quantify the amounts of dissolved gases released or trapped during these processes.

SEM has clear disadvantages: it requires expensive equipment that needs $N_2(l)$, and obtaining a representative number of pictures takes much longer than making a SSA measurement using adsorption. Thus, this technique cannot be used for routine SSA estimation. Yet, its use for a limited number of selected samples can bring unique data on the three-dimensional shapes of snow crystals, especially if an orientable stage is available. SEM can also be valuable to observe subtle changes in snow morphology during metamorphism in a manner more accurate than OM. This may be valuable to differentiate between adsorption/desorption and evaporation/condensation processes.

Stereology is another possible method to obtain SSA values. However, we cannot comment on it here, and future studies will be aimed at comparing SSA values obtained by CH_4 adsorption and that method.

Regarding snow microphysics, two conclusions can be derived here. First, our data cast doubt on the validity of relationships such as R2. The presence of both plates and needles in sample 2 shows that different parts of the cloud

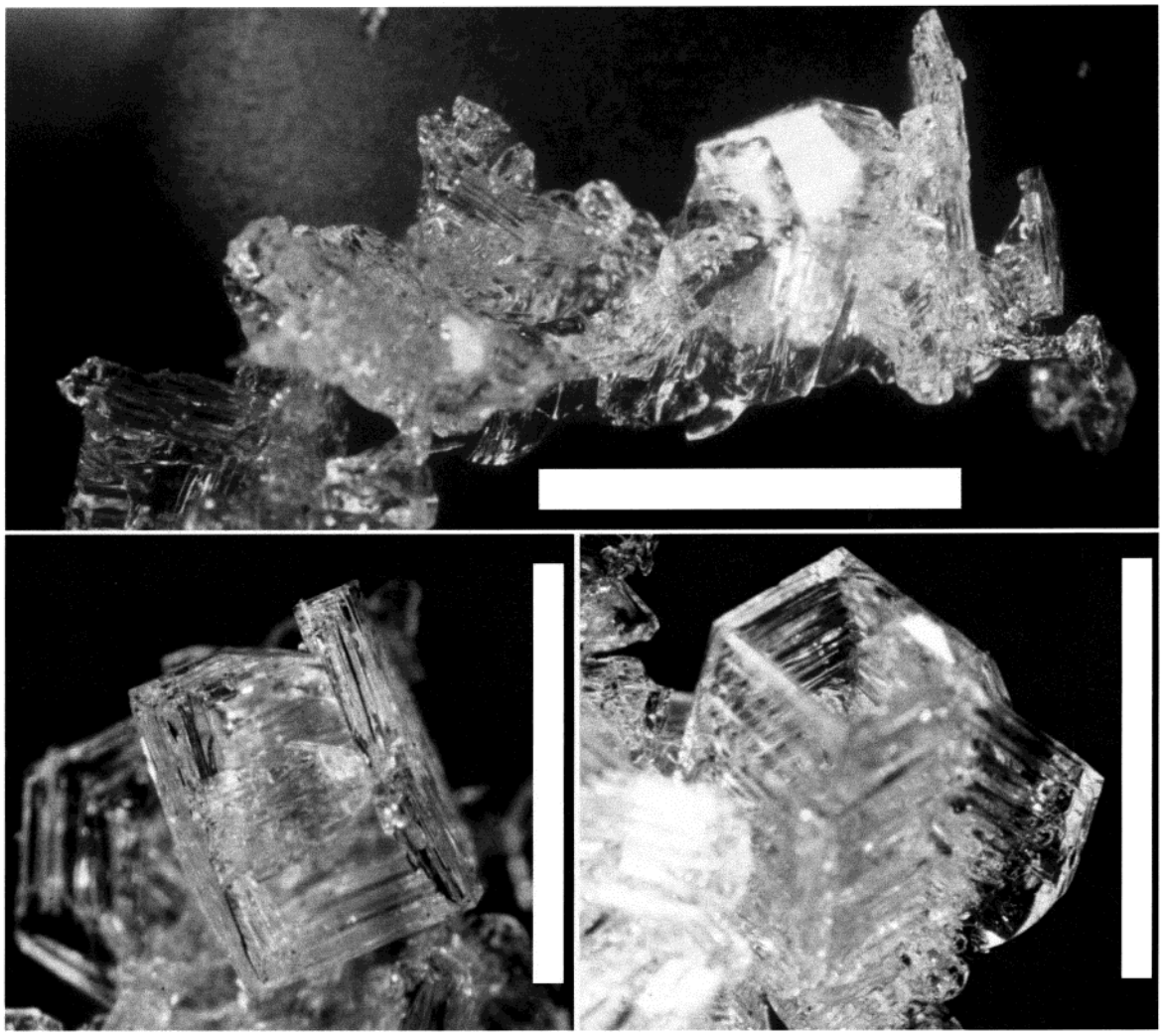

FIGURE 7. Optical microscopy pictures of crystals from sample 4. Top: Cluster of faceted crystals. Bottom: Columnar crystals with square symmetry, indicating preferential growth of the prismatic faces. Scale bars: 5 mm.

were at different temperatures and/or that temperature varied during ice crystal growth. Thus, R2 may apply to crystals growing under constant conditions but not to our case and probably not to many others.

Second, the microstructure of the Graupel crystal of Figure 2 is very different from what can be deduced from OM images (ref *19*, p 50). The most interesting observation is that rime drops do not coalesce and retain their individuality. Trace gases in rime ice are almost always supersaturated with respect to the atmosphere (*25*−*26*), and will tend to re-equilibrate by releasing trace gases. Figure 2 shows that modeling this release cannot be made by assuming condensed phase diffusion out of the 1-mm particle of Figure 2. The model should include condensed phase diffusion out of 50-μm structures, followed by gas-phase diffusion out of the particle using a tortuous path. This last process will be slowed by adsorption/desorption events on the ice surface. The accurate description of these processes will require the knowledge of (i) the structure of rime ice, and in particular whether the supersaturated gases are dissolved in ice or remain in veins of concentrated liquid solutions, and (ii) the interactions of the trace gas with the ice surface.

Acknowledgments

We thank Jacqueline Boumendil for assistance in obtaining SEM data at Centre de Microscopie Appliquée à la Biologie et la Géologie, University Lyon I; our colleague Jacques Meyssonnier for the use of the optical microscope; and Dominique Lecorps, Météo-France, for the use of the photomicrography equipment at Alert. The efforts of Peter Brickell to provide us with a continuous supply of liquid nitrogen at Alert are greatly appreciated. The alpine part of this work was funded by CNRS through Programme National de Chimie Atmosphérique (PNCA). The Arctic part was funded by the French Polar Institute (IFRTP), with the logistics assistance of the Meteorological Service of Canada, within the framework of Polar Sunrise Experiment 2000, coordinated by Jan Bottenheim and Paul Shepson. Numerous helpful suggestions by three anonymous reviewers are gratefully acknowledged.

Literature Cited

(1) Robinson, D. A.; Dewey, K. F.; Heim, R. R., Jr. *Bull. Am. Meteorol. Soc.* **1993**, *74*, 1689.
(2) Sumner, A. L.; Shepson, P. B. *Nature* **1999**, *398*, 230.
(3) Hutterli, M. A.; Röthlisberger, R.; Bales, R. C. *Geophys. Res. Lett.* **1999**, *26*, 1691.
(4) Couch, T. L.; Sumner, A.-L.; Dassau, T. M.; Shepson, P. B.; Honrath, R. E. *Geophys. Res. Lett.* **2000**, *27*, 2241.
(5) Honrath, R. E.; Peterson, M. C.; Guo, S.; Dibb, J. E.; Shepson, P. B.; Campbell, B. *Geophys. Res. Lett.* **1999**, *26*, 695.
(6) Weller, R.; Minikin, A.; König-Langlo, G.; Schrems, O.; Jones, A. E.; Wolff, E. W.; Anderson, P. S. *Geophys. Res. Lett.* **1999**, *26*, 601.
(7) Dominé, F.; Thibert, E. *Geophys. Res. Lett.* **1996**, *23*, 3627.
(8) Thibert, E.; Dominé, F. *J. Phys. Chem. B* **1998**, *102*, 4432.

(9) Gregg, S. J.; Sing, K. S. W. *Adsorption, Surface Area and Porosity*; Academic Press: London, 1982.
(10) Hanot, L.; Dominé, F. *Environ. Sci. Technol.* **1999**, *33*, 4250.
(11) Hoff, J. T.; Mackay, D.; Wania, F.; Jia, C. Q. *Environ. Sci. Technol.* **1998**, *32*, 58.
(12) Chaix, L.; Ocampo, J.; Dominé, F. *C. R. Acad. Sci. Ser. II* **1996**, *322*, 609.
(13) Narita, H. *Low Temp. Sci.* **1971**, *A29*, 69.
(14) Perla, R.; Dozier, J.; Davis, R. E. *J. Microsc.* **1986**, *141*, 111.
(15) Nishida, K.; Narita, H. *J. Geophys. Res.* **1996**, *101*, 21331.
(16) Brzoska, J. B.; Lesafre, B.; Coléou, C.; Xu, K.; Pieritz, R. A. *Eur. Phys. J.: Appl. Phys.* **1999**, *7*, 45.
(17) Wergin, W. P.; Rango A.; Erbe, E. F. *Scanning* **1995**, *17*, 41.
(18) Fassnacht, S. R.; Innes, J.; Kouwen, N.; Soulis, E. D. *Hydrol. Process.* **1999**, *13*, 2945.
(19) Pruppacher, H. R.; Klett, J. D. *Microphysics of Clouds and Precipitation*; Reidel: Dordrecht, The Netherlands, 1978.
(20) Cabanes, A.; Legagneux, L.; Dominé, F. Manuscript in preparation.
(21) Wergin, W. P.; Rango, A.; Erbe, E. F. *Scanning* **1998**, *20*, 285.
(22) Döppenschmidt, A.; Butt, H.-J. *Langmuir* **2000**, *16*, 6709.
(23) Haynes, D. R.; Tro, N. J.; George, S. M. *J. Phys. Chem.* **1992**, *96*, 8502.
(24) Iwai, K. *Mem. Natl. Inst. Polar Res.* 4, **1986**, *5*, 38.
(25) Snider, J. R.; Montague, D. C.; Vali, G. *J. Geophys. Res.* **1989**, *94*, 7569.
(26) Iribarne, J. V.; Pyshnov, T. *Atmos. Environ.* **1990**, *24A*, 383.

Received for review April 7, 2000. Revised manuscript received November 27, 2000. Accepted November 28, 2000.

ES001168N

III.4. Structure, microphysics, and surface area of the Arctic snowpack near Alert during the ALERT 2000 campaign.

Cet article (avec l'**article 4, § III.5.**) présente les résultats obtenus lors de la campagne de terrain ALERT 2000 qui s'est déroulée en Février et Avril 2000 dans l'Arctique canadien près d'Alert (82°30'N, 62°20'W, Ile d'Ellesmere, Canada).

Ici, l'objectif principal est d'obtenir des données permettant de quantifier les processus ayant lieu à la surface de la glace et interagissant sur la chimie atmosphérique en région Arctique. Il s'agit en fait de déterminer la surface totale développée par le manteau neigeux afin d'estimer notamment sa capacité de stockage à la surface de la glace. Pour cela, nous avons étudié la stratigraphie du manteau neigeux recouvrant le sol et la glace de mer. La SS et la densité de la plupart des couches étudiées ont été mesurées. Les autres ont été estimées à partir des valeurs obtenues pour des couches similaires. L'exemple de l'acétone, qui s'adsorbe fortement à la surface de la glace, a été pris pour mettre en évidence l'impact du manteau neigeux sur la répartition de ce gaz entre la phase gaz et la neige.

Une interprétation du mécanisme de formation et d'évolution du manteau neigeux est également présentée dans cet article.

Le principe de la mesure de SS est détaillé dans l'article 1(cf. **§ III.2**.), il n'est donc pas utile de le relire ici.

Structure, microphysics, and surface area of the Arctic snowpack near Alert during the ALERT 2000 campaign

Florent Dominé*, Axel Cabanes and Loic Legagneux

CNRS, Laboratoire de Glaciologie et Géophysique de l'Environnement, BP 96, 38402 St Martin d'Hères cedex, France

Abstract

The seasonal snowpack at Alert (North coast of Ellesmere Island, 82°29.94' N, 62°20.55'W) was studied in February and April 2000, on land and on sea ice. The stratigraphy was studied, and the density and specific surface area (SSA) of each snow layer were measured. SSA was measured by CH_4 adsorption at 77K using a volumetric method. On land, the snowpack was 10 to 50 cm thick and consisted of a depth hoar layer covered by one or more hard wind-packed layers with densities between 0.35 and 0.52. These were sometimes separated by soft layers of more or less faceted crystals. The surface was covered by recent precipitation and surface hoar. The stratigraphy on sea ice was more variable, with numerous hard wind-packed layers alternating with soft layers of depth hoar or faceted crystals. SSA values ranged from 125 cm^2/g for depth hoar to 1500 cm^2/g for diamond dust and dendritic snow. The total surface area of the snowpack was calculated from the thickness, density, and SSA of each layer, and ranged from 1160 to 3710 m^2 of snow surface area per m^2 of ground. These values were used to estimate the potential impact of the snowpack on atmospheric chemistry, by adsorption/desorption of trace gases. Using the example of acetone, whose adsorption behavior on ice is estimated, it is found that the snowpack may sequester most of the acetone of the (snow + boundary layer) system most of the year. The release during metamorphism of trace gases dissolved in snow is also discussed. We propose that the frequency and intensity of wind storms will strongly affect the release of trace gases, as this will determine whether intense metamorphism leading to depositional depth hoar can happen.

Key words: Snow, surface area, density, metamorphism, stratigraphy

*Corresponding author. Phone: (33) 476 82 42 69; e-mail : florent@glaciog.ujf-grenoble.fr

Submitted, Atmospheric Environment, 7 june 2001

Revised,30 november 2001

Introduction

Recent studies have revealed the potential impact of the snow cover on polar atmospheric chemistry. Production of nitrogen oxides in the snowpack (Dibb et al., 1998; Weller et al, 1999; Honrath et al., 1999, 2000a), by photolysis of the nitrate ion, NO_3^- (Honrath et al., 2000b), and their release to the atmosphere has been observed in Greenland and Antarctica. The snowpack then reactivates NO_3^-, usually considered as irreversibly oxidized, and extends the lifetime of anthropogenic NO_x.

Similarly, carbonyl compounds are released to the atmosphere by the snowpack (Hutterli et al., 1999; Sumner and Shepson, 1999, Couch et al., 2000). Considering the importance of carbonyls on the oxidizing capacity of the atmosphere (Lary and Shallcross, 2000), it is again clear that the presence of snow, that can affect up to 50% of northern land masses (Robinson et al., 1993), may strongly impact tropospheric chemistry.

To model the impact of the snowpack on tropospheric chemistry, the processes that cause exchanges of gases between the snow and the atmosphere must be understood (Michalowski et al., 2000). These include adsorption/desorption from the surface of snow crystals (Hutterli et al., 1999, Hanot and Dominé, 1999), formation and subsequent sublimation of ice-trace gas solid solutions (Dominé and Thibert, 1996), photolysis of dissolved precursors (Honrath et al., 1999, 2000b; Weller et al, 1999), heterogeneous reactions on the surface of snow crystals, as observed in stratospheric ozone depletion (Chu et al., 1993), and solid state diffusion in and out of ice crystals (Thibert and Dominé, 1998).

The main purpose of this work is to provide data that will allow the quantification of surface processes such as adsorption/desorption and heterogeneous reactions, and we have measured the surface area (SA) and density of snow samples. By surface area of a snow sample we mean the area of the snow sample that is accessible to gases (Gregg and Sing, 1982), and this is expressed in m^2. The ratio of the SA of a snow sample over its mass yields the specific surface area (SSA) of the sample, expressed in m^2/g, or rather in cm^2/g as snow SSA is usually small. The product of SSA, density, and thickness of each snow layer yields the total surface area (TSA) of the layer, which is a dimensionless parameter, expressed in m^2 of snow per m^2 of ground. Values of snowpack TSA can be used to quantify surface processes in models. Another purpose of this work is to understand the mechanism of snowpack formation and the extent of metamorphism, to assist in the modeling of sublimation/condensation cycles that can trap or release dissolved species.

Here we report observations of the snowpack stratigraphy near Alert (82°29.94' N, 62°20.55'W, Canadian Arctic) in February and April 2000, during the dark and sunlit phases of the ALERT 2000 experiment. The densities and SSA of many snow layers were measured, and macrophotographs of each sample were taken. Observations were made on land, on sea ice a few km NW of the base, and at a remote location on the Arctic ocean.

Experimental methods

General considerations

Snowpack observations were made in winter between 4 and 23 February 2000, and in spring between 11 and 30 April 2000. The snowpack at Alert is seasonal. Over flat areas its thickness was usually 10 to 25 cm in winter and 20 to 50 cm in spring. Winter observations were limited by low temperatures and darkness, that was complete until mid February, requiring the use of a head lamp. More detailed observations were made in spring.

The experimental systems were located in the FTX building (82°27.28' N, 62°29.69' W), at about 200 m elevation, 5.4 km SW of the Alert base. Observations and samplings were mostly done 300 m SE of the FTX building (hereafter: site A). In winter, snow was also sampled on the sea ice in Joliffe bay, about 1 km North of the coast, and 4 km W-NW of Alert station. In spring, snow was also sampled at an ice camp (82°31.74' N, 62°44.39' W) on sea ice near Williams Island, 2 km N of the winter sea ice site. A plane trip also allowed snow sampling on the Arctic Ocean, at about 85 °N.

Snow sampling

Vertical faces were dug in the snow to observe the stratigraphy. The density of each layer was measured using a 500 ml plexiglas sampler for soft snow layers, and a 100 ml metal sampler for hard layers. The density of thin surface snow layers lying on hard wind-packed snow was estimated by scraping 400 cm^2 of snow into a bag after having measured the layer thickness at 10 different spots. For SA measurements, snow was sampled into glass vials. At site A, the vials were immediately immersed in liquid nitrogen. Often, snow was also sampled directly into the containers used for SA measurements.

Sampling vials used on sea ice were kept in a cooler, and immersed in liquid nitrogen upon returning to the laboratory, 2-3 hours later. Considering the rate of snow SSA evolution (Cabanes et al., this issue) at the low temperatures involved, this procedure probably did not affect snow SSA in a detectable manner. For hard snow, snow chunks as large as possible (3 to 8 cm^3) were sampled. To minimize the creation of extra surface area, great care was taken to remove any loose snow grains upon transfer into the SA measurement apparatus.

Macrophotographs

Snow macrophotographs were taken with a reflex camera, bellows, and a 38 mm macro lens with a minimum aperture of f16. The maximum magnification (size of the object on film/its real size) was 7.

Surface area measurements

Snow surface area was measured using a volumetric method with BET analysis (Chaix et al., 1996; Hanot and Dominé, 1999, Legagneux et al., in press). The principle of the method is to determine the number of CH_4 molecules that can be adsorbed on the snow surface, and to deduce the sample SA knowing the cross sectional surface area of a CH_4 molecule on ice (19.18×10^{-20} m^2, Chaix et al., 1996). The volumetric system consisted of 2 containers, one of which (V_e) contained the snow

immersed in liquid nitrogen, and the other (V_i) was at room temperature, and was connected to a capacitance manometer. CH_4 was leaked into V_i and the number of CH_4 molecules was deduced from the ideal gas equation. The valve between V_i and V_e was then opened. The new pressure was measured. A molar balance yielded the number of CH_4 molecules adsorbed. Increments of CH_4 were added into V_i, and the adsorption isotherm was recorded. A BET analysis (Brunauer et al., 1938) yielded the SA from the isotherm. SSA was derived as the ratio of SA over mass. The precision on SSA is 6%, the accuracy 12% (Legagneux et al., in press).

Results

Meteorology

Understanding the formation and properties of the snowpack is facilitated if meteorological conditions are known. These are routinely measured at the GAW lab, about 300 m from sampling site A, and at the Alert base, at an elevation of about 30 m, with conditions probably similar to the ice camp. Meteorological parameters between both meteorological stations may slightly vary. However, for the purpose of understanding snowpack formation, this difference will have little effect.

Data from the Alert base over the period 1951-1995 show that the mean monthly temperature is above freezing 2 months per year, in July and August. The Alert area is snow-covered 10 months of the year. Precipitation is about 150 mm per year, with maximum in summer (24 mm in August and September) and minimum in February (6 mm). The most important parameters to understand snow formation are temperature, wind speed, precipitation, and snow accumulation. Precipitation and accumulation are not monitored, and only data on snowfalls observed during the campaigns are available.

In winter, light snow falls deposited about 1 cm of snow on 3 and 7 February. Surface hoar grew on the snow surface and became clearly visible on 15 February. On 21 February, before a wind storm modified surface snow, surface hoar consisted of feather-shaped clusters of crystals that had reached 15 mm in length. In spring, light snow falls were observed on 13 and 14 April, that deposited 2 and less than 1 mm of snow, respectively. Surface hoar grew rapidly on the snow surface to form again feather-shaped clusters of crystals that were 20 mm long on 24 April. A large snow fall deposited about 5 cm of snow between 25 and 28 April under windy conditions. Finally, less than 1 mm of snow fell on 30 April.

Temperature and wind speed measured at the GAW lab between 1 September 1999 and 2 May 2000 are shown in Fig. 1.

Temperature stayed below –10°C from October to May, and reached –44.5°C on 6 February. October had many wind storms, but wind speed is usually low at Alert. In winter, calm periods of up to 4 weeks were separated by wind storms, with speeds up to 29 m/s (105 km/h) on 2 February. These storms were accompanied by temperature increases, caused by mixing with higher and warmer air layers.

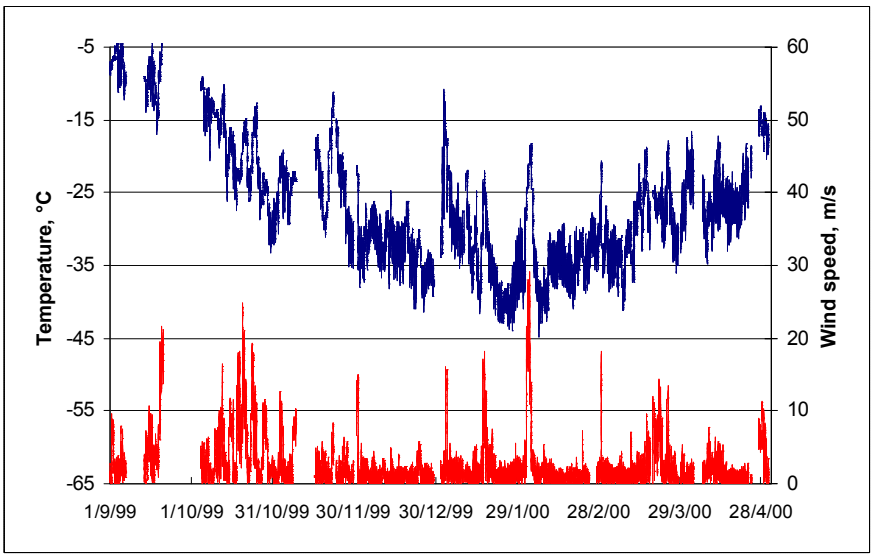

Figure 1: Temperature and wind speed measured at the GAW lab, 300 m from sampling site A, between September 1999 and May 2000.

Snow stratigraphy

The snow stratigraphy of site A on 8 February 2000 (Fig. 2) is typical of the snowpack stratigraphy on land.

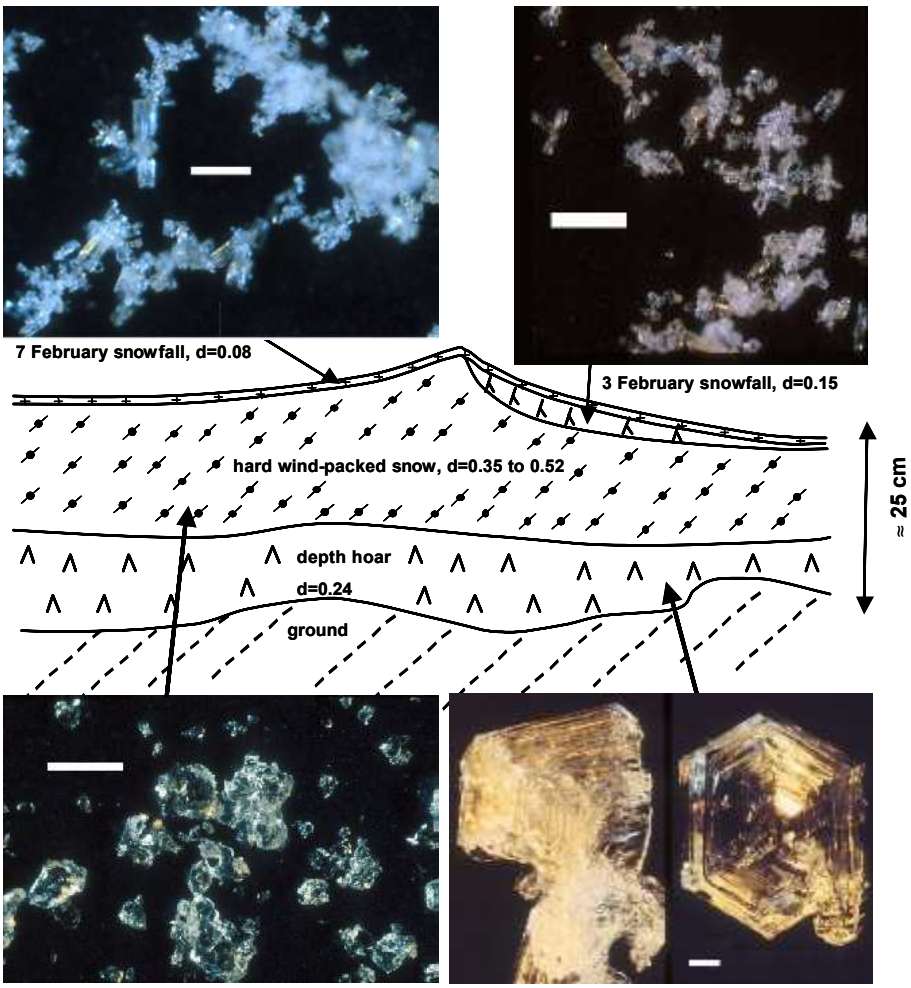

Figure 2: Typical snowpack stratigraphy at site A (on land) on 8 February 2000, with macrophotographs of snow crystals. Scale bars : 1 mm.The layer lying on the ground consisted of

5 to 15 cm of depth hoar, i.e. large faceted crystals of hexagonal or square symmetry, that are often cup-shaped. This layer had little or no cohesion, and its density was 0.18 to 0.25 g/cm^3. Over the depth hoar was a hard to very hard (a pencil could not penetrate it) wind-blown layer, of density 0.35 to 0.52, but usually close to 0.5. It consisted of rounded and heavily sintered crystals 0.1 to 0.6 mm in size. Loose surface layers consisted of a discontinuous layer 3 to 8 cm thick overlaid by a continuous layer 0.5 to 1.5 cm thick. The discontinuous layer was formed by snow fallen on 3 February, at the end of a violent wind storm. Wind speed during precipitation was 8 to 10 m/s at the beginning, dropping to 3 to 4 m/s at the end. This wind mobilized the snow, that accumulated in hollows or in the lee of sastrugi (i.e. wind-generated snow dunes that were 5 to 30 cm high around Alert). This layer, with a density of 0.15, consisted of submillimetric columns and bullet combinations. Such snow, when it falls under clear sky conditions, is usually called diamond dust. Here, some clouds were present during precipitation but the term diamond dust will nevertheless be used to refer to such snow. More diamond dust fell on 7 February under calm conditions, to form a layer of density 0.08, with crystals similar to those of the 3 February layer, although smaller crystals were also present (Fig. 2).

At the end of the winter campaign, twilight revealed moderate variability of the land snow cover. Over 80% of flat areas were snow-covered, usually by 10 to 25 cm of snow, although thicknesses of 0 to 45 cm were observed. The simplest stratigraphy consisted of a thin hard wind-packed layer overlaid by the 7 February diamond dust layer. Depth hoar was almost always present, however, even though it was sometimes only 1 to 2 cm thick. Uncovered areas were outcropping rocks and small ridges. Up to 50% of the surface of hill sides exposed to the prevailing SSW winds were uncovered. Downwind slopes were almost entirely snow covered.

The snow stratigraphy on sea ice in Joliffe bay was more variable, both in terms of thickness (0 to 50 cm, about 30 % of bare ice observed) and stratigraphy. Trips to Joliffe bay were made on 11 and 17 February. The stratigraphy of a snow bank is shown in Fig. 3.

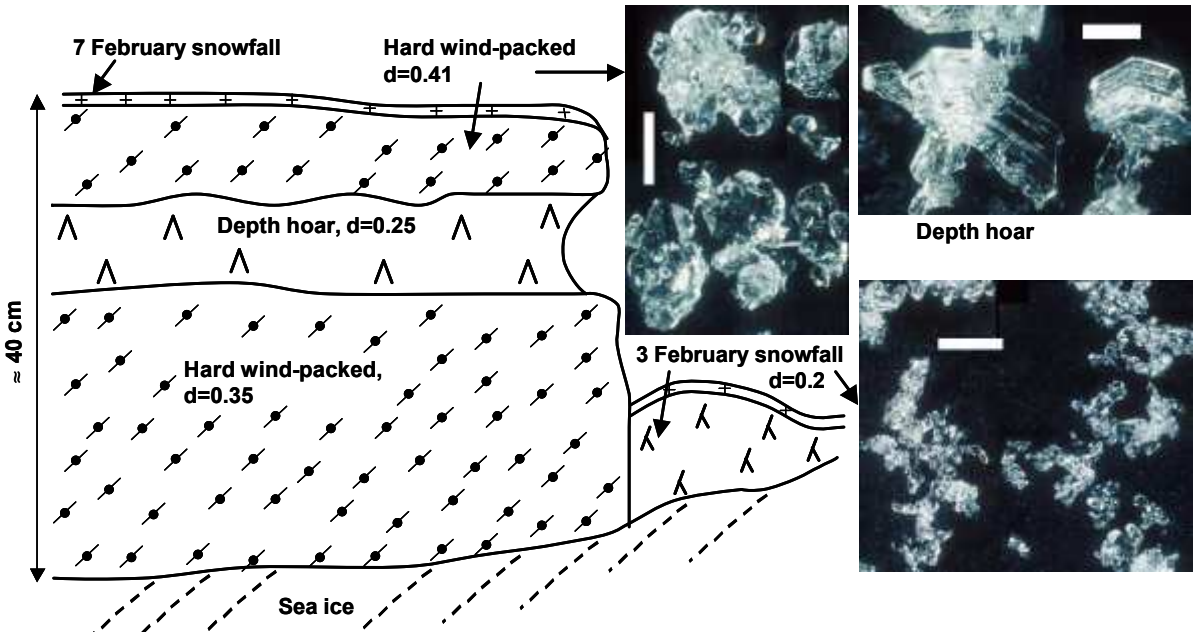

Figure 3: Example of snowpack stratigraphy on Joliffe bay (on sea ice) on 11 February 2000, with macrophotographs of snow crystals. Scale bars : 1 mm. Crystals of the 3 February layer shown were sampled on 17 February.

Such a bank seemed representative of fairly numerous structures around the sampling site, but this is deduced from limited observations during 30 minutes of exploration in total darkness using a head lamp. A 20 cm thick wind-packed layer of density 0.35 and of moderate hardness was on the ice. That layer was not sampled. Over it was 10 cm of depth hoar of density 0.25, with crystals smaller than those of the depth hoar at site A. Over the depth hoar was a hard wind-packed layer of density 0.41, with crystals similar to those of the wind-packed layer of site A. The 1 cm thick top layer was made of diamond dust fallen on 7 February. It was not sampled. Next to the snow bank, soft snow of density 0.2 had accumulated. Most likely, this was the 3 February diamond dust layer, also covered by the 7 February layer. On 17 february, extensive crystal rounding had taken place in the 3 february layer and the initial crystals were difficult to recognize.

The stratigraphy at site A on 18 April is shown in Fig. 4.

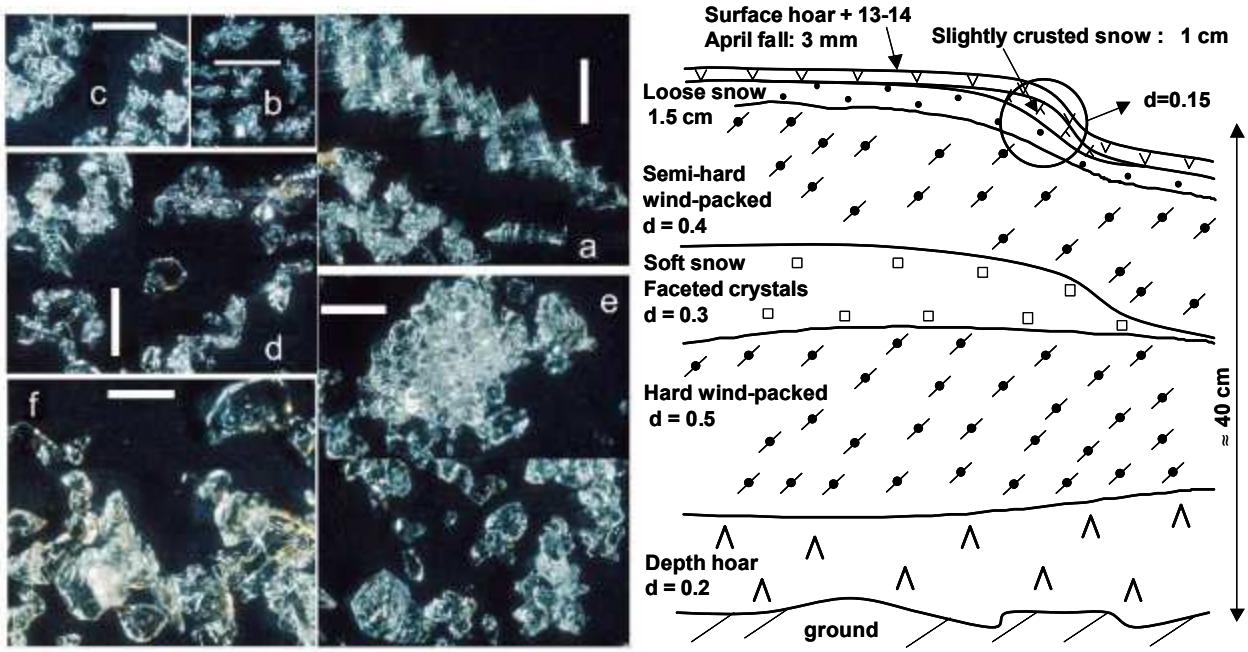

Figure 4: Typical snowpack stratigraphy at site A (on land) on 18 April 2000, with macrophotographs of snow crystals. All scale bars : 1 mm (a) Surface hoar and aged diamond dust crystals, sampled on 19 and 20 April (b) Diamond dust crystals fallen on 13 and 14 April, sampled on 15 and 16 April. (c) Crystals from the slightly crusted surface layer. (d) Crystals from the loose surface layer. (e) Crystals from the semi-hard wind-packed layer. A cluster of unseparated grains is shown. (f) Faceted crystals from the soft snow layer.The depth hoar and hard wind-packed layers observed in the winter displayed no detectable change. A soft, uncohesive layer of density 0.3, made up of mostly unsintered crystals 0.3 to 1.5 mm in size was present on top of this winter hard layer. The crystals were mostly rounded, but some facets were present. This discontinuous layer was absent in 20% of the pits that were dug. Above this soft layer was a hard wind-packed layer of density 0.4 made up of small (0.1 to 0.8 mm) rounded and highly sintered crystals. It was not as hard as the winter wind-packed layer.

Three thin layers were seen near the surface. The lowest one consisted of unsintered crystals 0.1 to 1 mm in size (Fig. 4d). Some crystals were elongated. Most shapes were rounded, but a significant number of facets were seen. This layer could be a mixture of buried diamond dust and surface hoar crystals that had undergone recent rounding, but metamorphism had also probably formed some facets. Crystal shapes suggested that this layer was deposited several days to 3 weeks earlier. The

middle layer was discontinuous and formed an easily breakable crust formed by slightly sintered crystals similar to the underlying layer, but in the size range 0.1 to 0.5 mm (Fig. 4c). The slightly crusted character of this layer was probably caused by moderate winds a few days or weeks earlier. These thin subsurface layers were covered by a thin layer of diamond dust that precipitated in 2 events on 13 and 14 April. This top layer grew in thickness with the progressive formation of surface hoar.

As in winter, the snowpack on sea ice was more variable than on land. Less bare ice was visible than in winter. The snowpack was up to 50 cm thick. Snow layers were more numerous and thinner than on land. Usually, several layers of depth hoar or of smaller faceted crystals with little or no cohesion alternated with wind-packed layers. One snow bank consisting of a large variety of layers was sampled on 23 April. Its stratigraphy (Fig. 5) will be described by numbering layers from the bottom.

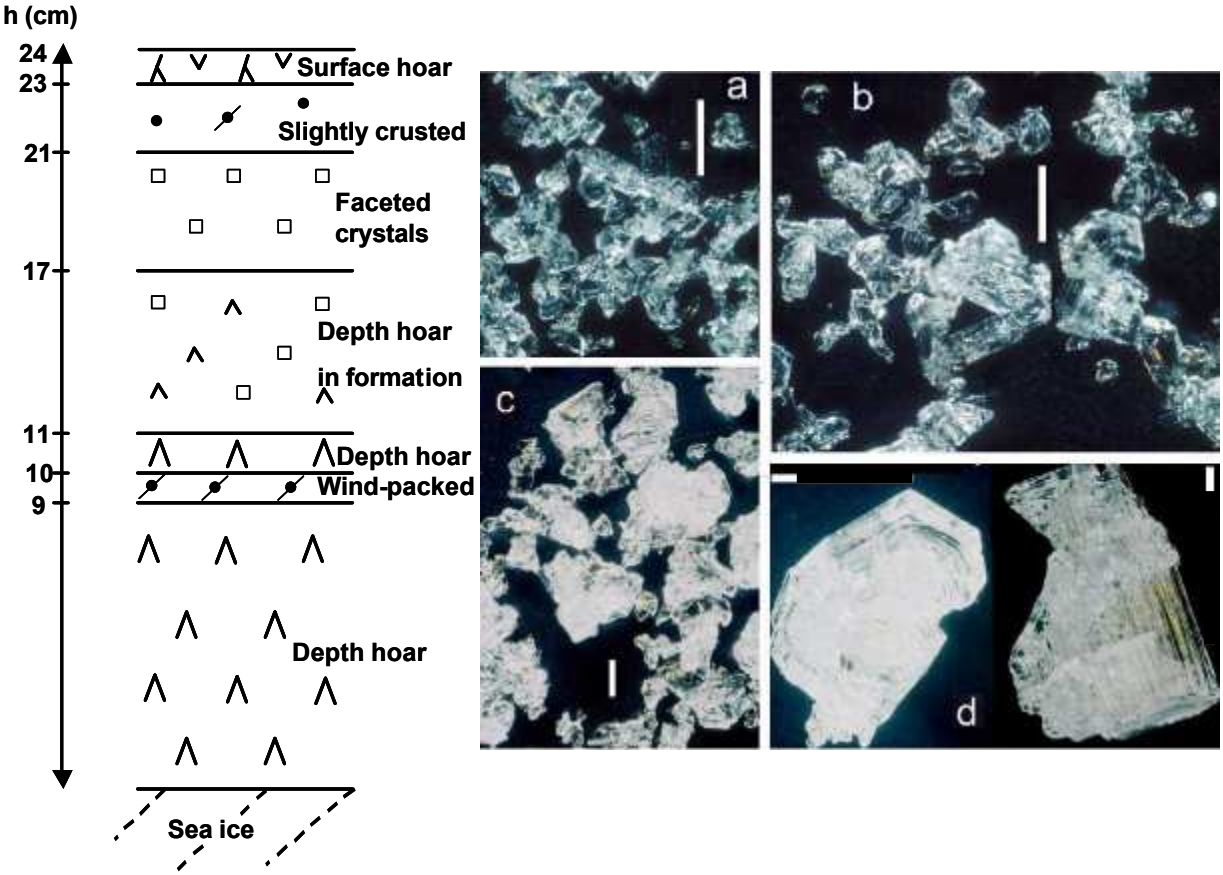

Figure 5: Example of snowpack stratigraphy at the ice camp (on sea ice) on 23 April 2000, with macrophotographs of snow crystals. All scale bars : 1 mm. (a) Surface hoar. (b) Faceted crystals. (c) Depth hoar in formation (d) Bottom layer of depth hoar.

Layer (1) consisted of depth hoar crystals 3 to 10 mm in size (Fig. 5d) that had a tendency to line up vertically, forming brittle columns of crystals with some cohesion. Layer (2) was a 1 cm thick wind-packed layer that was not sampled. Layer (3) was 1 cm thick and consisted of uncohesive depth hoar, that was not sampled. Layer (4) was 6 cm thick and consisted of faceted, sometimes striated, crystals (Fig. 5c) 1 to 3 mm in size, that were lined up to form brittle vertical columns, similar in structure to layer (1) except that the crystals were smaller rarely cup-shaped. Layer (4) resembled depth hoar at an early stage of formation. Layer (5) consisted of faceted crystals 0.3 to 1.5 mm in size (Fig. 5b). Its cohesion varied from slightly cohesive to uncohesive. Layer (6) was formed by small crystals that were

not sampled. It looked similar to the middle, discontinuous and slightly crusted surface layer observed on land at site A, but was slightly more cohesive. The top layer (7) was made up mostly of highly faceted crystals 0.2 to 1.5 mm in size. They were surface hoar crystals at an early stage of growth (Fig. 5a), difficult to identify with the naked eye. Some highly metamorphosed columns and bullet combinations, precipitated on 13 and 14 April, may have been present.

A plane trip was made on the Arctic ocean (85°N) on 25 April. The limited time spent on the sea ice allowed a few observations and a preliminary description. Most of the ice seen from the plane was formed at the beginning of the winter or was multi-year ice. Recently refrozen leads, covered by a limited amount of snow, made up less than 5% of the ice pack. Snow stratigraphy was observed on aged ice, that appeared to have accumulated all the precipitation and wind-blown snow from the winter season. Ten pits were dug. Snow thickness was 70 cm in 2 pits dug at the top of sastrugi. The other 8 pits had thicknesses between 15 and 25 cm. The stratigraphy of one of those pits is shown in Fig. 6.

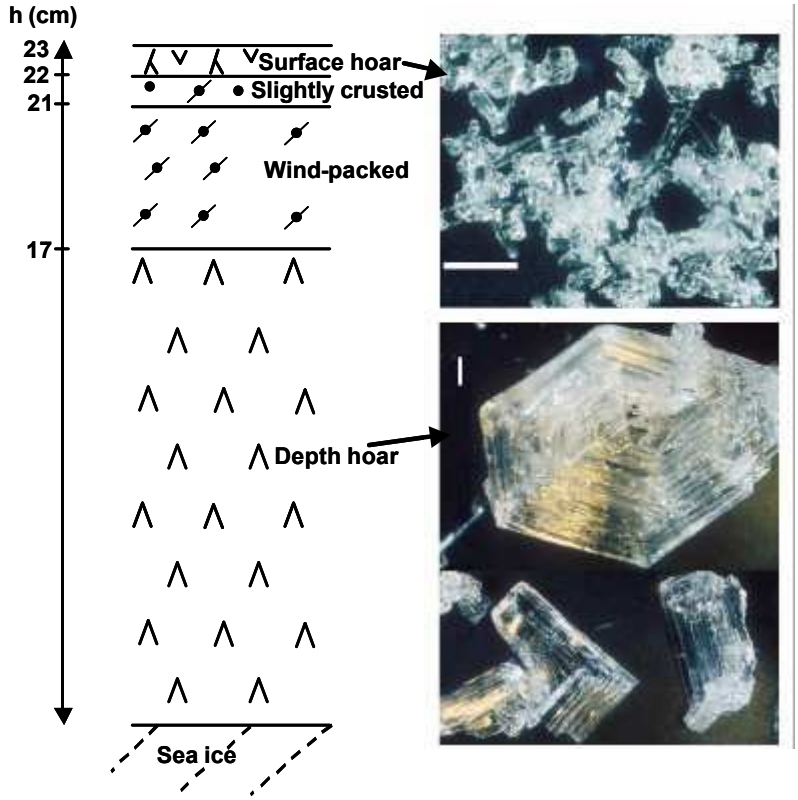

Figure 6: . Example of snowpack stratigraphy on the Arctic ocean (85°N) on 25 April 2000, with macrophotographs of snow crystals. All scale bars : 1 mm.

Layer (1) was 17 cm thick and consisted of unusually cohesive depth hoar with crystals 5 to 15 mm in size. Layer (2) was wind-packed snow of moderate hardness, 5 cm thick and was subdivided into sublayers of variable hardnesses. That layer was not sampled. Layer (3) was 1 cm thick and consisted of slightly crusted small crystals, that seemed similar to the surface light crust seen on land and at the sea ice camp. It was not sampled. Layer (4) was 1 cm thick and, as at the ice camp, consisted of small surface hoar crystals with the possible presence of highly metamorphosed diamond dust crystals.

Snowpack surface area

The SSAs of all snow layers on land and of most layers on sea ice were measured, along with their densities and thicknesses. These values, summed up in Table 1, were used to determine the TSA of the snowpacks shown in Figs. 2 to 6. Densities and SSAs values not measured were estimated by comparison with similar snow layers.

The TSA of the snowpack on land at site A increased from 1720 m^2 of snow surface area per m^2 of ground in winter to 2740 m^2/m^2 in spring. This increase is real and corresponds to increased snow accumulation between February and April. Besides the thin diamond dust falls of 3 and 7 February, the snow layers seen in winter were observed again in spring, and their SSA showed no significant change in 2 months. The stratigraphies observed on land (Figs. 2 and 4) were also representative of the snowpack found within several km of the FTX building.

On the contrary, the decrease suggested in snow TSA on sea ice from 3710 to 1160 m^2/m^2 between winter and spring is probably not representative of the actual trend. Firstly, only 2 days were spent on the sea ice in winter and in spring. Secondly, the much greater snowpack variability, both in terms of thickness and stratigraphy, means that numerous snowpits should have been studied to obtain a representative estimate. The difficult winter conditions imply that the observations were not representative. It actually seemed that the sea ice spring snow cover was more extensive and thicker than in winter. The large winter value can be explained by the presence of 2 thick wind-packed layers. These windpacks have the largest TSA values, even though their SSA is low (Table 1). On the contrary, the spring snow bank of Fig. 5 had almost no windpack, which explains its low TSA.

Table 1. Specific surface areas (SSA) of snow from each snow layer and total surface area (TSA) of the snow pack at different locations and times.

TSA of the snowpack on land at site A on 8 February 2000, shown in Fig. 2					
Layer number	Description	Mean thickness cm	Mean density g/cm^3	SSA, cm^2/g	TSA of layer m^2/m^2
4	DD[a] precipitated on 7 feb.	1	0,08	1460	117
3	DD[a] precipitated on 3 feb.	1	0,15	760	114
2	hard wind-packed	15	0,48	160	1152
1	depth hoar	10	0,22	155	341
			TSA of snowpack		1720

TSA of the snowpack on the sea ice, Joliffe bay on 11 February 2000 shown in Fig. 3					
Layer number	Description	Mean thickness cm	Mean density g/cm^3	SSA, cm^2/g	TSA of layer m^2/m^2
4	DD[a] precipitated on 7 feb.	1	0,1*	680*	68
3	hard wind-packed	10	0,41	240	984
2	depth hoar	7	0,22	200	308
1	hard wind-packed	24	0,35	280*	2352
			TSA of snowpack		3710

TSA of the snowpack on land at site A on 18 April 2000, shown in Fig. 4					
Layer number	Description	Mean thickness cm	Mean density g/cm^3	SSA, cm^2/g	TSA of layer m^2/m^2
7	Surface hoar and DD[a]	0,3	0,16	400	19
6	slightly crusted surface snow	0,5	0,16	450	36
5	loose surface snow	1,5	0,16	350	84
4	hard wind-packed	10	0,4	240	960
3	uncohesive snow	3	0,3	350	315
2	hard wind-packed	15	0,48	150	1080
1	depth hoar	10	0,2	125	250
			TSA of snowpack		2740

TSA of the snowpack at the sea ice camp on 23 April 2000 shown in Fig. 5					
Layer number	Description	Mean thickness cm	Mean density g/cm^3	SSA, cm^2/g	TSA of layer m^2/m^2
7	Surface hoar and DD[a]	1	0,15*	330	50
6	slightly crusted surface snow	2	0,2*	400*	160
5	faceted crystals	4	0,3*	231	277
4	depth hoar in formation	6	0,25*	168	252
3	depth hoar	1	0,2*	175*	35
2	hard wind-packed	1	0,45*	160*	72
1	depth hoar	9	0,2*	175	315
			TSA of snowpack		1160

TSA of the snowpack on the Arctic Ocean, 85°N on 25 April 2000, shown in Fig. 6					
Layer number	Description	Mean thickness cm	Mean density g/cm^3	SSA, cm^2/g	TSA of layer m^2/m^2
4	Surface hoar and DD[a]	1	0,15*	405	61
3	slightly crusted	1	0,2*	400*	80
2	wind-packed	5	0,35*	280*	490
1	depth hoar	16	0,2*	170	544
			TSA of snowpack		1175

[a] DD = diamond dust

* These values were not measured. They were estimated by comparison with similar snow layers.

Discussion

Snowpack formation

Understanding the metamorphism involved in the formation of the snowpack is needed to quantify the incorporation and release of solutes in future models. Current theories of snow metamorphism (Colbeck, 1983) seem applicable to the snowpack studied. Around Alert, precipitation is low (150 mm per year), and wind storms violent enough to affect surface snow happen fairly frequently. Wind, rather than accumulation, is then the main factor determining snowpack structure. Our observations indicate that in the winter, the growth of the snowpack proceeds in the following steps:

- Fresh snow falls on the surface.

- Fresh snow undergoes metamorphism: crystals shapes and sizes change. This process is quite slow around –40°C (Cabanes et al., this issue).

- Surface hoar forms continuously on top of fresh snow.

- A wind storm takes place. Snow is blown around. Grains are rounded by sublimation and broken up. Snow accumulates in sheltered areas. Old sastrugi are eroded, while others form elsewhere. Previously undisturbed snowfalls accumulate on a fraction of the surface, while older snow is exposed on the remaining part of the surface. Wind deposition results in compacting, which increases density and hardness. Under strong wind conditions, density can be as high as 0.52. While snowfalls usually deposit only a few mm of snow, accumulation in sheltered spots can reach several cm.

- Other snowfalls and wind storms take place. Exposed wind-blown layers deposited under low wind speed can be remobilized by stronger winds. If wind speed increases progressively, soft low density layers can progressively be covered and sheltered by denser and denser layers. This explains the presence of low density (< 0.35) layers between high density (> 0.45) layers. Wind storms cause considerable changes in snow topography. Previously sheltered spots can become exposed spots in the next storm. Sastrugi can be eroded if they were formed by a weaker storm. They also facilitate accumulation on their downwind side. The net result is that an homogeneous-looking snow surface can actually be the combination of many different outcropping layers, formed between October and May. Fig. 7 shows the exposition of 3 different wind-packed layers, formed or exposed during the 25-29 April storm. Two of these layers were formed during the storm, while the other is much older. A few meters away, early winter or fall layers were exposed as evidenced by their light brown colors, caused by wind-blown soil dust raised when snow cover was partial. Huge lateral variations in the composition of wind-packed surface snow can then be expected, which should be taken into account when quantifying exchanges.

This chemical heterogeneity was confirmed by analyses of anions in the middle of the wind-packed layer at site A, and at a spot with similar stratigraphy near the FTX. The snow from site A had 20 times as much chloride (876 ppbw vs. 44 at the FTX), more nitrate (94 vs 77 ppbw) and more sulfate (186 vs. 144 ppbw). These differences are greater than the variability of the triplicate samples taken (<5%), demonstrating that the snow at both sites came from different precipitation and/or wind events.

Figure 7. Snow surface near site A on 30 April 2000. Right of the continuous line is snow that is at least several weeks old, and that has been exposed by the wind storm of 25-29 April. The snow inside the dotted lines was deposited on 29 April by southerly winds. The eroded sastrugi were formed on 26-28 April by northerly winds and were subsequently remodeled and eroded when the wind direction changed on 29 April. The stratifications on the eroded sastrugi were caused by variations in wind speed.

Depth hoar formation is not explained by the above sequence, as it requires low snow densities (<0.3) and high temperature gradients (>20°C/m, Marbouty, 1980). The first snow layers were probably initially very dense. Temperatures were <0°C in the second half of August and were below –5°C in September when precipitations are most abundant. A snow cover was then probably present in September. Several windstorms with wind speed >15 m/s took place in September and October (Fig. 1), which formed hard windpacks. In the summer and early fall, the snow surface can be radiatively heated and become 4 to 5°C warmer than the overlying air (Alley et al., 1990), resulting in sublimation, fast mass loss, and density reduction of 0.1 g/cm^3 in a few days. This process probably reduced snow density below the threshold for depth hoar formation. Calculations (Colbeck, 1989) and observations (Gow, 1965; Alley, 1988; Alley et al. 1990) indicate that such conditions result in the rapid growth of depth hoar. These previous observations were made on ice caps, but such diagenetic formation of depth hoar probably also applies to the seasonal snowpacks. Strong gradient metamorphism in low density surface layers deposited under calm conditions also forms depth hoar. Given the frequency of wind storms at Alert, it appears fairly unlikely that a 10 cm thick continuous layer of depositional depth hoar could have formed. Depositional depth hoar forms layers less than 1 cm on ice caps (Alley, 1988).

Depositional depth hoar can still form at Alert, however. The spring stratigraphy at site A (Fig. 3) shows a discontinuous layer of density 0.3 with slightly faceted crystals that was probably formed by a wind storm of moderate intensity. The next wind storm, as its wind speed increased, deposited denser and denser snow without disturbing the low density layer, that was then preserved, and where the growth of faceted crystals, and eventually depth hoar, would have been possible, given sufficient temperature gradients. The preservation of such low density snow has been observed in Greenland (Alley, 1997).

We also observed the preservation of light snow during the 25-29 April storm that deposited very light dendritic snow whose density in sheltered areas was as low as 0.016. Stronger and stronger winds deposited denser and denser snow above light snow. Sastrugi formed, with a top crust of density of 0.3 to 0.35, while snow underneath had a density 0.1 to 0.25. We could not observe snow metamorphism in these light layers because we left Alert, but the density conditions were met for the formation of a discontinuous depth hoar layer without requiring mass loss. The numerous layers of depth hoar and faceted crystals observed on sea ice in the spring where probably formed in layers whose low densities were caused by depositional, rather than diagenetic processes.

Impact of the snowpack on atmospheric chemistry

The snowpack can effect atmospheric composition through many processes. Here we first discuss the impact of metamorphism on exchanges of trace gases between the snowpack and the atmosphere, and then the exchanges of trace gases through adsorption/desorption processes.

Metamorphism can be summed up as sublimation of ice and its solutes, and co-condensation of water vapor and solutes. Solute incorporation depends on both kinetic and thermodynamic processes (Dominé and Thibert, 1996) and the composition of condensed ice will be different from that of sublimating ice. As observed here and by Cabanes et al. (this issue), metamorphism of surface snow is slow in the absence of wind and should not result in major exchanges. In contrast, the formation of windpacks and depth hoar leads to grains where most or all the ice has undergone at least one sublimation/condensation cycle during which its solutes could be released to the atmosphere. Perrier et al. (this issue) showed that the formaldehyde content of snow was lower in the windpacks than in surface snow, and yet lower in the depth hoar, which has undergone the most extensive metamorphism, in terms of intensity of water vapor remobilization. This suggests that metamorphism leads to the release of formaldehyde, and that the efficiency of this release increases with metamorphic intensity.

Intense metamorphism means formation of large faceted crystals, which needs low density snow to take place. From our observations, and others in Greenland and Antarctica mentioned above, diagenetic depth hoar formation is frequent in autumn in polar regions. Depositional depth hoar, however, requires that fresh snow be sheltered from winds that form windpacks. This will be facilitated if strong winds are absent, or if their speed increases progressively. We thus suggest that snow-atmosphere exchanges of solutes by metamorphism will be enhanced in low wind speed regions. High wind speeds increase ventilation, which may compensate for less intense metamorphism. However, the formation of fairly impermeable windpacks will considerably reduce the ventilation of lower, more permeable layers (Albert and Schultz, this issue), and detailed physical and microphysical modelling is needed to quantify these effects.

Adsorption/desorption of trace gases on snow surfaces also lead to snow-atmosphere exchanges. To quantify these effects, the adsorption isotherms of the trace gases on ice must be known. Unfortunately, no detailed adsorption data are available at -45 to –15°C for gases of tropospheric interest. We will use the example of acetone, for which some adsorption parameters can be estimated semi-quantitatively.

Acetone is important for HO_x chemistry (Arnold et al., 1986) and its emission by the snowpack is documented (Couch et al., 2000). Limited laboratory data exist at 140 K (Schaff and Roberts, 1998) and around 200 K (Rey-Hanot, 1999), which suggest an adsorption enthalpy in the range 40-60 kJ/mol. Molecular dynamics calculations suggest a value around 50 kJ/mol (Picaud et al., 2000).

Using those data, we have calculated the partitioning of acetone between the snowpack and the boundary layer over a year's time with simplified conditions. Climatological data yielded the monthly mean temperatures shown in Fig. 8.

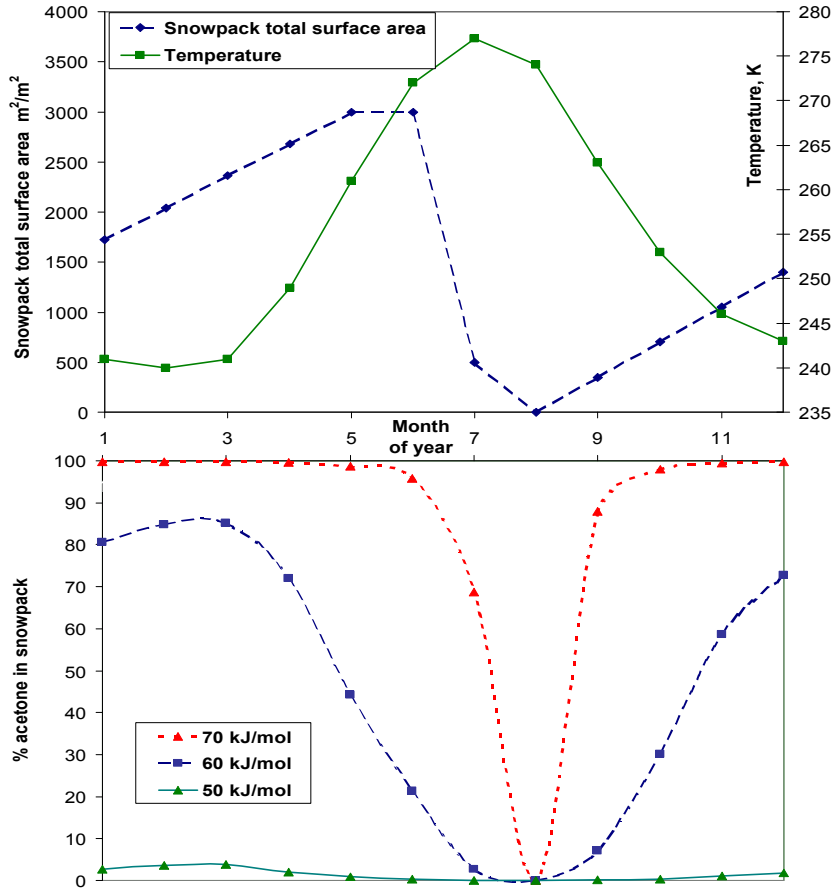

Figure 8 : Mean monthly temperatures and snowpack total surface area (top panel) used to calculate the partitioning of acetone between the snowpack and the boundary layer, for 3 values of the adsorption enthalpy of acetone on ice.

The variation of snowpack TSA assumes a linear increase from August to May and rapid snow melt in july. Other assumptions include a 300 m thick boundary layer, a constant amount of acetone in the (snow + boundary layer system), and acetone adsorption following Henry's law: $N_{ads} = A_0 \exp(E/RT) P_{acetone}$. $A_0=2.17\times10^7$ molecule m^{-2} Pa^{-1} was derived from the preliminary data of Rey-Hanot (1999). Considering the uncertainties on the adsorption enthalpy E, partitioning was calculated for E values of 50, 60 and 70 kJ/mol (Fig. 8). With E=40 kJ/mol, adsorption was negligible. With E=50 kJ/mol the effect of the snowpack is hardly detectable. If E=60 kJ/mol, up to 85% of the acetone in the (snow + boundary layer) system is sequestered in the snowpack in winter. Part of this acetone will be released to the atmosphere in spring as temperature increases, and the rest will be re-emitted as the snow melts. If E=70 kJ/mol, almost all of the acetone is sequestered in the snowpack throughout the year,

except in summer. This shows that predicting the impact of the snowpack through adsorption/desorption processes requires an accurate knowledge of adsorption enthalpies.

Summary and conclusions

This study shows that some characteristics of the seasonal snowpack near Alert are similar to those of the permanent snowpack on polar ice caps. Our observations indicate that diagenetic depth hoar forms in late summer or in the fall by mass loss from wind-packed layers by sublimation, followed by the growth of large crystals in large temperature gradients. Wind-packed layers then accumulate over depth hoar. Depositional depth hoar can also form, but the mechanism seems different from that observed in Antarctica, certainly because accumulation is more important here. The preservation of layers of low to moderate densities was observed, where faceted crystals can grow without mass loss by sublimation. If the layer density is low enough and if a high temperature gradient is maintained long enough, several cm of depth hoar can form, while in Antarctica, depositional depth hoar is thin and is generated by surface hoar (Alley, 1988; Gow, 1965). Depth hoar formation leads to intense sublimation/condensation cycles that can result in the release of solutes such as formaldehyde, and the occurrence of these large crystals can therefore be expected to effect the tropospheric concentration of ice-soluble gases more than the presence of windpacks.

We have obtained the first measurement of the SSA of Arctic snow layers on land and on sea ice. SSA values ranged from 125 to about 1500 cm^2/g and in general decreased with depth, the lowest values being for depth hoar. The TSA of the snowpack ranged from 1160 to 3710 m^2 of snow surface per m^2 of ground, so that the snowpack amplifies ground surface area by 3 to 3.5 orders of magnitude.

Calculations performed for acetone, using preliminary adsorption data, indicate that the snowpack may sequester large amounts of trace gases by adsorption. A reliable evaluation of the impact of these adsorption processes on lower tropospheric chemistry will however require the accurate measurement of the adsorption isotherms of the trace gases of interest on ice.

Acknowledgements

This work was funded by the French Polar Institute (IFRTP) and CNRS (PNCA program). We are most grateful to Peter Brickell for his constant efforts to supply liquid nitrogen at Alert. Ionic analyses were kindly performed by Roberto Sparapani. We thank Leonard Barrie for inviting us to ALERT 2000 and Jan Bottenheim and Paul Shepson for coordinating the campaign. FD thanks James H. Morison for the invitation to fly to the Arctic ocean.

References

Albert, M.A., Schultz E.F. Snow and firn properties and air-snow transfer properties at Summit, Greenland. This issue.

Alley, R.B. (1988) Concerning the deposition and diagenesis of strata in polar firn. J. Glaciol. 34, 283-290.

Alley, R.B., Saltzman, E.S., Cuffey, K.M., Fitzpatrick, J.J. (1990) Summertime formation of depth hoar in central Greenland. Geophys. Res. Lett, 17, 2393-2396.

Alley, R.B., Shuman, C.A., Meese, D.A., Gow, A.J., Taylor, K.C., Cuffey, K.M., Fitzpatrick, J.J., Grootes, P.M., Zielinski, G.A., Ram, M., Spinelli, G., Elder, B. (1997) Visual-stratigraphic dating of the GISP2 ice core: basis, reproducibility, and application. J. Geophys. Res. 102, 26367-26381.

Arnold, F., Knop, G., Ziereis, H. (1986) Acetone measurements in the upper troposphere and lower stratosphere – implications for hydroxyl radical abundances. Nature, 321, 505-507.

Brunauer, S., Emmet, P.H., Teller, E., (1938). Adsorption of gases in multimolecular layers. J. Am. Chem. Soc. 60, 309-319.

Cabanes, A., Legagneux, L., Dominé, F. Evolution of the specific surface area and of crystal morphology of fresh snow near Alert during Polar Sunrise experiment 2000**.** This issue.

Chaix, L., Ocampo, J., Dominé, F. (1996) Adsorption of CH4 on laboratory-made crushed ice and on natural snow at 77K. Atmospheric implications. Comptes Rendus Acad. Sciences, 322, série II, 609-616

Chu, L.T., Leu, M.T., Keyser, L.F., (1993). Heterogeneous reactions of HOCl + HCl → Cl_2 + H_2O and $ClONO_2$ + HCl → Cl_2 + HNO_3 on ice surfaces at polar stratospheric conditions. *J. Phys. Chem*. 97, 12798-12804.

Colbeck, S.C., (1983) Theory of metamorphism of dry snow, J. Geophys. Res. 88, 5475-5482.

Colbeck, S.C., (1989), Snow crystal growth with varying surface temperatures and radiation penetration, J. Glaciol. 35, 23-29.

Couch, T.L.; Sumner, A.-L.; Dassau, T.M.; Shepson, P.B. Honrath, R.E. (2000) An Investigation of the Interaction of Carbonyl Compounds with the Snowpack, *Geophys. Res. Lett.*, **27**, 2241-2244.

Dibb, J., Talbot, R., Munger, D., Jacob, D., Fan S.-M. (1998) Air-snow exchange of HNO_3 and NO_y at Summit, Greenland. *J. Geophys. Res.*, 103, 3475-3486.

Dominé, F., Thibert, E (1996) Mechanism of incorporation of trace gases in ice grown from the gas phase. *Geophys. Res. Lett.*, **23,** 3627-3630

Gow, A.J. (1965) Snow studies in Antarctica. *CRREL Res. Rep.* 177.

Gregg, S.J., Sing, K.S.W., (1982). Adsorption, surface area and porosity. Academic Press, London.

Hanot, L., and Dominé, F. (1999) Evolution of the surface area of a snow layer. *Environ. Sci. Technol*. **33**, 4250-4255.

Honrath, R.E., Peterson, M.C., Guo, S., Dibb, J.E., Shepson, P.B., Campbell, B. (1999) Evidence of NO_x production within or upon ice particles in the Greenland snowpack. *Geophys. Res. Lett.*, **26** 695-698.

Honrath, R.E., Peterson, M.C., Dzobiak, M.P., Dibb, J.E., Arsenault, M.A.; Green, S.A. (2000a) Release of NO_x from sunlight-irradiated Midlatitude Snow. *Geophys. Res. Lett.*, **27** 2237-2240.

Honrath, R.E., Guo, S., Peterson, M.C., Dzobiak, M.P., Dibb, J.E., Arsenault, M.A. (2000b) Photochemical production of gas phase NO_x from ice crystals NO_3^-. *J. Geophys. Res.* 105, 24183-24190.

Hutterli, M. A., Rothlisberger, R., Bales, R. C. (1999) Atmosphere-to-snow-to-firn transfer studies of HCHO at Summit, Greenland, Geophys. Res. Lett., 26, 1691-1694.

Lary, D.J., Shallcross, D.E. (2000) Central role of carbonyl compounds in atmospheric chemistry. J. Geophys. Res. 105, 19771-19778.

Legagneux, L., Cabanes, A., Dominé, F. Measurement of the Specific Surface Area of 176 Snow Samples Using Methane Adsorption at 77 K. J. Geophys. Res. In press.

Marbouty, D. (1980) An experimental study of temperature gradient metamorphism ; *J. Glaciol*. **26**, 303-312.

Michalowski, B.A., Francisco, J.S., Li, S.-M., Barrie, L., Bottenheim, J.W. and Shepson, P..B. (2000) A computer model study of multiphase chemistry in the arctic boundary layer during polar sunrise. J. Geophys. Res., 105, 15131-15145.

Perrier, S., Houdier, S., Dominé, F., Cabanes, A., Legagneux, L., Sumner, A.L., Shepson, P.B., Formaldehyde in the snowpack near Alert during ALERT2000 field campaign Snowpack composition, incorporation processes and atmospheric impact. This issue.

Picaud, S., Toubin, C., Girardet, C. (2000) Monolayers of acetone and methanol molecules on ice. *Surf. Sci. 454-456*, 178-182.

Rey-Hanot, L.. (1999) Adsorption de gaz traces sur la glace. Applications à la chimie des nuages et du manteau neigeux. Thesis, Université Joseph Fourier, Grenoble, 295 pp.

Robinson, D. A., Dewey, K. F., Heim, R. R.Jr. (1993). Global snow cover monitoring: an update. Bull. Amer. Meteor. Soc. 74, 1689-1696.

Schaff, J.E., Roberts, J.T. (1998) The adsorption of acetone on thin films of amorphous and crystalline ice. *Langmuir, 14*, 1478-14

Sumner, A.L., Shepson, P.B. (1999) Snowpack production of formaldehyde and its effect on the Arctic troposphere. Nature, 398, 230-233.

Thibert, E., F. Dominé (1998) Thermodynamics and kinetics of the solid solution of HNO_3 in ice. J. Phys. Chem. B. 102, 4432-4439.

Weller, R., Minikin, A., König-Langlo, G., Schrems, O., Jones, A.E.; Wolff, E.W., Anderson, P.S. (1999) Investigating possible causes of the observed diurnal variability in Antarctic NO_y. *Geophys. Res. Lett*. 26, 601-604.

III.5. Evolution of the specific surface area and of crystal morphology of Arctic fresh snow during the ALERT 2000 campaign.

Dans le manteau neigeux, les couches de surface ont un potentiel d'interaction avec l'atmosphère plus important que les couches profondes. Comme elles sont plus récentes, elles ont également un plus grand potentiel d'évolution. Ainsi, la concentration d'une espèce localisée principalement à la surface de la glace est susceptible de changer rapidement suite à une évolution météorologique entraînant une variation de température, ou/et un déséquilibre avec sa concentration atmosphérique. Il est donc nécessaire d'étudier en détail l'évolution de la SS des neiges fraîches.

Ici, nous présentons l'étude de 4 couches de neige fraîche formées durant les deux campagnes de Février et Avril 2000. Des macrophotographies ont été prises pour suivre l'évolution morphologique des couches de neige et nous aider à interpréter l'évolution de leur SS.

La majorité des échantillons de neige ont été prélevés sur le site A ; deux ont été collecté sur la banquise à Joliffe bay. Ces deux sites ont été décrits dans l'**article 3**; et il n'est donc pas utile de lire le paragraphe décrivant les prélèvements.

Evolution of the specific surface area and of crystal morphology of Arctic fresh snow during the ALERT 2000 campaign

Axel Cabanes, Loïc Legagneux, and Florent Dominé*

CNRS, Laboratoire de Glaciologie et Géophysique de l'Environnement, B.P. 96,
54 Rue Molière, 38402 Saint Martin d'Hères, cedex, France.

*Corresponding author. Phone: (33) 476 82 42 69; e-mail : florent@glaciog.ujf-grenoble.fr

Abstract

Metamorphism of surface snow results in a decrease in specific surface area (SSA), which causes the release of adsorbed trace gases. This process contributes to the impact of the snowpack on atmospheric chemistry and must be quantified. The SSA evolution of fresh snow layers was measured in February and April 2000 during the ALERT 2000 campaign at Alert (Canadian Arctic: 82°29'94"N, 62°20'55"W). Measurements were made using CH_4 adsorption at 77 K. Numerous photomacrographs of snow crystals were also taken to interpret observed SSA decreases. Five snow falls were studied. Four snowfalls consisted of fine snow called diamond dust, whose initial SSA ranged from 1460 to 770 cm^2/g, and decreased to about 500 cm^2/g in winter, and to about 300 cm^2/g in spring after 10 days. The fifth one consisted of rimed dendritic crystals, whose SSA decreased from 1540 to 450 cm^2/g in 3 windy days. The continuous growth of surface hoar at the surface of the snowpack diluted surface diamond dust and contributed to their SSA decrease. Our data indicate that the total surface area of surface snow layers is sufficient to sequester adsorbable gases. The example of HNO_3 shows that the release of this gas by SSA decrease may indeed lead to a significant increase in its atmospheric concentration.

Keywords : Adsorption ; Surface Area ; Diamond Dust ; Snow ; Metamorphism.

Submitted, Atmospheric Environment, 7 June 2001

Revised, 6 December 2001

Accepted, 7 December 2001

Introduction

Ice represents 45 % of the cloud water mass and snow covers up to 50 % of land masses in the northern hemisphere (Robinson et al., 1993). A strong potential therefore exists for atmospheric trace gases to interact with ice and impact atmospheric chemistry. Springtime ozone depletion studied in the Arctic troposphere for over a decade (Barrie et al., 1988) illustrates this impact. Other effects of snow observed more recently include the emission of formaldehyde by the Arctic snowpack (Sumner and Shepson, 1999; Hutterli et al., 1999), exchanges of nitrogen oxides between the snowpack and the atmosphere (Dibb et al., 1998) and the photochemical production of NO_x (Honrath et al., 1999) in Greenland. Models of Arctic atmospheric chemistry systematically underestimate the mixing ratios of these species (De Serves, 1994; Sander, 1995; Sumner and Shepson, 1999) and snowpack chemistry must be taken into account to reproduce observations, and to model tropospheric ozone depletion (Michalowski et al., 2000).

The mechanisms of exchange of trace gases between the snow and the atmosphere are still not understood, however. Processes involved include adsorption/desorption from the snow surface, sublimation/condensation of snow and solutes, diffusion of chemical species in the ice lattice, and reactions on the ice surface. Understanding and quantifying these various processes requires the knowledge of several physical parameters, among which the specific surface area (SSA) of snow.

As detailed in Dominé et al. (2001), snow SSA represents the surface area of snow accessible to gases per mass unit and is expressed in m^2/g or here in cm^2/g, as values found for snow are small. Knowing snow SSA is necessary to evaluate surface uptake capacity of species by the snowpack, to quantify the rate of surface reactions, and to model the evolution of the composition of snow in adsorbed species such as persistent organic pollutants (Wania, 1997). During winter and spring 2000, snow SSA was measured at Alert, Ellesmere Island (82°29'94"N, 62°20'55"W) as part of the ALERT 2000 campaign. These SSA measurements, together with those of Dominé et al. (this issue) are the first reported for polar snow.

The method used is CH_4 adsorption at 77 K, described in Hanot and Dominé, (1999) and in Legagneux et al. (in press). It has been preferred to others such as N_2 adsorption (Hoff et al., 1998), stereology (Narita, 1971) or image analysis (Fassnacht et al., 1999), as is faster and/or more accurate (Dominé et al., 2000 and 2001; Legagneux et al., in press).

Here, we focus on the evolution of the SSA of fresh snow layers. Fresh snow layers are obviously on the surface of the snowpack and have the highest potential of interaction with the atmosphere. Moreover, they have the highest potential for evolution, as their SSAs are higher than those of aged snow, and their crystals contain microstructures that are unstable and disappear after a few days (Hanot and Dominé, 1999; Dominé et al., 2001). We studied five snowfalls during the campaign: two in February, and three in April.

To understand SSA evolution, we also studied changes in snow crystal morphology associated with snow metamorphism using photomacrographs. The impact of temperature and wind on SSA evolution is also discussed. Finally, using the example of HNO_3 release, we evaluate the possible impact of the observed SSA decrease on tropospheric composition.

Snow sampling

Surface snow layers were studied from 4 to 23 February and from 11 to 30 April. Snow was collected at two sites. Most samples were collected at site A, 300 m southeast from the Far Transmitter building (FTX: 82° 27.28' N, 62°29.69' W), 5.4 km south from the Alert base. The other sampling site was Joliffe bay, on the sea ice about 1 km from the coast, and 4 km West-Northwest of Alert base. Only two samples of recent snow were collected in Joliffe bay in February, but these could be compared with samples taken at site A to evaluate spatial variations in snow SSA. For each sampling, air temperature and snow temperatures near the surface and at several depths were measured with a mercury thermometer with a 0.5°C accuracy. Wind speed and air temperature were monitored continuously at the GAW laboratory, 300 meters South of site A.

For each sample, about 150 cm^3 of snow were collected with a spatula in two glass vials that were immediately immersed in liquid nitrogen to stop metamorphism. Snow samples were kept in liquid nitrogen until being transferred to the stainless steel volume used for SSA measurement. This transfer was made in a room whose temperature was below – 30°C in February and –15 °C in April. Sometimes, the stainless steel volume was used directly for sampling.

Experimental methods

Snow SSA was determined by CH_4 adsorption at liquid nitrogen temperature (77.15K). A volumetric method was used and required the measurement of the adsorption isotherm of CH_4. More details are given by Dominé et al. (this issue) and Legagneux et al. (in press) who estimated the reproducibility of the method at 6% and its accuracy at 12%. Snow density was measured as described by Dominé et al. (this issue). Briefly, a container of known volume was used to sample snow that was then weighed. For thin layers, the thickness was measured and snow was scrapped from a surface of known area, and weighed.

Fifteen photomacrographs were taken for each snow sample in the transfer room mentioned above, using a reflex camera with a macro lens (focal length: 38 mm; minimum aperture: f16) allowing a magnification of 7.

Results

Winter snow falls

During the winter campaign, two snowfalls were observed on 3 and 7 February. The first fall took place at the end of a southwesterly wind storm whose speed decreased from 10 m/s at the beginning of the fall to 4 m/s at the end of it. This storm had raised the air temperature to –19 °C just before the snowfall started. This snow formed a discontinuous layer that had accumulated in wind-sheltered spots such as the lee of sastrugi. Accumulations were mostly 3 to 8 cm thick, with a density around 0.15. The second snowfall took place on 7 February in the absence of wind while the air temperature was around -38 °C, and covered the surface with a continuous layer about 1 cm thick with a density around 0.08. Afterwards, we observed the continuous formation of surface hoar at the top of the snowpack. This growth was stopped on 22 February when a northerly wind blowing at up to 7.2 m/s

raised and mixed both surface layers with surface hoar. Under the surface layers were a hard wind-packed layer and a depth hoar layer, bringing the total thickness of the snow pack to about 25 cm (Dominé et al., this issue).

Snow crystals fallen on 3 and 7 February and sampled one day after their fall consisted of columns and bullet combinations (Figs. 1a and 1c).

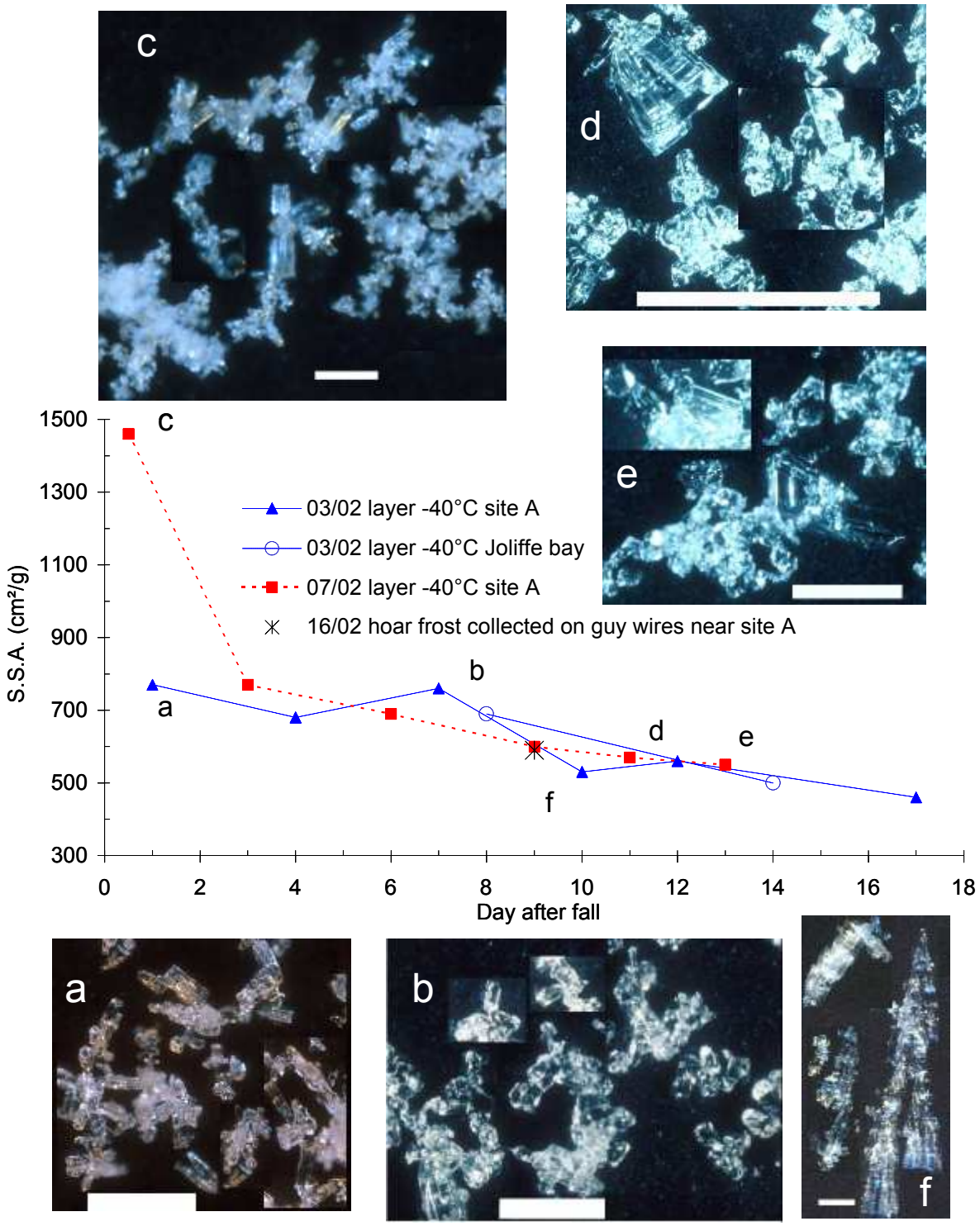

Figure 1: SSA evolution and morphological changes of fresh snow layers in February 2000. Scale bars: 1 mm. (a) Fresh snow samples collected on 4 February. (b) Sample from the 3 February layer collected on 10 February. (c) Snow precipitated on 7 February, collected on 8 February. (d) Sample from the 7 February layer collected on 18 February. (e) Sample from the 7 February layer collected on 20 February. (f) Hoar frost collected on antenna guy wires on 16 February.

Bullets combinations form after a supercooled droplet freezes into an ice polycrystal, and each crystal leads to a bullet. Such combinations usually form under low temperature and moisture contents (Gow, 1965). They often fall lightly under clear sky conditions and are then called diamond dust (DD). At Alert, the sky was partly cloudy during these snowfalls, but we nevertheless use the term diamond dust to refer to them, because of the morphological similarities. Our photographs (Fig. 1a) indicate that the 3 February crystals were 0.1 to 0.2 mm in diameter and 0.2 to 0.4 mm long, with a few crystals under 0.1 mm. Crystals fallen on 7 February and collected on 8 February seem to show a bimodal size distribution. Most crystals were small (< 0.1 mm long) but a few were large (0.5 mm long) (Fig. 1c).

The altitude and temperature of formation of the snow was determined from vertical profiles of temperature and relative humidity (RH), measured by a Vaisala sonde. Profiles regarding the 7 February fall are shown on Fig. 2.

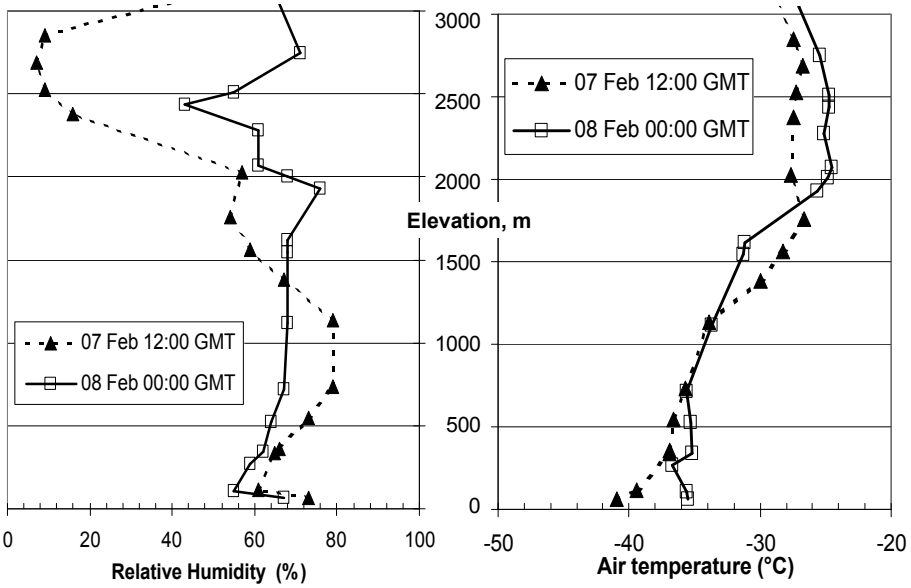

Figure 2: Vertical profiles of relative humidity and air temperature measured with a Vaisala sonde on 7 February 2000 above Alert.

The height of formation was assumed to be when RH reached a maximum, keeping in mind that several artifacts in RH measurements are possible, including hysteresis and underestimation (Sherlock et al., 1999). According to Fig. 2, 7 February crystals formed at about –35 °C around 900 m (7 Feb. 12:00 GMT). However, Fig. 2 shows a maximum in RH at 1900 m at about –26 °C on 8 February 0:00 GMT. Unless this is a measurement artifact, the bimodal size distribution mentioned above may have been caused by a varying temperature of formation. Other profiles showed that the 3 February crystals formed at about 800 meters around –24°C.

Fig. 1 shows the SSA decrease of the 3 and 7 February layers. The SSA of the 3 February snow decreased by a factor of 1.5 in 17 days, from 770 to 460 cm^2/g. That of the 7 February snow decreased by a factor of 3 in 13 days from 1460 to 550 cm^2/g. SSA values from samples of the 3 February layer collected in Joliffe bay on 11 and 17 February (Fig. 1) lie on the curve of the snow collected at site A, about 10 km away, demonstrating very small SSA spatial variability in this case.

In both winter and spring, we observed the continuous growth of surface hoar. In winter, the hoar overlaid the 7 February layer so that DD and surface hoar could not be sampled separately. To compare the SSA of DD and surface hoar, we collected hoar frost growing on antenna guy wires between the FTX and site A on 16 February. This hoar, with a SSA of 590 cm^2/g, consisted of feather–shaped clusters of crystals (Fig. 1f), that had grown up to 30 mm long on 21 February. Surface hoar crystals observed on the 7 February layer were similar in morphology, but smaller than those collected on wires. Whether their SSA was similar to that of hoar frost is unknown, but a reasonable suggestion is that surface hoar had a SSA similar to that of hoar frost, and that its growth contributed to the observed SSA decrease of surface snow.

Photomacrographs were examined to understand the physical changes associated with SSA decrease. Figs. 1a and 1b show pictures of snow samples from the 3 February layer collected on 4 and 10 February. Fig. 1a shows submillimetric crystals with sharp angles, as expected from fresh snow. Fig. 1b shows that some crystals rounding has taken place, indicating early stages of metamorphism. However, this rounding had negligible effects on SSA, which decreased insignificantly from 770 to 760 cm^2/g.

From photomacrographs, we estimated the proportion of surface hoar in the 7 February snow. On 13 February, it made up about 10% of the sample mass while DD crystals still had fairly sharp edges, and the SSA was 690 cm^2/g, a factor of 2 decrease from the 8 February value. Pictures of snow collected 11 and 13 days after the fall (Figs. 1d and 1e) lead to estimates of 25% and 50% respectively. DD crystals were then clearly rounded while surface hoar remained sharp, consistent with fast growth under high temperature gradients, that form facets (Marbouty, 1980, Colbeck, 1983a). The SSA was then 570 and 550 cm^2/g, respectively, lower than that of hoar frost collected on guy wires (590 cm^2/g).

On 22 February, wind blowing at speeds up to 7.2 m/s raised surface snow and mixed the 3 and 7 February layers, and surface hoar. The wind was too weak to affect the underlying very hard wind-packed layer, and formed a fairly soft discontinuous snow layer, of density 0.28, which accumulated in sheltered spots. This wind-blown snow had a SSA of 650 cm^2/g, greater than both SSA values of the 3 and 7 February layer just before the storm, that were 460 and 550 cm^2/g, respectively. Photomacrographs of snow crystals from this mixed layer (Fig. 3) show a few broken surface hoar crystals among crystals of DD with various degrees of rounding and sintering.

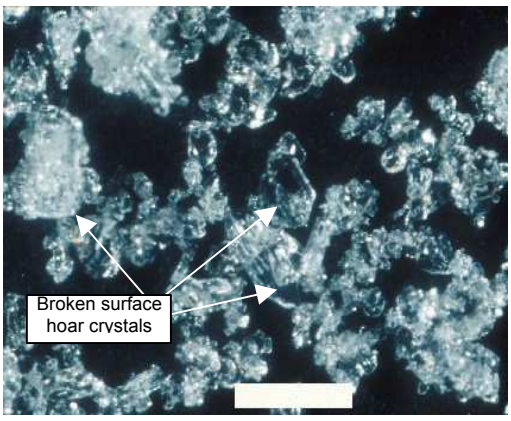

Figure 3: Photomacrograph of snow collected on 22 February during the wind storm. Scale bar: 1 mm.

Spring snowfalls

Three snowfalls were observed in spring: (i) two diamond dust (DD) falls on 13 and 14 April, that could not be distinguished from each other after the fall and will be treated as a single snowfall; (ii) a long dendritic snowfall on 25 to 28 April, (iii) another diamond dust fall on 30 April, that was sampled only once just before our departure.

On 13 and 14 April, two distinct DD falls consisting of columns and bullet combinations, deposited 2 and 1 mm of snow. The density was about 0.07, with a large uncertainty due to the very thin layers. As in winter, precipitations took place under a partly cloudy sky and the term diamond dust does not perfectly apply. Crystals were about 200 µm long with a few columns 500 µm long (Fig. 4a). The air temperature was –27°C to –23°C during precipitation, and there was no wind. From vertical temperature and humidity profiles, we deduce that both snowfalls formed between 1500 and 2500 m at around –26°C.

No precipitation or wind storms took place until 25 April when a snowfall lasting until 28 April, deposited 5 cm of dendritic snow under northerly winds reaching 11 m/s, while temperature was –15°C. About 50% of snow crystals were rimed (Fig. 5), i.e. covered by supercooled droplets that froze upon impacting the snow crystal, but the degree of riming showed a large temporal variation during the fall. Vertical profiles indicate that this snow formed at about –15 °C, consistent with the dendritic shape (Pruppacher et Klett, 1978). Crystals were 1 to 5 mm in diameter. The snow density was as low as 0.016 in sheltered areas where it was not wind-packed. The density reached 0.21 in wind-packed accumulations.

On 30 April, 1 mm of DD precipitated under calm conditions, under an air temperature of –18°C. This snow formed at 1500 to 2500 m with temperatures around –20°C. Crystals were 0.2 to 0.5 mm long with a density of 0.10, with a large error associated to this value, that is probably overestimated.

As in winter, feather-shaped surface hoar crystals grew continuously over the 13-14 April snowfalls. They reached a length of 20 mm on 24 April. Surface hoar also grew over a 3x6 m Teflon sheet laid on the snow to allow separate sampling. This surface hoar looked identical to the one growing of snow (Fig. 4e) indicating that the water vapor that formed it did come from the atmosphere.

Fig. 4 shows the SSA evolutions of spring snowfalls. Day zero for the 13-14 April layer is 14 April. The SSA of the DD that fell on 13-14 April decreased by a factor of 2.4 in 9 days, from 779 to 326 cm^2/g, faster than winter DD layers. SSA of dendritic snow fallen on 26 April decreased very rapidly from 1530 to 456 cm^2/g on 29 April, while conditions remained windy. On 28 April, we collected three different snow samples. The first one was deposited in a sheltered area and had a SSA of 1015 cm^2/g with a density of 0.066. The other two were wind-packed and slightly crusted with a density of 0.21. Their SSA was half as high: 540 and 435 cm^2/g. On 29 April snow samples from both spots had SSA values closer to each other : 575 cm^2/g for wind-sheltered snow and 456 for wind-packed snow. Fresh DD precipitated on 30 April had a SSA of 802 cm^2/g. Surface hoar collected on 21 April on the Teflon sheet had a SSA of 354 cm^2/g.

The changes in the shapes of DD crystals fallen on 13-14 April are shown in Fig. 4. A slight rounding appeared on snow sample on 15 April (not shown here) associated to a SSA decrease from 779 to 725 cm^2/g. The first visible presence of surface hoar on snow occurred on 16 April (fig. 4b), when SSA had decreased to 608 cm^2/g, and rounding was clearly visible. Pictures of snow crystals collected on

17 and 19 April (Fig. 4c and 4d) show the growth of surface hoar, that made up an estimated 25% of the snow mass on 17 April, and 80% on 19 April. Meanwhile, DD crystals became more and more rounded, as visible on Fig. 4c and on other pictures not shown. It is noteworthy that the SSA of this layer tends towards that of the surface hoar sampled on the teflon sheet, in agreement with the observation that surface hoar made up most of the layer on 19 April.

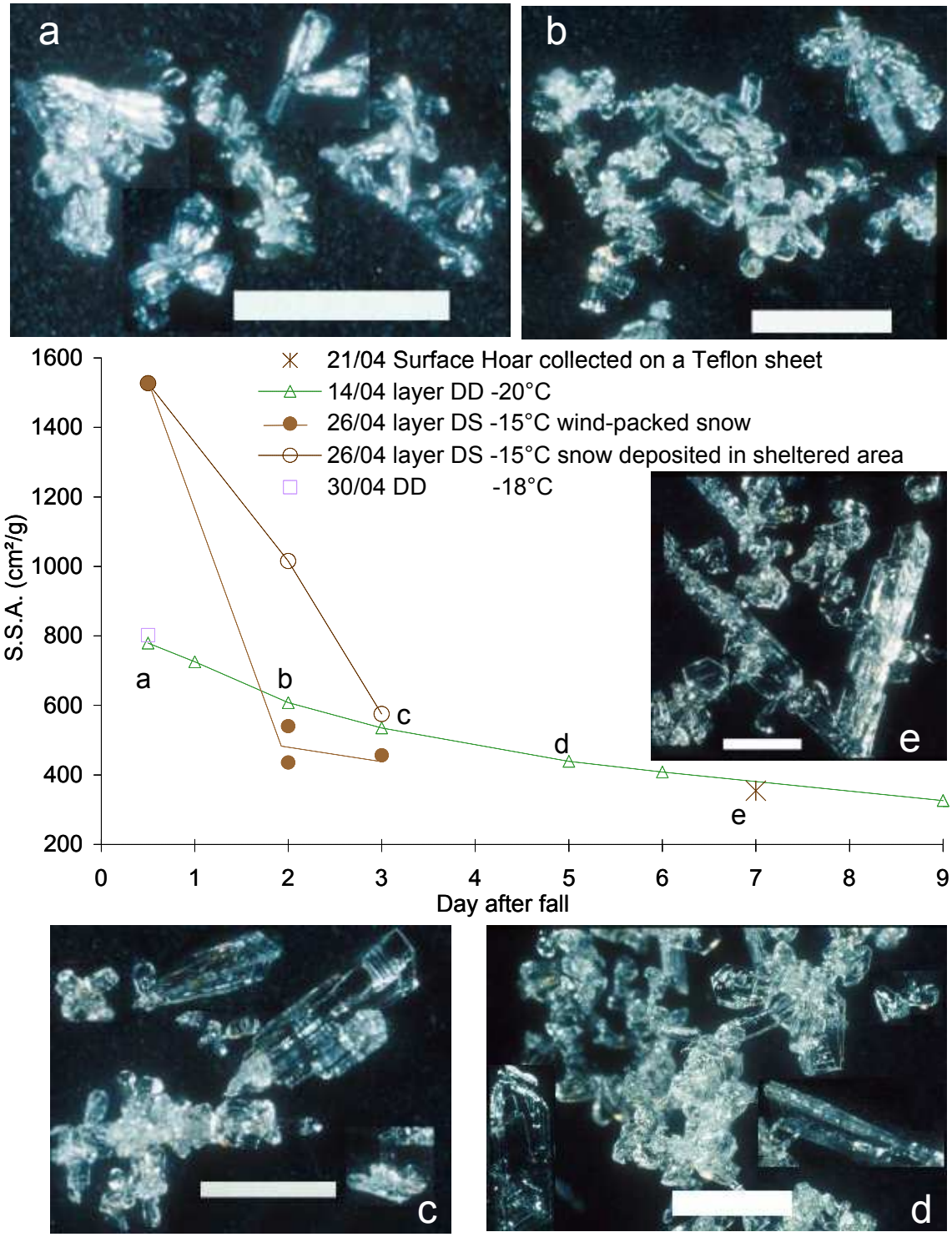

Figure 4: SSA evolution of fresh snow layers in April 2000 and morphological changes of crystals from the 13-14 April layer. DD: diamond dust. DS: dendritic snow. Scale bar: 1 mm. (a) Fresh DD collected on 14 April. (b) Surface snow collected on 16 April. (c) Surface snow collected on 17 April. (d) Surface snow collected on 19 April. (e) Surface hoar crystals collected on a teflon sheet on 21 April.

Changes in snow crystal morphology for snow precipitated on 26 April are illustrated in Fig. 5.

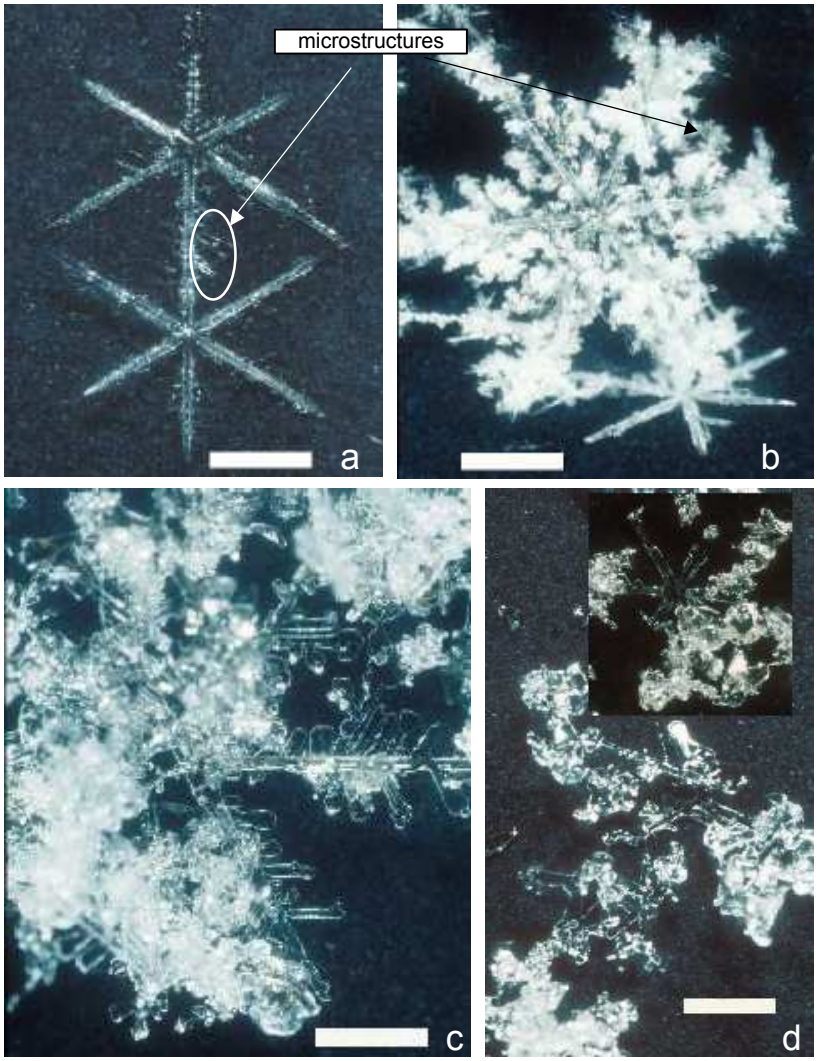

Figure 5: Photomacrographs of dendritic crystals from the 25-28 April snowfall. Scale bar: 1mm. (a) Fresh crystal without rime. (b) Heavily rimed fresh crystal. (c) Snow deposited in a sheltered area, collected on 28 April. b. Snow exposed to strong winds, collected on 28 April.

Fresh dendritic crystals (Figs. 5a and 5b) are bigger than DD, but have dendrites and numerous microstructures with ramifications. Snow crystals collected on 28 April and deposited in a sheltered area (Fig. 5c) still have recognizable dendrites. Edges are only slightly rounded but microstructures have totally disappeared. On the other hand, wind-packed crystals were broken and clearly rounded (Fig. 5d). The presence of bigger rounded grains suggests that snow had been mixed with older snow layers by strong winds. These pictures, together with the data in Figure 4, show that wind accelerated the SSA decrease by favoring sublimation that leads to rounding (Nelson, 1998) and to the disappearance of microstructures.

Discussion

Aspects of this work discussed here are the explanation of fresh snow SSA, its kinetics of decrease, and the potential impact of this decrease on atmospheric composition, through the release of adsorbed gases.

SSA of fresh snow

The SSA of four fresh DD samples were measured. The 7 February snowfall had a SSA of 1460 cm^2/g, while the other three had SSA values in the range 770-802 cm^2/g. Approximating column and bullet shapes by solid hexagonal prisms, their SSA is estimated by equation (1), where d (cm), L (cm) and ? (g/cm^3) are the diameter, length and volumic mass.

$$\text{SSA } (cm^2/g) = \frac{8/\sqrt{3}}{d * ?} + \frac{2}{L * ?} \qquad (1)$$

The ratio L/d is generally high and the second term is often negligible. Therefore, SSAs of 800 and 1500 cm^2/g imply mean diameters of 63 and 34 µm, respectively, significantly less than observed on photomacrographs (Figs. 1a, 1c and 4a). Using equation (1), Dominé et al. (2001) estimated the SSAs of 33 columns and bullets from the 13-14 April DD fall and obtained SSA=420 cm^2/g, i.e. about half the value obtained here by CH_4 adsorption, from which they concluded that the columns and bullet combinations were hollow, as suggested by photographs presented here and in Dominé et al. (2001). This suggestion also agrees with scanning electron microscopy (SEM) data presented by Wergin et al. (1995), who show numerous hollow columns.

The presence of hollows then appears to explain the SSA of the 4 DD falls studied. As mentioned above, the higher value of the 7 February fall can be explained by the presence of smaller crystals (Fig. 1c), formed at –35°C, while the other DD crystals formed around –25°C, where moisture is more abundant and can lead to larger crystals.

Falling dendritic snow collected on 26 April had a high SSA: 1540 cm^2/g. Crystals are much bigger than DD crystals, but may be very thin, and have numerous microstructures with very high SSA. The dendritic crystals in Fig. 5a have microstructures consisting of small elongated needles about 10 µm diameter whose SSA can be estimated at about 5000 cm^2/g, approximating their shapes by cylinders. Rime can also contribute to a high SSA value. On Fig. 5b, the size of rime droplets cannot be accurately estimated. Dominé et al. (2001) used SEM to study rime on dendritic snow collected at –4°C in the Alps. Rime was not spherical, but the shape of frozen droplets could be approximated by cylinders capped by a half sphere. From their mean diameter and height, 59 and 100 µm, they estimated the SSA of rime at 790 cm^2/g. Wergin et al. (1995) also used SEM to study rime formed on the edges of an hexagonal plate, that consisted of elongated structures with multi-faceted shapes having sharp edges, whose diameter did not exceed 3 µm, and whose SSA can be estimated at 15000 cm^2/g. The detailed analysis of our photomacrographs suggests that rime droplets may have had dimensions as small as 15 to 20 µm, and they may thus have contributed to the observed high SSA value. Microstructures and rime may then both have contributed to the high SSA of this dendritic snow.

Mechanism of SSA decrease

For all snow layers, SSA decreased with time. The cases of the DD fall of 3 February and of the dendritic snowfall of late April will be discussed first, as they were not affected by the growth of surface hoar.

From photomacrographs (Fig. 1b and 5), the SSA decrease is associated with rounding of crystal shapes. Rounding is commonly observed in snow metamorphism, and can be caused by (i) sublimation (Nelson, 1998) and overall loss of solid matter; (ii) transfer of matter via the gas phase by sublimation of convex structures such as edges followed by condensation on flat surfaces and on concave structures (Pahaut et Sergent, 1991). This phenomenon is usually referred to a low temperature gradient metamorphism; (iii) slow crystal growth (Marbouty, 1980; Colbeck, 1983b).

In the case of dendritic snow, the disappearance of microstructures and the enhanced ventilation caused by strong winds suggest that the SSA decrease was caused by sublimation, which also resulted in the rounding of larger structures. The observations that snow more exposed to wind experienced faster SSA decrease supports this interpretation: stronger winds led to faster sublimation and greater SSA decrease. In contrast, it is noteworthy that the wind storm of 22 February increased surface snow SSA. In that case, wind affected aged snow and broke up the grains, thus creating new surfaces. The effect of wind on snow SSA thus appears complex and depends on the snow involved.

In the case of the 3 February DD, the growth of surface hoar a few cm above this snow forces us to consider slow growth as a factor responsible for rounding. Fast growth produced the sharp features of the surface hoar, but slower growth may have taken place in underlying layers. Rounding by transfer of water vapor between structures of different curvatures can probably be ruled out, as is can only be significant under low temperature gradients. Microphysical modeling appears necessary to determine whether sublimation or slow growth was responsible for the SSA decrease. Observations at higher magnifications would also be an advantage.

We note that the decrease in SSA of the 3 February layer is not quite as monotonous as those of the other layers. Because our experimental method has a reproducibility of 6%, we think this behavior is not caused by analytical error. This snow was deposited under windy conditions, and we suggest that these variations were due to different wind compaction during deposition. Even though one sampling site was only about 30 cm away from the previous one, observations during the 25-28 storm suggest that even this small distance is sufficient to lead to differences in wind compaction, and therefore in SSA.

The 7 February and 13–14 April layers were affected by the growth of surface hoar. In winter, the surface hoar may have had a SSA similar to hoar frost: 590 cm^2/g. In spring, surface hoar had a SSA of 354 cm^2/g. It is then clear that DD dilution by surface hoar contributed to the SSA decrease. Crystal rounding of the 7 February DD can also be observed on Fig. 1d. Rounding of the 13-14 April layer is less well marked (Fig. 4), but an examination of a larger number of pictures nevertheless shows slight but detectable rounding. Again, rounding of surface DD may have been caused either by slow growth or by sublimation of edges. The SSA decrease of both these surface DD layers can then be explained by a combination of rouding of edges and by dilution by surface hoar of lower SSA.

Kinetics of SSA decrease

The rate of SSA decrease is different in winter and spring. Except for the fast initial decrease, the SSA of the 7 February layer decreased by 23 cm^2/g per day, while that of the 13-14 April layer decreased by 34 cm^2/g per day. The faster decrease in spring can be related to the higher average temperatures that induced higher water vapor pressures: at –37°C, P_{H_2O} =17.8 Pa, while at -27°C and P_{H_2O}=51.3 Pa (Marti and Mauersberger, 1993). This will contribute to higher fluxes and faster metamorphism.

At site A, the SSA of the 3 February layer decreased by 19 cm^2/g per day between 4 and 20 February. A comparison is not very meaningful, however, because both DD layers were not affected by the same processes. The growth of surface hoar may have contributed to the slightly faster decrease of the 7 February DD, but detailed microphysical modelling is required to answer such questions.

The SSA of the dendritic snow of 26 April decreased by up to 1090 cm^2/g in 1.5 day. This fast rate is explained by the warmer temperature (-15°C, P_{H_2O}=165 Pa) but especially by the strong winds. Snow microphysics also certainly influence the rate of SSA decrease. When microstructures are present, such as observed on dendritic snow, their disappearance by sublimation will lead to a fast initial decrease. This may also have contributed to the rapid SSA decrease of the 7 February DD, but the magnification of our pictures was insufficient to observe the relevant changes.

Atmospheric implications

Our results show that the SSA of fresh surface snow decreases significantly in 2 weeks, even under very cold conditions. On the contrary, the SSA of older underlying snow remained stable (Dominé et al.; this issue). The release of adsorbed trace gases due to SSA decrease can then be evaluated by considering surface layers only, and this effect will be illustrated with the example of HNO_3, that adsorbs strongly to ice surfaces (Abbatt, 1997; Zondlo et al., 1997). We consider here a column of 1 m^2, where exchanges take place between both February DD layers and a 400 m-thick boundary layer. On 8 February, the total surface area (TSA) of the surface snow, given as the product of SSA (cm^2/g), density (g/cm^3), and thickness (cm) is 222 m^2 of snow per m^2 of ground. Values taken for the 7 February and 3 February layers are 1460 and 700 cm^2/g for SSA, 0.08 and 0.15 for density, and 1 cm each of average thickness. On 20 February, the TSA had decreased to 113 m^2 of snow per m^2 of ground: SSA values of both layers were then 550 and 460 cm^2/g, while the products of densities and thicknesses remained unchanged, to a first approximation.

Hypotheses used are: (i) temperature is constant at –37°C. (ii) The HNO_3 partial pressure, P_{HNO3}, is $5x10^{-7}$ Pa (5 pptv, Dominé and Thibert, 1996) (iii) The HNO_3 surface coverage ? follows a Henry's law and is 0.1 monolayer at -37°C. This value is consistent with the data of Abbatt (1997), although he did not perform measurements at the low P_{HNO3}. (iv) The cross sectional surface area a_m of a HNO_3 molecule is $20x10^{-20}$ m^2. From eq. (2) we deduce a Henry's law constant H(236K) = $1x10^{24}$ molec Pa^{-1} m^{-2}.

$$H = \frac{?/a_m}{P_{HNO_3}} \qquad (2)$$

Under these conditions, Table 1 indicates that the snow surface layers sequester 99.94% of the HNO_3 contained in the (surface snow + boundary layer) system. When the snow TSA decreases from 222 to 113 m^2/m^2, P_{HNO3} increases by a factor of 2.

Table 1. Partitioning of HNO_3 between the atmospheric boundary layer and surface snow layers, in a $1m^2$ column.TSA: Total Surface Area.

	Atmospheric boundary layer (molec m^{-2})	**Surface snow layers (molec m^{-2})**
8 February 233K TSA: 222 m^2/m^2	$6.2x10^{16}$ 5 pptv	$1.109x10^{20}$
20 February 233K TSA: 113 m^2/m^2	$1.2x10^{17}$ 9.8 pptv	$1.108x10^{20}$
Warming ? 253K TSA: 113 m^2/m^2	$8.7x10^{17}$ 76 pptv	$1.101x10^{20}$

Warming also leads to desorption. Table 1 shows the effect of a 20°C warming, at constant TSA=113 m^2/m^2. Using Clapeyron's law, and an enthalpy of adsorption of 60 kJ/mol, close to the value of the partial molar heat of sublimation of HNO_3 from ice (Thibert and Dominé, 1998), we get H(256K)= $1.3x10^{23}$ molec Pa^{-1} m^{-2}. P_{HNO3} then increases by a factor of 8 to 76 pptv. Of course, other effects such as mixing and chemical reactions would also take place, but these calculations nevertheless show the potential contribution of the snowpack to changes in mixing ratios of adsorbable gases. More accurate predictions would require the knowledge of the adsorption isotherms of HNO_3 on ice at various temperatures.

Another potential impact of the snowpack is through metamorphism, as ice sublimation leads to solute release. From Figs. 5c and 5d and other similar pictures, we estimate that 20 to 40 % of the mass of dendritic snow crystals sublimated under strong winds. Perrier et al. (this issue) determined that formaldehyde (HCHO) in snow was dissolved in the ice volume. Its concentration in the April dendritic snow was 5 ppbw, while the gas phase value was P_{HCHO}=100 pptv. Due to the short HCHO lifetime (6h), exchanges have to be considered between surface snow and a 14 m-thick air layer. In this case sublimation of 20% of a 5 cm snow layer of density 0.2 will release $2x10^{17}$ molecule m^{-2} of HCHO. If this release were instantaneous, it would lead to an increase in P_{HCHO} of 480 pptv. It thus appears worthwhile to include snow sublimation as an HCHO source in models.

Conclusion

The initial SSA values of fresh snow measured here were between 770 and 1540 cm^2/g. In all cases, these values decreased with time at rates that increased with increasing temperature and wind speed. The mechanisms of SSA decrease were rounding of edges, sublimation of microstructures, and dilution of snow by surface hoar of lower SSA. Simple calculations show that the total surface areas developed by surface layers are sufficient to greatly influence the atmospheric mixing ratios of gases that adsorb strongly to ice, such as HNO_3. However, the accurate quantification of these effects require the laboratory measurement of the adsorption isotherms of trace gases on ice at several temperatures.

Acknowledgments

This work was funded by the French Polar Institute (IFRTP) and CNRS (PNCA program). We are most grateful to Peter Brickell for his constant efforts to supply liquid nitrogen at Alert. We thank Leonard Barrie for inviting us to ALERT 2000, Jan Bottenheim and Paul Shepson for coordinating the campaign, and Al Gallant for constant logistical assistance.

References

Abbatt, J.P.D., 1997. Interaction of HNO_3 with water-ice surfaces at temperatures of the free troposphere. Geophys. Res. Lett. 24, 1479-1482.

Barrie, L..A., Bottenheim, J.W., Schnell, P.J., Crutzen, P.J., Rasmussen, R.A., 1988. Ozone destruction and photochemical reactions at polar sunrise in the lower Arctic atmosphere. Nature, 334, 138-141.

Brunauer, S., Emmet, P.H., Teller, E., 1938. Adsorption of gases in multimolecular layers. J. Am. Chem. Soc. 60, 309-319.

Chaix, L., Ocampo, J., Dominé, F., 1996. Adsorption of CH_4 on laboratory-made crushed ice and on natural snow at 77K. Atmospheric implications. Comptes Rendus Acad. Sciences, 322, série II, 609-616.

Colbeck, S.C., 1983 Ice crystal morphology and growth rates at low supersaturations and high temperatures. J. Appl. Phys., 54, 2677-2682.a

Colbeck, S.C. 1983. Theory of metamorphism of dry snow. J. Geophys. Res. 88, 5475-5482., 1983.b

De Serves, C., 1994. Gas phase formaldehyde and peroxide measurements in the arctic atmosphere. J. Geophys. Res., 99D, 25391-25398.

Dibb J. E., R. W. Talbot, M. H. Bergin, 1994. Soluble acidic species in air and snow at Summit. Greenland. Geophysical Research Letters, 21(15), p. 1627-1630.

Dominé, F., Thibert, E, 1996. Mechanism of incorporation of trace gases in ice grown from the gas phase. Geophys. Res. Lett., 23**,** 3627-3630.

Dominé, F., Chaix, L., Hanot, L., 2000. Reanalysis and new measurements of N_2 and CH_4 adsorption on ice and snow. J. Colloid. Interf. Sci., 227, 104-110.

Dominé, F., Cabanes, A., Taillandier A.-S., Legagneux, L., 2001. Specific surface area of snow samples determined by CH_4 adsorption at 77 K, and estimated by optical microscopy and scanning electron microscopy. Environ. Sci. Technol. 35, 771-780.

Dominé, F., Cabanes, A., Legagneux, L., Structure, microphysics, and surface area of the Arctic snowpack near Alert during the ALERT 2000 campaign. this issue.

Fassnacht, S.R. ; Innes, J. ; Kouwen, N., Soulis, E.D., 1999. The specific surface area of fresh dendritic snow crystals. Hydrol. Process. 13, 2945-2962.

Gow, A.J., 1965. Snow studies in Antarctica. CRREL Res. Rep. 177.

Gregg, S.J., Sing, K.S.W., 1982. Adsorption, surface area and porosity. Academic Press, London.

Hanot, L., Dominé, F., 1999. Evolution of the surface area of a snow layer. Environ. Sci. Technol. 33, 4250-4255.

Hoff, J. T., Mackay, D., Jia, C.Q., Wania, F., 1998. Measurement of the specific surface area of snow using the nitrogen adsorption technique, *Environ. Sci. Technol*., 32, 58-62.

Honrath, R.E., Peterson, M.C., Guo, S., Dibb, J.E., Shepson, P.B., Campbell, B., 1999. Evidence of NO_x production within or upon ice particles in the Greenland snowpack. Geophys. Res. Lett., 26 695-698.

Hutterli, M. A., Rothlisberger, R., Bales, R. C., 1999. Atmosphere-to-snow-to-firn transfer studies of HCHO at Summit. Greenland. Geophys. Res. Lett., 26, 1691-1694.

Legagneux, L., Cabanes, A., Dominé, F., Measurement of the specific surface area of 176 snow samples using methane adsorption at 77 K. J. Geophys. Res., in press.

Marbouty, D., 1980. An experimental study of temperature gradient metamorphism. J. Glaciol. 26, 303-312.

Marti, J., Mauersberger, K., 1993, A survey and new measurements of ice vapor pressure at temperature between 170 and 250K, Geophys. Res. Lett. 20, 363-366.

McElroy M. B., Salawitch, R. J., Wofsy, S. G., Logan, J. A., 1986. Reduction of antarctic ozone due to synergistic interaction of chlorine and bromine. Nature, 321, p. 759-762.

Michalowski, B.A., Francisco, J.S., Li, S.-M., Barrie, L., Bottenheim, J.W., Shepson, P., 2000. A computer model study of multiphase chemistry in the arctic boundary layer during polar sunrise. J. Geophys. Res., 105, 15131-15145.

Narita, H., 1971. Specific surface of deposited snow II. Low Temp. Sci., A29, 69-81.

Nelson, J., 1998. Sublimation of ice crystals. J. Atmos. Sciences, 55, 910-919.

Pahaut , E. and Sergent, C., 1991. La neige Formation et Evolution. Centre d'Etude de la Neige, Météo-France.

Perrier, S., Houdier, S., Dominé, F., Cabanes, A., Legagneux, L., Sumner, A.L., Shepson, P.B., Formaldehyde in the snowpack near Alert during ALERT2000 field campaign Snowpack composition, incorporation processes and atmospheric impact. This issue.

Pruppacher, H.R. and Klett, J.D., 1978. Microphysics of clouds and precipitation. Reidel, Dordrecht.

Robinson D.A., Dewey K.F., Heim R.R., Jr; 1993. Global snow cover monitoring: an update, Bull. Amer. Meteor. Soc., 74, 1689-1696.

Sander, R., Vogt, R., Harris, G.W., Crutzen, P.J., 1997. Modeling the chemistry of ozone, halogen compounds, and hydrocarbons in the Arctic troposphere. Tellus, 49B, 522-532.

Sherlock, V.; Garnier, A.; Hauchecorme, A. Keckhut, P., 1999. Implementation and validation of a Raman lidar measurement of middle and upper tropospheric water vapor. *Applied Optics*, **38**, 5838-5850.

Thibert, E., Dominé, F., 1998. Thermodynamics and kinetics of the solid solution of HNO_3 in ice. Journal of Physical Chemistry B, 102, 4432-4439.

Wania, F., 1997. Modeling the fate of non-polar organic chemicals in an ageing snow pack, Chemosphere, 35, 2345-2363.

Wergin, W. P., Rango A., Erbe, E.F., 1995. Observations of Snow Crystals Using Low-Temperature Scanning Electron Microscopy. Scanning, 17, 41-49.

Zondlo, M.A., Barone, S.B. Tolbert, M.A., 1997. Uptake of HNO_3 on ice under upper tropospheric conditions. *Geophys.Res. Lett.* 24*,* 1391-1394.

III.6. Evolution of the specific surface area of surface snow layers

Différentes couches de neige ont pu être étudiées dans les Alpes et l'Arctique. Les résultats de la campagne ALERT 2000 montrent une décroissance de la SS avec le temps, et les résultats de l'**article 1** (cf. **§ III.2**.) indiquent également que les neiges âgées ont une SS plus faible que les neiges récentes.

L'objectif de cet article est de comparer l'évolution de la SS des différentes couches de neige fraîche étudiées dans les Alpes et l'Arctique. Nous tentons de montrer quels sont les paramètres impliqués dans la vitesse d'évolution de la SS. Nos données nous permettent ici de proposer une paramétrisation de cette vitesse d'évolution en fonction de la température. D'autres paramètres influencent la vitesse d'évolution mais nos données ne sont pas suffisantes pour les quantifier.

Evolution of the specific surface area of surface snow layers

Axel Cabanes, Loïc Legagneux, and Florent Dominé*

CNRS, Laboratoire de Glaciologie et Géophysique de l'Environnement, B.P. 96,
54 Rue Molière, 38402 Saint Martin d'Hères, cedex, France.

*Corresponding author. Phone: (33) 476 82 42 69; e-mail : florent@glaciog.ujf-grenoble.fr

ABSTRACT

The snowpack can impact atmospheric chemistry by exchanging adsorbed or dissolved gases with the atmosphere. Modeling this impact requires the knowledge of the specific surface area (SSA) of snow and its variations with time. We have therefore measured the evolution of the SSA of 8 recent surface snow layers in the Arctic and the French Alps, using CH_4 adsorption at liquid nitrogen temperature (77K). The SSA of fresh snow layers has been found to decrease with time. This is explained by snow metamorphism, which causes modifications in crystal shapes, here essentially crystal rounding and the disappearance of microstructures.

A parameterization of the rate of SSA decrease is proposed. We fit the SSA decrease to an exponential law, and find that the time constant α_{exp} (day^{-1}) depends on temperature according to $\alpha_{exp} = 60.3 \exp(-1642/T)$, with T in kelvin. Our parameterization predicts that the SSA of a snow layer evolving at - 40 °C will decrease by a factor of 2 after 14 days, while a similar decrease at –1°C will only require 5 days. Wind has also been found to increase the rate of SSA decrease, but insufficient data did not allow a parameterization of this effect.

Index terms: 1863: Snow and Ice; 3947: Surfaces and interfaces; 0399: General or miscellaneous; 0320: Cloud physics and chemistry

Submitted, JGR, 2 October 2001

1. INTRODUCTION

For over a decade, numerous studies of atmospheric chemistry in polar regions have revealed that the snowpack could interact chemically with the atmosphere. Spring-time Arctic ozone depletion (Barrie et al., 1988) is among the most studied aspects. Recently, studies have shown that significant exchanges of reactive gases between the snowpack and the lower troposphere were taking place, increasing the interest of studying air-snow interactions. Production of NO_x by the snowpack has been observed in Greenland and Antarctica (Dibb et al., 1998; Weller et al., 1999; Honrath et al., 1999; Jones et al., 2001). Emission of carbonyl compounds from the snowpack have also been observed. Formaldehyde emissions have been reported in Greenland and the Canadian Arctic (Hutterli et al., 1999, Sumner and Shepson, 1999), and emissions of formaldehyde, acetaldehyde and acetone have been measured at middle latitudes (Couch et al., 2000). Emissions of persistent organic pollutants have also been observed and modeled (Wania,1997, and references therein).

Numerous models of atmospheric chemistry over snow-covered surfaces (Sander et al., 1997; Michalowski et al., 2000) lead to calculated values lower than measured values (De Serves, 1994; Sumner and Shepson, 1999), which demonstrates than the impact of the snowpack must be included to yield reliable gas phase values. However, the inclusion of this impact requires the knowledge of the physical processes responsible for it, but these are insufficiently understood. Possible processes include sublimation/condensation of snow and solutes, adsorption/desorption of trace gases from the snow crystals surfaces, diffusion of species in the ice lattice and reaction on crystals surfaces.

Many physical parameters such as the specific surface area (SSA) of the snow must be known to quantify processes involving the surface of snow crystals. SSA is the surface area accessible to gases for a given mass of snow, and is expressed in cm^2/g rather than m^2/g because snow SSA values are usually low (Dominé et al., 2001; Dominé et al., in press; Cabanes et al., in press; Legagneux et al., in press). Fresh snow layers have the highest interaction potential with the atmosphere. Fresh crystals are at the surface of the snowpack and have the highest potential for physical evolution, and their SSA decrease can be rapid (Hanot and Dominé, 1999). The rate of SSA decrease is an essential parameter to quantify the amounts of a given species released by desorption, as mentioned by Hutterli et al. (1999) in the case of HCHO. However, there are almost no data on the rate of decrease of snow SSA shortly after precipitation.

We have therefore studied the SSA evolution of 8 fresh snow layers, sampled in the French Alps and in the Arctic. A wide range of rates were obtained, and these seemed to be affected by temperature, wind speed, and other environmental parameters, whose values are also reported. We then hope that this first, and necessarily incomplete, set of data will assist modelers of snow-air interactions in estimating the rate of SSA decrease of fresh snow.

We also present photomacrographs of snow crystals, taken to understand the physical processes involved in SSA decrease. These photographs are necessary for a future physical model of SSA evolution, that may be incorporated into comprehensive models of atmospheric chemistry over snow-covered areas.

2. SNOW SAMPLING

Snow layers studied in this work were sampled in the French Alps in early 1999 and 2001, hereafter referred to as winters 1999 and 2001, respectively, in the Canadian Arctic during winter and spring 2000, and in Svalbard during spring 2001. In the French Alps, snow samples were collected at three sites. Two of them were located at col de Porte (45°12'N, 5°44'E) at an elevation of 1330 m, in the Chartreuse range, about 10 km north of Grenoble. The first sampling site was located within the meteorological station of Centre d'Etude de la Neige (CEN). This site is referred to as site P. Continuous monitoring of air temperature and humidity, surface snow temperature, snowpack height, liquid and solid precipitation rates, wind speed at 10 m height, are performed by CEN. Air temperature was recorded in a ventilated shelter 1.5 m above the snow surface. Snow surface temperature was measured by its IR emission (Hanot et Dominé, 1999).

The second site was located 500 m west of CEN in a flat forest clearing of about 3 000 m^2. This site, referred to as site P', was preferred to site P when chemical measurements were coupled to our physical measurements because it is further from the road. Meteorological parameters were assumed to be similar to those at site P. This was verified for air temperature, that was found to be within 0.5°C of the CEN values on several occasions.

The third site was located at Col du Lautaret (45°02'N, 6°24'E), 55 km east of Grenoble, in a small south-facing sheltered basin at an elevation of 2058 m. This higher elevation site, referred to as site L, had to be used because of the unusually warm temperature during winter 2001, that resulted in rare snow events at site P. Unfortunately, there is no meteorological station at or near site L.

In the Canadian Arctic, snow samples were collected near the Alert base (Ellesmere Island 82°30' N, 62°21'W) during the ALERT 2000 campaign. The sampling site, referred to as site A, was located 5.4 km south from the base at about 180 m above sea level (Dominé et al., in press).

In Svalbard, the snow was sampled at Ny-Alesund (78°55' N, 12°56' E) during the NICE campaign in April-may 2001. The sampling site N was located about 50 m south of the Italian station, at the edge of the Ny-Alesund village.

The sampling method was similar to that described by Hanot and Dominé (1999) and Dominé et al. (in press): vertical faces were dug to observe the stratigraphy and to locate the snow layer of interest. For each sample, about 150 cm^3 of snow was collected in two glass vials which were immediately dropped in liquid nitrogen to stop metamorphism. Snow samples were kept in liquid nitrogen until being transferred in the volume used to measure SSA. Snow and air temperature were measured at different heights with a mercury or alcohol thermometer, or with a thermocouple. According to the thickness of the layer, snow was sampled at up to three levels, and density was measured using a sampler of known volume.

3. EXPERIMENTAL METHOD

The SSA of each snow sample was determined by CH_4 adsorption at liquid nitrogen temperature (77.15 K), as already described by Hanot and Dominé (1999), and recently detailed by Legagneux et al. (in press). Briefly, we used a volumetric method which requires the measurement of the adsorption isotherm of CH_4 on snow, followed by a BET treatment (Brunauer et al., 1938). This yields the SSA of the snow sample as well as the net heat of adsorption of CH_4 on ice, ΔQ_{CH4} . This latter parameter was used to test the reliability of SSA measurements as a value $\Delta Q_{CH4} = 2240 \pm 200$ J/mol must be obtained for the measurement to be considered reliable (Legagneux et al., in press). Legagneux et al. estimated that the reproducibility of the method was 6%, and that its accuracy, taking into account systematic errors due to the BET treatment, was 12%.

4. RESULTS

The characteristics of the 8 snow layers studied are summed up in table 1.

Table 1: Snow layers studied in the French Alps and the Arctic..

N°	Date of snowfall	Period of study	Sampling site	Initial layer thickness (cm)	Mean air Temp.	Initial snow density	Fresh snow crystal shape
1	6-9 Feb 99	10 Feb 99 16 Feb 99	Col de Porte Site P	105	-10	0.21(1)	Plates, needles and columns
2	4 Mar 99	4 Mar 99 9 Mar 99	Col de Porte Site P'	38	-1	0.10	Plates, needles and columns
3	9 Feb 01	9 Feb 01 15 Feb 01	Col du Lautaret Site L	24	-0.5	0.20(1)	Dendritic crystals
4	3 Feb 00	4 Feb 00 22 Feb 00	Alert Site A	3 to 8	-40	0.16	Columns, bullets combination
5	7 Feb 00	7 Feb 00 22 Feb 00	Alert Site A	1	-40	0.08	Columns, bullets combination
6	13-14 Apr 00	14 Apr 00 23 Apr 00	Alert Site A	0.3	-27	0.07	Columns, bullets combination
7	25-28 Apr 00	25 Apr 00 29 Apr 00	Alert Site A	5	-15	0.016 to 0.21(2)	Variably rimed dendritic crystals
8	27 Apr 01	27 Apr 01 3 May 01	Ny-Alesund Site N	6	-2.0	0.14	Columns, rimed dendritic crystals

(1) : density measured at the bottom of the layer

(2) : in wind-packed accumulation

4.1. Description of the snow layer fallen on 6-9 February 1999 at col de Porte

This snow fall, (n°1 in table 1), was studied at col de Porte at site P. It was 105 cm-thick and was above a hard melt-freeze layer. It was made up of a mixture of plates, needles and columns with the presence of rime on crystals in the middle of the layer. Figure 1 and table 2 sum up the samplings which were performed at three heights on 10, 12 and 16 February.

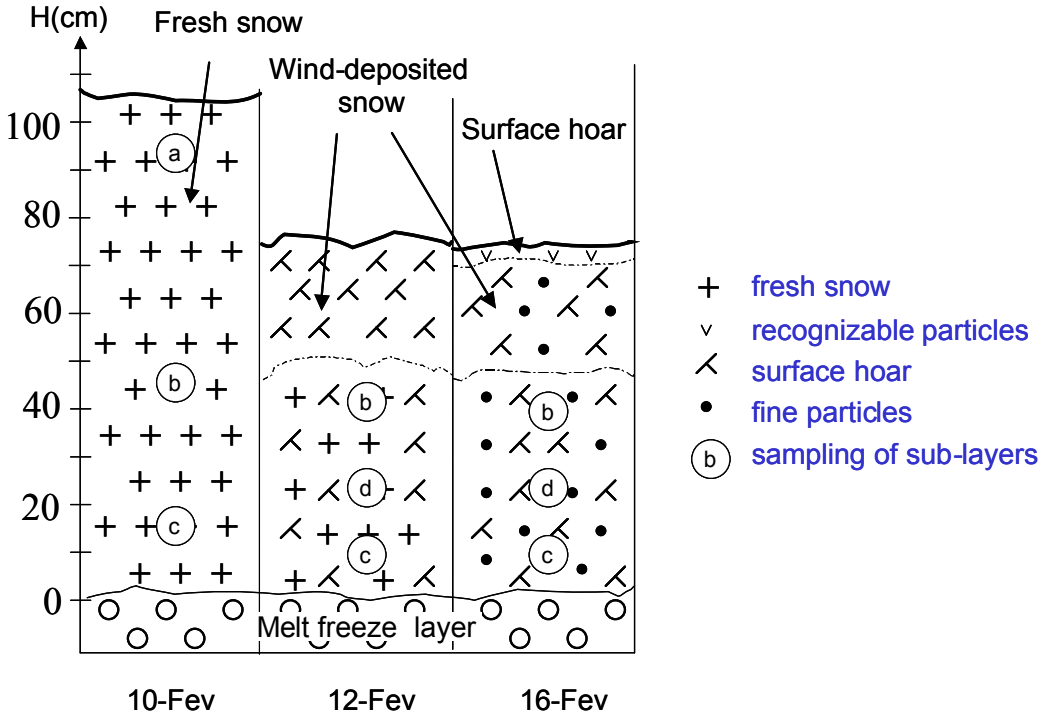

Figure 1: Stratigraphy of the snowpack studied at col de Porte in mid-February 1999 (snow fall n°1). Sampling levels are shown

Table 2 : Snow sampling conditions and SSA for snow fall n° 1 (6-9 Feb. 99) at col de Porte (site P).

Date time	Weather conditions	T air (°C)	Sub-layer	depth (cm)	T snow (°C)	Density	SSA (cm²/g)
10-Feb 12:00	Snowing Northerly wind	-9.4	a	10	-7.9	0.107	801
			b	60	-3.0	0.178	396
			c	90	-2.7	0.214	414
12-Fev 10:00	Cloudy Slight north wind	-12.3	b	35	-8.2	0.178	673
			d	50	-6.2	0.178	599
			c	65	-4.7	0.250	341
16-Fev 10:00	Cloudy No wind	-1.8	b	38	-5.9	0.245	404
			d	57	-5.0	0.224	372
			c	68	-4.7	0.275	272

Figure 2 shows snowpack height and precipitation rates monitored at CEN. Air and snow surface temperature measured at CEN are shown in figure 3. Figure 2 indicates that snow fell during six major precipitation events from 6 February to 9 February: 3 events were on 6 February, one on 7 February, one on 8-9 February, and the last one on 9 February. During these four days, air temperature varied between -10.0 to - 0.5 °C. Afterwards, a few showers occurred on 10 and 11 February, including one during our first sampling. Then, a wind event started on 10 February around

4 pm and lasted until 12 February morning, that disturbed the upper part of the layer, so that only the middle and bottom sub-layers referred to as b and c respectively, could be monitored. Note that the second sample (referred to as “d”) collected on 12 February did not correspond to any sub-layer d collected on 10 February (fig.1 and table 2).

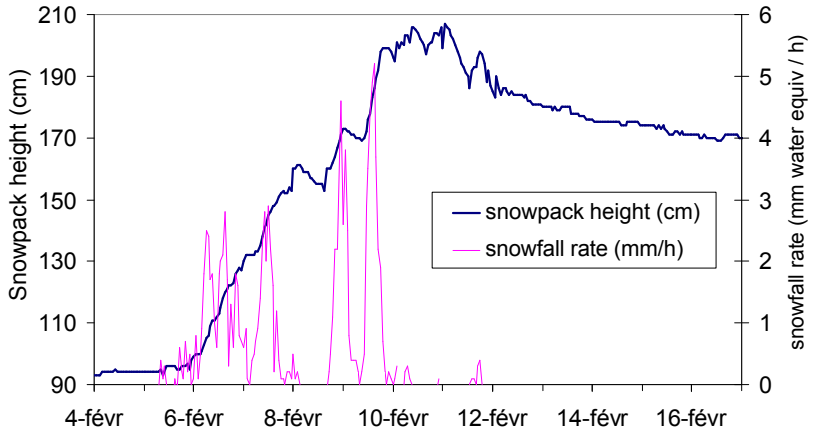

Figure 2: Snowpack height and snowfall rate at col de Porte in early February 1999. Time is GMT.

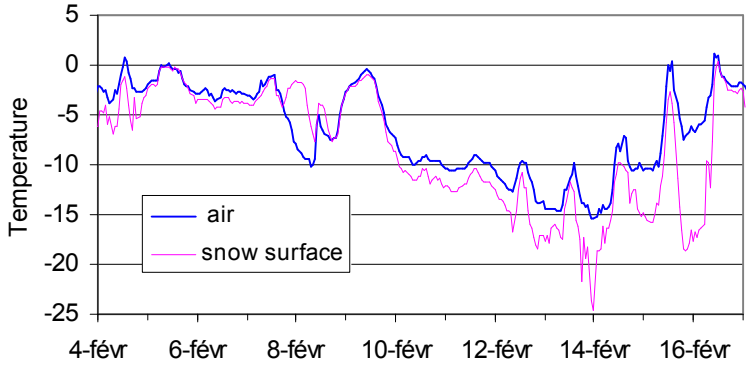

Figure 3: Air temperature (1.5 m above the surface) and snow surface temperature (measured by IR emission) in early February 1999.

After 12 February, the air temperature continued its overall decrease down to -15 °C on 14 February, with visible diurnal variations, while wind speed stayed low (less than 5 m/s). Then, a warming up to +1.0 °C occurred on 16 February, when we performed the last sampling. All snow samples collected on 16 February corresponded to the same sub-layers as on 12 February, and rounded grains made up a large fraction of the snow.

The SSA evolution of the bottom sub-layer c is reported in figure 4. The age of the sub-layer was estimated according to snowfall rates and densities. The SSA decreased from 414 to 272 cm^2/g in 6 days. The SSA evolution of the middle sub-layer b (fig.4) presents an unusual increase from 396 to 673 cm^2/g after 2 days, followed by a decrease to 404 cm^2/g. This unusual behavior will be addressed in the discussion section.

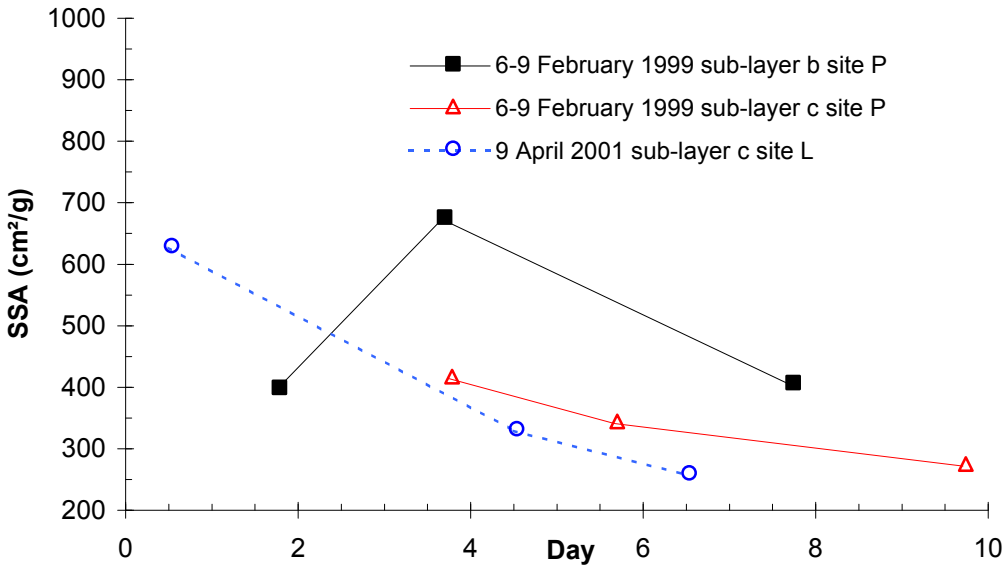

Figure 4: Evolution of the SSA of several snow layers studied in the French Alps.

4.2. Description of the 4 March 1999 snow layer at col de Porte

The snow fall, (n°2 in table 1) that precipitated at site P' on 4 March 1999 was sampled five times until 9 March (fig.5). Values of physical parameters measured during sampling are reported in table 3.

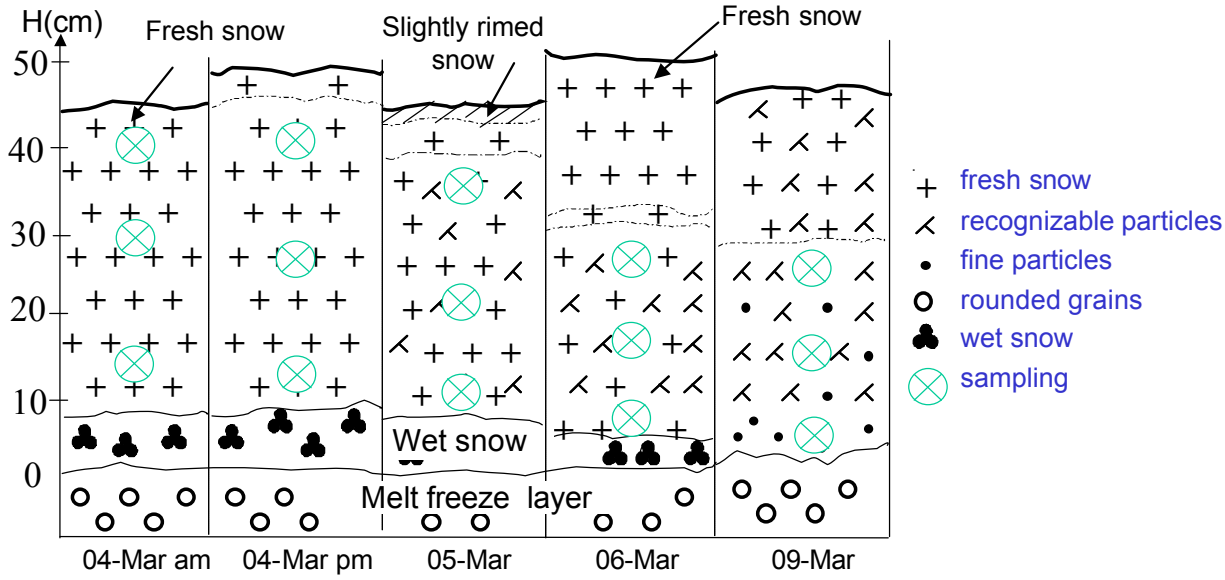

Figure 5: Stratigraphy of the snowpack studied at col de Porte during early March 1999 (snow fall n°2). Sampling levels are shown

Table 3 : Snow sampling conditions and SSA for snowfall n°2 (4 March 1999) at col de Porte (site P').

Date time	Weather conditions	T air (°C)	Sub layer	depth (cm)	Tsnow (°C)	Density	SSA (cm²/g)
4-Mar 10:00	Snowing	-0.7	a	5	-1.1	0.092	780
			b	15	-1.0	0.097	654
			c	30	-0.4	0.112	613
4-Mar 16:00	Slightly snowing	-0.6	a	8	-0.4	0.10	702
			b	19	-0.4	0.117	596
			c	35	-0.4	0.16	604
5-Mar 10:00	Cloudy No wind	-1.8	a	7	-1.8	0.122	557
			b	22	-1.0	0.112	496
			c	35	-0.1	0.163	454
6-Mar 09:00	Slightly snowing	-2.9	a	23	-2.4	0.133	469
			b	33	-1.5	0.152	431
			c	44	-0.5	0.183	410
9-Mar 10:00	Cloudy No wind	+2.2	a	20	-0.8	0.194	369
			b	30	-0.7	0.194	269
			c	40	-0.3	0.229	349

Figure 6 shows snowpack height and precipitation rates monitored at CEN. Air and snow surface temperatures measured at CEN are shown in figure 7.

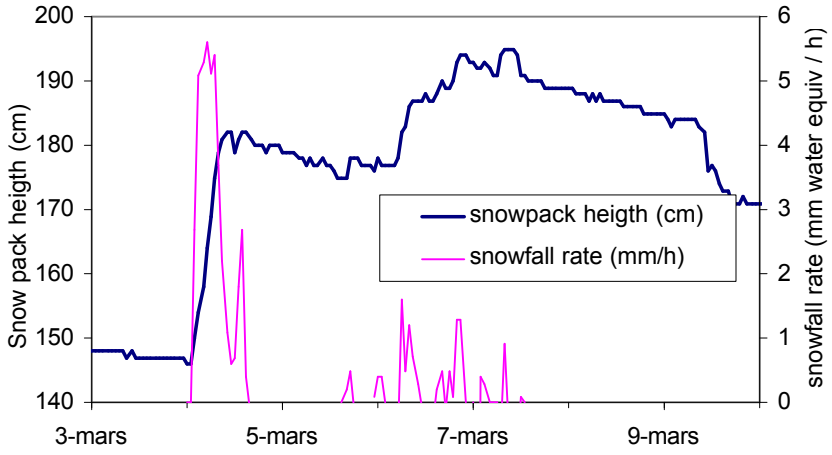

Figure 6: Snowpack height and snowfall rate at col de Porte in early March 1999.

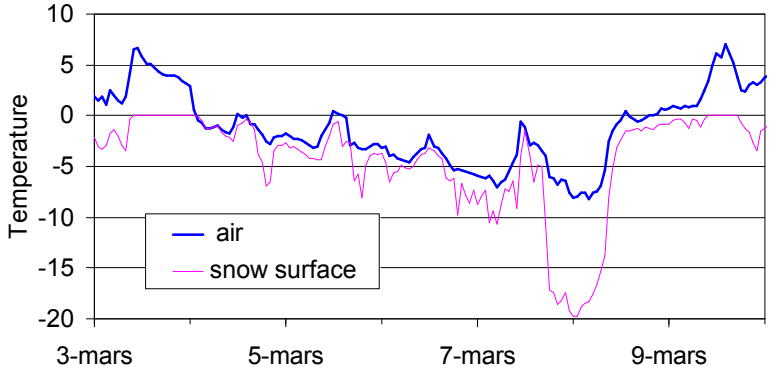

Figure 7: Air temperature (1.5 m above the surface) and snow surface temperature (measured by IR emission) in early March 1999.

Figure 6 shows that precipitation began on 4 March at 1 am when the air temperature was fluctuating between –0.5 to – 2.0 °C and finished around 4 pm while the air temperature was also fluctuating between –0.5 and –2.0 °C. The snowfall could be subdivided in two parts: First, 38 cm of snow were deposited in 10 hours over a 7 cm-thick layer of wet snow, and precipitation almost stopped around 11 am after the first sampling. Then, while the initial snow was settling, snow started falling again around 1 pm increasing snowpack height by 4 cm while a slight warming occurred (fig.7).

From 5 to 7 March, several light snowfalls took place, adding about 15 cm of new snow at site P'. Note that at CEN, 20 cm were recorded (fig.6). Afterwards, a temperature drop was observed during the night from 7 to 8 March followed by a warming after 8 March which forced us to stop our study on 9 March.

As determined with a magnifying glass and with an optical microscope, this snow consisted of a very variable mixture of stellar crystals, plates, needles and columns. The initial density of the fresh snow ranged from 0.092 at the top of the layer to 0.112 at the bottom. Snow was collected at three heights for each sampling. In order to locate easily the top of the layer, an aluminum sheet was deposited over the snow surface after the first sampling. The evolution of the snow stratigraphy over our sampling period is detailed in figure 5. Pictures of a few snow crystals coming from the top sub-layer and collected between 4 to 9 March are shown in figure 8, showing the effect of rounding with time.

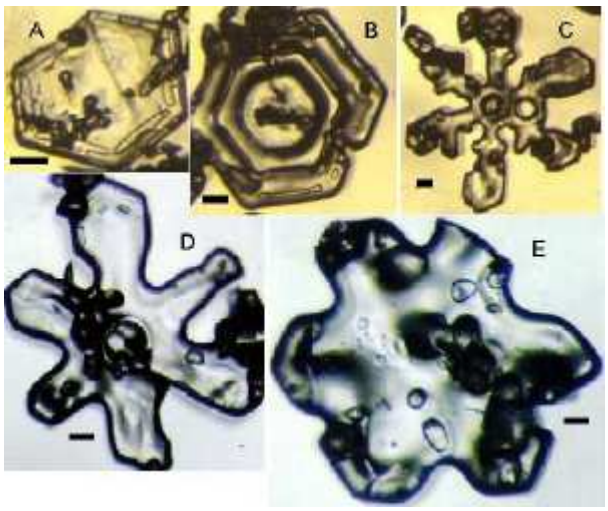

Figure 8: Pictures of snow crystals from the top of the 4 March 1999 snowfall at Col de Porte. Pictures were taken from 4 to 9 March, to show rounding with time. Scale bars: 100 µm. Dates of crystal sampling are A: 4 March am; B: 4 March pm; C: 5 March; D: 6 March; E: 9 March.

The SSA evolutions of the 3 levels sampled are shown in figure 9, and show a decrease with time. The top sub-layer had an initial SSA of 780 cm^2/g, which decreased to 369 cm^2/g in 5 days. For the middle and bottom sub-layers, SSA decreased from 654 to 269 cm^2/g and from 613 to 349 cm^2/g respectively. Figures 8 and 9, and table 3 show that the SSA decrease is correlated to crystal rounding and to a density increase.

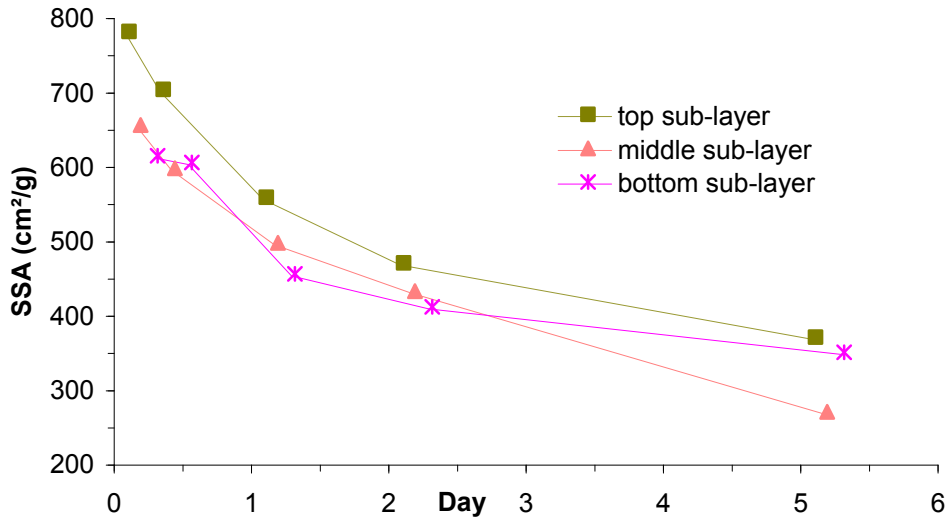

Figure 9: SSA evolution of the snow fall of 4 March 1999 (snow fall n°2) at col de Porte.

4.3. Description of the 9 February 2001 snow layer studied at col du Lautaret

This snow fall, (n°3 in table 1) consisted of dendritic snow and fell on 9 February 2001 in the early morning at site L. It fell over a 15 cm-thick wet snow layer, and was sampled three times on 9, 13 and 15 February (fig.10).

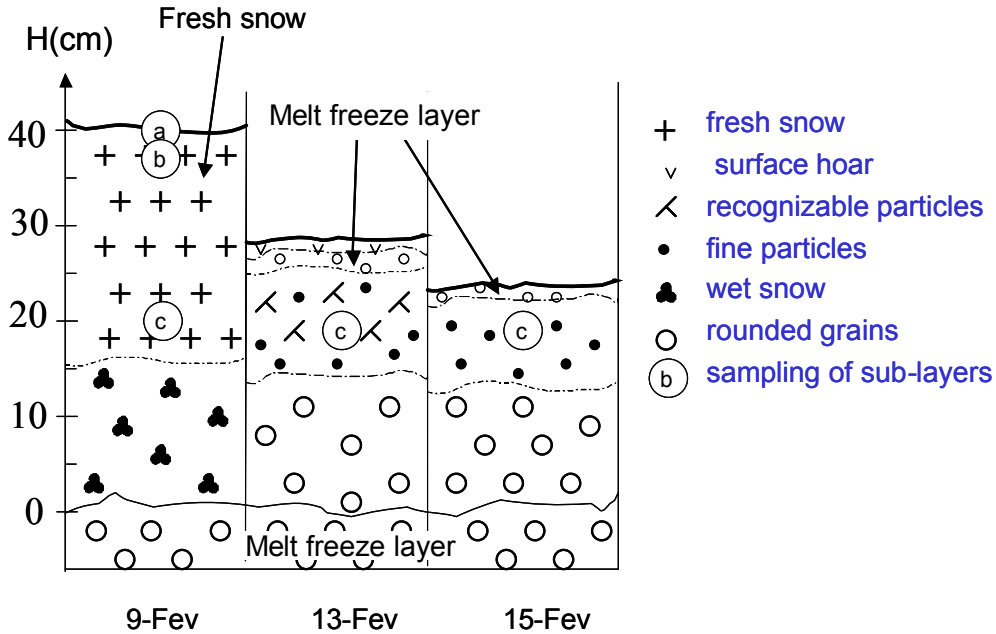

Figure 10: Stratigraphy of the snowpack studied at col du Lautaret during February 2001 (snow fall n°3). Sampling levels are shown.

The snow layer had a thickness of 24 cm and its density increased with depth from 0.10 to 0.20 (table 4).On 13 February, the layer had shrunk down to 10 cm-thick. The crystals were made up of recognizable particles and of rounded crystals. A 2 cm-thick melt-freeze layer and 1 cm of surface hoar had formed on its surface. No weather station is present near site L, but weather observations near Grenoble, and data from other alpine meteorological stations suggest warm temperatures, most likely above freezing, in the day time, and clear sky conditions at night, which can easily explain the formation of the melt-freeze layer and of the surface hoar. The snow layer was sampled at 3 levels on

9 February, but the modification of the stratigraphy resulted in a single sampling (“c”) on 13 February (fig.10 and table 4).

Table 4 : Snow sampling conditions and SSA for snow fall n°3 (9 February 2001) at col du Lautaret (site L).

Date time	Weather conditions	T air (°C)	Sub layer	Depth (cm)	T snow (°C)	Density	SSA (cm²/g)
9-Feb 11:00	Cloudy Light west wind	-2.0	a	0	-2.5	/	690
			b	2	-2.5	0.10	666
			c	20	-2.0	0.20	627
13-fev 11:00	Sunny No wind	+1.2	c	8	-1.5	0.19	329
15-fev 11:00	Sunny Light east wind	+1.0	c	5	-0.5	0.20	257

On 15 February, the top of the layer consisted of a 1 cm-thick melt-freeze layer. The presence of wind-deposited snow in sheltered area indicated that wind had blown between 13 and 15 February. Only the sub-layer c sampled on 13 February was sampled again on the 15. The SSA evolution of this sub-layer c is reported in figure 4, which shows a decrease from 627 to 257 cm^2/g.

4.4. Winter and spring snow layers studied near Alert during winter 2000

In the Canadian Arctic, four fresh snow layers were studied near Alert at site A. Two fell on 3 and 7 February 2000, and another two fell on 13-14 and 25-28 April (table 1). The description of the snow layers and the evolution of their SSA have been detailed recently (Dominé et al., in press; Cabanes et al., in press) and only the main data are briefly recalled here.

4.4.1. Description of the 3 and 7 February 2000 snow layers

The 3 February fall, (n°4 in table 1) fell by –19 °C at the end of a south-westerly wind event. Snow formed a wind-blown discontinuous layer 3 to 8 cm-thick. It consisted of columns and combination of bullets, as usually observed in Polar regions at low temperature (Gow, 1965). The density was 0.16.

New snow (n°5 in table 1) consisting of columns and combination of bullets fell on 7 February by - 38 °C under calm conditions and covered the 3 February layer with a continuous 1 cm-thick layer of density 0.08. The air temperature then remained around - 40°C and surface hoar grew continuously on the snow surface, until 22 February when a northerly wind event remobilized both layers and the surface hoar. Both layers were sampled several times between 3 and 22 February 2000.

As observed for Alpine snow, the SSA of Arctic snow essentially decreased with time. The SSA of the 3 February snow shows an overall decreasing trend: from 770 cm^2/g to 460 cm^2/g in 17 days (fig.11). We note here that this decrease is not perfectly monotonous, and that this layer was affected by wind, whose effect will be addressed in the discussion section. For the 7 February layer, the decrease was by a factor of 2.7 from 1460 cm^2/g to 550 cm^2/g in 13 days (fig.11). Photomacrographs of snow samples were taken to attempt to understand the processes responsible for the SSA decrease

(Cabanes et al., in press). They showed that crystal rounding was the main observed change in the 3 February layer. For the 7 February layer, the SSA decrease was explained by two processes: (i) rounding of crystals; (ii) dilution by surface hoar of lower SSA (590 cm^2/g).

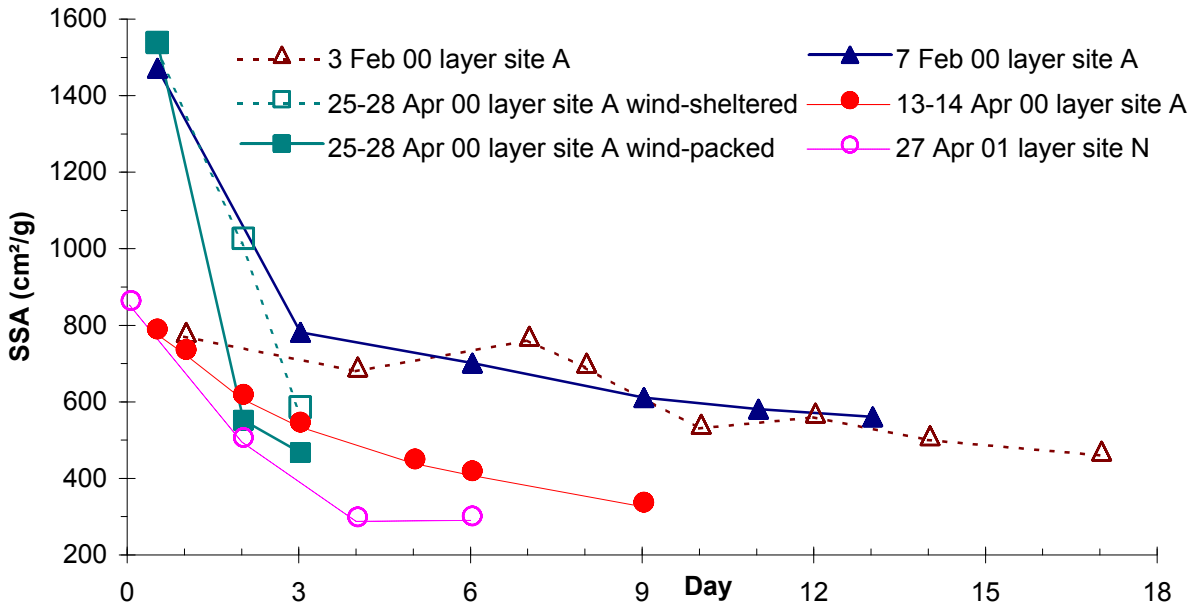

Figure 11: Evolution of the SSA of several snow layers studied in the Arctic.

4.4.2. Description of the 13-14 April snow layer

On 13 and 14 April 2000, two snowfalls (n°6 in table 1) deposited 2 and 1 mm of snow, under temperatures of –27 and –23°C, respectively, under calm conditions. As in winter, snow was made up of columns and bullet combinations and its density was 0.07. We studied the SSA evolution until 25 April, while the average air temperature was – 27°C. Until then, no precipitation or wind occurred. Snow fallen on 13 and 14 April had an initial SSA of 779 cm^2/g which decreased by a factor of 2.4 to 326 cm^2/g in 9 days (fig.11). As in winter, surface hoar of low SSA, 354 cm^2/g, was observed to grow over the 13-14 snow layer and, together with crystal rounding, contributed to the SSA decrease.

4.4.3. Description of the 25-28 April snow layer

This snow layer (n°7 in table 1) fell from 25 to 28 April by –15 °C during a continuous northerly wind event and consisted of variably rimed dendritic crystals. It formed a 5 cm-thick layer of variable density. Values as low as 0.016 were measured in wind-sheltered areas, while values as high as 0.21 were found in wind-packed accumulations. The SSA decrease was also dependent on the wind conditions. In wind-exposed accumulations, the SSA decrease was very rapid: from 1530 to 540 cm^2/g in just 1.5 day. In wind-sheltered areas, the decrease was from 1530 to only 1015 cm^2/g in 1.5 day (fig.11). Photomacrographs (fig.12) show that the quick decrease was associated with crystal rounding and to the disappearance of microstructures such as small sub-dendrites with diameters in the 10 to 20 µm size range. From geometrical considerations (Dominé et al., 2001), we estimate that such structures have a SSA of about 4000 cm^2/g.

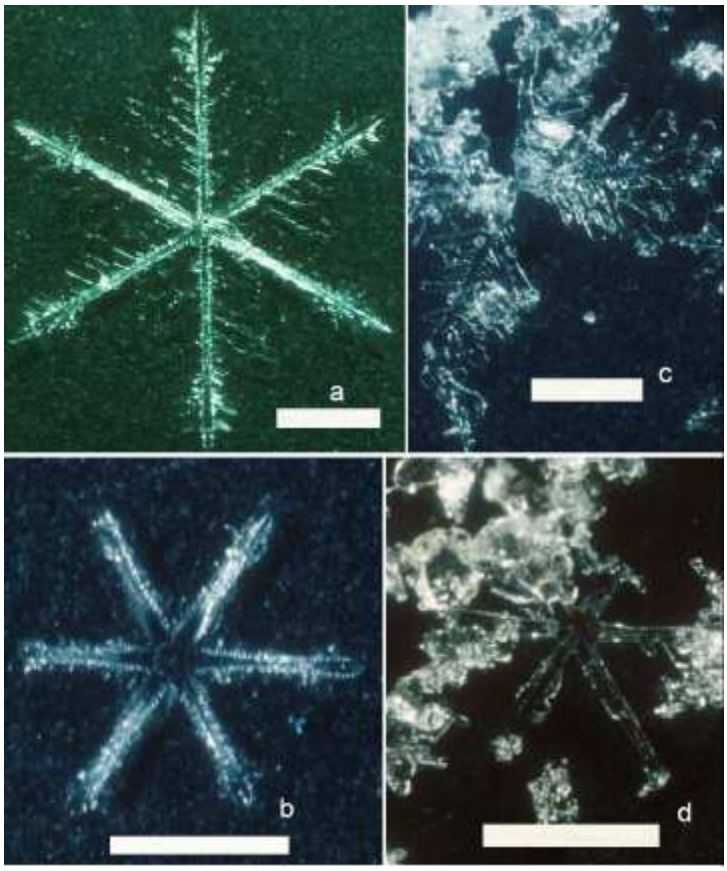

Figure 12: Photomacrographs of snow crystals fallen near Alert on 25-28 April 2000 (snow fall n°7) showing crystal rounding and the disappearance of small sub-dendrites in the 10 to 20 µm size range. Scale bars : 1mm. a and b: Fresh dendritic snow crystal. c: Snow crystal collected on 28 April in a wind-sheltered area. d. Snow crystal collected on 28 April in a wind-exposed accumulation.

4.5. Description of the 27 April 2001 snow layer studied at Ny-Alesund

This 6 cm-thick snow layer formed on 27 April at site N. It precipitated by a temperature around -0.3°C under calm conditions and was mostly made up of columns and rimed dendritic crystals. The density of fresh snow was 0.14. This layer was then sampled on 28 and 30 April and 2 may.

On 28 April, a melt-freeze crust formed on the surface. The lower part of the layer was sampled, and consisted of still recognizable particles. A new snowfall deposited about 55 mm of fresh snow by a temperature around 0°C on 29 April. Then, temperature decreased to around –2.5°C and a new snowfall fell on 30 April. From 30 April to 2 may, temperature evolved between –2.0°C and -3.5°C while the density of the studied layer increased, up to 0.29 on 2 may. SSA of snow was initially 853 cm^2/g and decreased to 290 cm^2/g after 6 days (fig.11).

5. DISCUSSION

The main purpose of this study is to quantify the rate of SSA decrease of fresh snow and to propose a parameterisation of this decrease that can be used in models of air-snow interactions.

The SSA evolutions of snow layers reported in figures 4, 9 and 11 always show a monotonous decrease with time except in two cases where wind was involved. In the third case where wind was involved (25-28 April '00 snow fall at Alert), wind was also observed to have an important effect, as it accelerated SSA decrease. In the case of the 3 February '00 fall at Alert, successive samplings progressed in the same wind-accumulated snow bank. It is easy to imagine that the properties of the snow in this bank were spatially variable, due to time-varying wind speed during deposition. This bank was then heterogeneous, which probably caused the variations observed in the plot of figure 11. This suggestion is consistent with the observations made at Alert on 25-28 April '00, but similar observations could not be made in early February, because of the complete darkness. Thus, we suggest that the non-monotonous SSA decrease of the 3 February layer is a wind-induced artefact.

Two processes may explain the SSA increase of sub-layer "b" of the 6-9 February '99 layer at col de Porte (fig. 4 and table 2). We first notice that the top sub-layer ("a") had a high initial SSA, 801 cm^2/g, while the middle sub-layer "b" had a lower initial SSA of 396 cm^2/g. It is possible that there was a sharp vertical discontinuity in SSA, because this snow accumulation was caused by several distinct events. Between the first and the second sampling, the top part of the layer was removed and locating sub-layer "b" was then difficult. It is then possible that sampling was done on the other side of a possible discontinuity. Another possibility is that sub-layer "b", whose surface was exposed during the wind storm, acted as a small crystal filter, while larger wind-blown crystals remained on top. Thus, an enrichment in small particles of high SSA could have resulted in an increased SSA. In any case, data from this sub-layer cannot be considered in the subsequent attempt to parameterize SSA decrease. Data from the 3 February '00 layer will be considered, however, as the variations observed can be considered as noise, while the overall decrease remains clearly apparent.

Photomacrographs presented here (figures 8 and 12) and in earlier work (Cabanes et al., in press) indicate that the observed SSA decreases are due to modifications in crystal shapes, essentially rounding due to metamorphism, and also, for the very surface layers in the Canadian Arctic, to dilution by surface hoar of lower SSA.

Quantifying SSA decrease rigorously would then require the physical modelling of crystal rounding, which is governed by numerous parameters such as temperature, temperature gradient, ventilation, permeability, air relative humidity, density increase, etc. Such an enterprise is well beyond the scope of this first paper on the subject. At this point, we will only seek empirical correlations between SSA and time, and investigate whether empirical parameters can be related to measurable physical variables.

Many possible equations can be used to fit our SSA decrease plots. Considering the complexity of the physics involved, and the preliminary character of our approach, any choice of an analytical

expression will at this point be largely arbitrary. We will here investigate 2 equations: a linear one (equation 1) and an exponential one (equation 2).

$$SSA = SSA_0 - \alpha_{lin} t \quad (1)$$

$$SSA = SSA_0 . e^{-\alpha_{exp} t} \quad (2)$$

In the above equations, SSA_0 is the initial SSA, at time t=0, i.e. when the snow is deposited, and α_{lin} and α_{exp} are the time constants in each equation. Table 5 shows the correlation coefficients R^2 as well as α values obtained for each snow layer. Except in one instance, the best R^2 value is obtained with the exponential equation, and we will continue our discussion by considering α_{exp} values only.

Table 5 :Correlation coefficients R^2 and factors α obtained by fitting the rate of SSA decrease to equations 1 (linear) and 2 (exponential).

Snow layer	R^2 linear	R^2 exponential	Average T °C	$\alpha_{lin,}$ day^{-1}	$\alpha_{exp,}$ day^{-1}
10 Feb 99 bottom	0.952	0.975	-10	22.79	0.0682
04 Mar 99 top	0.822	0.893	-1	74.87	0.141
04 Mar 99 middle	0,942	0.987	-1	71.97	0.171
04 Mar 99 bottom	0,770	0.827	-1	51.03	0.110
03 Feb 00	0.811	0.823	-40	20.7	0.0343
07 Feb 00	0.682	0.781	-40	59,60	0.0672
13-14 Apr 00	0.919	0.972	-27	52.73	0.103
25-28 Apr 00[a]	0.995	0.957	-15	377.7	0.381
25-28 Apr 00[b]	0.890	0.925	-15	446.5	0.500
09 Feb 01	0.978	0.996	-0.5	63.5	0.150
27 Apr 01	0.844	0.885	-1.5	95.2	0.190

[a]: wind sheltered
[b]: wind exposed

The data presented here indicate that temperature strongly affects the rate of SSA decrease. For example, the 3 February 2000 layer evolved by around - 40 °C at Alert and its SSA decreased only by a factor of 1.5 in 17 days while the SSA of the 4 March 1999 top sub-layer, evolving around - 1 °C, decreased by a similar ratio in just 5 days. Of course, our data also show that other factors come into play. Wind accelerates SSA decrease: data from the 25-28 April 2000 layer show that SSA decrease in a wind-sheltered area is much slower than in a wind–exposed one (fig.11).

However, we will first seek to quantify the effect of what appears to be the most important parameter, temperature. SSA decrease appears strongly linked to metamorphism, as suggested by numerous photomacrographs, such as those of figures 8 and 12. If this is indeed the case, then what is involved is essentially sublimation and condensation of water molecules. This is a thermally activated process, and a description of its rate may be made with an Arrhenius equation. Keeping in mind that we are

grossly simplifying the problem, we present in figure 13 an Arrhenius plot of α_{exp}. We have excluded the data from the 25-28 April '00 layer at Alert, because it was strongly affected by wind. The correlation coefficient is fairly large, 0.68, which suggests that temperature does indeed explain a large fraction of the rate of SSA decrease observed.

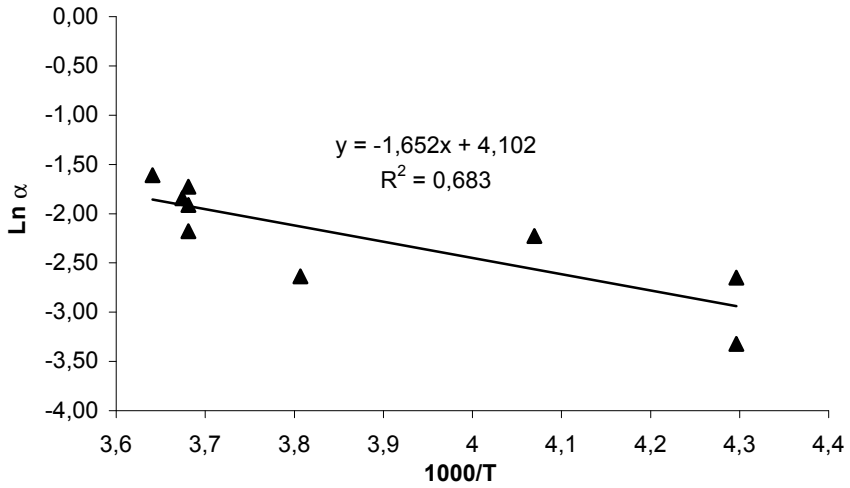

Figure 13: Evolution of the parameter α_{exp} as a function of 1/T. Values of α_{exp} are summed up in table 5. The 25-28 April 00 snow layer affected by wind has not been included in the data.

We then propose that the rate of SSA decrease of fresh snow can be parameterized by equation (2), with α_{exp} given by:

$$\alpha_{exp}(day^{-1}) = 60.3 \quad \exp^{-\frac{1652}{T(K)}} \qquad (3)$$

According to the limited data of figure 13, equation (3) will give the rate within 50% at the 1 σ confidence level. Thus, for snow layers evolving by -1 and - 40°C, we can deduce that the SSA will decrease by a factor of 2 after 5 and 14 days, respectively.

As indicated by the data, wind can also strongly influence the rate of SSA decrease. The rate of SSA decrease of the 25-28 April '00 layer at Alert, which took place at –15°C, is thus the fastest we observed, and this demonstrates that strong wind can have the same effect of the rate of SSA decrease as a temperature increase of several tens of degrees. Thus our parameterization is valid when the action of wind is small. More observations are necessary before we can include wind speed in a more general parameterization.

Yet other factors influence SSA decrease. Increases in snow density, either caused by wind or by the weight of subsequent layers, will increase contact points between crystals and reduce SSA. This is consistent with the anti-correlation between SSA and density obtained by Narita (1971) and Legagneux et al. (in press). Snow permeability is also an important parameter, as it will affect the motion of water vapor throughout the snowpack, and therefore the crystal transformations that lead to SSA decrease. Permeability varies greatly as a function of density and snow type (Albert, 2000), and should also be measured to accurately predict the rate of SSA decrease.

6. SUMMARY AND CONCLUSION

The present work shows that (i) the evolution of SSA can be described by an exponential law; (ii) the kinetics of decrease appear mostly determined by temperature and by the presence of wind. The limited data presented here only allow a parameterization of the rate of SSA decrease as a function of temperature, in the absence of strong winds. It is then obvious that a more rigorous parameterization of snow SSA decrease should be a function of several parameters, and not of temperature only, but many more measurements are needed before this can be achieved.

Moreover, the photographs taken during this study strongly suggest that the study of crystal shapes and their evolution is relevant to the understanding of SSA decrease. The microphysics of snow crystals will clearly influence the rate of SSA decrease. For example, snow made up of homogenous structures of about 50 µm in size, as described in Dominé et al. (2001) with an initial SSA of 1300 cm^2/g should show a regular SSA decrease. On the other hand, snow having a similar initial SSA but made up of a mixture of microstructures in the 10 µm size range (SSA=6500 cm^2/g) and in the 100 µm size range (SSA=650 cm^2/g) should show a decrease in two stages with different time constants. Such snow would be similar to the dendritic snow of 25-28 April ’00 at Alert, where an initial fast decrease was observed, even for wind-sheltered accumulations. Thus, the study of snow microphysics may also be required for a proper understanding of the kinetics of SSA decrease.

ACKNOWLEDGMENTS

Work in the Alps was funded by CNRS through Programme National de Chimie Atmosphérique (PNCA). Work in the Arctic was funded by the French Polar Institute (IFRTP). At col de Porte, meteorological data were supplied by Centre d’ Etude de la Neige operated by Météo-France. We especially thank Yves Lejeune for supplying meteorological data. The Alert 2000 campaign was coordinated by Jan Bottenheim (Meteorological Service of Canada) and Paul Shepson (Purdue University). We thank CFS Alert and Al Gallant (MSC) for logistical and technical support, and Peter Brickell (MSC) for his efforts to supply us with liquid nitrogen at Alert. Work in Svalbard was done in collaboration with the NICE campaign, coordinated by Harry Beine (CNR Rome). The efforts of Roberto Sparapani (CNR Rome) to ensure that we had optimal working conditions are gratefully acknowledged. Liquid nitrogen in Svalbard was very graciously supplied by Kay Krüger (AWI).

REFERENCES

Albert, M.R., E.F. Shultz, and F.E. Perron. Snow and firn permeability at Siple Dome, Antarctica. Ann. Glacio., 31, 353-356, 2000

Barrie, L.A., J.W. Bottenheim, R.C. Schnell, P.J. Crutzen, and R.A. Rasmussen. Ozone destruction and photochemical reactions at polar sunrise in the lower Arctic atmosphere. Nature, 334, 138-141, 1988.

Brunauer, S., P.H. Emmet, and E. Teller. Adsorption of gases in multimolecular layers. *J. Am. Chem. Soc.,* **60**, 309-319, 1938.

Cabanes, A., L. Legagneux, and F. Dominé. Evolution of the specific surface area and of crystal morphology of Arctic fresh snow during the ALERT 2000 campaign, *Atm. Env.*, in press.

Couch, T.L.; A.-L. Sumner, T.M. Dassau, P.B. Shepson, and R.E. Honrath. An Investigation of the Interaction of Carbonyl Compounds with the Snowpack. *Geophys. Res. Lett.*, **27**, 2241-2244, 2000.

De Serves, C. Gas phase formaldehyde and peroxide measurements in the arctic atmosphere. J. Geophys. Res., **99D**, 25391-25398, 1994.

Dibb, J.E. Talbot, D. Munger, D. Jacob, and S.-M. Fan. Air-snow exchange of HNO_3 and NOy at Summit, Greenland. *J. Geophys. Res.*, **103**, 3475-3486, 1998.

Dominé, F., A. Cabanes, A.-S. Taillandier. and L. Legagneux. Specific surface area of snow samples determined by CH_4 adsorption at 77 K, and estimated by optical microscopy and scanning electron microscopy. *Environ. Sci. Technol. **35***, 771-780, 2001.

Dominé, F., A. Cabanes, and L. Legagneux. Structure, microphysics, and surface area of the Arctic snowpack near Alert during the ALERT 2000 campaign. *Atm. Environ*., in press.

Gow, A.J. Snow studies in Antarctica. CRREL Res. Rep. 177, 1965.

Hanot, L., and F. Dominé. Evolution of the surface area of a snow layer. *Environ. Sci. Technol*., **33**, 4250-4255, 1999.

Honrath, R.E., M.C. Peterson, S. Guo, J.E. Dibb, P.B. Shepson, and B. Campbell. Evidence of NO_x production within or upon ice particles in the Greenland snowpack. *Geophys. Res. Lett*., **26**, 695-698, 1999.

Hutterli, M.A., R. Rothlisberger, and R. C. Bales. Atmosphere-to-snow-to-firn transfer studies of HCHO at Summit. Greenland. *Geophys. Res. Lett*., **26**, 1691-1694, 1999

Jones, A. E., R. Weller, P.S. Anderson, H.-W. Jacobi, E. W. Wolff, O. Schrems, H. Miller , Measurements of NOx emissions from the Antarctic snowpack. *Geophys. Res. Lett*., **28,** 1499-1502, 2001.

Legagneux, L., A. Cabanes, and F. Dominé. Measurement of the specific surface area of 176 snow samples using CH_4 adsorption at 77 K. *J. Geophys. Res*., in press.

Michalowski, B.A., J.S. Francisco, S.-M. Li, L.A. Barrie, J. W. Bottenheim, and P.B. Shepson. A computer model study of multiphase chemistry in the arctic boundary layer during polar sunrise*. J. Geophys. Res.*, **105**, 15131-15145, 2000.

Narita, H. Specific surface of deposited snow II, *Low Temp. Sci.* **A29**, 69-81, 1971.

Sander, R., R. Vogt, G.W. Harris, and P.J. Crutzen. Modelling the chemistry of ozone, halogen compounds, and hydrocarbons in the Arctic troposphere. Tellus, **49**B, 522-532, 1997.

Sumner, A.L. and P.B. Shepson. Snowpack production of formaldehyde and its effect on the Arctic troposphere. *Nature*, **398**, 230-233, 1999.

Wania, F. Modelling the fate of non-polar organic chemicals in an ageing snow pack. *Chemosphere*, **35**, 2345-2363, 1997.

Weller, R.; A. Minikin, G. König-Langlo, O. Schrems, A.E. Jones, E.W. Wolff, and P.S. Anderson. Investigating possible causes of the observed diurnal variability in Antarctic NOy. *Geophys. Res. Lett*., **26**, 601-604, 1999.

III.7. Evolution of crystal shapes and of the specific surface area of a snowfall determined by scanning electron microscopy and CH_4 adsorption

Les macrophotographies optiques couplées aux mesures de SS ont montré que la décroissance de la SS au cours du métamorphisme était associée à un arrondissement des cristaux et une sublimation des microstructures. Cependant, la résolution des images obtenues est limitée pour visualiser correctement les transformations morphologiques. De plus, l'estimation de la quantité de glace remobilisée au cours du métamorphisme, ne peut pas être faite précisément. Les images obtenues en MEB (**article 2, § III.3**.) ont un bon champ de profondeur et permettent ainsi une meilleure visualisation de la surface des cristaux de glace.

Nous avons eu donc recours à l'utilisation de la microscopie électronique à balayage pour étudier simultanément les changements morphologiques d'une couche de neige et l'évolution de sa SS. Les images obtenues ont permis notamment de mettre en évidence la remobilisation de la vapeur d'eau résultant de la métamorphose de la neige.

Evolution of crystal shapes and of the specific surface area of a snowfall determined by scanning electron microscopy and CH_4 adsorption

Axel Cabanes[1] , Loïc Legagneux[1], Florent Dominé[1], W.F. Kuhs[2], T Heinrichs[3], K. Techmer[2]

[1] CNRS, Laboratoire de Glaciologie et Géophysique de l'Environnement, B.P. 96, 54 Rue Molière, 38402 Saint Martin d'Hères, cedex, France.

[2] GZG, Abt. Kristallographie, Universität Göttingen, Goldschmidtsts.1, 37077 Göttingen, Germany
[3] IGDL Universität Göttingen, Goldschmidtsts.3, 37077 Göttingen, Germany

Corresponding author: Florent Dominé, phone: (33) 476 82 42 69; e-mail : florent@glaciog.ujf-grenoble.fr

ABSTRACT

Understanding the impact of the snowpack on atmospheric chemistry requires the detailed knowledge of snow microphysics and their changes during metamorphism. The specific surface area (SSA) of snow, i.e. the surface area accesible to gases per unit mass, expressed in cm^2/g, is needed to quantify all surface processes, and its evolution has been measured in a fresh snow fall. Scanning electron microscopy and optical pictures were also taken to observe morphological changes associated with SSA decrease. The 24 cm-thick snow fall studied was subjected to intense thermal cycling that led to surface hoar formation and to melting of the first few cm, while crystal rounding and sintering, as well as the growth of flat crystal faces, were observed in the bottom part of the layer. This metamorphism led to SSA decreases in 6 days from 666 to 118 cm^2/g in the top part, and from 627 to 257 cm^2/g in the bottom part of the layer. The potential impact of SSA reduction, melting, and ice remobilization on atmospheric chemistry are discussed, as well as the role of temperature on the rate of SSA decrease.

Draft, 21 December 2001

To be submitted to Journal of Glaciology

1. Introduction

Snow can cover up to 50 % of land masses in the Northern hemisphere in winter (Robinson et al., 1993) and its potential for interaction with the atmosphere has been demonstrated by studies in polar regions. Spring-time ozone depletion in the Arctic troposphere (Barrie et al., 1988) is one of the most studied aspects. Recently, production of nitrogen oxides in the snowpack and their release to the atmosphere have been observed in Greenland and Antarctica (Dibb et al., 1998; Honrath et al. 1999; Weller et al., 1999). Similarly, exchanges of aldehydes between the snowpack and the troposphere have been observed in the Arctic and at mid-latitudes (Hutterli et al., 1999; Sumner and Shepson, 1999; Couch et al., 2000). The atmospheric mixing ratios of these species is higher than predicted by models (Sander et al., 1997; Michalowski et al., 2000), showing that snow chemistry and snow-air interactions have to be taken into account to describe adequately atmospheric chemistry over snow-covered regions.

Exchanges of trace gases between the snowpack and the atmosphere can proceed by different processes that include heterogeneous reactions on the snow surface, adsorption/desorption of gases, sublimation of snow and its solutes and co-condensation of water vapor and other gases (Dominé et al., in press). Quantifying these processes requires the knowledge of physical parameters, among which the specific surface area (SSA) of snow and the amount of ice remobilized during metamorphism. Snow SSA must be known to quantify all surface processes. It represents the surface area accessible to gases per mass unit (Hanot et Dominé, 1999; Dominé et al., 2001) and we express it in cm^2/g rather than m^2/g because of the low values found for snow (Legagneux et al., in press). Snow SSA decreases during metamorphism (Hanot and Dominé, 1999; Cabanes et al., in press) and this can lead to the release of adsorbed gases, and to the decrease of the rate of heterogeneous reactions. Understanding the mechanisms responsible for the observed rates of SSA decrease requires detailed morphological analyses of snow crystals for subsequent predictive modeling. Morphological studies are also necessary to quantify ice remobilization by metamorphism and exchanges of solutes with the atmosphere.

Optical photomacrographs and SSA measurements of Arctic snow layers have been reported by Cabanes et al. (in press). These showed that SSA decrease during metamorphism were associated with rounding of sharp edges and sublimation of small structures. However, magnification and depth of field of pictures taken were not sufficient to visualize all the subtle morphological changes involved. Moreover, quantifying ice remobilization could not be done accurately.

In this paper, we report the simultaneous use of electron microscopy and of SSA measurements to correlate SSA decrease to changes in crystal shapes. Optical photomacrographs were also obtained for samples for which electron microscopy was not used. Electron microscopy allows large magnifications and images have a good depth of field (Wergin et al., 1995 and 1998; Dominé et al., 2001). Furthermore, because ice is not transparent to the electron beam, images obtained allow a good visualization of crystal surfaces, and also allow a better quantification of ice remobilization.

2. Sampling and experimental methods

2.1. Sampling

Snow samples were collected in the French Alps in February 2001 at Col du Lautaret (45°02'N, 6°24'E), 55 km East of Grenoble. The sampling site was located in a small south-facing sheltered basin at an elevation of 2058 m. This elevated site was used despite the absence of nearby meteorological station, because during winter 2000-2001, there was no snow at the lower elevations where stations are located.

The sampling method was similar to that described by Hanot and Dominé (1999) and Dominé et al. (in press): vertical faces were dug to observe the stratigraphy of the snowpack and to locate the different snow layers to sample. Snow and air temperatures were measured at different heights with an alcohol thermometer. Density was measured at different depths using a 500 ml Plexiglas sampler. For each snow sample, about 150 cm^3 were collected in two glass vials which were immediately immersed in liquid nitrogen ($N_{2(liq)}$) to stop metamorphism. Snow was kept in $N_{2(liq)}$ until being transferred to the SSA measurement volume or into the electron microscope, or used for photomacrographs.

2.2. Measurements of the specific surface area of snow

SSA was measured by CH_4 adsorption at liquid nitrogen temperature (77.15 K), as described by Hanot and Dominé (1999), and recently detailed by Legagneux et al. (in press). The principle is to determine the number of CH_4 molecules that can be adsorbed on the snow surface. This in fact requires the measurement of the adsorption isotherm of CH_4 on the snow sample, which is interpreted with a BET method (Brunauer et al., 1938) to obtain the SSA of the snow sample as well as the net heat of adsorption of CH_4 on ice, ΔQ_{CH4}. This latter parameter can be used to test the reliability of SSA measurements, as a value of 2240 $\pm$ 200 J/mol has been recommended (Legagneux et al., in press). The reproducibility of the method and its accuracy, taking into account systematic errors due to the BET treatment, were estimated at 6 and 12 %, respectively (Legagneux et al., in press).

2.3. Observation of snow crystals morphology

Observations of snow crystals were made with a field-emission scanning electron microscope (FE-SEM). The size of a SEM sample holder was about 15 mm^2, so only a few mg of snow were used. The vial containing the snow sample was filled with $N_{2(liq)}$ and the snow was transferred onto the sample holder in the $N_{2(liq)}$. The sample holder was then rapidly inserted into a mobile transfer chamber, so that the snow was in contact with the atmosphere for only a fraction of a second. The mobile transfer chamber was then connected to the SEM transfer chamber, that was $N_{2(liq)}$-cooled and had windows that allowed the inspection of the sample prior to its introduction in the main chamber of the SEM, where the sample holder was in thermal contact with a $N_{2(liq)}$-cooled stage. The FE-SEM was operated at an acceleration voltage of 1 to 1.5 kV. Metal-coating the snow surfaces was therefore not necessary and was never done, even though occasional charging was observed.

Magnifications greater than 25000 were obtained, with a resolution better than 0.1 µm. 60 to 100 pictures were taken for each sample.

Optical photomacrographs of all snow samples were taken in a cold room at –15°C, using a reflex camera with bellows, allowing a maximum magnification of 7.

3. Snowpack stratigraphy

Snow fallen in the early morning of 9 February 2001 was sampled three times at Col de Lautaret on 9, 13 and 15 February. Meteorological conditions during sampling and the stratigraphy of the snowpack are summed up in Table 1 and Figure 1.

Table 1 : Snow sampling conditions and SSA of different snow layers.

Date time (GMT)	Weather conditions	T air (°C)	Sub layer	Depth (cm)	T snow (°C)	Density	SSA (cm²/g)
9-Feb 11:00	Cloudy Light west wind	-2.0	A_1	0	-2.5	/	690
			A_2	2	-2.5	0.10	666
			A_3	20	-2.0	0.20	627
			B_1	27	-2.0	/	240
			E	90	-0.5	0.33	100
			H	120	0.0		116
13-Fev 11:00	Sunny No wind	+1.2	A_4	0	0.0	/	316
			A_5	2	0	/	134
			A_6	8	-1.5	0.19	329
			B_2	20	-3.5	0.30	225
			G	75	-1.0		106
15-fev 11:00	Sunny Light east wind	+1.0	A_7	1	0.0	0.12	473
			A_8	3	0.0	/	118
			A_9	8	-0.5	0.20	257
			B_3	20	-2.7	0.30	207

On 9 February, the snowpack had a total thickness of 135 cm. Fresh dry snow with a significant proportion of small stellar crystals formed a 24 cm-thick layer (hereafter: layer A) on the surface. Its density increased with depth from 0.10 to 0.20. Sample A_1 was taken on the very surface, sample A_2 was taken 2 cm below the surface, and sample A_3 was taken in the bottom half of the layer. This fresh snow overlaid a 16 cm-thick wet snow layer “B” fallen on 8 February under temperatures near 0°C. Underneath, older snow sub-layers referred as “C” to “H” in Figure 1 were observed.

On 13 February, the fresh snow layer “A” had shrunk down to 13 cm in thickness. On its surface, 1 cm of surface hoar had formed, from which sample A_4 was taken. The top of layer A had been subjected to partial melting, and a 2 cm-thick melt-freeze sub-layer had formed, that consisted of nearly spherical rounded grains about 0.5 mm in size, from which sample A_5 was taken. A visual examination with a magnifying glass indicated that the bottom of the layer was unaffected by melting and was made up of small rounded grains and of recognizable particles, from which sample A_6 was

taken. The wet snow layer “B” had also slightly shrunk down to 13 cm while no modification was observed for lower layers.

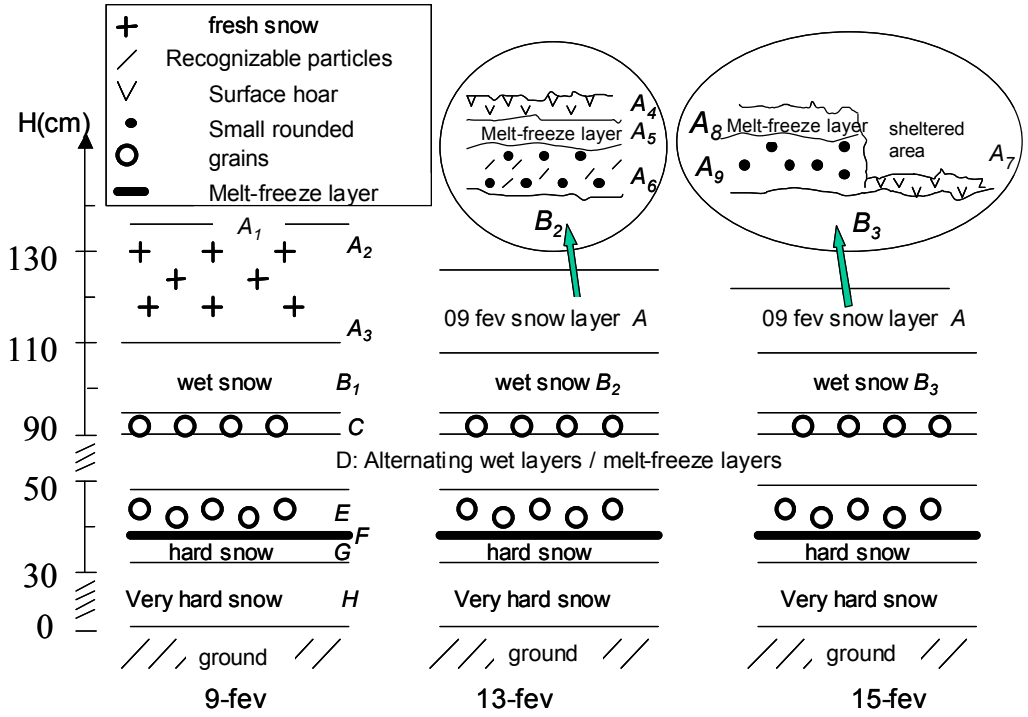

Figure 1: Stratigraphy of the snowpack observed at col du Lautaret in February 2001. Surface hoar on 15 February (A_7) was only observed in wind-sheltered areas.

On 15 February, surface hoar had been wind-blown from the top of the snowpack, and had accumulated in hollows. It was sampled in a shallow pit that we had dug on 13 February, and where only layer A had been removed. There, it formed a soft 2 cm-thick layer consisting of recognizable surface hoar crystals (Fig.1). from which sample A_7 was taken. Around the pit, the top of the snowpack consisted of a melt-freeze sub-layer as observed under the surface hoar on 13 February. Sample A_8 was taken from this melt-freeze layer. Underneath, the rest of layer A had visibly metamorphosed to rounded crystals mixed with faceted grains, where sample A_9 was taken. No morphological change was visible for lower layers.

4. SSA evolution of the snow and associated structural changes

This work focuses on layer A fallen on 9 February, because more important morphological changes were observed there. Data regarding other layers were nevertheless obtained, and are summed up in Table 1 because they are of some use to interpret metamorphism observed in layer A.

4.1 Variation of SSA and morphology with depth

Table 1 shows that on 9 February, the SSA of layer A decreased with depth from 690 cm^2/g for sample A_1 to 627 cm^2/g for sample A_3. It was difficult to detect clear changes in morphology between these 3 samples from optical photomacrographs. As shown on Figure 2a, only stellar and dendritic crystals, with a maximum size of about 2 mm and with slightly rounded arms, can be clearly identified

on optical pictures. Smaller crystals are obviously present, but their shapes cannot be clearly distinguished. FE-SEM was used, and SEM pictures of crystals from samples A_1, A_2 and A_3 are shown in Figures 3, 4, and 5, respectively.

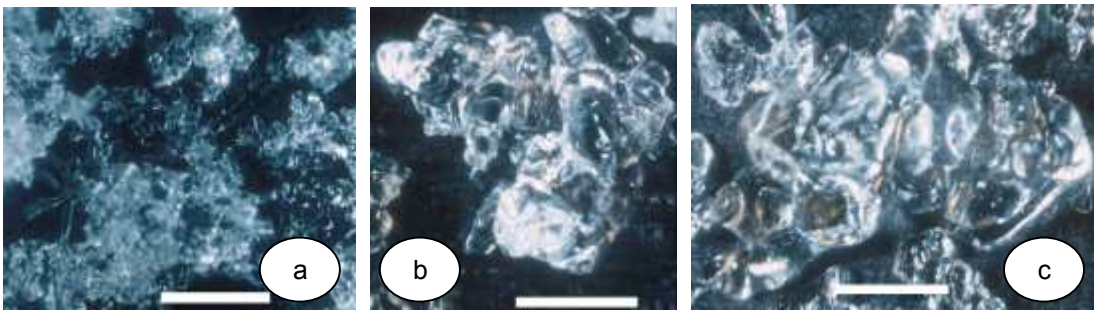

Figure 2: Optical photomacrographs showing the structural evolution with time of the top of the layer A. (a) Sample A_2 collected on 9 February. (b) Sample A_5 collected on 13 February. (c) Sample A_8 collected on 15 February. Scale bars : 1 mm.

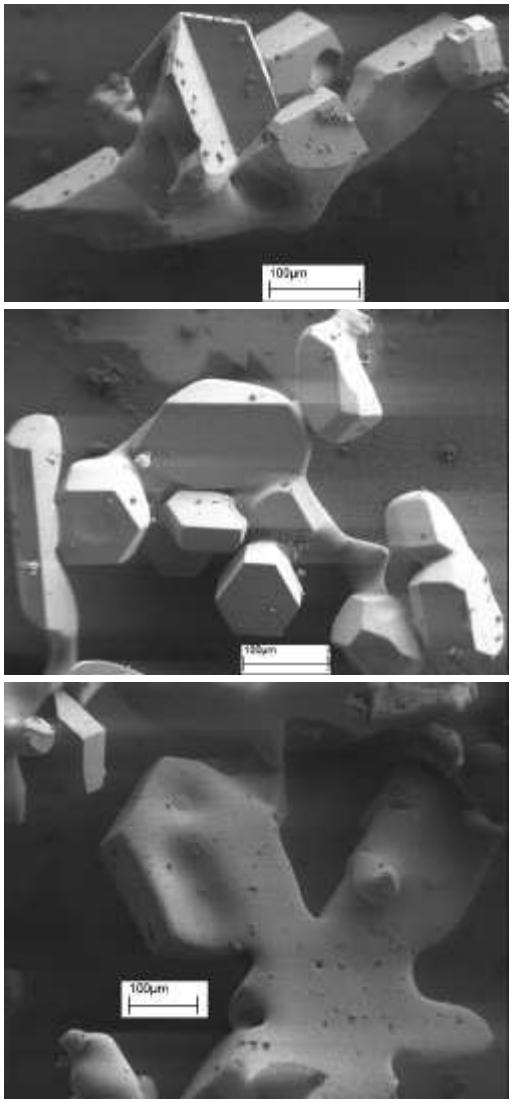

Figure 3: Scanning electron microscopy (SEM) images of snow sample A_1 collected on the very surface of the snowpack on 9 February.

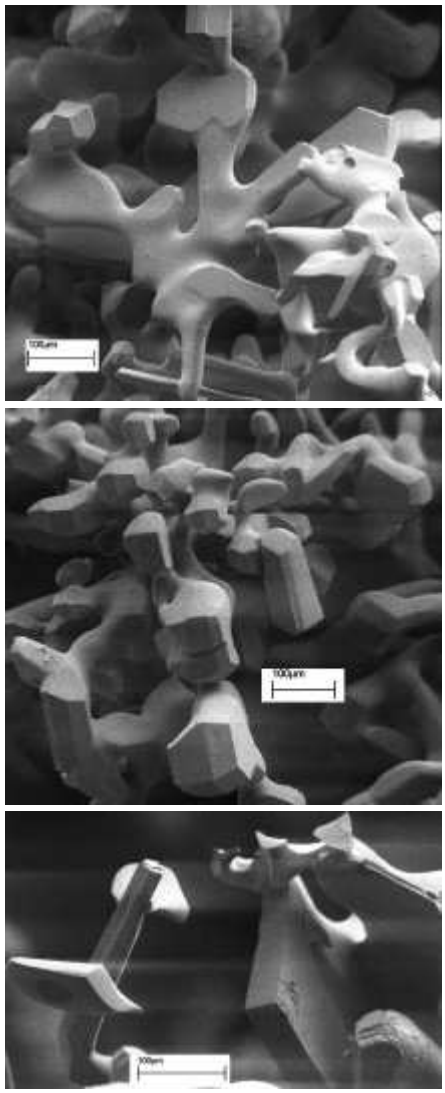

Figure 4: SEM pictures of sample A_2 collected at a depth of 2 cm on 9 February.

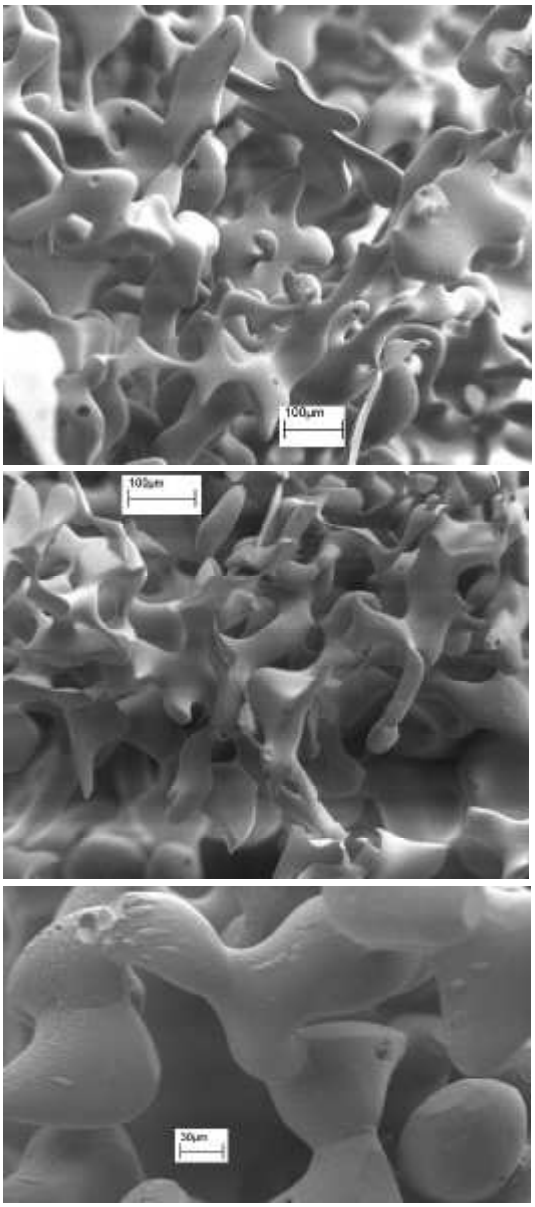

Figure 5: SEM pictures of sample A_3 collected at the bottom of layer A on 9 February.

Figures 3 and 4 show that samples A_1 and A_2 contained numerous plates and short columns, 0.1 to 0.5 mm in size, as well as stellar crystals that seemed more numerous in sample A_2. Irregular shapes were more common that perfect symmetrical forms although basic hexagonal shapes were often clearly visible. Moreover, slight rounding of crystal edges is obvious in sample A_2 (Fig. 4) whereas most crystals from sample A_1 have sharp edges (Fig. 3).

Figure 5 shows that sample A_3 contains more stellar crystals than samples A_1 and A_2, and that all crystals are more rounded. Overall shapes have also been altered, and sintering has started to take place, leading to the formation of a tortuous 3-D network, where stellar arms remain visible. From these observations, it appears that layer A was not homogeneous over its whole thickness.

4.2 Time-evolution of the SSA of layer A

On 13 February, partial melting of the top of layer A and formation of surface hoar prevented the monitoring of the SSA of snow similar to samples A_1 and A_2. The very surface and subsurface layers distinguished on 9 February were considered as merged on 13 February, and represented by sample A_5. We now characterize the evolution of the top of layer A by the sample sequence A_2, A_5 and A_8, while the evolution of the bottom of layer A will be characterized by the sequence A_3, A_6 and A_9. Figure 6 shows the SSA evolution of both sequences. Surface hoar formed by the deposition of water vapor onto the snow surface during night-time radiative cooling of course cannot be included in a time series of the evolution of layer A.

Figure 6 shows that the SSA of both sequences decreased with time, but the decrease is faster for the upper sequence. The melt-freeze episode caused a factor of 5 drop in SSA of the upper sequence, from 666 to 134 cm^2/g on 13 February which stabilized to 118 cm^2/g on 15 February. The bottom sequence had a slower and more regular SSA decrease to 329 cm^2/g on 13 February, then to 257 cm^2/g on 15 February.

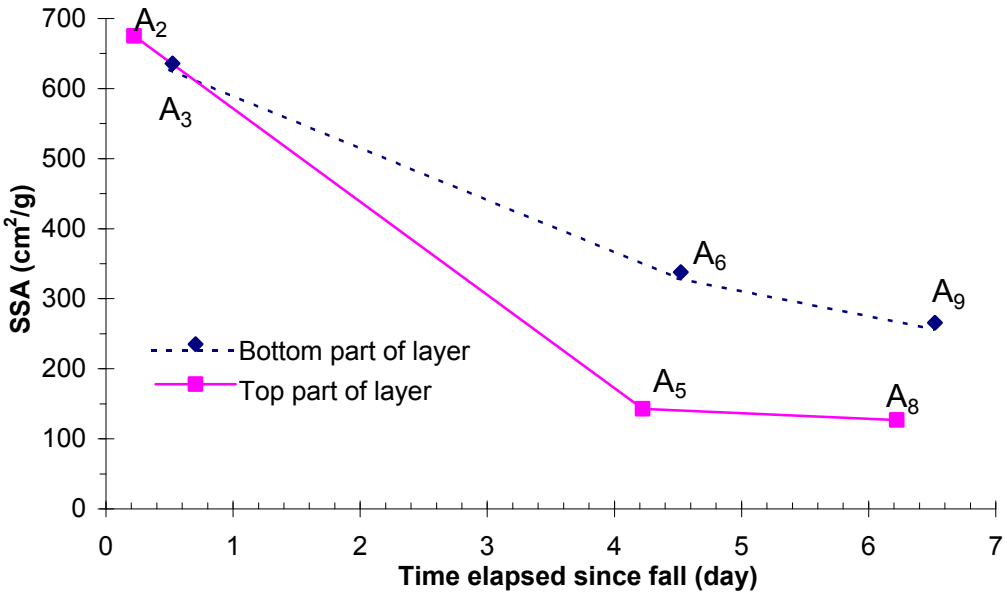

Figure 6: Time-evolution of the SSA of the top part (sequence A_2, A_5, A_8) and bottom part (sequence A_3, A_6, A_9) of layer A.

Unfortunately, no SEM pictures could be obtained for the melt-freeze layer. Optical photomacrographs were nevertheless obtained and are shown in Figures 2b and 2c. They show clusters of rounded grains about 0.5 mm in size, where individual grains can still be distinguished, as typical of wet snow with a low to moderate liquid water content (Colbeck, 1986). No clear morphological changes can be observed between samples A_5 and A_8 collected on 13 and 15 February.

Figures 7 and 8 show SEM pictures of snow crystals taken from samples A_6 and A_9, respectively (bottom sequence). Observations of numerous pictures show that many changes had occurred since 9 February, even though no indication of melting is observed in this deeper sub layer. A comparison between Figures 5 and 7 show that in 4 days, crystal size has increased and grain boundaries are more abundant and thicker. While large rounded shapes are widespread on 13 February (Fig. 7a), flat crystal faces, than may be newly formed, are also present (Fig. 7c). On 15 February (Fig. 8), flat crystal faces are now abundant and some of them have dimensions of several hundred microns, indicating clearly that they are neoformed. Grain boundaries with large cross sections are also present (Fig. 8a). A summary of the evolution of the lower part of the snowfall is that average grain size became larger, grain boundaries increased in cross section, the number of crystals decreased, flat crystalline faces up to 0.7 mm in size, with hexagonal symmetry and rounded edges, appeared in large numbers.

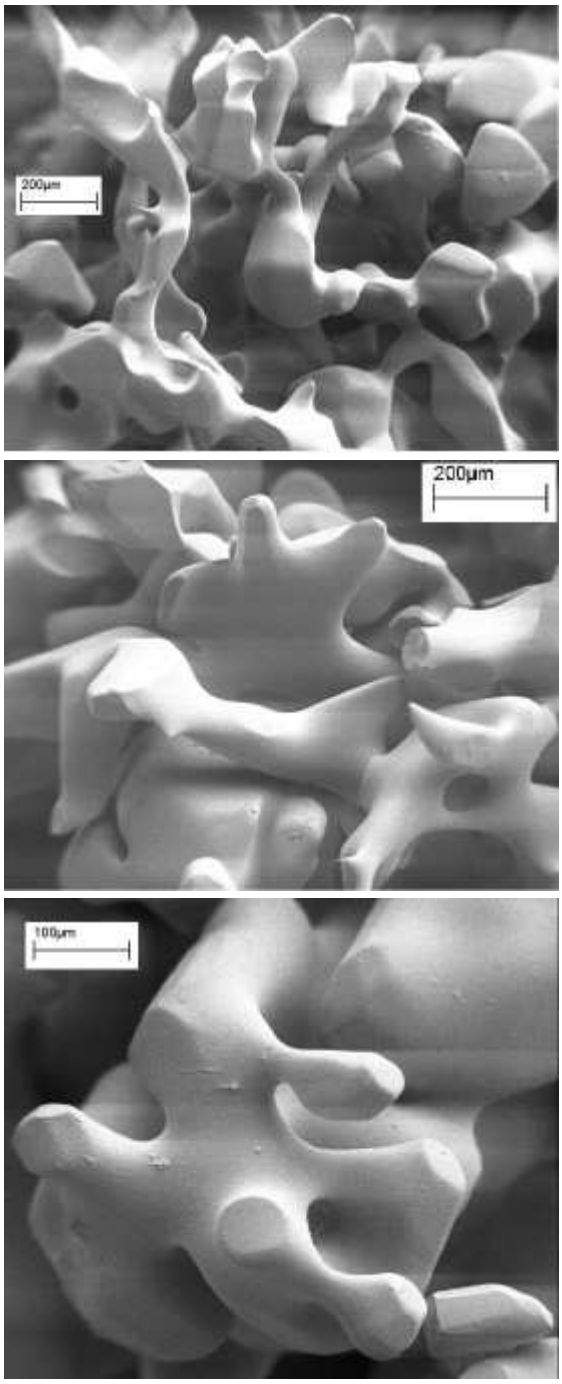

Figure 7: SEM pictures of sample A_6 collected at the bottom of layer A on 13 February.

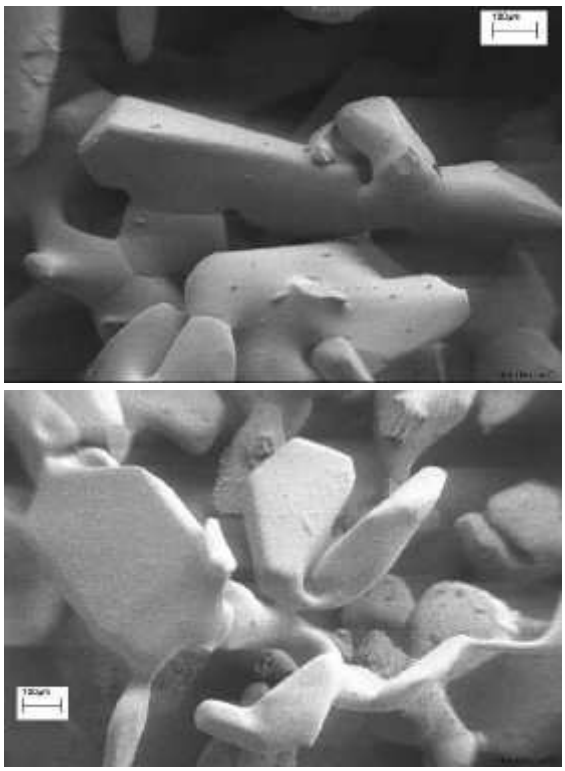

Figure 8: SEM pictures of sample A_9 collected at the bottom of layer A on 15 February.

5. Discussion

5.1. Low SSA variation with depth on 9 February

On 9 February, a low SSA decrease (10%), that is significant according to our experimental reproducibility (6%), was measured from the very surface to the bottom of layer A. This decrease can be due to 2 factors: (i) variation of the microphysics of precipitating snow over the course of the snow fall, or (ii) a decrease in SSA of the bottom part of the layer, caused by metamorphism following deposition. Considering that we observed slightly different snow microphysics between the top and the bottom of the layer, factor (i) cannot be ruled out. However, crystal rounding visible in Figure 3 clearly shows that metamorphism had already had an effect on the bottom part of layer A on 9 February. Rounded crystals are the equilibrium form of snow crystals (Colbeck, 1983a), and this evolution is driven by the minimization of surface free energy. Rounding then leads to a decrease in SSA, as already described by Cabanes et al. (in press) for Arctic snow falls. In that earlier work, rounding was much slower because of the low temperatures involved (-35 to –40°C). Here, the high temperature (-2°C) during precipitation leads to rounding after only a few hours, because of the higher water vapor pressure that impose larger fluxes, at equal temperature gradients.

These data show that snow metamorphism at warm temperatures have the potential to affect atmospheric composition a few hours after precipitation. The SSA decrease leads to the release of adsorbed gases (Hanot and Dominé, 1999; Dominé et al., in press) and water vapor remobilization can lead to the release or uptake of dissolved trace gases (Dominé and Thibert, 1996) that can be exchanged with the atmosphere. Figures 3 to 5 indicate that FE-SEM images can potentially be used to quantify the amount of water vapor remobilized, and can therefore be useful in elaborating improved models of air-snow interactions. They also show that SSA variations as low as 10% can translates into significant morphological changes.

5.2. Time-evolution of the SSA of layer A

Between 9 and 15 February, layer A was subjected to intense thermal cycling. Even though we do not have detailed meteorological data, daily trips to the surrounding mountains by laboratory personnel show that days were sunny, leading to surface warming and melting, while nights were clear, leading to intense radiative cooling that caused refreezing of surface snow and deposition of surface hoar. Thus, the upper and lower parts of layer A evolved differently, and both sequences studied will be discussed separately.

5.2.1 Evolution of the upper sequence

Optical pictures from Figure 2 show that the rapid SSA decrease of the upper sequence is associated with dramatic morphological changes. Figures 2b and 2c show unambiguously that daily solar heating led to the formation of liquid water (Colbeck, 1986) that refroze the following night. Latent heat exchanges then contributed to important metamorphic changes (Brun, 1989) whose result is that no initial shapes present on 9 February can be recognized on 13 February. These major morphological changes are associated to a very rapid SSA decrease: 80% of the initial SSA is lost in just 4 days.

Such changes can lead to exchanges of gases with the atmosphere. As mentioned above, adsorbed gases will be released, and in this case, the formation of liquid water can lead to the sequestration of soluble gases that will therefore be removed from the atmosphere. If refreezing is rapid, kinetic factors may prevent these dissolved gases to be released back to the atmosphere (Iribarne and Pyshnov, 1990).

5.2.2 Evolution of the lower sequence

Figures 5, 7 and 8 show that the evolution of the deeper sequence was characterized by both crystal rounding and by the growth of new flat crystallographic faces. Overall, the largest dimension of crystals increased by a factor of 3 or more, while SSA decreased by 59%, from 627 to 257 cm^2/g.

Rounding can be caused by sublimation (Nelson, 1998) or slow growth (Marbouty, 1980, Colbeck, 1983b) whereas flat faces are the kinetic growth form (Colbeck, 1983b) and are produced by rapid crystal growth (Marbouty, 1980). Intense thermal cycling doubtless produced very large temperature gradients near the surface of the snowpack (see e.g. Hanot and Dominé, 1999). At night, this resulted in the condensation of atmospheric water vapor on the snow surface, and to upward fluxes of water vapor from the warmer, lower layers. Our observations indicate that at the base of layer A, the temperature gradient was near the threshold for the growth of facetted crystals, 20°C/m (Marbouty, 1980).

The rounded edges suggest that the thermal gradient may not have quite reached this threshold. Alternatively, rounding may also have been caused by the warm day-time temperatures, that did produce morphological changes, as indicated by the rapid sintering and growth of grain boundaries.

The large increase in crystal size resulting from rapid growth led to a significant water vapor remobilization. An examination of the numerous SEM pictures taken in this lower sequence indicate that at least 80% of the water vapor was remobilized, and exchanges of trace gases with the atmosphere may then have been extensive. Our SSA measurements also indicate that about 60% of adsorbed gases could have been released.

6. Summary and conclusion

We have reported SSA measurements and shown FE-SEM pictures of a snow layer where the top and the bottom parts underwent two very different metamorphic conditions, caused by intense thermal cycling during warm days and cold nights. The top layer was subjected to melting and refreezing. Its SSA decreased by about 80% in just 4 days, while crystals transformed into large rounded clusters several mm in size. The bottom layer was subjected to crystal rounding and to crystal growth, that produced large flat crystal faces several hundred microns long. Its SSA decreased only by about 60 % in 6 days.

These results confirm an intuitive guess that wet metamorphism leads to a much faster SSA decrease than dry metamorphism. These different metamorphic scenarios can be speculated to have quite different impacts on atmospheric composition. SSA decrease leads to the release of adsorbed gases, and this process will be more important in the case of wet metamorphism. The presence of

liquid water can lead to the uptake of soluble gases, that may not be released entirely during refreezing, because of kinetic factors (Iribarne and Pyshnov, 1990). Dry metamorphism under moderate to large temperature gradients, as experienced by the bottom part of the layer, led to the remobilization of over 80% of the snow crystals mass, and to the potential release of trace gases sequestered in the ice lattice. Coupled chemical and microphysical studies are necessary to quantify these processes.

The warm temperatures involved in this dry metamorphism episode led to a fairly rapid SSA decrease (59% in 6 days). This is to be compared to the SSA decrease of a subsurface layer in the arctic during winter (Cabanes et al., in press) that evolved at temperatures between –35 and –40°C, and whose SSA decreased by only 43% in 16 days. This clearly illustrates the crucial role of temperature in the rate of SSA decrease, but more snow layers evolving over a wide variety of temperatures must be studied for a better quantification of this role.

Acknowledgements

This work was funded by CNRS through PNCA and GDR RS-Glace programs.

References

Barrie, L.A., Bottenheim, J.W., Schnell, R.C., Crutzen, P.J. and Rasmussen, R.A., 1988. Ozone destruction and photochemical reactions at polar sunrise in the lower Arctic atmosphere. *Nature*, 334, 138-141.

Brun, E. 1989. Investigation on wet-snow metamorphism in respect of liquid-water content. *Ann. of Glaciol.*, 13, 22-26,.

Brunauer, S., Emmet, P.H., and Teller, E. 1938. Adsorption of gases in multimolecular layers. *J. Am. Chem. Soc.,* 60, 309-319.

Cabanes, A., L. Legagneux, and F. Dominé. 2002. Evolution of the specific surface area and of crystal morphology of Arctic fresh snow during the ALERT 2000 campaign, *Atm. Environ.*, in press.

Colbeck, S.C., 1983a. Ice crystal morphology and growth rates at low supersaturations and high temperatures. *J. Appl. Phys.,* 54, 2677 –2682.

Colbeck, S.C., 1983b. Theory of metamorphism of dry snow, *J. Geophys. Res.* 88, 5475-5482.

Colbeck, S.C. 1986. Classification of seasonal snow cover crystals, *Water Ressources Res.* 22, 59S-70S.

Couch, T.L.; A.-L. Sumner, T.M. Dassau, P.B. Shepson, and R.E. Honrath. 2000. An Investigation of the Interaction of Carbonyl Compounds with the Snowpack, *Geophys. Res. Lett.*, 27, 2241-2244.

Dibb, J.E. Talbot, D. Munger, D. Jacob, and S.-M. Fan. 1998. Air-snow exchange of HNO_3 and NOy at Summit, Greenland. *J. Geophys. Res*, 103, 3475-3486.

Dominé, F. and Thibert, E. 1996. Mechanism of incorporation of trace gases in ice grown from the gas phase. *Geophys. Res. Lett.*, 23, 3627-3630.

Dominé, F., Cabanes, A., Taillandier A.-S. and Legagneux., L. 2001. Specific surface area of snow samples determined by CH_4 adsorption at 77 K, and estimated by optical microscopy and scanning electron microscopy. *Environ. Sci. Technol. 35*, 771-780.

Dominé, F., A Cabanes., and L. Legagneux. 2002. Structure, microphysics, and surface area of the Arctic snowpack near Alert during the ALERT 2000 campaign, *Atm. Environ*., in press.

Hanot, L., and F. Dominé. 1999. Evolution of the surface area of a snow layer. *Environ. Sci. Technol*., 33, 4250-4255.

Honrath, R.E., M.C. Peterson, S. Guo, J.E. Dibb, P.B. Shepson, and B. Campbell. 1999. Evidence of NO_x production within or upon ice particles in the Greenland snowpack. *Geophys. Res. Lett*., 26, 695-698.

Hutterli, M.A., R. Rothlisberger, and R. C. Bales. 1999. Atmosphere-to-snow-to-firn transfer studies of HCHO at Summit. Greenland. *Geophys. Res. Lett*., 26, 1691-1694.

Iribarne, J.V. and Pyshnov, T. 1990. The effect of freezing on the composition of supercooled droplets. I - Retention of HCl, HNO_3, NH_3 and H_2O_2, *Atmos. Environ*. 24A, 383-390.

Legagneux, L., A. Cabanes, and F. Dominé. Measurement of the specific surface area of 176 snow samples using CH_4 adsorption at 77 K, *J. Geophys. Res*., in press.

Marbouty, D. 1980. An experimental study of temperature gradient metamorphism. *J. Glaciol*., 26, 303-312,

Michalowski, B.A., J.S. Francisco, S.-M. Li, L.A. Barrie, J. W. Bottenheim, and P.B. Shepson. 2000. A computer model study of multiphase chemistry in the arctic boundary layer during polar sunrise*. J. Geophys. Res.*, 105, 15131-15145.

Nelson, J. 1998. Sublimation of ice crystals, *J. Atmos. Sciences,* 55, 910-919.

Robinson, D. A., K. F. Dewey, and R. R. Heim, Jr. 1993. Global snow cover monitoring: an update. *Bull. Amer. Meteor. Soc*. 74, 1689-1696.

Sander, R., R. Vogt, G.W. Harris, and P.J. Crutzen. 1997. Modeling the chemistry of ozone, halogen compounds, and hydrocarbons in the Arctic troposphere. Tellus, 49B, 522-532.

Sumner, A.L. and P.B. Shepson. 1999. Snowpack production of formaldehyde and its effect on the Arctic troposphere. *Nature*, 398, 230-233.

Weller, R.; A. Minikin, G. König-Langlo, O. Schrems, A.E. Jones, E.W. Wolff, and P.S. Anderson. 1999. Investigating possible causes of the observed diurnal variability in Antarctic NOy. *Geophys. Res. Lett*., 26, 601-604.

Wergin, W. P., Rango A., and Erbe, E.F., 1995. Observations of Snow Crystals Using Low-Temperature Scanning Electron Microscopy, *Scanning*, 17, 41-49.

Wergin, W. P., Rango A., and Erbe, E.F. 1998. Image comparisons of snow and ice crystals photographed by light (video) microscopy and low temperature scanning electron microscopy, *Scanning*, 20, 285-296.

III.8. Applications atmosphériques. Impact de la neige sur la concentration atmosphérique en formaldéhyde. Etude des processus d'incorporation.

III.8.1. Introduction

Récemment, des mesures de terrain ont mis en évidence des émissions de formaldéhyde (HCHO) par le manteau neigeux dans l'Arctique (Hutterli et al., 1999 ; Sumner and Shepson, 1999) ainsi qu'aux moyennes latitudes (Couch et al., 2000). Ceci a permis d'expliquer au moins partiellement pourquoi les modèles de chimie atmosphérique (Sander et al.,1997 ; Michalowski et al., 2000) au-dessus des régions enneigées conduisent à des concentrations beaucoup plus basses que celles mesurées lors des campagnes de terrain (De Serves, 1994 ; Sumner et Shepson, 1999).

En région polaire, la photolyse du formaldéhyde produit indirectement deux radicaux OH et est une source importante de l'agent oxydant principal de l'atmosphère (Grannas et al., sous presse). Comprendre les processus qui déterminent la concentration de HCHO dans la troposphère, est donc nécessaire pour prédire le temps de vie de nombreuses espèces chimiques.

Un des objectifs de la campagne ALERT 2000 était donc de comprendre l'impact de la neige sur la concentration du HCHO dans la basse troposphère. Dans le manteau neigeux, la détermination des processus responsables de modifications chimiques nécessite la connaissance de paramètres physiques de la neige, dont sa surface spécifique. Nos mesures de SS ont donc été utilisées dans cet objectif.

L'étude du formaldéhyde a nécessité des mesures simultanées du formaldéhyde dans la neige et dans la phase gaz, et des mesures de la SS de la neige. Ce travail collaboratif a été mené par :

S. Perrier et S. Houdier pour les mesures de HCHO dans la neige ;

A.-L. Sumner et P. Shepson pour les mesures de HCHO dans la phase gaz ;

F. Dominé, L. Legagneux et moi-même pour l'étude du manteau neigeux et les mesures de SS de la neige.

Les résultats de cette étude ont fait l'objet d'un article récemment accepté dans le journal Atmospheric Environment (Perrier et al., sous presse).

III.8.2. Démarche adoptée

Le formaldéhyde présent ou produit dans le manteau neigeux et émis vers l'atmosphère peut être soit adsorbé à la surface des cristaux de neige, soit dissout dans le réseau cristallin de la glace. Modéliser les échanges neige-air de formaldéhyde nécessite de savoir si ce composé est adsorbé ou dissout. En effet, les processus de surface sont très rapides et leur constante de temps est généralement de l'ordre de quelques minutes comme l'ont montré les expériences faites par Hanson et Ravishankara (1992) sur l'adsorption/desorption de HCl sur la glace dans un tube à écoulement. Les processus de diffusion sont par contre beaucoup plus lents. La constante de diffusion D du formaldéhyde n'est pas connue. Si elle est voisine de celles de HNO_3 et HCl qui sont de l'ordre de 10^{-12} à 10^{-10} cm^2 s^{-1} aux températures qui nous intéressent (Thibert et Dominé, 1997 et 1998), et en supposant une distance de diffusion x de 30 µm, et D= 10^{-11} cm^2 s^{-1}, on obtient une constante de temps $t=x^2/D$ de l'ordre de 10 jours. Ainsi, si HCHO est localisé à la surface de la glace plutôt que dans son volume, les échanges entre le manteau neigeux et la phase gaz pourront être rapides, et donc susceptibles de modifier rapidement la composition de l'atmosphère.

L'objectif de ce travail était donc dans un premier temps de déterminer le partage du HCHO entre la phase gaz et la neige afin d'estimer le potentiel du manteau neigeux en tant que réservoir de formaldéhyde, puis de discuter nos résultats afin d'en extraire des informations sur le mécanisme d'incorporation du HCHO dans la neige, c'est à dire s'il est préférentiellement dissout dans le volume de la glace ou plutôt localisé en surface. Ces deux objectifs ont donc nécessité des mesures couplées de la surface spécifique de la neige et de sa concentration en HCHO.

III.8.3. Résultats

III.8.3.1. Concentration en formaldéhyde dans les différentes couches de neige

Afin d'estimer la quantité totale de formaldéhyde contenue dans le manteau neigeux, les concentrations moyennes des différentes couches de neige $[HCHO]_{neige}$ ont été déterminées. Elles sont reportées dans la Table 1 avec les épaisseurs et densité de neige des différentes couches. Les parts relatives (pour chaque couche) du HCHO total contenu dans le manteau neigeux ont pu ainsi être déterminées. La numérotation des couches reprend celle décrite dans l'article 3 (cf. § **III.4**.) où les symboles H et P ont été rajoutés pour distinguer les mesures faites en hiver et au printemps

Table 1: HCHO total contenu dans le manteau neigeux en hiver avant le 22 Février et au printemps avant le 25 Avril.

Numéro de couche	Couche	Epaisseur (cm)	Densité	$[HCHO]_{neige}$ ppbw	HCHO total (ng/cm^2)	Contribution %
Hiver						
4H	7 Février	1	0,08	12,5	1	2.58
3H	3 Février	1,5	0,15	8	1,8	4.64
2H	Dure	15	0,48	4,7	33,84	87.32
1H	Givre de profondeur	8	0,22	1,2	2,112	5.45
	Total	25.5			**38.8**	100

Numéro de couche	Couche	Epaisseur (cm)	Densité	$[HCHO]_{neige}$ ppbw	HCHO total (ng/cm^2)	Contribution %
Printemps						
7P	13-14 Avril	0,3	0,16	6,5	0,31	0.52
6P	Faiblement croûtée	1	0,16	7	1.12	1.86
5P	Légère	1,5	0,16	6,5	1,56	2.59
4P	Dure	10	0,4	6,2	24.8	41.24
3P	Non cohésive	5	0,3	6,2*	9,3	15.47
2P	Dure	12	0,48	3,5	20.16	33,53
1P	Givre de profondeur	8	0,2	1,8	2,88	4,79
	Total	37.8			**60.1**	100

*non mesurée: supposée identique à la couche 4P

III.8.3.2. Evolution des concentrations en formaldéhyde

L'ensemble des mesures de formaldéhyde dans la neige obtenues par Perrier et al. indique des concentrations similaires en hiver et au printemps pour les couches âgées, ce qui suggère que les échanges de HCHO entre ces couches et l'atmosphère ont été limités entre les deux campagnes.

Les différentes couches de surface ont par contre montré une évolution de $[HCHO]_{neige}$ après leur dépôt. Au printemps, les concentrations ont décru puis se sont stabilisées à un niveau proche des couches sous-jacentes (5P et 6P) qui s'étaient déposées plusieurs jours à quelques semaines avant le début de la campagne de printemps. En hiver, l'évolution a été différente : la couche de surface précipitée le 7 Février (4H) a montré une $[HCHO]_{neige}$ stable. Pour la couche précipitée le 3 Février (3H), la $[HCHO]_{neige}$ a décru avec des variations significatives puis s'est stabilisé.

III.8.3.3. Partage de HCHO entre la neige et l'atmosphère

La Table 1 indique que la quantité totale de formaldéhyde contenu dans le manteau neigeux en hiver et au printemps est de 38.8 et 60.1 ng/cm^2 (colonne de $1cm^2$ de section). Connaissant les épaisseurs d'échange et les concentrations moyennes dans l'atmosphère, il est possible de calculer le partage du formaldéhyde entre la neige et la phase gaz. En hiver, l'obscurité totale implique que le temps de vie de HCHO est de l'ordre de τ = 160 jours (De Serves, 1994), et les échanges se font sur toute la couche limite qui a été estimé à 300 m (Perrier et al., sous presse). Au printemps, le temps de vie de HCHO est réduit à environ τ = 6 heures. Avec une diffusivité verticale K_z= 95 cm^2/s (Gimbaud et al., sous presse), on peut déduire que le HCHO émis est détruit vers une hauteur $h=(K_z x \tau)^{1/2}$ =14 m. C'est cette hauteur d'échange que nous avons considérée. Les concentrations de HCHO supposées verticalement homogènes dans l'atmosphère ont été prises égales à 200 pptv en hiver et à 150 pptv au printemps (Perrier et al., sous presse, Grannas et al., sous presse). Nous avons ainsi calculé que 80.7% et 99.5% du formaldéhyde étaient contenu dans le manteau neigeux en hiver et au printemps, ce qui en fait un important réservoir. Cependant les couches de surfaces qui ont une épaisseur et une densité réduite n'en contiennent que 7 et 5%, respectivement.

III.8.4. Discussion

III.8.4.1. Equations régissant les mécanismes d'incorporation de HCHO dans la neige

HCHO dans la neige peut être incorporé soit (i) par adsorption à la surface des cristaux de neige, (ii) dissolution dans le volume de la glace, ou (iii) une combinaison des deux (Bales et Choi, 1996 ; Dominé et al., 1995 ; Dominé et Thibert, 1996 ; Thibert et Dominé, 1997, 1998). Les équations régissant les deux processus possibles doivent tout d'abord être rappelées avant d'être testées avec nos mesures.

a) Adsorption à la surface de la glace

Si HCHO est adsorbé à la surface de la glace, sa concentration $[HCHO]_{snow}$ est déterminée par la température T, sa pression partielle dans l'air P_{HCHO}, et la surface spécifique SS de la neige. Sa fraction molaire à l'équilibre dans la neige (X_{HCHO}) est donnée par l'équation (III.1):

$$X_{HCHO} = A \times SS \times (P_{HCHO})^{1/n} \exp\left(\frac{\Delta H_{ads}}{nRT}\right) \qquad \text{(III.1)}$$

où A est une constante, n le nombre d'entités créées par l'adsorption d'une molécule de HCHO à la surface de la glace (Thibert and Dominé, 1997), et ΔH_{ads} l'enthalpie d'adsorption de HCHO sur la glace.

b) Dissolution dans le volume des cristaux de glace

SI HCHO est dissout dans la glace en formant une solution solide, il peut être en équilibre thermodynamique avec l'atmosphère ou au contraire sa concentration peut être déterminée par des processus cinétiques.

Dans le cas de l'équilibre thermodynamique, la fraction molaire dépendant de T et de P_{HCHO} sera

$$X_{HCHO} = A' \times (P_{HCHO})^{1/n'} \exp\left(\frac{\Delta H_{sub}}{n'RT}\right) \qquad \text{(III.2)}$$

où A' est une constante, ΔH_{sub} l'enthalpie molaire partielle de sublimation de HCHO, et n' le nombre de défauts créés dans le réseau de la glace. Une variation de P_{HCHO} ou de T va conduire à un échange avec l'atmosphère par diffusion dans la glace.

Si la concentration est déterminée par des processus cinétiques, la fraction molaire X_{HCHO} au moment de l'incorporation sera déterminée par le nombre relatif de molécules de HCHO et H_2O qui heurtent et s'adsorbent à la surface de la glace (Dominé et al., 1995, Dominé and Thibert, 1996) selon l'équation III.3 :

$$X_{HCHO} = \frac{P_{HCHO}}{P_{H2O}} \frac{\alpha_{HCHO}}{\alpha_{H2O}} \sqrt{\frac{M_{H2O}}{M_{HCHO}}} \qquad \text{(III.3)}$$

où α and M sont les coefficients de collage et les masses molaires. Dans ce cas également, l'équilibre avec l'atmosphère se fera par diffusion solide

Comme nous l'avons vu précédemment, les processus de surface sont plus rapides que la diffusion en phase solide.

III.8.4.2 Test de détermination du(des) processus d'incorporation de HCHO dans la neige

SI HCHO est adsorbé à la surface de la neige, et en supposant une isotherme d'adsorption linéaire, l'équation (III.1) indique que l'on devrait observer une dépendance linéaire entre $Ln[X_{HCHO}/(SSA \times P_{HCHO})]$ et 1/T. Les différents couples de points obtenus sont représentés sur la figure III.1 où l'on peut voir qu'aucune corrélation n'existe pour n=1. Le même résultat a été obtenu pour n=2. Bien que des approximations aient été faites pour ce calcul, on peut conclure que l'adsorption n'est pas le mécanisme d'incorporation dominant du formaldéhyde dans la neige.

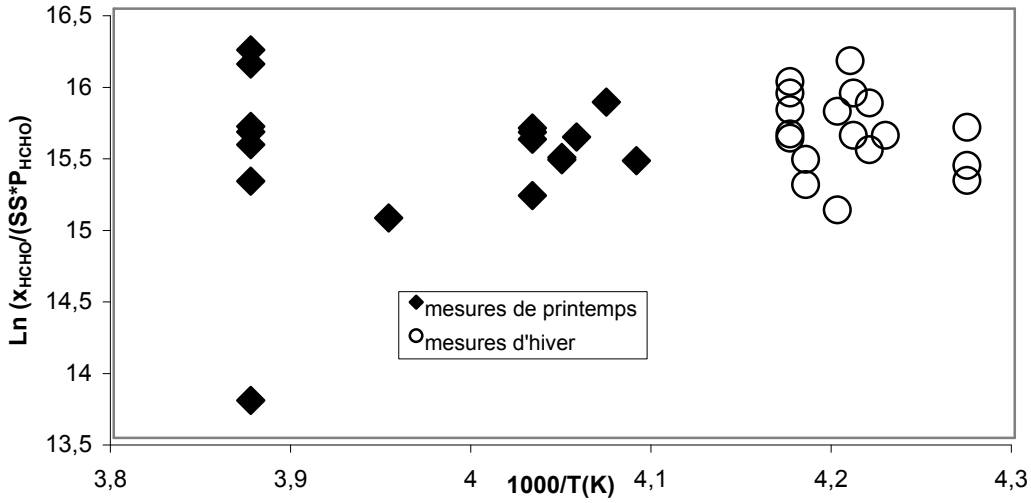

Figure III.1 : Diagramme d'Arrhenius testant l'hypothèse d'une incorporation de HCHO par adsorption à la surface des cristaux de glace, d'après l 'équation (III.1). On a utilisé n=1.

Un test similaire a été fait pour tester l'hypothèse d'une dissolution de HCHO dans le volume des cristaux de glace à l'équilibre thermodynamique (équation III.2). Les résultats obtenus sont reportés en figure III.2.

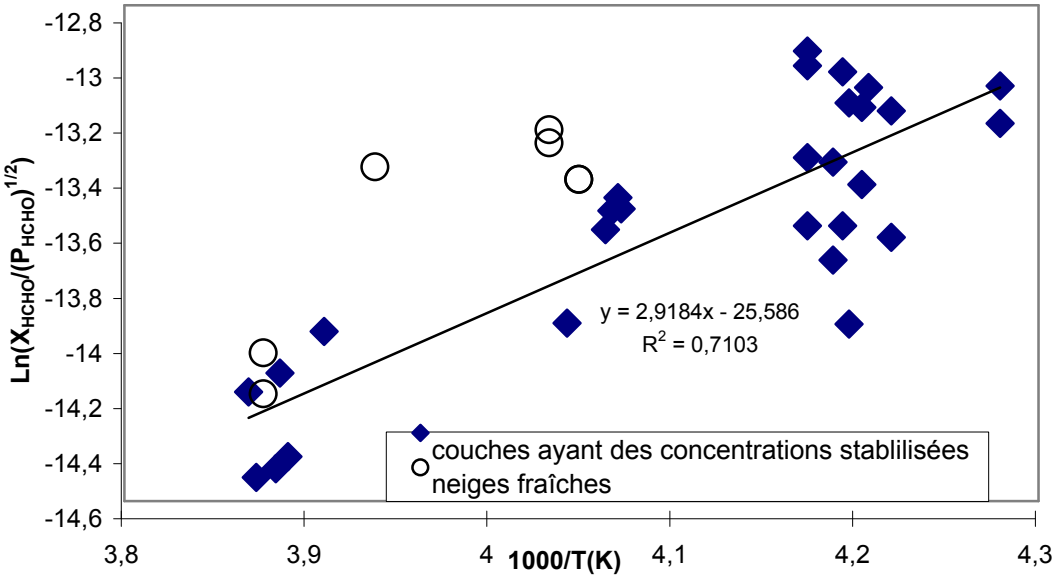

Figure III.2 : Diagramme d'Arrhenius testant l'hypothèse d'une solution solide à l'équilibre thermodynamique d'après l 'équation (III.2). Le calcul a été fait pour n'=2. La droite de corrélation n'incluse que les neige dont la concentration en formaldéhyde est stable dans le temps.

Comme le processus d'équilibre par diffusion solide est lent, seules les valeurs de concentration stabilisées ont été prises en compte. Une tendance est nettement visible, avec un coefficient de corrélation de 0.71 pour n'=2. Avec n'=1 le coefficient de corrélation obtenu est de 0.60.

Ces résultats indiquent que la diffusion en solution solide apparaît comme le processus dominant conduisant à une stabilisation de $[HCHO]_{neige}$. Bien que la valeur de n' ne soit pas connue, une comparaison de ΔH_{sub} (48.5 kJ mol^{-1} pour n'=2) avec l'enthalpie molaire partielle d'évaporation de HCHO (59.8 kJ mol^{-1}, Betterton et Hoffman, 1988) indique que l'incorporation de HCHO en solution solide en formant deux entités (n'=2) est raisonnable. Contrairement aux acides tels que HCl et HNO_3 (Thibert et Dominé, 1997 et 1998), HCHO ne se dissocie probablement pas dans la glace, et il apparaît probable que la dissolution d'une molécule de HCHO dans la glace s'accompagne de la formation d'un défaut.

Sur la figure III.2, les points obtenus pour les neiges fraîches sont tous au-dessus de la droite de régression ce qui suggère qu'elles étaient sursaturées par rapport à l'équilibre thermodynamique. L'hypothèse d'une solution solide avec des concentrations déterminées par les processus cinétiques a donc été testée pour les neiges fraîches et les résultats obtenus se sont révélés compatibles avec un tel processus (Perrier et al., sous presse).

L'ensemble de ces résultats permet de suggérer que HCHO dans la neige est probablement incorporé dans le volume de la glace plutôt qu'à la surface des cristaux de glace, et que sa concentration initiale est déterminée par des processus cinétiques.

III.8.3. Conclusion

Les mesures effectuées dans ce travail montrent que le manteau neigeux contient la majorité du HCHO présent dans le système (neige + couche d'échange) : 80.7 % en hiver et 99.5 % au printemps, ce qui en fait un important réservoir.

Nos mesures de surface spécifique couplées aux mesures de HCHO ont permis de montrer que HCHO n'est pas significativement localisé à la surface des cristaux de neige. Ceci ne rend pas pour autant nos mesures de surface spécifique inutiles, puisqu'elles ont permis d'écarter le processus de d'adsorption/desorption comme un possible mécanisme d'incorporation de HCHO. Ce résultat est d'autant plus important que jusqu'à maintenant, la désorption de HCHO était considérée comme l'un des processus probables pour expliquer le relargage de HCHO par le manteau neigeux (Hutterli et al., 1999). Ce résultat montre que la modélisation des échanges neige-air de formaldéhyde doit décrire la diffusion de ce gaz dans la phase glace. Il est donc nécessaire de mesurer au laboratoire le coefficient de diffusion du formaldéhyde dans la glace, ainsi que sa solubilité à l'équilibre thermodynamique en fonction de la température et de P_{HCHO}, afin d'apprécier l'écart à l'équilibre et la quantité qui pourra être ré-émise.

CONCLUSIONS ET PERSPECTIVES

L'objectif de notre travail était de fournir des données de surface spécifique (SS) de la neige qui servent dans la quantification de l'impact de la neige sur la chimie atmosphérique. La première étape a consisté à mettre au point une méthode expérimentale qui soit fiable et précise pour mesurer la SS de la neige, celle-ci étant généralement faible (< 0.15 m^2/g). Nous avons utilisé la méthode d'adsorption de méthane à la température de l'azote liquide (77 K). Bien que le principe de cette méthode soit simple, nous avons du mettre au point un protocole expérimental afin de réduire les possibles artéfacts et les sources d'erreurs susceptibles de fausser les résultats. La reproductibilité et l'erreur absolue de la méthode d'adsorption ont été estimées à 6 et 12 % respectivement. L'incertitude prend notamment en compte les approximations faites par le modèle BET utilisé pour calculer la SS des échantillons de neige. La chaleur nette d'adsorption ΔQ_{CH4}, déterminée à partir de la théorie BET, a été utilisée pour tester la fiabilité des mesures de SS. L'ensemble de nos résultats nous permet de proposer $\Delta Q_{CH4} = 2240 \pm 200$ J mol^{-1}.

Nous avons également tenté d'estimer la SS d'échantillons de neige en utilisant des méthodes d'analyses d'image de cristaux obtenues par microscopies optique et électronique à balayage (MEB). Bien que moins précises que la technique d'adsorption, ces méthodes permettent néanmoins d'obtenir une estimation raisonnable de la SS d'échantillons de neige. L'analyse d'image peut également servir de complément aux mesures d'adsorption car elles permettent de corréler l'évolution morphologique et la décroissance de la SS.

La mise au point de la méthode d'adsorption nous a permis d'étudier la SS de la neige dans les Alpes et L'Arctique, où nous avons réalisé la première étude détaillée de la microphysique du manteau neigeux. L'ensemble de nos données, soit 176 mesures de SS, nous ont montré que la SS de la neige présente une grande variabilité: elle est comprise entre 1540 et 400 cm^2/g pour les neiges fraîches et peut descendre jusqu'à 100 cm^2/g pour des vieilles neiges. Afin de permettre l'estimation rapide de la SS d'échantillon de neige à l'aide de quelques macrophotographies, nous avons proposé une classification des types de neige, en fonction de leur age et de la forme des cristaux. Ainsi, 14 catégories de neige ont été proposées, qui permettent de proposer une estimation de la SS dans une intervalle de confiance comprise entre 25 et 40 %, suivant le type de neige observé. Pour 13 de ces catégories, nous avons également observé une corrélation entre la SS de la neige et sa densité, celle-ci pouvant être utilisée afin d'améliorer encore la précision de l'estimation.

L'étude de l'évolution de la SS pour différentes couches de neige a montré que la SS décroît au cours du temps. Cette décroissance est due au métamorphisme de la neige qui entraîne une modification de la structure des cristaux. il s'agit essentiellement d'un arrondissement et d'un grossissement des cristaux, et de la sublimation des petites structures. La croissance de givre de surface, dont la SS est inférieure à celle de la neige fraîche, peut également contribuer à la décroissance de la SS d'une couche de neige de surface par effet de dilution.

L'étude de l'évolution de neiges fraîches dans une large gamme de température, nous a permis de proposer une paramétrisation de la vitesse de décroissance de la SS en fonction de la température. La température et le vent sont les deux principaux facteurs qui déterminent la cinétique de décroissance de la SS, car ils déterminent les flux de vapeur d'eau responsables du métamorphisme de la neige. En raison d'un manque de données, il n'a pas été possible de quantifier l'effet du vent. Cet effet semble complexe. En effet, le vent peut entraîner une augmentation de la SS en fractionnant les cristaux de neiges âgées à faible surface spécifique. A l'inverse, le vent peut considérablement accélérer la décroissance de neige fraîche à forte SS, en facilitant la sublimation de microstructures. D'autres travaux s'avèrent nécessaires pour paramétrer ces divers effets. L'apparition d'eau liquide peut aussi accélérer la décroissance de la SS, mais les résultats obtenus sont en nombre insuffisant pour proposer une paramétrisation.

A Alert, l'étude détaillée de la microphysique du manteau neigeux a permis de mesurer directement la capacité d'adsorption de gaz traces réactifs par le manteau neigeux. Sa surface totale a été mesurée entre 1160 et 3710 m^2/m^2. Nous avons ainsi montré que la neige pouvait séquestrer une grande partie des espèces chimiques s'adsorbant à la surface de la glace, et présentes dans le système (neige + couche limite). Dans le cas d'un échange limité entre les couches de neige de surface et la couche limite de la basse troposphère, nous avons montré que la désorption d'une espèce à la suite d'un réchauffement et/ou d'une diminution de la SS, entraîner une forte augmentation de sa concentration atmosphérique, bien que la surface totale de ces couches de neige de surface ne représente qu'une faible fraction de la surface totale du manteau neigeux.

Nos mesures de SS ont également servi à étudier les processus d'échange de gaz traces entre la neige et l'atmosphère. Dans le cas de formaldéhyde, nous avons pu démontrer que dans le manteau neigeux, ce composé n'était pas localisé à la surface des cristaux de neige, mais était dissout dans le réseau cristallin de la glace. Ce résultat contredit des spéculations d'autres auteurs et contraint la paramétrisation des échanges neige-air de formaldéhyde, qui doit faire appel à la diffusion en phase solide. Ce processus est lent, avec une constante de temps de l'ordre de la dizaine de jours, alors qu'une paramétrisation faisant appel à l'adsorption aurait impliqué une constante de temps de quelques minutes.

La remobilisation de la glace résultant des processus du métamorphisme a également été mise en évidence et il a été montré que ce mécanisme pouvait conduire à une redistribution importante des solutés dissous dans le volume de la glace.

L'ensemble de nos résultats ont montré que l'étude de la microphysique de la neige et de l'évolution de la SS sont nécessaires pour comprendre la chimie de la neige et le rôle du manteau neigeux sur la chimie atmosphérique. De plus, il a été montré que l'impact de la neige sur la chimie de la troposphère peut être important et confirme que sa prise en compte est indispensable pour améliorer la compréhension de la chimie atmosphérique au-dessus des régions enneigées.

Dans le cadre de l'étude de la SS, de nombreuses études restent à faire. En ce qui concerne la méthode expérimentale, la méthode d'adsorption qui nous utilisons semble bien adaptée car elle

détermine la surface accessible aux gaz et est sensible aux structures les plus petites. Nous pensons que notre méthode est plus précise que la stéréologie (utilisée dans des travaux précédents) pour les neiges saisonnières ayant une SS supérieures à 100 cm^2/g. Dans le cas de neige plus âgées, la précision de notre méthode diminue et la stéréologie pourrait être mieux appropriée. Une comparaison des deux méthodes sur des échantillons identiques est nécessaire pour confirmer cette hypothèse. Une comparaison avec la tomographie par rayons X qui est une technique beaucoup plus récente pourrait également être envisagée, mais cette dernière technique aura une utilisation assez limitée, car elle est très lourde à mettre en oeuvre.

D'autres mesures sont nécessaires pour améliorer la précision de nos estimations de SS. Ceci concerne notamment les précipitations de l'Arctique aux faibles températures, les neiges humides fraîches et récentes ainsi que les neiges récentes perturbées par le vent. Le givre de surface qui croit durant l'hiver polaire nécessité également d'autres mesures.

Enfin, la prédiction de l'évolution de la SS de la neige devra sans doute faire appel à l'expérimentation en chambre froide, ou il est alors facile de contrôler la température, son gradient, et les autres paramètres influant sur le métamorphisme. De tels résultats seront sans doute essentiel dans la réussite de toute tentative de modéliser l'évolution de la SS.

Dans le cadre plus large de l'étude l'impact du manteau neigeux sur la chimie atmosphérique, de nombreuses études restent à faire. Pour les processus de surface, la connaissance de la SS est très utile mais les isothermes d'adsorption des gaz à la surface de la glace sont aussi indispensables pour estimer correctement les échanges avec l'atmosphère. Dans le cas des espèces localisées dans le volume de la glace, la prédiction de ces échanges requiert la quantification de la diffusion en phase solide. Cela nécessite donc la détermination des coefficients de diffusion des gaz dans la glace ainsi que leur solubilité à l'équilibre thermodynamique. Ainsi de nombreuses études de laboratoires sont souhaitables pour améliorer la compréhension du rôle du manteau neigeux sur la chimie atmosphérique.

REFERENCES BIBLIOGRAPHIQUES

Abbatt, J.P.D., Heterogeneous reaction of HOBr with HBr and HCl on ice surfaces at 228 K, Geophys. Res. Lett., 21, 665-668, 1994.

Abbatt, J.P.D., Interaction of HNO_3 with water-ice surfaces at temperatures of the free troposphere, *Geophys. Res. Lett.*, 24, 1479-1482, 1997.

Adamson, A.W., Dormant, L.M., et Orem, M., Physical adsorption of vapors on ice, *J. Colloid Interface Sci.*, 25, p. 206-217, 1967.

Anlauf, K.G., Mickle, R.E., Trivett, N.B.A., Measurement of ozone during Polar Sunrise Experiment 1992, *J. Geophys. Res.*, 99D, 345-353, 1994.

Auer A.H. Jr, et Veal D.L., The dimensions of ice crystals in natural clouds, *J. Atm. Sci.*, 1970.

Auer, A.H., Jr, Inferences about nucleation from ice crystal observations, *J. Atm. Sci.*, 29, 311-317, 1972.

Bales, R.C., et Choi, J., Conceptual framework for interpretation of exchange processes in chemical exchange between the atmosphere and polar snow, 43, NATO ASI 319-338, Springer, 1996.

Barnes, W.H., *Proc. R. Soc*. A125, p 670, 1929.

Barrie, L.A., Bottenheim, J.W., Schnell, R.C., Crutzen, P.J. et Rasmussen, R.A., Ozone destruction and photochemical reactions at polar sunrise in the lower Arctic atmosphere, *Nature*, 334, 138-141, 1988.

Barrie, L.A., Georgi, B., den Hartog, G., Landsberger, S., Staebler, R., Toom, D., et Wu, D., Arctic aerosol size-segregation chemical observations in relation to ozone depletion during polar sunrise 1992, *J. Geophys. Res*., 99D, 439-451, 1994.

Beaglehole, D., et Nason, D., Transition layer on the surface of ice, *Surf. Sci.*, 96, 357-363, 1980.

Bentley, W.A., et Humphries, W.J., Snow crystals, *reissue by Dover Publications Inc.: New York, 1962), McGraw-Hill: New York*, 226 p, 1931.

Bergeron, T., On the physics of cloud and precipitation, *Int. union Geod. Geophys. En. Assem. Lisbon., Int Assoc Hydrol. Sci. Publi*. 20, p 156, 1935.

Bernal, J.D., et Fowler, R.H., A theory of water and ionic solution, with particular reference to hydrogen and hydroxyl ions, *J. Chem. Phys.*, 1, 515-548, 1933.

Betterton, E.A., et Hoffmann, M.R., Henry's law constants of some environmental important aldehydes. Environmental Science and Technology 22, 1415-1418, 1988

Bjerrum, N., K. danske Vidensk selsk Skr., 27, p 1, 1951.

Bottenheim, J.W., Gallant, A.J., et Brice, K.A., Measurements of NO_y species and O_3 at 82°N latitude. *Geophys. Res. Lett.*, 13, 113-116, 1986.

Bottenheim, J.W., Barrie, L. W., Atlas, E., Heidt, L. E., Niki, H., Rasmussen, R. A., et Shepson, P.B., Depletion of lower tropospheric ozone during Arctic spring: The Polar Sunrise Experiment 1988, *J. Geophys. Res*., 95, 18555 –18568, 1990.

Bragg, W.;H., *Proc. Phys. Soc*., 34, p. 98, 1922.

Brunauer, S., Emmett, P., H., and Teller, E., *J. Amer. Chem. Soc*., 60, 309, 1938.

Brunauer, S., Deming, L.S., Deming, W.S., and Teller, E., *J. Amer. Chem. Soc*., 62, 1723, 1940.

Brun, E., Investigation on wet-snow metamorphism in respect of liquid-water content, *Annals of Glaciol*., 13, 22-26, 1989.

Burton, W.K., Cabrera, N., et Frank, F.C. ; The growth of crystals and the equilibrium structure of their surfaces, *Phil. Trans. Roy. Soc., London*, A243, 299-358, 1951.

Chaix, L., Ocampo, J., et Dominé, F., Adsorption of CH_4 on laboratory-made crushed ice and on natural snow at 77 K. Atmospheric implications, *C.R. Acad. Sci.Série II, Paris*, 322, 609-616, 1996.

Chaix, L. Influence de la méthode de fabrication de la glace et de son histoire thermique sur ses propriétés de surface, *Thèse de 3ème cycle, Université Joseph Fourier, Grenoble, France*, 1997.

Chu, L.T., Leu, M.T., et Keyser, L.F., Heterogeneous reactions of HOCl + HCl → Cl_2 + H_2O and $ClONO_2$ + HCl → Cl_2 + HNO_3 on ice surfaces at polar stratospheric conditions. *J. Phys. Chem*., 97, 12798-12804, 1993.

Colbeck, S.C., Theory of metamorphism of dry snow, *J. Geophys. Res.* 88, 5475-5482., 1983a.

Colbeck, S.C., 1983 Ice crystal morphology and growth rates at low supersaturations and high temperatures, *J. Appl. Phys.,* 54, 2677-2682, 1983b.

Colbeck, S.C., Classification of seasonal snow cover crystals, *Water Ressources Res.* 22, 59S-70S, 1986.

Couch, T.L.; Sumner, A.-L.., Dassau, T.M., Shepson, P.B., et Honrath, R.E., An Investigation of the Interaction of Carbonyl Compounds with the Snowpack. *Geophys. Res. Lett.*, 27, 2241-2244, 2000.

Debye, P., Polar Molecules, *Chemical Catalog Company, Reinhold, New York*., 1929.

Dennison, D.M., The crystal structure of ice, *Phys. Rev*., 17, p.20, 1921 .

Denoth, A., An electronic device for long-term snow wetness recording, *Annals of Glaciol*., 19, 104-106, 1994 .

De Serves, C. Gas phase formaldehyde et peroxide measurements in the arctic atmosphere. J. Geophys. Res., 99D, 25391-25398, 1994..

Dibb, J., Talbot, R., Munger, D., Jacob, D., et Fan S.-M., Air-snow exchange of HNO_3 et NOy at Summit, Greenland. *J. Geophys. Res.*, 103, 3475-3486, 1998.

Dominé, F., Thibert, E., Silvente, E., Legrand, M. & Jaffrezo, J.-L., Determining past atmospheric HCl mixing ratios from ice core analyses. *J. Atmos. Chem*., 21, 165-186., 1995.

Dominé, F., et Thibert, E., Mechanism of incorporation of trace gases in ice grown from the gas phase, *Geophys. Res. Lett.*, 23, 3627-3630, 1996.

Fan, S.-M., et Jacob, D.J., Surface ozone depletion in Arctic spring sustained by bromine reactions on aerosols, *Nature*, 359: 522-524, 1992.

Fassnacht, S.R. ; Innes, J. ; Kouwen, N. et Soulis, E.D. The specific surface area of fresh dendritic snow crystals. *Hydrol. Process.* 13, 2945-2962, 1999.

Ferry, D., Glebov, A., Senz, V., Suzanne, J., Toennies, J.P., and Weiss, H., Observation of the second ordered phase of water on the MgO (100) surface: Low energy electroin diffraction and helium atom scattering studies, *J. Chem. Phys*., 105, 4, 1996.

Fletcher, N.H., Surface structure of water and ice II. A revised model, *Philosoph. Mag*. 18, p. 1287, 1968.

Franck, F.C., The influence of dislocations on crystal growth, *Disc. Faraday Soc*., 5, 48-54, 1949.

Frank, F.C., Snow crystals, *Contemp. Phys*. 23, 3-22, 1982.

Frank, F.C., Foreword, Handbook of crystal growth 1, Fundamentals part A: Thermodynamics and Kinetics, *D.T.J. Hurle, Ed;, North Holland, xi-xii*, 1993.

Frei, A., et Robinson, D.A., Evaluation of snow extent and its variability in the Atmospheric Model Intercomparison Project, *J. Geophys. Res*., 103, 8859-8871, 1998.

Furukawa, Y., Yamamoto, M., et Kuroda, T., Ellipsometric study of the transition layer on the surface of an ice crystal, *J. of Cryst. Growth*, 82, 665-677, 1987.

Furukawa, Y., "Snow Crystals" (en Japonais), *Snow Crystals Museum, Asahikawa, Hokkaido, Japan*, 1991, copyright © 2000 Yoshinori Furukawa, http://www.lowtem.hokudai.ac.jp/~frkw/english/aletter.html.

Girardet, C, et Toubin, C., Molecular atmospheric pollutant adsorption on ice: a theoretical survey, *Surface Sci. Reports*, 2001, sous presse.

Glen, J.W., et Perutz, M.F., The growth and deformation of ice crystals, *J. Glaciol.*, 2, 397-403, 1954.

Golecki, I., et Jaccard, C., The surface of ice near 0°C studied by 100 keV proton channeling, *Phys. Lett., A* 63, 374-376, 1977.

Granberg, H.B., Distribution of grain sizes and internal surface area and their role in snow chemistry in a sub-arctic snow cover, *Annals of Glaciol.*, 7, 149-152, 1985.

Grannas, A.M., Shepson, P.B., Guimbaud, C., Sumner, A.L., Albert, M., Simpson, W., Dominé, F., Boudries, H., Bottenheim, J.W., Beine, H.J., Honrath, R., Zhou, X., A study of carbonyl compounds and photochemistry in the arctic atmospheric boundary layer, *Atm. Env.*, sous prese.

Gregg, S. J., and Sing, K.S.W., Adsorption, Surface Area and Porosity, *Academic Press*, 1982.

Guimbaud C., Grannas, A.M., Shepson, P.B., Boudries, H., Bottenheim, J.W., Fuentes, J.D., Dominé, F., Houdier, S., Perrier, S., Biesenthal, T.B., Splawn, B.G.. Importance of the snowpack in processing acetaldehyde and acetone in the arctic atmospheric boundary layer, *Atm. Env.*, sous presse

Hanot, L., et Dominé, F., Evolution of the surface area of a snow layer, *Environ. Sci. Technol.*, 33, 4250-4255, 1999.

Hallett J. et Mason B.J., The influence of temperature and supersaturation on the habit on ice crystals grown from the vapour, *Proc. Roy. Soc., London* A247, 440-453, 1958.

Hanson, D.R. et Ravishankara, A.R., Investigation of the reactive and nonreactive processes involving $ClONO_2$ and HCl on water and nitric acid doped ice, *J. Phys. Chem.,* 96, 2682-2691, 1992.

Hausmann, M., et Platt, U., Spectroscopy measurement of bromine oxyde in the hight Arctic during Polar Sunrise Experiment 1992, *J. Geophys. Res.,* 99, 399-413, 1994.

Higashi, A., et Sakai, N., Movement of small angle boundary of ice crystal, *J. Phys. Soc. Japan,* 16, 2359-2360, 1961.

Hobbs, P. V., Ice Physics; *Clarendon Press, Oxford, England*, 1974.

Hobbs, P. V., Radke, L.F., Weiss, R.R., Atkinson, D.G., Locatelli, J.D., Biswas, K.R., et Robertson, C.E., *Res. Rep. No VIII, Dec. 1974, Cloud Physic Group, Dept. Atmospheric Sci., University of Washington, Seattles; Washington*, 1974.

Hoff, J. T., Wania, F., Mackay, F., et Gillham, R., Sorption of nonpolar organic vapors by ice and snow, Environ. Sci. Technol., 29, 1995.

Hoff, J. T., Mackay, D., Jia, C.Q., et Wania, F., Measurement of the specific surface area of snow using the nitrogen adsorption technique, *Environ. Sci. Technol.*, 32, 58-62, 1998.

Hondoh, T., Azuma, K., et Higashi, A., Self interstitials in Ice, *J. de Physique* 48, 183-187, 1987.

Honjo, G., Kitamura, N., Shimaoka, K., et Mihama, K., Low temperature specimen method for electron diffraction and electron microscopy, *J. Phys. Soc. Japan,* 11, 527-536, 1956.

Honrath, R.E., Peterson, M.C., Guo, S., Dibb, J.E., Shepson, P.B. et Campbell, B., Evidence of NO_x production within or upon ice particles in the Greenland snowpack. *Geophys. Res. Lett.*, 26, 695-698, 1999.

Honrath, R.E., Peterson, M.C., Dzobiak, M.P., Dibb, J.E., Arsenault, M.A., et Green, S.A., Release of NO_x from sunlight-irradiated Midlatitude Snow, *Geophys. Res. Lett.*, 27, 2237-2240, 2000a.

Honrath, R.E., Guo, S., Peterson, M.C., Dzobiak, M.P., Dibb, J.E., Arsenault, M.A., Photochemical production of gas phase NO_x from ice-crystal NO_3^-, *J. Geophys. Res.*, 105:,183-24,190, 2000b.

Houdier, S., Perrier, S., Dominé, F., Grannas, A.M., Guimbaud, C., Shepson, P.B., Boudries, H., Bottenheim, J.W., Acetaldehyde and acetone in the Arctic snowpack during the ALERT 2000 field campaign. Snowpack composition, incorporation processes and atmospheric impact, *Atm. Env*., 2001, sous presse.

Hutterli, M. A., Rothlisberger, R., et Bales, R. C., Atmosphere-to-snow-to-firn transfer studies of HCHO at Summit, Greenland, *Geophys. Res. Lett., 26*, 1691-1694, 1999

Impey, G.A., Shepson, P.B, Hastie, D.R., Barrie, L.A., et Anlauf, K.G., Measurements of photolyzable chlorine and bromine sources during the Polar Sunrise Experiment 1995, *J. Geophys. Res*., 95, 16005-16010, 1997.

Impey, G.A., Mihele, C.M., Anlauf, K.G., Barrie, L.A., Hastie, D.R., et Shepson, P.B., Measurements of photolyzable halogen compounds and bromine radicals during the Polar Sunrise Experiment 1997, *J. Atm. Chem*., 34, 21-37, 1999.

Israelachvili, J.N., Intermolecular and Surface Forces*, Academic Press, New-York*, 1985.

Itoo, K., *Tokyo Papers in Meteor. And Geophys*., 8, 220, 1957.

Jaffrezo, J.-L., Dibb, J., Bales, R., et Neftel A., Current atmospheric studies at Summit (Greenland) and implications for future research in R.J. Delmas (ed.), NATO ARW: Ice Core Chemistry of Global Biogeochemical Cyles, *Springer-Verlag, Berlin*, p. 435, 1994.

Jellinek, K., et Ibrahim, S., Sintering of powdered ice, *J. Colloid Interface Sci.,* 25, 245-254, 1967.

Jobson, B. T., et al., Measurements of C2-C6 hydrocarbons during the Polar Sunrise Experiment: Evidence for Cl atom and Br atom chemistry, *J. Geophys. Res*., 99, 355-368, 1994.

Jones, A.E., R. Weller, P.S. Anderson, H.-W. Jacobi, E. W. Wolff, O. Schrems, H. Miller, Measurements of NOx emissions from the Antarctic snowpack. *Geophys. Res. Lett*., 28, 1499-1502, 2001.

Judson, A., et Doesken, N., Density of freshly fallen snow in the Central Rocky Mountains, *Bull. Amer. Meteor. Soc.,* 81,1577-1587, 2000.

Ketcham, W.M., et Hobbs, P.V., Step growth on ice during the freezing of pure water. *Phil. Mag*., 18, 659-661,1968.

Kittel, C., Introduction to Solid State Physics, *3rd Ed., Wiley International Ed., U*SA, 1968.

Kobayashi, T., The growth of snow crystal at low supersaturation, *Phil. Mag*., 6, 1363-1370, 1961.

Kobayashi, T., et Kuroda, T., Morphology of crystals*, Part B, édition Sunagawa I., Terra Scientific*, 1987.

Lamb, D., et Hobbs, P.V., Growth rate and habits of ice crystals grown from the vapor phase, *J. Atmos. Sci*., 28, 1506-1509, 1971.

Lamb, D. et Scott, W.D., Linear growth rates of ice crystals grown from the vapor phase, *J. Crystal. Growth,* 12, 21-31, 1972a.

Lamb, D. et Scott, W.D., The mechanism of ice growth and habit formation, *J. Atmos. Sci.*, 31, 570-580, 1972b.

Langmuir, I., *J. Amer. Soc*., 38, 2221, 1916.

La Placa, S.J., et Post, B., Thermal expansion of ice, *Acta Crystallogr*, 13, 503-505, 1960.

Leu, M.T., Laboratory studies of sticking coefficients and heterogeneous reactions important in the Antarctic stratosphere, *Geophys. Res. Lett.*, 15, 17-20, 1988.

Libbrecht, K. G., The Patty Rasmussen 2000 Collection, Copyright © 2000 Patty Rasmussen, *site web http://www.snowcrystals.net* , *Caltech, USA*.

London, F., Z. *Physik. Chem*., 11, p 222, 1930.

Lundberg., A., Laboratory calibration of TDR-probes for snow wetness measurements, *Cold Reg. Sci. Technol*., 25, 197-205, 1997.

Magano, C, Lee, C.W., Meteorological classification of natural snow crystals*, J. of the faculty of Sci,. Hokkaido university*, 1966.

Marbouty, D., An experimental study of temperature gradient metamorphism ; *J. Glaciol*., 26, 303-312, 1980.

Mason, B. J., The Physics of clouds, *Oxford: Clarendon Press*, 481p, 1957.

McKnight, C.V., et Hallett, J, X-ray topographic studies of dislocations in vapor-grown crystals, *J. of Glaciol*., 21, 397-408, 1968.

Michalowski, B.A., Francisco, J.S., Li, S.-M., Barrie, L.A., Bottenheim, J.W., et Shepson, P.B., A computer model study of multiphase chemistry in the arctic boundary layer during polar sunrise*. J. Geophys. Res.*, 105, 15131-15145, 2000.

Mickle, R.E., Bottenheim, J.W., Leaitch, W.R., et Evans, W., Boundary layer ozone depletion during AGASP-II, *Atmospheric Environment*, 23, 2443-2449, 1989 .

Mizuno, Y., *J. of Glaciol.*, 85, p 409, 1978

Mizuno, Y., et Hanafusa, N., Studies of surface properties of ice using nuclear magnetic resonance, *J. de physique*, C1, 48, 511-517, 1987.

Mullins, W. W., et Sekerka, R. F. Morphological stability of a particle growing by diffusion or heat flow, *J. Appl. Phys*, 34,1965, 323-329, 1963.

Mulvaney R., Wolff, E.W., et Oates, K., Sulphuric acid at grain boundaries in Antarctic ice, *Nature* 331, 247-249, 1988.

Nakaya, U., Snow *Crystals:* Natural and Artificial*, Harvard University Press*, 174p, 1954.

Narita, H., Specific surface of deposited snow II, *Low Temp. Sci.,* A29, 69-81, 1971 (en japonais).

Nelson, H., Baker, M.B., New theoretical framework for studies of vapor growth and sublimation of small ice crystals in the atmosphere, *J. of Geophys. Res*., 101, 7033-7047, 1996.

Nelson, J., Sublimation of ice crystals, *J. Atmos. Sciences,* 55, 910-919, 1998.

Nelson, J., et Knight, C., Snow crystal habit change explained by layer nucleation, *J. Atmos. Sciences,* 55, 1452-1465, 1998.

Orem, M.W. et Adamson, A.W., Physical adsorption of vapors on ice. II. n-Alkanes. *J. Colloid Interface Sci.*, 31, 278-286, 1969.

Oum, K. W., Lakin, M. J., et Finlayson-Pitts, B. J., Bromine activation in the troposphere by the dark reaction of O_3 with seawater ice, Geophys. Res. Lett., 25, 3923-3926, 1998.

Pahaut, E., et Sergent, C., La Neige Formation et Evolution, *Centre d'Etude de la Neige, Météo France*, 1991.

Pauling L., The structure and entropy of ice and other crystals with randomness of atomic arrangement, *J. Am. Chem. Soc.* 57, 2680-2684, 1935.

Paterson, W.S.B., The physics of glaciers*, 3^{ième} édition, Pergamon*, 1994 .

Perla, R., Dozier, J., et Davis, R.E., Preparation of serial sections in dry snow specimens. *J. Microsc,.* 141, 111-114, 1986..

Perrier, S., Houdier, S., Dominé, F., Cabanes, A., Legagneux, L., Sumner, A.L., et Shepson, P.B., Formaldehyde in Arctic snow. Incorporation into ice particles and evolution in the snowpack, *Atm. Env*., 2001, sous presse .

Petrenko, V. F., et Withworth, R. W., Physics of ice; *Oxford University Press: New York*, 1999.

Plummer P.L.M., in Physics and Chemistry of Ice*, Hokkaido University Press, Sapporo*, 1992.

Pruppacher, H. R., et Klett, J. D., Microphysics of Clouds and Precipitation; *D. Reidel: Dordrecht, Boston*, 1978.

de Quervain, M.R., On the metamorphism and hardening of snow under constant pressure and temperature gradient, *IAHS publication* 46, 225-239, 1958.

de Quervain, M.R., On the metamorphism of snow*, in Ice and Snow: Properties, Proceses and Applications, edited by W.D. Kingery,* p. 377-390*, MIT Press, Cambridge, MA*, 1963.

Rey, Laurent, La Neige, ses Métamorphoses, les Avalanches, *Centre d'Etude de la Neige, Météo France*, 1986.

Rey, Laurence, Comparaison des propriétés de surface de la neige naturelle et de la glace préparée au laboratoire, *D.E.A. 3eme cycle, Université Paris VII, France*, 1995.

Rey-Hanot, Laurence, Adsorption de gaz traces sur la glace. Application à la chimie des nuages et du manteau neigeux. *Thèse 3ème cycle, Université Joseph Fourier, Grenoble, France*, 295p., 1999.

Rinne, F., *Ber. Verth. Sächs Acad. Wiss., Math.- Phys*., K1, 69, p. 57, 1917.

Robinson, D. A., Dewey, K. F., et. Heim, R. R. Jr., Global snow cover monitoring: an update, *Bull. Amer. Meteor. Soc.,* 74, 1689-1696, 1993.

Rottner, D., et Vali, G., *J. Atm. Sci.*, 31, p 560, 1974

Schmitt, B., La surface de la glace. Structure, dynamique et Interactions. Implications astrophysiques, *Thèse 3emecycle, Université de Grenoble, France*, 272p, 1986.

Sander, R., R. Vogt, G.W. Harris, et P.J. Crutzen. Modelling the chemistry of ozone, halogen compounds, and hydrocarbons in the Arctic troposphere, Tellus, 49B, 522-532, 1997.

Sei, T., et Gonda, T., The growth mechanism and the habit change of ice crystals growing from the vapor phase, *J. Crystal Growth*, 94, 697-707, 1989.

Seligman, G., Snow structure and Ski Fields, *International Glaciological Society, Cambridge*, 1936 (reprinted 1980).

Snider, J.R., and Murphy, T. Airborne hydrogen peroxide measurements in supercooled clouds, *J. Geophys. Res*., 100, 23039-23050, 1995.

Solomon, S., The mystery of the Antarctic ozone "hole", *Rev. Geophys.,* 26, 132-148, 1988.

Solberg, S., Hermansen, O., Joranger, E, Schmidtbaeur, N., Stordal, F., et Hov, O., Tropospheric ozone depletion in the Arctic during spring measurements on the Zeppelin mountain on Spitsbergen, *NILU Report OR 27/94 ISBN 82-425-0575-6*, 1994.

Sumner, A.L., et. Shepson., P.B., Snowpack production of formaldehyde and its effect on the Arctic troposphere. *Nature*, 398, 230-233, 1999.

Tang, T., et Mc Connell, J. C., Autocatalytic release of bromine from arctic snow pack during polar sunrise, *Geophys. Res.Lett., 23, 2633-2636,* 1996.

Thibert, M., Thermodynamique et cinétique des solutions solides HCl-H_2O et HNO_3-H_2O, Implications atmosphériques, *Thèse de 3ème cycle, Université Joseph Fourier, Grenoble , France*, 274p, 1996.

Thibert, E., et Dominé, F. Thermodynamics and kinetics of the solid solution of HCl in ice, *J. Phys. Chem. B*., 101, 3554-3565, 1997

Thibert, E., et Dominé, F., Thermodynamics and kinetics of the solid solution of HNO_3 in ice, *J. Phys. Chem. B*, 102, 4432-4439, 1998

Van de Veen, C.J., State of balance of the cryosphere*. Review of Geophys*., 29 ,3 , 433-455, 1991.

Voisin, D.; Legrand, M. et Chaumerliac, N., Scavenging of acidic gases (HCOOH, CH_3COOH, HNO_3, HCl and SO_2) and ammonia in mixed liquid-solid water clouds at the Puy de Dôme mountain (France), *J. Geophys. Res*., 105, 6817-6835, 2000.

Wania, F., Modelling the fate of non-polar organic chemicals in an ageing snow pack, *Chemosphere*, 35, 2345-2363, 1997.

Weller, R.; Minikin, A.; König-Langlo, G.; Schrems, O.; Jones, A.E.; Wolff, E.W.; et Anderson, P.S., Investigating possible causes of the observed diurnal variability in Antarctic NOy. *Geophys. Res. Lett.*, 26, 601-604, 1999.

Wergin, William P., Rango A., et Erbe, E.F., Observations of snow crystals using low-temperature Scanning Electron Microscopy, *Scanning*, 17, 41-49, 1995. Images de cristaux de neige obtenues par SEM disponible sur internet : http://www.lpsi.barc.usda.gov/emusnow .

Zaretskii, A.V., Petrenko, V.F. et Chesnakov, V.A., The protonic conductivity of heavily KOH-doped ice, *Physica Status Solidi (a)* 109, 373-381, 1988.